HIGH-RESOLUTION ATMOSPHERE-OCEAN CLIMATE MODELLING IN THE ADRIATIC SEA

Pranić, Petra

Doctoral thesis / Doktorski rad

2023

Degree Grantor / Ustanova koja je dodijelila akademski / stručni stupanj: **University of Zagreb, Faculty of Science / Sveučilište u Zagrebu, Prirodoslovno-matematički fakultet**

Permanent link / Trajna poveznica: https://urn.nsk.hr/urn:nbn:hr:217:621020

Rights / Prava: In copyright / Zaštićeno autorskim pravom.

Download date / Datum preuzimanja: **2025-02-28**

Repository / Repozitorij:

Repository of the Faculty of Science - University of Zagreb

University of Zagreb

Faculty of Science
Department of Geology

Petra Pranić

HIGH-RESOLUTION ATMOSPHERE-OCEAN CLIMATE MODELLING IN THE ADRIATIC SEA

DOCTORAL DISSERTATION

Zagreb, 2023

University of Zagreb

Faculty of Science
Department of Geology

Petra Pranić

HIGH-RESOLUTION ATMOSPHERE-OCEAN CLIMATE MODELLING IN THE ADRIATIC SEA

DOCTORAL DISSERTATION

Supervisors: Dr. Ivica Vilibić, Dr. Cléa Denamiel

Zagreb, 2023

Sveučilište u Zagrebu

Prirodoslovno-matematički fakultet
Geološki odsjek

Petra Pranić

ATMOSFERSKO-OCEANSKO KLIMATSKO MODELIRANJE VISOKE RAZLUČIVOSTI ZA PODRUČJE JADRANSKOGA MORA

DOKTORSKI RAD

Mentori: Dr. sc. Ivica Vilibić, Dr. sc. Cléa Denamiel

Zagreb, 2023.

This doctoral dissertation was written as part of the University Postgraduate Doctoral Study in Oceanology at the Department of Geology, Faculty of Science, University of Zagreb, under the supervision of Dr. Ivica Vilibić and Dr. Cléa Denamiel. The research was carried out in the Physical Oceanography Laboratory of the Institute of Oceanography and Fisheries in Split as part of the "Adriatic Decadal and Interannual Oscillations: Observations, Modeling and Consequences" project (ADIOS; IP–2016–06–1955) of the Croatian Science Foundation.

ACKNOWLEDGMENTS

I thank my supervisors Dr. Ivica Vilibić and Dr. Cléa Denamiel for their invaluable guidance, help and advice during my doctoral studies and the creation of this doctoral dissertation. I also thank the members of my supervisory committee, Prof. Danijel Belušić, Asst. Prof. Dr. Žarko Kovač and Dr. Ivan Güttler, for their contributions.

I would like to express my gratitude to all my colleagues at the Institute of Oceanography and Fisheries. A special thanks to my colleague and friend, Dr. Petra Zemunik, for her selfless help during our time working together and numerous discussions about our doctoral research.

I acknowledge the work and efforts of the various organizations, researchers, and technicians who participated in collecting the observational data used in this doctoral research. Also, I would like to acknowledge the European Centre for Medium-Range Weather Forecasts (ECMWF) for providing their computing and archive facilities to support this research.

I am thankful to my family and friends who have been with me throughout this journey. Finally, I want to express my deepest gratitude to my mother, Ita, for making everything possible and for her endless love and support.

University of Zagreb
Faculty of Science
Department of Geology

Doctoral thesis

HIGH-RESOLUTION ATMOSPHERE-OCEAN CLIMATE MODELLING IN THE ADRIATIC SEA

Petra Pranić

ABSTRACT

The Adriatic region is characterized by extremely complex geomorphology and atmospheric and oceanic processes occurring at various temporal and spatial scales. Due to the relatively coarse horizontal resolution, regional climate models are not capable to resolve the coastal morphology of the Adriatic Sea nor reproduce the processes that occur on smaller spatial and shorter temporal scales. High-resolution climate modeling can be used to overcome these challenges and improve our understanding of the complex processes that drive the Adriatic atmospheric and oceanic circulation. Hence, a high-resolution atmosphere-ocean climate model, the Adriatic Sea and Coast (AdriSC), has been developed for the Adriatic and northern Ionian seas. In order to describe the climate properties of the Adriatic, a 31-year-long (1987–2017) climate simulation was carried out with the AdriSC model. In this thesis, the performance of the AdriSC ocean simulation was thoroughly evaluated by comparing the model results with a comprehensive collection of remote sensing and *in situ* observational data. Furthermore, the results of the AdriSC simulation, the latest reanalysis product for the Mediterranean Sea and a long-time-running Adriatic Sea atmosphere-ocean forecast model used in both hindcast and data assimilation modes were compared in their ability to reproduce the Adriatic dense-water dynamics during the 2014–2015 period. The main advantages and disadvantages of the different modelling approaches were quantified and discussed. Lastly, a climatology of the Adriatic dense-water dynamics was derived from the results of the AdriSC climate simulation by analyzing the thermohaline properties of the Adriatic Sea during the 1987–2017 period.

(170 pages, 62 figures, 3 tables, 186 references, original in English)

Keywords: Adriatic Sea, thermohaline circulation, climate model, high resolution, evaluation, data assimilation, reanalysis, dense water, dense-water climatology

Supervisors: Dr. Ivica Vilibić
Dr. Cléa Denamiel

Reviewers: Prof. Danijel Belušić
Asst. Prof. Dr. Žarko Kovač
Dr. Ivan Güttler

Sveučilište u Zagrebu
Prirodoslovno–matematički fakultet
Geološki odsjek

Doktorski rad

ATMOSFERSKO-OCEANSKO KLIMATSKO MODELIRANJE VISOKE RAZLUČIVOSTI ZA PODRUČJE JADRANSKOGA MORA

Petra Pranić

SAŽETAK

Područje Jadrana obilježava vrlo složena geomorfologija te procesi u atmosferi i moru koji se odvijaju na različitim vremenskim i prostornim skalama. Zbog relativno grube horizontalne razlučivosti, regionalni klimatski modeli nisu sposobni razlučiti obalnu morfologiju Jadranskoga mora ni reproducirati procese koji se odvijaju na manjim prostornim i kraćim vremenskim skalama. Za prevladavanje navedenih izazova i poboljšanje razumijevanja složenih procesa koji pokreću jadransku atmosfersku i oceansku cirkulaciju može se koristiti klimatsko modeliranje visoke razlučivosti. S tim ciljem razvijen je atmosfersko-oceanski klimatski model visoke razlučivosti Adriatic Sea and Coast (AdriSC) za područje Jadranskog i sjevernog Jonskog mora. Kako bi se opisala klimatska svojstva Jadrana, izvršena je 31-godišnja (od 1987. do 2017. godine) klimatska simulacija modelom AdriSC. U ovom radu, napravljena je temeljita evaluacija oceanske simulacije modela AdriSC usporedbom rezultata modela s opsežnim skupom podataka daljinskih i *in situ* mjerenja. Nadalje, rezultati simulacije AdriSC, najnovije reanalize za Sredozemno more i prognostičkog atmosfersko-oceanskog modela za Jadransko more korištenog za simulacije sa i bez asimilacije podataka, uspoređeni su na temelju njihove sposobnosti reproduciranja dinamike guste vode u Jadranu u razdoblju od 2014. do 2015. godine. Kvantificirane su i raspravljene glavne prednosti i nedostaci različitih pristupa numeričkom modeliranju guste vode. Naposljetku, analizom termohalinih svojstava Jadranskoga mora iz rezultata klimatske simulacije AdriSC u razdoblju od 1987. do 2017. godine načinjena je klimatologija dinamike jadranske guste vode.

(170 stranica, 62 slike, 3 tablice, 186 literaturnih navoda, jezik izvornika: engleski)

Ključne riječi: Jadransko more, termohalina cirkulacija, klimatski model, evaluacija, visoka razlučivost, asimilacija podataka, reanaliza, gusta voda, klimatologija guste vode

Mentori: dr.sc. Ivica Vilibić
dr.sc. Cléa Denamiel

Ocjenjivači: prof. dr. sc. Danijel Belušić
doc. dr. sc. Žarko Kovač
dr. sc. Ivan Güttler

TABLE OF CONTENTS

1. INTRODUCTION

In the present day, the study of the dynamics and variability of atmospheric and oceanic processes heavily relies on continuous developments and improvements in available numerical modelling tools, particularly due to the temporal and spatial sparsity of *in situ* observations.

Over the years, the modelling community in the Adriatic region, has made significant progress in addressing the challenges posed by the complex orography, bathymetry and coastline of the Adriatic area (Fig. 1). The elongated semi-enclosed Adriatic basin is surrounded by mountain ranges – the Alps in the north, the Apennines in the west, and the Dinarides in the east. The bathymetry of the Adriatic Sea is characterized by the shallow northern Adriatic shelf (averaging 30 m in depth), gradually deepening towards the ~ 280-m-deep Jabuka Pit in the middle Adriatic. The pit is separated from the ~ 1230-m-deep Southern Adriatic Pit by the Palagruža Sill, whereas in the very south, the Strait of Otranto (~ 780 m deep) connects the Adriatic with the northern Ionian Sea. Also, the Adriatic coastline is very complex with over 1200 islands, islets and rocks along its eastern side.

Apart from its geomorphological features, the Adriatic is characterized by atmospheric and oceanic processes that occur on different temporal and spatial scales, ranging from long-term phenomena on larger spatial scales (e.g. thermohaline circulation) to short-term events that vary on smaller spatial scales (e.g. bora wind). Consequently, the Adriatic presents an extremely challenging region for the numerical modelling of atmospheric and oceanic processes.

1.1. Adriatic thermohaline circulation

The thermohaline circulation is one of the main processes influencing the Adriatic Sea dynamics. On the one hand, the river Po in the northern Adriatic drives the outward Western Adriatic Current (WAC) along the western coast. On the other hand, the inward Eastern Adriatic Current (EAC) flows along the eastern side of the Adriatic Sea and transports water masses from the Mediterranean Sea and, in coastal regions, from large rivers located in northern Albania and southern Croatia.

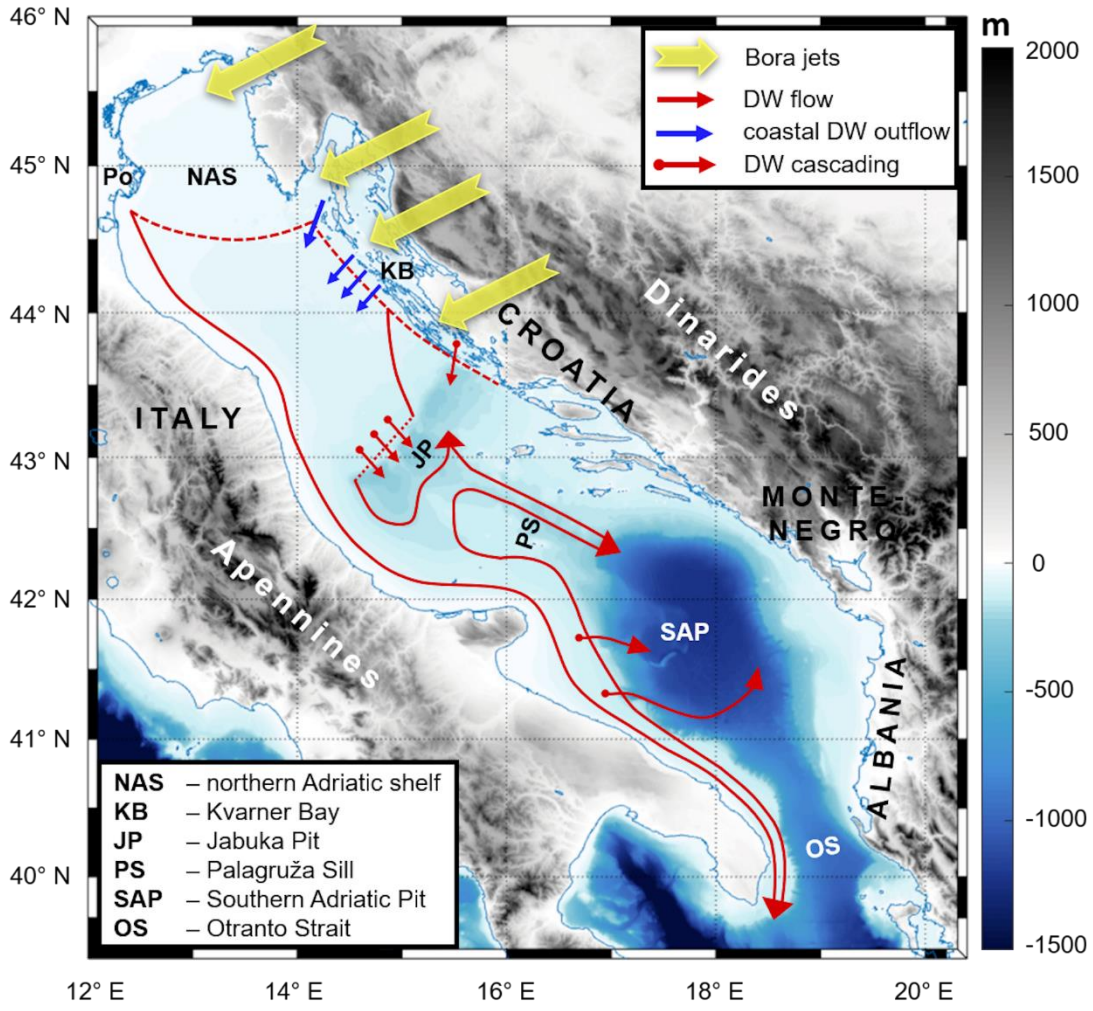

Figure 1. Bathymetry and orography of the Adriatic Sea area, with indicated North Adriatic Dense Water formation sites (NAS – northern Adriatic shelf, KB – Kvarner Bay), NAddW pathways (arrows) and accumulation sites (JP – Jabuka Pit or middle Adriatic depressions, SAP – Southern Adriatic Pit, KB – Kvarner Bay). Dominant bora wind patterns associated with the NAddW formation are also indicated. Adapted from Vilibić et al. (2023).

Another important driver of the thermohaline circulation is the formation of the densest water mass in the whole Mediterranean Sea (Melanotte-Rizzoli i sur., 1997; Cushman-Roisin i sur., 2001), known as the North Adriatic dense Water (NAddW; Zore-Armanda, 1963). On average, the density of NAddW is around 1029.5 kg m^{-3}, but it can surpass 1030 kg m^{-3} during extreme events (Vilibić, 2003; Mihanović et al., 2013; Benetazzo et al., 2014). The formation of NAddW is known to occur in winter during severe bora events associated with hurricane-strength gusts up to 50 m s^{-1} (Belušić and Klaić, 2004). Bora events tipically last for about two days but can extend up to a week (Belušić et al., 2013; Grisogono and Belušić, 2009; Stiperski et al., 2012). They are strongly influenced by the orography of the region and are most frequent

and intense along the northern Velebit mountain range (e.g. Belušić et al., 2007; Gohm et al., 2008; Grubišić, 2004; Klemp and Durran, 1987; Kuzmić et al., 2015; Smith, 1987). Practically, the alternation of major mountain gaps and peaks along the Velebit mountain range leads to the formation of gap jets and wakes (e.g. Alpers et al., 2009; Jiang and Doyle, 2005; Signell et al., 2010) which results in the ocurrence of bora jets at specific locations (Fig. 1). The Trieste jet has the northernmost location, the Senj jet is the most intense and furthest reaching at sea, while the Karlobag and Sukošan jets strongly impact the upper middle Adriatic (Dorman et al., 2007; Pullen et al., 2007; Janeković et al., 2014; Denamiel et al., 2020a, b). Several jets also occur along the eastern coast in the middle and southern Adriatic (Grisogono and Belušić, 2009; Horvath et al., 2009).

During the most extreme bora events, the intensity of the upward sea surface heat fluxes – taking out heat from the sea – is largely increased along the jets, inducing negative buoyancy fluxes associated with sea surface cooling at hourly to daily timescales (e.g. Janeković et al., 2014; Denamiel et al., 2021a). This cooling, in addition to the homogenization of the coastal waters during the late autumn and winter seasons, results in the formation of dense waters over the northern Adriatic and the Kvarner Bay (e.g. Janeković et al., 2014; Ličer et al., 2016; Vilibić et al., 2018). In the days to weeks following these bora events, a strong thermohaline circulation – mostly driven by bottom density currents – starts in the Adriatic–Ionian basin and generally lasts for months (Orlić et al., 2007). Indeed, the dense waters, generated in the northern Adriatic or within the Kvarner Bay, travel along the Italian coast following the Po River plume (Artegiani and Salusti, 1987; Vilibić and Mihanović, 2013). Dense waters are partly collected within the Jabuka Pit (Marini et al., 2006), the SAP (Querin et al., 2016) but also within the Kvarner Bay, which serves as an area of both generation and deposition of dense waters. The remaining part leaves the Adriatic basin through the Strait of Otranto towards the northern Ionian Sea (Buljan and Zore-Armanda, 1971; Bensi et al., 2013).

Along with the bora-induced surface heat losses, another important factor preconditioning dense-water formation are the surface water fluxes, particularly river discharge, with the river Po being the most influental (Beg-Paklar et al., 2001). A reduction in river discharge up to four months prior to dense-water formation has been found to precondition strong formation events (Vilibić and Supić, 2005). Another preconditioning factor is also the advection of the water masses from the Ionian Sea (Vilibić and Supić, 2005), influenced by the Adriatic–Ionian Bimodal Oscillating System (hereafter reffered as BiOS; Gačić et al., 2010, 2014).

Thus, bora-driven dense-water formation in the northern Adriatic, jointly with the deep waters generated through bora-driven open convection in the SAP (Gačić et al., 2002), has a crucial impact on the Adriatic thermohaline circulation (Orlić et al., 2006; Vilibić et al., 2013) which presents large seasonal and interannual variability (Vilibić et al., 2014). Also, dense-water formation greatly impacts the biogeochemical properties of the Adriatic Sea (Boldrin et al., 2009; Bensi et al., 2013; Gačić et al., 2010; Batistić et al., 2014; Jasprica et al., 2022) among which the most important is the transport of oxygen to the deep layers, in particular to the middle Adriatic depressions, which are a nursery for many benthic species (Chiarini et al., 2022; Vilibić et al., 2023). Besides the Adriatic Sea, dense-water formation on shelves and its subsequent sinking along shelf breaks (i.e. cascading; Shapiro and Hill, 1997, 2003) have been observed and studied in many other areas of the world ocean and particularly in higher latitudes (Borenas et al., 2002; Shapiro et al., 2003; Wahlin, 2002, 2004; Ivanov et al., 2004; Heggelund et al., 2004; Leredde et al., 2007; Garcia-Quintana et al., 2021).

1.2. Numerical modelling in the Adriatic Sea

In general, numerical models are widely applied in oceanography and they differ in their ability to reproduce different oceanographic properties and processes. One of the main features of these models is their spatial and temporal resolution which largely influences the model performance. This concept is particularly important in modelling of small- and short-scale processes, especially in complex coastal areas such as the Adriatic Sea. Moreover, in multi-decadal (climate) simulations, increasing the resolution substantially increases the computational costs (Prein et al., 2015). Consequently, in the past few decades, high-resolution numerical studies in the Adriatic have predominantly focused on shorter time periods of up to several years, while kilometre-scale climate model simulations have only recently been performed in the Adriatic.

Historically, numerous studies have focused on the numerical modelling of dense-water dynamics in the Adriatic due to its vital role in many ocean processes. The initial numerical efforts to study dense-water formation in the Adriatic, with ocean model resolutions up to 3 km, mainly concentrated on the NAddW formation within the northern Adriatic shelf (Bergamasco et al., 1999; Beg-Paklar et al., 2001) and the formation of Adriatic Deep Water (AdDW) within the southern Adriatic Pit, along with its interannual variability (Mantziafou and Lascaratos, 2004, 2008). During this period, the atmospheric fields used for forcing ocean models were mostly climatological data (May, 1982; Artegiani et al., 1997) or global datasets

from the European Centre for Medium-Range Weather Forecasts (ECMWF; e.g., ERA 40, ERA-I; Vested et al., 1998; Zavatarelli et al., 2002; Oddo and Guarnieri, 2011). However, many studies demonstrated that ECMWF reanalyses, due to their spatial homogeneity and coarse resolution, could not properly reproduce the extreme bora events that drive dense-water formation in the northern Adriatic Sea. In particular, Cavaleri and Bertotti (1997) highlighted that the underestimation of bora wind speeds could reach up to 50 %, consequently leading to a strong underestimation of NAdDW production rates (Vilibić and Supić, 2005). Therefore, in some studies, ECMWF wind speeds were increased by up to 20 % to in order improve the representation of ocean dynamics during bora events (e.g. Mantziafou and Lascaratos, 2004). Indeed, the resolution of the atmospheric model was found to be one of the most important factors influencing bora wind speeds due to an improved reproduction of orography and enhancement of jet flows in finer grids (Belušić et al., 2017).

More recently, the implementation of a modelling system by Janeković et al. (2014), based on the Regional Ocean Modeling System (ROMS; Shchepetkin and McWilliams, 2009) at a 2 km resolution, forced by the operational atmospheric model ALADIN/HR (Aire Limitée Adaptation Dynamique développement InterNational; Tudor et al., 2013), has allowed for a better representation of the atmosphere-ocean dynamics during bora events in the northern Adriatic (Vilibić et al., 2016; Mihanović et al., 2018; Vilibić et al., 2018), which is also substantially influenced by the ocean feedback to the atmosphere (Pullen et al., 2006, 2007; Ličer et al., 2016). Over the last decade, several other studies have also used kilometre-scale limited-area models to simulate various ocean processes driven by extreme conditions in the Adriatic Sea. These processes include extreme waves and storm surges, sea surface cooling, water column mixing, dense-water formation and long-term thermohaline circulation occurring during severe bora and sirocco windstorms (e.g., Cavaleri et al., 2010, 2018; Ricchi et al., 2016; Carniel et al., 2016; Denamiel et al., 2020a).

Nevertheless, apart from atmospheric forcing, other sources of errors have been identified as factors that influence the quality of numerical modelling in the Adriatic region, including the representation of the river discharges and the choice of the open boundary conditions. Regarding the issues related to river discharges, the use of an outdated river runoff climatology (Raicich, 1994) and the absence of recent river load observations, particularly along the eastern Adriatic coast, led to a large overestimation (multiplied by at least 5) of discharges in the northeastern Adriatic (Janeković et al., 2014). This climatology has been used in numerous Adriatic modelling studies (e.g. Zavatarelli and Pinardi, 2003; Oddo et al., 2005; Chiggiato and

Oddo, 2008; Benetazzo et al., 2014). However, it has been demonstrated to prevent dense-water generation in the coastal eastern Adriatic area (Mihanović et al., 2013) and reduce the ocean density by up to 0.5 kg m^{-3} in the primary dense-water formation sites on the northern Adriatic shelf (Vilibić et al., 2016). Thus, it has been replaced by a more recent climatology based on up-to-date observations (Janeković et al., 2014), significantly improving the representation of dense-water formation, particularly at its secondary source location in the Kvarner Bay (Vilibić et al., 2016, 2018; Mihanović et al., 2018).

Concerning the propagation of errors from the open boundaries, particularly at the Strait of Otranto, they have mostly been documented as an underestimation of salinity, also linked to incorrect freshwater forcing (Janeković et al., 2014). Other sources of errors, such as improper parameterization of vertical mixing and diffusion, can also affect the performance of Adriatic models, and better ocean modelling solutions may be reached through a data assimilation procedure (Janeković et al., 2020).

Notwithstanding the corrections of the aforementioned sources of error, a common key conclusion of all recent Adriatic studies was still the need for higher-resolution atmospheric models and longer-term simulations to capture the coastal ocean dynamics in the Adriatic Sea. In terms of long-term climate modelling, the Adriatic Sea has, until now, predominantly been studied with regional climate models (RCMs) developed for the entire Mediterranean Sea within the Med-CORDEX initiative (e.g. Somot et al., 2006; Sevault et al., 2014). However, these RCMs have been shown to be incapable of properly reproducing the processes at the coastal scale, mainly due to their relatively coarse horizontal resolution (of the order of 10 km), which is insufficient to resolve the complexity of the coastal morphologies of the Adriatic (McKiver et al., 2016; Dunić et al., 2019). In addition, some quasi-climate ocean studies were carried out to quantify interannual variability of the Adriatic dense-water dynamics (e.g. Mantziafou and Lascaratos, 2004, 2008), while quantification of the sources for Adriatic–Ionian decadal thermohaline variability required multi-decadal climate simulations of the eastern Mediterranean (Theocharis et al., 2014).

Therefore, to quantify the impacts of climate change in the Adriatic, it is crucial to obtain an adequate representation at climate scales of the atmosphere-ocean interactions during extreme events, such as those driving the formation of dense water within the basin. Atmospheric RCMs generally fail to provide such a representation, especially in the northern Adriatic where they cannot be used to study the extreme bora dynamics (Denamiel et al., 2020b,

2021a). Additionally, it has also been recently demonstrated that the latest higher-resolution ECMWF reanalysis dataset – the ERA5 product (Hersbach et al., 2018) – cannot be used as a reference for climate model evaluation or as a forcing for ocean models during bora events in the northern Adriatic as it also strongly underestimates the extreme bora speeds (Denamiel et al., 2021a). Consequently, in the recent study of Liu et al. (2021) – which investigated the BiOS variability using a regional ocean circulation model at 9 km resolution driven by the ERA-20C atmospheric forcing (Poli et al., 2016) with a 101-year-long simulation – the impact of bora events not properly represented by the atmospheric forcing was mimicked by artificially setting the 2 m air temperature and the dew point temperature over the entire Adriatic Sea to 0 °C in January, February, November, and December.

The proper representation of the bora-driven dense-water dynamics in the Adriatic Sea remains challenging, whether it is for research purposes, such as hindcast simulations and reanalysis products, or for operational purposes, such as forecast simulations. Based on the findings of previous research, there is a need for higher-resolution atmospheric models that can reproduce wind dynamics and air-sea interactions in the northern Adriatic. Consequently, data assimilation has recently been explored as an avenue to improve free model simulations, including the representation of dense-water dynamics in the Adriatic Sea (Yaremchuk et al., 2016; Janeković et al., 2020). More particularly, the four-dimensional variational scheme (4D-Var; Courtier et al., 1994; Janeković et al., 2013; Iermano et al., 2015; Sperrevik et al., 2017) was applied during the 2014–2015 period when a large number of *in situ* salinity, temperature, and current observations were available (Janeković et al., 2020).

Further, the high-resolution atmosphere-ocean Adriatic Sea and Coast (AdriSC; Denamiel et al., 2019) climate model has been developed and used to perform an evaluation simulation over the Adriatic basin for the 1987–2017 period. These types of simulations, also referred to as "control runs" in the climate community, produce several-decade-long results, forced by reanalysis products (without the use of data assimilation), and are primarily used for evaluation purposes in climate studies. The AdriSC climate simulation is a free run, meaning it remains dynamically consistent over decades, unlike reanalysis products, which depend on the availability of observations (Thorne and Vose, 2010).

In general, a proper evaluation of a high-resolution climate model is not a trivial task often presenting significant challenges related to the availability, incompleteness, and scarcity of observational data, as well as the imperfections of the observing systems, which further

constrain the evaluation process (Horak et al., 2021). More specifically, the evaluation of ocean climate models is recognized as particularly challenging due to the sparsity and temporal inhomogeneity of ocean observations (Somot et al., 2018). Additionally, the absence of standardized gridded products in the Adriatic Sea significantly complicates the intercomparison of the performance of such ocean climate models.

1.3. Overview of the dissertation

The objective of this doctoral research is to conduct a comprehensive evaluation of the kilometre-scale AdriSC climate simulation against measurements for the 1987–2017 period. Additionally, the research aims to apply model results to investigate dense-water dynamics in the Adriatic Sea by (i) comparing different modelling approaches for the 2014–2015 period, and (ii) creating a climatology of dense-water dynamics for the entire duration of the AdriSC simulation.

Chapter 2 provides descriptions of models, observational data and data analysis methods used in this thesis.

In chapter 3, the performance of the ocean component of the AdriSC climate simulation is assessed thorugh an extensive comparison with observations during the 1987–2017 period.

Chapter 4 is dedicated to the intercomparison of currently available numerical modelling strategies for reproducing bora-driven dense-water dynamics in the Adriatic Sea. The objective of this chapter is to quantify the main advantages and disadvantages of different modelling approaches during a 1-year-long simulation period.

In Chapter 5, the Adriatic dense-water dynamics climatology estimated using the results of the AdrisSC model for the 31-year-long period is presented.

Lastly, the main conclusions of the preceding chapters are summarized in Chapter 6.

2. MODELS, OBSERVATIONS AND METHODS

2.1. Adriatic Sea and Coast (AdriSC) climate modelling suite

This section gives a detailed description of the Adriatic Sea and Coast (AdriSC) model which is later evaluated and used to study the Adriatic dense-water dynamics.

The Adriatic Sea and Coast modelling suite has been developed with the aim of properly representing the processes driving the atmospheric and oceanic circulation at different temporal and spatial scales over the Adriatic and northern Ionian seas. AdriSC comprises two different modules: (1) a basic module providing the Adriatic atmospheric and oceanic baroclinic circulation at the deep sea and coastal scales, and (2) a dedicated nearshore module used to reproduce atmospherically driven extreme sea level events and meteotsunamis (Denamiel et al. 2019).

The Adriatic Sea and Coast climate model, hereafter referred as AdriSC, is based on a modified version of the Coupled Ocean-Atmosphere-Wave-Sediment Transport (COAWST V3.3) modelling system developed by Warner et al. (2010). In its climate configuration (Fig.2; Table 1), the Adriatic atmospheric processes, which depend on both local orography and Mediterranean regional forcing, are simulated with the Weather Research and Forecasting (WRF v3.9.1.1) model (Skamarock et al., 2005), hereafter referred as AdriSC-WRF. The AdriSC-WRF 3 km grid covers the entire Adriatic and northern Ionian Sea and is nested in a 15 km outer grid (horizontal size: 140 $\times$ 140 grid points) that approximately covers the central Mediterranean basin.

In the ocean, the Regional Ocean Modeling System (ROMS svn 885; Shchepetkin and McWilliams, 2005, 2009; hereafter referred as AdriSC-ROMS) is used to simulate the exchanges of the Adriatic Sea with the Ionian Sea. ROMS is a 3-D, free surface, bathymetry following, s-coordinate model in which primitive equations are solved with a finite-difference approximation and a time-splitting method. AdriSC-ROMS has a 3 km grid identical to the atmospheric domain, while an additional one-way nested 1 km grid (676 $\times$ 730 grid points) represents more accurately the complex geomorphology of the Adriatic Sea. The 1 km grid receives temperature, salinity, ocean currents and sea-surface elevation at its boundaries from the AdriSC-ROMS 3 km model.

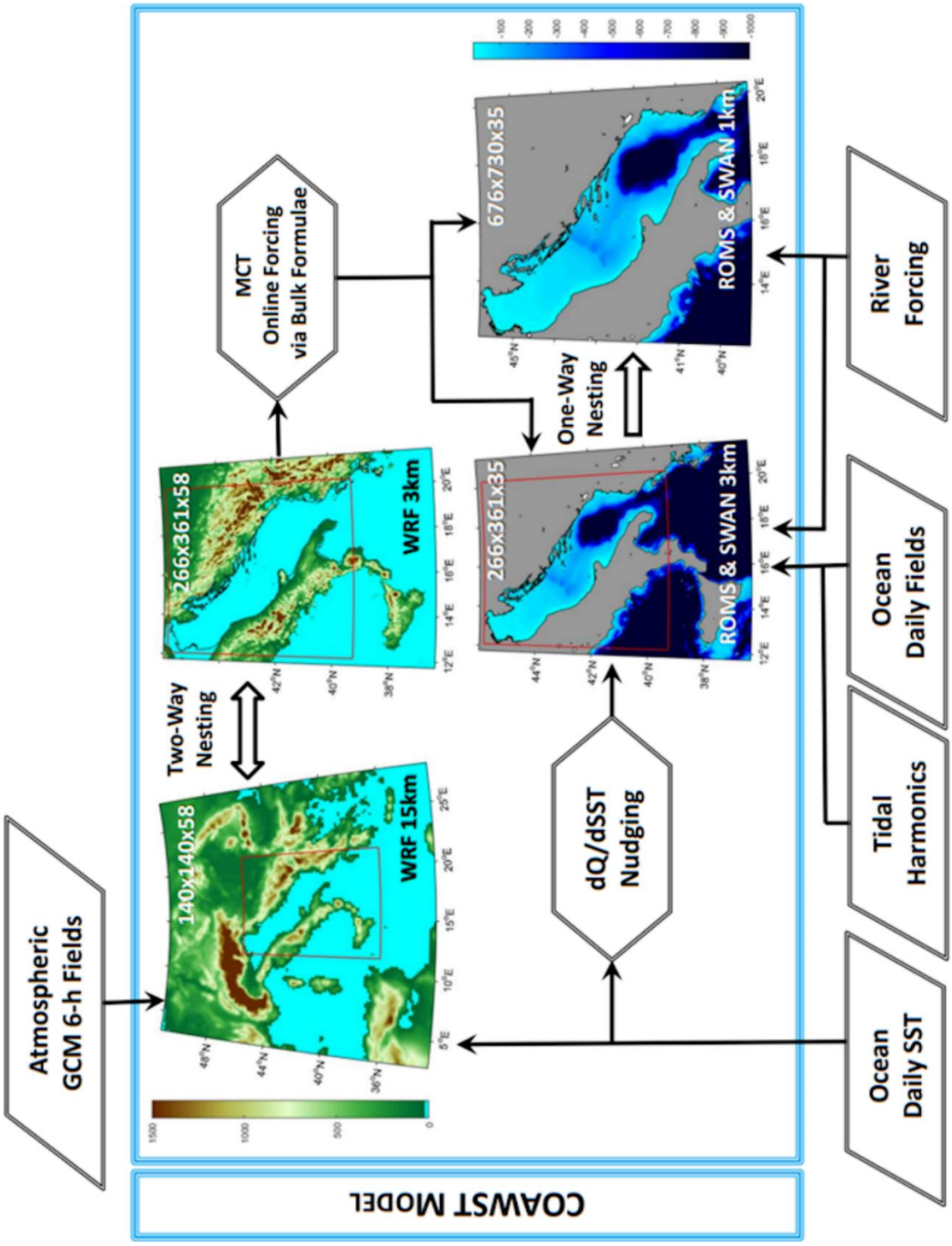

Figure 2. Scheme of the main components of the AdriSC climate model. Adapted from Denamiel et al. (2019).

Table 1. Summary of the main features of the AdriSC climate simulation. Adapted from Denamiel et al. (2021).

	Atmosphere		**Ocean**	
Model	WRF		ROMS	
Number of domains	2		2	
Horizontal resolution	15 km	3 km	3 km	1 km
Vertical resolution	58 levels		35 levels	
Time step	60 s	12 s	150 s	50 s
Initial and boundary conditions (frequency)	ERA-Interim (6-hourly)		MEDSEA (daily)	
Duration of run (time period)	31 years (1987–2017)			
Frequency of outputs	Hourly			

Furthermore, a Digital Terrain Model (DTM) incorporating topography from GEBCO 30 arc-second grid 2014 (Weatherall et al., 2015), offshore bathymetry from ETOPO1 (Amante and Eakins, 2009), nearshore bathymetry from navigation charts CM93 2011 and coastline data generated by the Institute of Oceanography and Fisheries (Split, Croatia), is providing the fine-resolution orography, bathymetry and coastline of all the AdriSC grids.

The data exchanges between the WRF and ROMS models are achieved with the Model Coupling Toolkit (MCT v2.6.0; Larson et al., 2005). The remapping weights between the WRF and both the ROMS 3 km and ROMS 1 km atmospheric and ocean grids are computed using the Spherical Coordinate Remapping and Interpolation Package (SCRIP). Additionally, as no ROMS grid was set up to entirely cover the spatial domain of the WRF 15 km grid, the ROMS sea surface temperature (SST) is not prescribed to the WRF models to avoid the generation of discontinuities along the border between the two-way nested WRF 15 km and WRF 3 km atmospheric grids. Consequently, the only grid exchanges in the AdriSC modelling suite consist of the WRF 3 km model providing atmospheric fields (i.e. horizontal wind at 10 m, temperature at 2 m, relative humidity at 2 m, mean sea level pressure, downward shortwave radiations, longwave radiations, rain and evaporation) to the ROMS 3 km and 1 km models which increases the efficiency of the AdriSC model.

Ideally, a two-way coupling, which imposes the SST of the ocean models on the atmospheric models, should be used in climate studies. Indeed, it allows for a better

representation of the SST, which is known to impact the local and regional precipitation (Mejia et al., 2018; Yang et al., 2019; Johnson et al., 2020). In the AdriSC modelling suite, implementing two-way coupling would require the use of an additional ROMS 9 km grid covering the WRF 15 km domain. However, due to limited numerical resources and the computational slowness of the AdriSC modelling suite, such a setup could not be implemented in this research. As a consequence, within the AdriSC modelling suite, the WRF models do not benefit from the more accurate simulation of the SST performed by the ROMS models. This limitation also applies to future scenario runs, which only add climatological changes (e.g., increase of SST up to 3.5 °C in summer) to the SST forcing used in the evaluation run, following the Pseudo-Global Warming (PGW) methodology originally developed for the atmosphere (Schär et al., 1996) and extended to the ocean by Denamiel et al. (2020a).

The AdriSC model was used to perform a climate simulation covering a 31-year period (1987–2017). It was initialized on the 1st of November 1986 in order to have a short two-month spin-up period allowing the ocean models to reach a steady state. Indeed, short experiments have shown that rapid equilibrium is reached within the AdriSC ocean models due to (1) the use, before the 1st of January 1987, of monthly (instead of daily) Mediterranean Forecasting System (MFS) reanalysis products with a relatively fine resolution of ~ 9 km, assimilating all available data in the Mediterranean Sea and (2) the relatively small size of the ROMS ocean domains. Preferably, several long-term simulations should have been run with different spin-up periods in order to better quantify the impact of the initial conditions on the long-term ocean model results. However, due to limitations in numerical resources, such systematic tests have not been carried out with the AdriSC climate model.

Additionally, within the AdriSC climate model, the COAWST model is compiled with the Intel 17.0.3.053 compiler, the PNetCDF 1.8.0 library and the MPI library (mpich 7.5.3) on the European Centre for Medium-range Forecast's (ECMWF's) High Performance Computing Facility (HPCF). In addition, ecFlow 4.9.0 – the workflow package used by all ECMWF operational suites, is set up to automatically and efficiently run the AdriSC long-term simulations in a controlled environment. In terms of workload, the AdriSC climate model optimally runs on 260 CPUs, with both WRF and ROMS grids decomposed into 10×13 tiles and without hyper-threading. Despite this optimal configuration of the models, which maximizes the running time of each individual model, as well as the time used to exchange data between the different grids, the AdriSC climate model runs at an extreme computational

cost and about 18 months are needed to complete each 31-year simulation within the ECMWF HPCF.

2.1.1. Atmospheric model set-up

The physics and parametrizations of the AdriSC-WRF 3 km atmospheric model are based on a configuration of high-resolution Adriatic WRF models as described by Kehler-Poljak et al. (2017) and include the following schemes: (1) Morrison double-moment bulk microphysics scheme (Morrison et al., 2005); Eta surface layer scheme (Janjić, 1994), which is based on the Mellor-Yamada-Janjić (MYJ) scheme for the planetary boundary layer (PBL), (2) a Rapid Radiative Transfer Model (RRTM) scheme (Mlawer et al., 1997), (3) a Dudhia scheme (Dudhia, 1989) for shortwave and longwave radiation, and (4) a five-layer thermal diffusion scheme for soil temperature (Dudhia, 1996). Additionally, the Kain-Fritch cumulus parameterization (Kain, 2004) was used only for the WRF 15 km grid. The vertical discretization of the grids is achieved with terrain-following coordinates distributed in 58 levels in the surface layer of the atmosphere (Laprise, 1992).

For the evaluation run, the initial conditions and boundary forcing of the WRF 15 km grid are provided by the 6-hourly ECMWF ERA-Interim reanalysis fields (Balsamo et al. 2015). However, because the spatial extent of the ocean grids does not entirely cover the WRF 15 km atmospheric domain, the SST from the AdriSC-ROMS grids is not prescribed to the AdriSC-WRF models. This approach prevents potential discontinuities along the border between the two-way nested WRF 15 km and WRF 3 km atmospheric grids and optimizes the balance between the efficiency and accuracy of the AdriSC model by reducing the exchanges between the different grids. Instead, the SST forcing is provided by the MFS MEDSEA v4.1 reanalysis (1/16° × 1/16° resolution; Simoncelli et al., 2016, 2019) distributed by the Copernicus Marine Environment Monitoring Service (CMEMS).

2.1.2. Ocean model set-up

In the AdriSC-ROMS model, the bathymetry (with the minimum depth of 2 m) is smoothed with the application of a Linear Programming (LP) method (Dutour Sikirić et al., 2009) to the ROMS 3 km and 1 km grids. In this way, the roughness factors are minimized while keeping the DTM bathymetric features. Also, the horizontal pressure gradient errors generated by the use of terrain-following coordinates with steep bathymetric gradients, are reduced. In the actual configuration of the AdriSC-ROMS models, 35 sigma layers – transformed ($V_{transform}$ = 2) and stretched ($V_{stretching}$ = 4) following Shchepetkin and McWilliams (2009) – are used with

increased resolution at the surface (θ_s = 6) and bottom (θ_b = 2), as well as a thickness of 50 m (h_c = 50).

Regarding the external forcing of the AdriSC-ROMS 3 km model, the initial conditions and boundary forcing – including sea-surface height, barotropic and baroclinic currents as well as baroclinic temperature and salinity – are provided daily by the MFS MEDSEA v4.1 reanalysis. The tidal forcing consists of eight tidal constituents (M2, S2, N2, K2, K1, O1, P1, Q1) extracted from the Mediterranean and Black Seas (2011) 1/30° regional solution of the OSU Tidal Inversion Software (OTIS; Egbert et al., 1994; Egbert and Erofeeva, 2002). The used tidal constituents were previously found to adequately reproduce the tidal dynamics in the Adriatic Sea (Cushman-Roisin and Naimie, 2002; Janeković and Kuzmić, 2005). Concerning the river forcing, 54 river flows in total (only 49 for the 1 km grid) are imposed over at least 6 grid points each (and 18 grid points for the Po river delta), with river mouths located along the coastline of: Italian peninsula, Sicily, Croatia, Slovenia, Albania, Montenegro and Greece. The monthly climatology of the river flow is acquired from the RivDis database (Vörösmarty et al., 1996), and studies from Pano and Abdyli (2002), Malačič and Petelin (2009), Pano et al. (2010), Janeković et al. (2014) and Ljubenkov (2015), whereas the river flow interannual variability is obtained from Ludwig et al. (2009). In addition, the river flows are linearly distributed between the 20 first sigma vertical levels – i.e. the discharge is multiplied by weights ranging from 20/210 at the surface, 19/210 at the 1st sigma level below the surface, to zero at the 20th sigma level below the surface.

Further, on one hand, the shallow parts of the Adriatic such as the eastern Adriatic Sea are characterized by high optical water clarity, which leads to a warming trend in SST due to the absorption of shortwave radiation reaching the seafloor. On the other hand, the low optical water clarity along the Italian coast due the muddy waters of the Po river plume tends to produce opposite trends. To address this issue, a dQ/dSST procedure, applied in previous studies (e.g., Escudier, 2015; Zhu et al., 2016), is used. Its purpose is to minimize the corrections of the heat fluxes produced by the WRF model while ensuring that no artificial SST trends emerge in the shallow parts of the ROMS grids (Denamiel et al., 2019). In brief, this method imposes a heat flux correction by calculating the kinematic surface net heat flux sensitivity to a reference SST. The 9 km SST forcing from the MEDSEA v4.1 reanalysis serves as the reference for calculation of the dQ/dSST procedure with the ROMS model. It should be noted that the use of this procedure should not be viewed as a permanent solution for climate studies in the Adriatic Sea. Indeed, the SST reference used in future climate scenario runs is

based either on other climate model predictions which are inherently uncertain or approximations using climatological changes. Consequently, long-term research focused on the fine tuning and parametrization of the solar radiation penetration using, for example, ocean colour, turbidity or even sediment transport modelling, is a prerequisite for achieving a better representation of the coupled atmosphere-ocean dynamics in the Adriatic Sea.

Finally, concerning the configuration of the physical options for the ROMS models, the MEDSEA barotropic velocities, surface elevations and baroclinic fields at the open boundaries are imposed with the Flather (Flather, 1976), Chapman (Chapman, 1985) and Orlanski (Orlanski, 1976) conditions. Additionally, the baroclinic structure is relaxed with a minimum folding time of three days, toward the fields provided by the MEDSEA v4.1 ocean climatology (Marchesiello et al., 2001). The relaxation occurs in two distinct nudging areas: (1) a ten-grid-point-wide zone along the open boundaries and (2) a zone covering the bathymetry deeper than 2000 m but only for temperature and salinity (in order to minimize the numerical diapycnal mixing). A sponge area of ten grid points (identical to the first nudging area) ensures that horizontal viscosities are smoothly interpolated from values four times greater at the open boundaries than those inside the domain. The tracer advection is provided with the Multidimensional Positive Definite Advection Transport Algorithm (MPDATA; Smolarkiewicz and Grabowski, 1990), while horizontal momentum advection utilizes a fourth–order centered scheme and the turbulence closure scheme following the generic length-scale (GLS) framework (Umlauf and Burchard, 2003).

2.2. Mediterranean Sea reanalysis

In this section, a description of a Mediterranean Sea reanalysis product used for a model intercomparison in reproduction of dense-water dynamics during the 2014–2015 period, is presented (Section 4).

The most recent high-resolution physical reanalysis product for the Mediterranean Sea (Escudier et al., 2020, 2021), hereafter referred to as MEDSEA, is distributed within the Copernicus Marine Environment Monitoring Service (CMEMS) framework (Escudier et al., 2020). MEDSEA covers the whole Mediterranean Sea and a part of the Atlantic Ocean for the 1987–2019 period. The reanalysis is generated by a numerical system composed of the Nucleus for European Modelling of the Ocean (NEMO) v3.6 model (Madec et al., 2017) and a three-dimensional variational (3D-Var) data assimilation scheme OceanVAR (Dobricic and Pinardi, 2008). NEMO is a non-linear, free surface, z-coordinate hydrodynamic model which solves the

primitive equations using time-splitting techniques. The model features a horizontal resolution of 1/24° (~ 4.5 km) and 141 unevenly distributed vertical levels (thickness varies from 2 m in the upper layers to 100 m in the deeper layers). The atmospheric forcing for the ocean model is sourced from the ECMWF ERA5 reanalysis, which has a horizontal resolution of 0.25° (~ 31 km) and temporal resolution of 1 h (Hersbach et al., 2020). The initial conditions are extracted from the SeaDataNet climatology (https://www.seadatanet.org/).

A 3D-Var data assimilation scheme, OceanVAR, is used to assimilate *in situ* data from Conductivity-Temperature-Depth (CTD), Argo profiling floats (ARGO; https://argo.ucsd.edu) and expendable bathythermograph (XBT) measurements, into the model, along with satellite altimetry observations. Further, a modified GEBCO 30arc-second grid (Weatherall et al., 2015) is used for topography. Nudging schemes are implemented to constrain heat and freshwater fluxes toward sea surface temperature (SST) and salinity observations. Also, a large-scale bias correction scheme is added to correct the model tendencies. Runoff data from 39 rivers is obtained from monthly mean climatological datasets and SST fields are used to adjust surface heat fluxes with a Gaussian relaxation coefficient dQ/dSST.

The MEDSEA reanalysis, assessed through a comparison against *in situ* and satellite observations as well as climatological data, demonstrated a better representation of the main dynamics of the Mediterranean region compared to the previous, coarser-resolution (1/16°) reanalysis (Simoncelli et al., 2016, 2019). A more detailed description of the state-of-the-art MEDSEA product and all the components of the model used to produce it, can be found in Escudier et al. (2021).

2.3. ROMS and ALADIN/HR modelling system

This section describes the ALADIN/HR and ROMS modelling system used for comparison with AdriSC climate simulation and MEDSEA reanalysis in the reproduction of dense-water dynamics during and after the winter of 2014–2015 (Section 4).

ROMS and ALADIN/HR is an atmosphere-ocean modelling system consisting of the ocean model ROMS and the atmospheric model ALADIN/HR (Aire Limitée Adaptation Dynamique Développement InterNational; Tudor et al., 2013, 2015). It has been running since 2008 for research purposes and has already been evaluated in several studies (e.g., Janeković et al., 2014; Vilibić et al., 2016, 2018).

Concerning the atmospheric model, a hydrostatic version of the ALADIN/HR (Aire Limitée Adaptation dynamique Développement InterNational; Tudor et al., 2013, 2015) model is used for the atmospheric forcing of the ocean model at the sea surface. ALADIN/HR is operationally run by the Croatian Meteorological and Hydrological Service four times a day with initial conditions computed using mesoscale data assimilation. It has a horizontal resolution of 8 km while the winds are dynamically downscaled to a horizontal resolution of 2 km (Ivatek-Šahdan and Tudor, 2004). In the vertical, 37 sigma layers are used in the model while the temporal resolution of all variables is 3 h. Lateral boundary conditions are obtained from the operational forecast runs of the Integrated Forecast System (IFS) in the ECMWF, where global analysis is performed using the 4D-Var data assimilation technique. The transfer of the surface variables into the ocean model is done via bulk parametrization (Fairall et al., 1996).

Regarding the ocean component, the horizontal ROMS grid resolution is 2 km and there are 20 vertically spaced sigma levels controlled by the following parameters: $V_{transform} = 2$ and $V_{stretching} = 2$ with $\theta_s = 7$ (increased resolution at the surface), $\theta_b = 0.5$, and $h_c = 30$ (critical depth of 30 m). Daily-averaged lateral boundary conditions are imposed north of the Otranto Strait from the Adriatic Forecasting System (AREG, Oddo et al., 2006). AREG is nested within the larger Mediterranean Forecasting System (MFS), which uses 3D-Var data assimilation (Pinardi et al., 2003; Pinardi and Coppini, 2010; Tonani et al., 2014). Furthermore, bathymetry smoothing achieved with the LP technique (Dutour Sikirić et al., 2009) is used to reduce numerical instabilities. A river discharge climatology is imposed at the freshwater point sources following Vilibić et al. (2016) data.

In the study of Janeković et al. (2020), a year-long (1 October 2014 – 30 September 2015) 4D-Var data assimilation experiment was applied to the Adriatic Sea. Three model simulations were integrated, but only two of them are used in this thesis: (1) a non-assimilative hindcast simulation, hereafter referred as ROMS-hind and (2) a fully assimilative simulation that used all available observations during the 4-day assimilation cycle, hereafter referred as ROMS-full. During the ROMS-full simulation, the Physical-Space Statistical Analysis System (PSAS) approach (Moore et al., 2011) was applied, splitting the one-year simulation into 91 4-day assimilation cycles, each restarting from the previous cycle using saved initial conditions. This window cycling was necessary to ensure the validity of the Tangent Linear model assumption (Powell et al., 2008) within the 4-day window. Concerning the Adjoint model, clamped boundary conditions were used instead of radiation nudging of 3-D fields. High-resolution

multi-platform observations were assimilated into the model, including SST measured by satellites, *in situ* temperature and salinity data measured by various moving (Argo floats, shipborne CTDs, sea glider, towed CTD profiler) and moored platforms, ocean current profiles measured by moored Acoustic Doppler Current Profilers (ADCPs), and 30-minute de-tided surface currents from high-frequency (HF) radars. More information about the observations, experiments and skill assessment of the model can be found in Janeković et al. (2020).

Lastly, the main features (type, coupling, time period, resolution, atmospheric and river forcing, data assimilation, initial and boundary conditions, bathymetry, evaluation etc.) of the four described models/products used for the analyses of the dense-water dynamics in the 2014–2015 period are summarized in Table 2.

Table 2. The summary of the main features of the four products/models used in for the analysis of the dense water dynamics in the 2014–2015 period (Pranić et al., 2023).

Product / model	Type / coupling	Time period	Ocean model / resolute-ion	Atmospheric forcing and resolution / hydrostatic	Data assimilation (DA)	Initial / bounday conditions	Bathymetry	River forcing	Evaluation
MEDSEA	Reanalysis/ uncoupled	1987–2019	NEMO v3.6 / 4.5 km, 141 levels	ERA5 reanalysis, 31 km	3D-Var OceanVAR	SeaDataNet climatology	GEBCO 30arc–second grid	Monthly climatol-ogies (39 rivers)	Escudier et al. (2021)
ROMS-hind	Operational model / uncoupled	2014–2015	ROMS / 2 km, 20 levels	ALADIN/HR, 8 km (2 km for winds), 37 levels /hydrostatic	No DA	AREG lateral boundary	Smoothing (Linear programming; LP)	Vilibić et al. (2016)	Janeković et al. (2020)
ROMS-full	Operational model / uncoupled	2014–2015	ROMS / 2 km, 20 levels	ALADIN/HR, 8 km (2 km for winds), 37 levels / hydrostatic	4D-Var DA scheme	AREG lateral boundary	Smoothing (LP)	Vilibić et al. (2016)	Janeković et al. (2020)
AdriSC	Climate model / one–way coupled	1987–2017	ROMS / 1 km, 35 levels	WRF v3.9.1.1, 3 km, 58 levels / non-hydrostatic	No DA	MEDSEA v4.1 reanalysis Simoncelli et al. 2016, 2019)	Digital Terrain Model (DTM); LP	Monthly discharge (54 rivers): Denamiel et al., 2019	Denamiel et al. (2021b), Pranić et al., (2021)

2.4. Observational datasets

This section gives a description of ocean observational data used in this thesis for a skill assessment of the AdriSC climate simulation in the 1987–2017 period and a comparative evaluation of the four simulations for the 2014–2015 period.

For the evaluation of the AdriSC-ROMS 3 km and AdriSC-ROMS 1 km models, a comparison is carried out against a comprehensive collection of observational data retrieved for the 1987–2017 period from *in situ* measurements and remote sensing gridded products. The first dataset used in this study is the Sea Surface Height Anomalies (SSHA) gap-free remote sensing (L4) product, SEA_SURFACE_HEIGHT_ALT_GRIDS_L4_ 2SATS_5DAY_6THDEG_V_JPL1812 (Zlotnicki et al., 2019; hereafter referred to as JPL MEASURES). It has been produced at the Jet Propulsion Laboratory (JPL) of the Physical Oceanography Distributed Active Archive Center (PODAAC) on a 1/6° grid every five days since October 1992. The final gridded product, obtained by a kriging method, is a combination of SSHA data derived from TOPEX/Poseidon, Jason-1, Jason-2, and Jason-3, as reference data, as well as ERS-1, ERS-2, Envisat, SARAL-AltiKa, and CRyosat-2, depending on the date.

Second, two sea surface temperature (SST) gap-free remote sensing (L4) products were chosen for this skill assessment. They were extracted from the datasets provided by the Group for High-resolution Sea Surface Temperature (GHRSST), which offers a framework for SST data sharing and processing. The first product, AVHRR_OI-NCEI-L4-GLOB-v2.0 (National Centers for Environmental Information, 2016; hereafter referred to as AVHRR), has been produced daily on a 0.25° grid at the National Oceanographic and Atmospheric Administration (NOAA) National Centers for Environmental Information (NCEI) since September 1981. It uses optimal interpolation (OI) by interpolating and extrapolating SST observations from the Advanced Very High-resolution Radiometer (AVHRR) and *in situ* platforms (i.e. ships and buoys), resulting in a smoothed complete field. The main advantage of AVHRR is that it covers the entire 1987–2017 period of the AdriSC simulation. However, its resolution is rather coarse and is likely to be insufficient to properly describe the coastal areas of the Adriatic basin. Consequently, a high-resolution second product is used for a shorter period. The MUR-JPL-L4-GLOB-v4.1 (JPL MUR MEaSUREs Project, 2015; hereafter referred to as JPL MUR) has indeed been produced daily on a global 0.01° grid at the JPL of the PODAAC since June 2002. It uses wavelets as basis functions in an OI approach. The Multiscale Ultrahigh Resolution (MUR) analysis is based upon nighttime GHRSST SST observations from several instruments

including the National Aeronautics and Space Administration (NASA) Advanced Microwave Scanning Radiometer-EOS (AMSR-E), the JAXA Advanced Microwave Scanning Radiometer 2 on GCOM-W1, the Moderate Resolution Imaging Spectroradiometers (MODIS) on the NASA Aqua and Terra platforms, the US Navy microwave WindSat radiometer, the AVHRR on several NOAA satellites, and *in situ* SST observations from the NOAA iQuam project.

The third dataset consists of a comprehensive collection of temperature and salinity *in situ* Conductivity-Temperature-Depth (CTD) observations with diverse temporal and spatial coverage (Fig. 3b). This dataset combines 17 different experiments and/or scientific cruises: (1) Argo floats – ARGO (https://argo.ucsd.edu), (2) ASCOP project Phase 2, Istituto Nazionale di Oceanografia e di Geofisica Sperimentale (OGS), (3) Corfu System Project – CSP01 cruise (https://isramar.ocean.org.il/PERSEUS_Data), (4) Dynamics of the Adriatic in Real Time – DART_CTD (Martin et al., 2009; Burrage at al., 2009), (5) CTD observations, Institute of Oceanography and Fisheries (IOR) – IOR_Data_CTD, (6) Palagruža transect long-term observations (IOR) – IOR_Pal_CTD, (7) Mediterranean Data Archaeology and Rescue project – MEDATLAS (http://www.ifremer.fr/medar/cdrom_database.htm), (8) Northern Adriatic Experiment CTD observations – NAdEx_CTD (Vilibić et al., 2018), (9) Otranto Gap Experiment, SACLANT Undersea Research Centre – OTRANTO, (10) PALMAS, OGS, (11) PCO, Consiglio Nazionale delle Ricerche (CNR), Istituto di Biologia del Mare, Venice, (12) Physical Oceanography of the Eastern Mediterranean project, Hellenic National Oceanographic Data Centre (HCMR/HNODC) – POEM, (13) Programma di RIcerca e Sperimentazione del Mare Adriatico Phase 2 (chemical stations) hosted at OGS – PR2_UR, (14) Programma di RIcerca e Sperimentazione del Mare Adriatico Phase 1 hosted at OGS – PRISMA, (15) PRV, CNR, Istituto di Biologia del Mare, Venice, (16) Northern Adriatic long-term observations, Ruder Bošković institute – RB_NAd (Vilibić et al., 2019), and (17) SIRIAD cruise hosted at OGS – SIRIAD_15.

This large dataset includes over 7000 locations in total and covers the Adriatic Sea almost entirely and the northern Ionian Sea partially. The data sampling frequency varies largely across locations and the observations, and the maximum depth of the measurements ranges from 40 to 2140 m. All CTD observations had already been independently quality-checked except IOR_DATA_CTD, which underwent quality control in this study to automatically and visually remove outliers, values with steep gradients, and vertical instabilities using standard procedures described in the SeaDataNet manual (https://www.seadatanet.org/Standards/Data-Quality-Control).

The last dataset is a collection of ocean current speed and direction combining Acoustic Doppler Current Profiler (ADCP) and Rotor Current Meter (RCM) *in situ* observations with diverse temporal coverage (Fig. 3c).

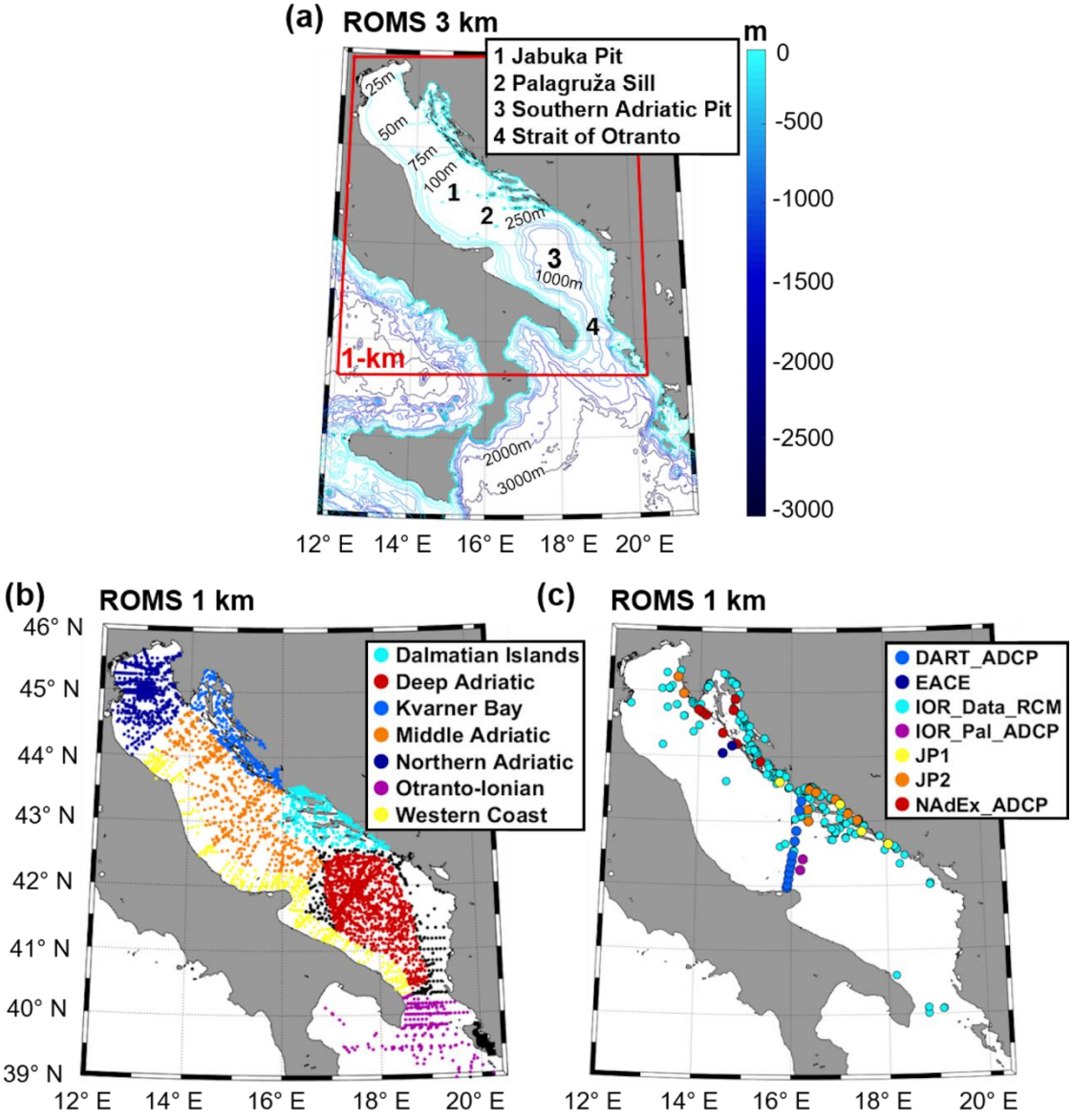

Figure 3. (a) AdriSC ROMS 3-km and ROMS 1-km domains and bathymetry as well as location of both (b) CTD observations separated in seven subdomains and (c) ADCP or RCM measurements from seven different sources.

This dataset combines seven different experiments and/or scientific cruises: (1) Dynamics of the Adriatic in Real Time – DART_ADCP (Martin et al., 2009; Burrage at al., 2009), (2) East Adriatic Coastal Experiment – EACE (http://www.izor.hr/eace/eace_g.htm), (3) historical RCM observations (IOR) – IOR_Data_RCM, (4) Palagruža transect ADCP observations

following the winter of 2012 – IOR_Pal_ADCP, (5) Jadranski project Phase 1 ADCP observations – JP1, (6) Jadranski project Phase 2 ADCP observations – JP2, and (7) Northern Adriatic Experiment ADCP observations – NAdEx_ADCP (Vilibić et al., 2018). All the observations had already been independently quality-checked except for IOR_Data_RCM, which underwent an additional quality control to automatically and visually remove obvious outliers, spurious data, and long strings of constant values.

A full list of the data collected to perform the AdriSC-ROMS 3 km and one-way nested 1 km model evaluations during the 1987–2017 period is provided in Table 3. The table includes, for each of the four datasets (i.e. SSHA, SST, CTD, and ADCP/RCM), the name of the corresponding observations (i.e. remote sensing products as well as CTD and ADCP/RCM experiments and/or scientific cruises), the time period covered, the number of locations, the number of records, and the maximum measured depth.

Table 3. The name and period of the observations, number of locations and records, as well as maximum measured depth for the four datasets – i.e. (1) SSHA, (2) SST, (3) CTD observations and (4) ADCP or RCM measurements.

Dataset	Observations	Period	No. locations	No. records (10^3)	Max. depth (m)
SSHA	JPL MEASURES	1992–2017	2065	3808	surface
SST	AVHRR	1987–2017	966	10938	surface
	JPL MUR	2002–2017	46777	266348	surface
CTD	ARGO	2012–2017	2182	569	1503
	ASCOP	1990–1991	96	4	39
	CSP01	1991	108	5	64
	DART_CTD	2005–2006	502	64	1202
	IOR_Data_CTD	1987–2017	3043	419	1214
	IOR_Pal_CTD	1987–2017	5	4	170
	MEDATLAS	1987–1990	254	63	2143
	NAdEx_CTD	2014–2015	19	4.5	93
	OTRANTO	1994–1995	332	231	1259
	PALMAS	1994	103	14	1154
	PCO	1987–1989	162	6	52
	POEM	1991–1992	85	44	1191
	PR2_UR	1996–1998	111	0.6	62
	PRISMA	1995–1996	538	236	1208
	PRV	1987–1988	283	1	38
	RB_NAd	1987–2017	6	9	40
	SIRIAD_15	2015	64	26	1199
	All data	1987–2017	7781	1700	2143
ADCP/RCM	DART_ADCP	2005–2006	11	2482	164
	EACE	2002–2003	2	282	68
	IOR_Data_RCM	1987–2004	321	268	930
	IOR_Pal_ADCP	2012	2	313	129
	JP1	2007–2009	4	430	82
	JP2	2013–2014	10	1784	79
	NAdEx_ADCP	2014–2015	8	940	83
	All data	1987–2015	358	9034	930

2.4.1. Northern Adriatic Experiment (NAdEx)

The NAdEx datasets are described in greater detail because the time period of the dense-water simulations investigated in this thesis is based on the NAdEx campaign which took place between late autumn 2014 and summer 2015.

The aim of the NAdEx campaign was to study the dense-water generation and transport within and off the Kvarner Bay. This involved the collection of temperature, salinity, and current data using several instruments and observing platforms. To measure the currents, ADCPs were deployed at nine locations between late November 2014 and mid-August 2015, while CTD probes measured salinity and temperature at five of the ADCP locations. Furthermore, vertical profiles of temperature and salinity were acquired at 19 CTD stations during two cruises, one from 3 to 6 December 2014 and another from 26 to 29 May 2015. An ocean glider was operated off the Kvarner Bay in a campaign lasting only 3 d, from 24 to 27 February 2015, while an Arvor-C profiling float was deployed on 19 February 2015 in the northern part of Kvarner Bay and was recovered on 15 March 2015 off the Istria coast. The full description of the NAdEx campaign is provided in Vilibić et al. (2018).

Notably, during the campaign, three severe bora episodes with gusts above 50 m s^{-1} in the Velebit channel occurred over the following dates: between 28 December 2014 and 1 January 2015, between 4 and 7 February 2015, and between the 3 and 6 March 2015. The NAdEx campaign was thus able to partially observe the dense-water generation within the Kvarner Bay during the 2014–2015 period. Due to the unique dataset collected during the NAdEx campaign, which has been used in data assimilation experiments (Janeković et al., 2020) and evaluation studies (Vilibić et al., 2018; Pranić et al., 2021), the 2015 bora events present a distinctive opportunity to compare the capabilities of different models (e.g. reanalysis, hindcast, assimilated simulations, and climate simulations) in reproducing the dense-water dynamics in the Adriatic basin**.**

2.5. Methods

2.5.1. Skill assessments

This section describes the methods used to prepare the observational data and model results for subsequent analyses and the methods used for the skill assessments of the AdriSC model.

Upon the completion of the evaluation run, the results of the AdriSC climate model are extracted and prepared for the skill assessments. The extraction of the AdriSC-ROMS 3 km and AdriSC-ROMS 1 km model hourly and daily results is achieved in two different ways. For the comparison with satellite observations, a bilinear interpolation to the coarser coordinates of the JPL MEASURES, AVHRR, and JPL MUR gridded products is carried out with the Earth System Modelling Framework (ESMF) software. For the *in situ* observational datasets, a nearest-neighbour method at points in time and space matching the coordinates of the CTD, RCM, and ADCP stations is used before linear interpolation to the vertical structure of the measurements following the depth.

In order to compare different simulations for the 2014–2015 period, model results with horizontal grid resolution coarser than 1 km are interpolated to the AdriSC-ROMS 1 km grid using regridding routines based on the ESMF software. Specifically, the results of the ocean models (MEDSEA, ROMS-hind and ROMS-full) and atmospheric models (ERA5, ALADIN/HR-hind, ALADIN/HR-full and AdriSC-WRF) are all regridded to a horizontal resolution of 1 km. However, model outputs were not interpolated in the vertical.

The performance of the ocean component of the AdriSC climate simulation is assessed separately for each type of observational dataset (i.e. SSHA and SST remote sensing gridded products, CTD observations, and ADCP/RCM measurements). Due to the relatively coarse temporal and spatial resolutions of the satellite observations, only the skill of the AdriSC-ROMS 3 km model is assessed against the selected sea level and sea surface temperature remote sensing products (i.e. SSHA from JPL MEASURES and SST from AVHRR and JPL MUR). For the sea level analysis, empirical orthogonal functions (EOFs) are used to compare the most important variability patterns in the Adriatic Sea and northern Ionian Sea in space and time. Indeed, Gačić et al. (2011) demonstrated that the BiOS, consisting of the decadal switch from cyclonic to anticyclonic of the circulation in the northern Ionian Sea and greatly impacting the thermohaline circulation of the Adriatic Sea, can be well described with the decadal change of sign of one of the main components of the EOF derived from SSHA products. The EOFs (also known as principal component analysis or eigen analysis) presented in this study, are

obtained via a covariance matrix and are normalized, meaning the sum of squares for each EOF pattern equals 1. The time series of the amplitudes (also known as principal components or expansion coefficients) associated with each eigenvalue in the EOF are derived via the dot product of the data and the EOF spatial patterns, and the mean is subtracted from the value of each component time series. Consequently, EOFs performed on SSHA from remote sensing products and sea surface height (hereafter referred to as SSH) results from the AdriSC-ROMS 3 km model can be directly compared, despite the different mean sea level references used to derive SSHA and SSH. For the SST analysis, the bias or difference between model results and observations is calculated at each point in time and space of the AVHRR and JPL MUR datasets. The biases are then analysed in space with statistical quantities such as the median and the 1st, 25th, 75th, and 99th percentiles.

The skill assessment of the AdriSC-ROMS 3 km and 1 km models against *in situ* temperature and salinity CTD data is divided into three main analyses. First, a basic assessment of the model performances is achieved with: (1) Taylor diagrams, (2) quantile-quantile (Q-Q) plots comparing the distributions of the observed and modelled temperature and salinity, and (3) scatter diagrams that are unique for the AdriSC-ROMS 1 km model, which is further used in the study as having a more precise matching of the nearest grid points with the CTD locations. It should be noted that, to obtain more robust statistics for the chosen geophysical quantities which are likely to have heavy-tailed distributions due to extreme conditions, the use of median and median absolute deviation (MAD) is preferred over the mean and standard deviation, which are typically recommended for normal distributions. The second analysis provides a more detailed examination of the spatial distributions of the median and MAD of the biases between the AdriSC-ROMS 1 km model and the CTD observations depending on the depth. The depth ranges considered in this analysis are: 0–50, 50–200, 200–500, and 500–2000 m). Furthermore, a climatological analysis of the AdriSC-ROMS 1 km results is performed for seven different subdomains named as follows: western coast, northern Adriatic, middle Adriatic, Kvarner Bay, deep Adriatic, Dalmatian Islands, and Otranto–Ionian (Fig. 3b). For each subdomain, the following results are presented: (1) monthly climatology of the median (and MAD as upper and lower bounds) of the modelled and observed temperature and salinity – this analysis is done without taking the same depth range for each month due to the vertical scarcity of the measurements, (2) seasonal variations of the vertical profiles of median temperature and salinity biases, which are interpolated to standard oceanographic depths selected appropriately for each subdomain – seasons are defined as January, February, and

March (JFM) for winter; August, May, and June (AMJ) for spring; July, August, and September (JAS) for summer; and October, November, and December (OND) for autumn, and (3) seasonal variations of temperature-salinity (T-S) diagrams, comparing observations and model results.

The evaluation of the AdriSC-ROMS 3 km and 1 km models against *in situ* ocean current speed and direction of the ADCP and RCM measurements is divided into two main analyses. First, a basic assessment of the model performances is achieved with: (1) Taylor diagrams, (2) Q-Q plots comparing the distributions of the observed and modelled current speed and direction, and (3) scatter diagrams that are unique for the AdriSC-ROMS 1 km model, which is further used for the other analyses. Second, a climatological analysis of the AdriSC-ROMS 1 km results is performed for the seven different datasets (Fig. 3c) collected from experiments and/or scientific cruises described in Sect. 2.4.2. For each dataset, the following results are presented: (1) monthly climatology of the median (and MAD as upper and lower bounds) of the modelled and observed current speed and direction – this analysis is done without taking the same depth range for each month due to the vertical sparsity of the measurements, (2) seasonal variations of the vertical profiles of the modelled and observed median current speed interpolated to standard oceanographic depths selected appropriately for each dataset (seasons are defined the same as for the CTD analysis), and (3) seasonal variations of the modelled and observed current direction presented in the form of polar histograms (i.e. rose plots) showing the ocean current direction distributions.

The final skill assessment method used in this thesis is a comparative evaluation of the four simulations for the 2014–2015 period against *in situ* temperature and salinity observations. The observational data is extracted from the NAdEx campaign (Vilibić et al., 2018), the Palagruža Sill long-term monitoring transect (IOR), as well as the CTD dataset described in section 2.4.2 and published in Vilibić (2021). The assessment is presented in the form of a Taylor diagram and probability density functions of the biases. The biases are calculated as differences between the daily results of the simulations and the available observations (i.e. they are daily instantaneous bias errors). Consequently, the model results are extracted at the location (i.e. near neighbour grid point), depth (i.e. linear interpolation from model depths to observation depth) and timing (i.e. approximated to daily average) of the observations. The biases are then obtained as the difference between model results and observations at each point in time, depth and space. The probability density functions are derived with a kernel-smoothing method (Bowman and Azzalini, 1997), which calculates the probability density estimate based on a

normal kernel function and is evaluated at 100 equally spaced points. Also, for each model, the median and MAD of the biases are calculated.

In addition, to determine the minimum horizontal resolution necessary to resolve the processes occurring in the Adriatic Sea, the baroclinic Rossby radii are calculated for the whole AdriSC-ROMS 1 km domain. The results are presented as spatial distributions of median and MAD of the Rossby radius as well as in the form of a time series of the Rossby radius for the four subdomains (northern Adriatic, Kvarner Bay, Jabuka Pit and deep Adriatic). The potential density method described in Chelton et al. (1998) is used to calculate the Brunt-Väisälä frequency and, hence, the first mode of the Rossby radii. This method can result in an underestimation of the Rossby radii if the vertical spacing is not fine enough. As the AdriSC-ROMS model provides results on 35 vertical sigma layers for the entire Adriatic Sea, this underestimation can only occur within the SAP area.

2.5.2. Analyses of the dense-water dynamics

This section outlines the methods used for the investigation of dense-water dynamics in the 2014–2015 period and for the creation of the 1987–2017 dense-water climatology.

Adriatic dense-water dynamics is analysed for the 2014–2015 period using four different simulations, while its climatology is derived for the 1987–2017 period using only the AdriSC-ROMS 1 km results. Hereafter, bottom potential density anomalies (PDAs) are calculated using the function available within the NCAR Command Language (NCL) library (Levitus et al., 1994a, 1994b; Dukowicz, 2000; https://www.ncl.ucar.edu/). Also, "dense waters" (DW) are defined as those having PDAs equal to or larger than 29.2 kg m^{-3} based on previous research dealing with DW in the Adriatic (e.g., Mantziafou and Lascaratos, 2008; Janeković et al., 2014; Vilibić et al., 2016).

For the analyses of the 1-year long simulations, the upward turbulent heat fluxes are computed as the sum of the latent and sensible heat fluxes based on the formulas provided in Denamiel et al. (2020a, 2021a). It should be noted that heat fluxes from the ALADIN/HR-full results are also modified by the 4D-Var data assimilation process.

In order to quantify the general conditions in the ocean and atmosphere throughout the whole 2014–2015 period, an analysis of the extremes is performed. For each of the four simulations, the results are presented as spatial distributions of extremes accompanied by spatial distributions of their associated timing (in days). This includes the spatial distributions

of the maximum wind stresses and the maximum upward turbulent heat fluxes in the atmosphere (at the sea surface), as well as the maximum bottom PDAs, minimum bottom temperatures and maximum bottom salinities in the ocean.

Further, to better capture the DW dynamics, two different temporal analyses of the results are also performed. First, time series of daily surface wind stresses and upward turbulent heat fluxes in the atmosphere, as well as daily bottom PDAs, temperatures and salinities in the ocean are presented as the spatial averages over different subdomains selected in areas where DW are known to be either generated or accumulated. These subdomains include the northern Adriatic and the Kvarner Bay for both atmosphere and ocean, and the Jabuka Pit and the deep Adriatic for the ocean only (Fig. 4a).

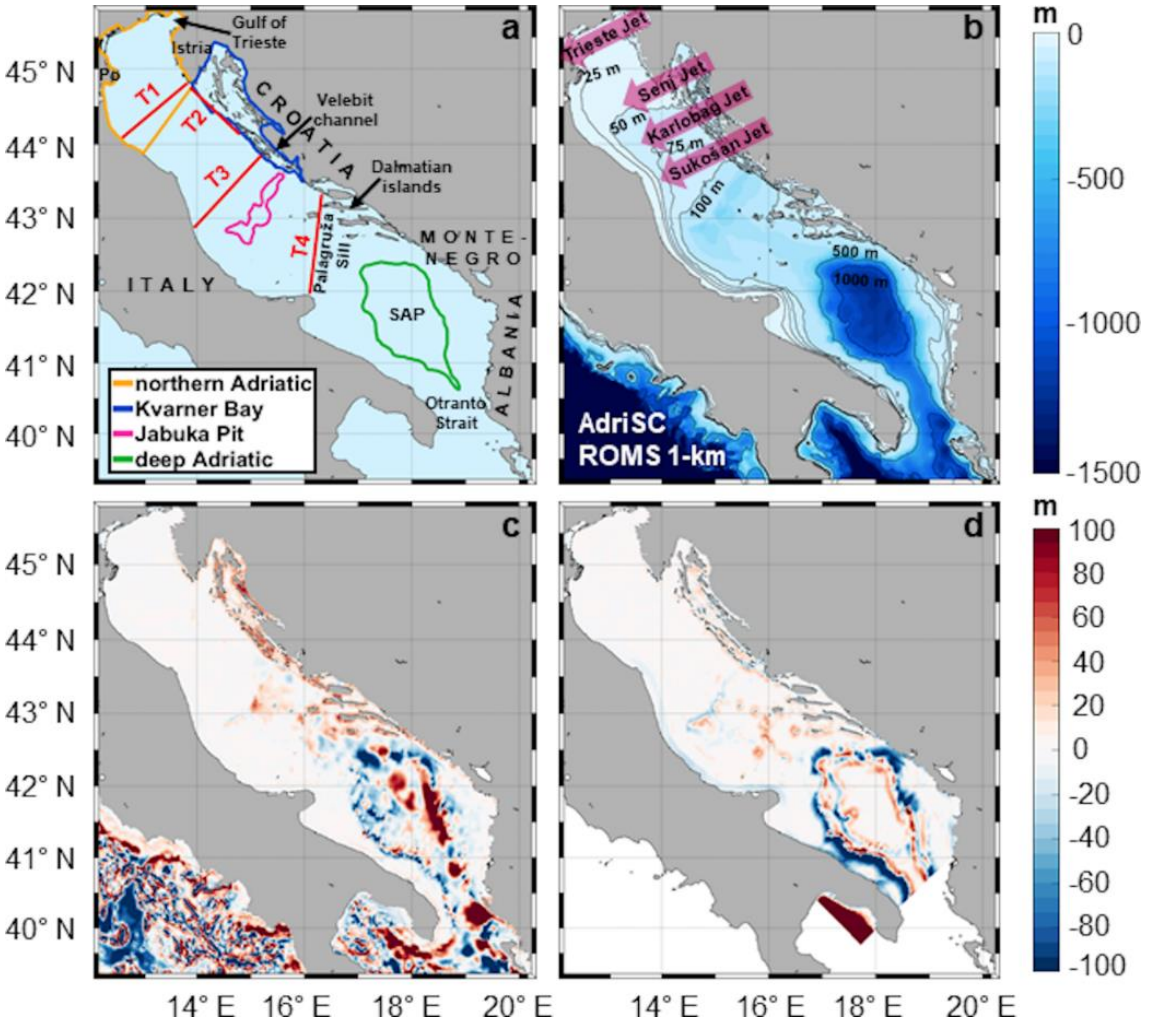

Figure 4. (a) Models domain with geographical locations, transects (red lines) and subdomains, (b) AdriSC-ROMS 1 km depths, (c) difference between AdriSC-ROMS 1 km and MEDSEA 1 km bathymetry, (d) difference between AdriSC-ROMS 1 km and ROMS 1 km bathymetry.

The daily bottom PDA time series are also presented without the mean and the seasonal signal (yearly and half-yearly) which are removed from the series at each point. More specifically, after subtracting the mean and detrending the time series, the seasonal signal is calculated using the least-squares method of a sine function and subtracted from the series. The final time series without the seasonality are obtained by adding back the trend. Also, the time evolution of the spatial distributions of the bottom PDAs is presented at selected dates – 1 March, 1 April, 1 May and 1 June 2015.

The final analysis for the 2014–2015 period quantifies the total daily volume transport of the outflowing DW across four transects (T1–T4; Fig. 4a) for all depths. The outward volume transport is calculated as a double integral of velocities normal to the transect over the area of the vertical plane of the transect.

For the 31-year long climatology (1987–2017), the Adriatic DW is derived from the AdriSC-ROMS simulation and the analyses are divided into three main phases of the DW dynamics: generation, spreading and accumulation. The analyses of DW generation are carried out for two generation sites – northern Adriatic and Kvarner Bay (Fig. 5). The results are presented in the form of daily time series of subdomain averaged bottom PDA, temperature and salinity for the whole time period of the simulation. The maximum bottom PDAs are calculated for each point of the subdomains in Januray, February and March (JFM). Also, the day of the year (DOY) in which the maximum PDA occured is considered. The results are presented as: 1) PDFs derived with a kernel-smoothing method (as in Sect. 2.5) for the maximum bottom PDAs, bottom temperature and salinity in the DOYs of maximum PDAs, and 2) box plots of maximum PDA, DOY, temperature and salinity in the DOYs, for all years.

Concerning the spreading phase, the analyses are performed for nine transects (T1, T2, T3, T4, T5a, T5b, T6, T7, T8) as depicted on Fig. 5. The outward DW flow rates are calculated only for the bottom layer and they are obtained by multiplying velocities normal to the transect by PDAs integrated over the area of the vertical plane of the bottom layer along the transect. The results are shown as monthly time series of median and maximum outward DW flow rates, as well as the cummulative DW mass transported outward through the transects. The obtained quantities are defined as positive in the northwest direction for all transects except T2, for which they are positive in the northeast direction. Also, the climatologies of the monthly median and maximum bottom DW outflow rate, as well as monthly bottom DW mass transported outward are presented as histograms for all transects.

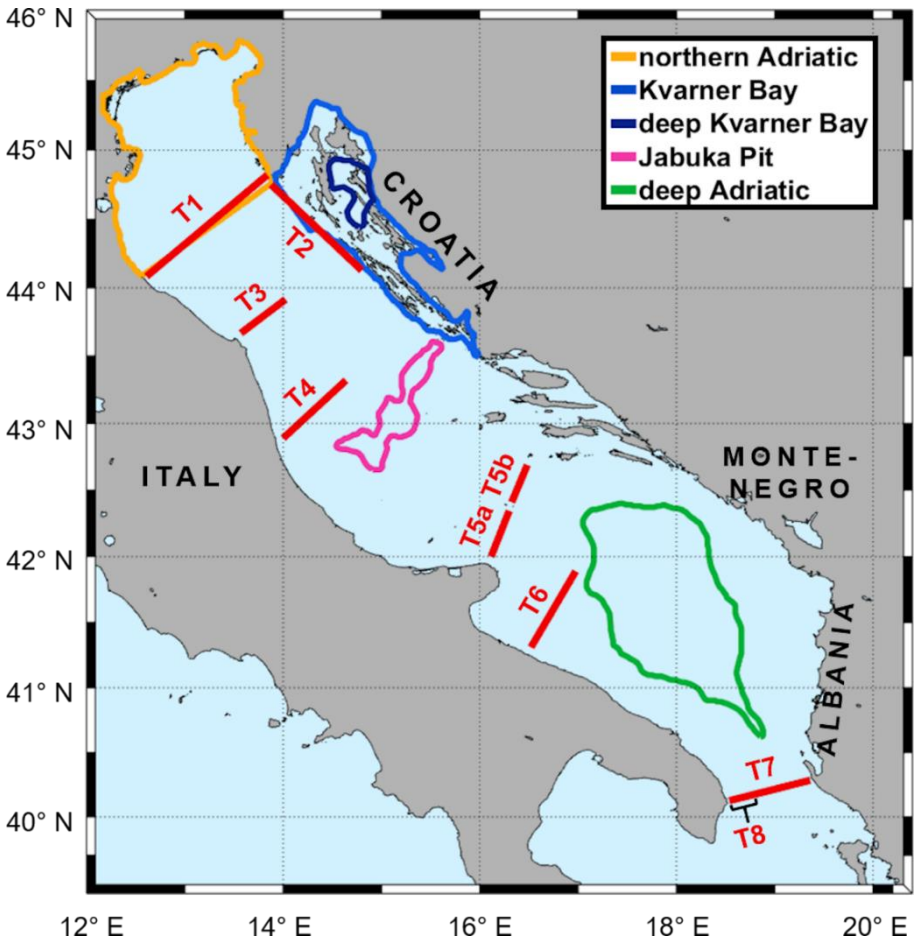

Figure 5. Subdomains and transects (red lines) used for the 1987–2017 Adriatic dense-water climatology.

Further, in order to quantify the DW accumulation for the whole simulation period, several analyses were conducted for three accumulation sites (subdomains) – deep Kvarner Bay (DKB) with depths above 80 m, Jabuka Pit (JP) with depths above 200 m and deep Adriatic (i.e. Southern Adriatic Pit; SAP) with depths above 1000 m (Fig. 5). Firstly, the time series of subdomain-averaged bottom PDAs are presented, while the PDA rate of change is calculated only for JP and SAP. The rate of change is calculated for specific years in which an abrupt change in subdomain averaged bottom PDA occurred after DW generation. The threshold chosen for the selection of years, above which the change of PDA should be, is 0.01 kg m^{-3}. The rate of change is calculated as the difference of PDA after and before the change divided by the time passed between those values. Additionally, the time series of subdomain-averaged bottom temperature and salinity are presented for the three subdomains. Secondly, maximum bottom PDA, DOY, bottom temperature and salinity in DOYs of maximum PDAs are analysed using box plots. Lastly, the monthly-averaged bottom PDAs, temperature and salinity are presented as box plots ranging between the 25th and 75th percentile.

3. EVALUATION OF THE ADRISC CLIMATE SIMULATION

In this section, the ocean results of the 31-year (i.e. 1987–2017) AdriSC climate simulation derived with AdriSC-ROMS 3 km and 1 km model are evaluated with respect to a comprehensive collection of remote sensing and *in situ* observational data (Pranić et al., 2021). The evaluation consists of three different kinds of assessments: (1) sea surface (sea surface height and temperature) properties, (2) thermohaline properties (temperature and salinity) and (3) dynamical properties (current speed and direction). The results of these skill assessments are thus presented and discussed in detail.

3.1. Modelled sea surface properties

First, the three main normalized spatial EOF components (Fig. 6) and their associated amplitude time series (Fig. 7), derived from the JPL_MEASURES SSHA gridded product and the AdriSC-ROMS 3 km SSH results, are analysed and compared. Overall, it can be seen that, for both the Adriatic Sea and northern Ionian Sea (Fig. 6), the first EOF component (EOF1) represents the seasonal variability of both AdriSC-ROMS 3 km and JPL_MEASURES results, with slightly stronger spatial signal and amplitudes in the model (i.e. 81.2 % of the total signal with amplitudes varying ±8.0; Fig. 7) compared to the observations (i.e. 74.5 % of the total signal with amplitudes ranging ±6.0; Fig. 7). Additionally, the correlation coefficient between the time variations of the observed and modelled EOF1 is only 0.65, associated with a normalized standard deviation of 1.19.

The two remaining EOF components are switched in the model compared to the observations (Fig. 6 and 7). In other words, the second ROMS 3 km EOF component (EOF2 representing 6.2 % of the total signal) corresponds to the third SSHA EOF component (EOF3 representing 3.0 % of the signal) and vice versa. Also, in the observations, the EOF2 component represents decadal variability, while the EOF3 component indicates interannual variability of the SSHA signal (Fig. 7). The comparison between modelled spatial EOF2 and observed spatial EOF3 (Fig. 6) reveals that, for the interannual variability, the model does not reproduce the observed eddies in the northern Ionian Sea and exhibits different spatial patterns in the northeastern Adriatic. Further, the interannual variability signal is generally stronger in the ROMS 3 km model (varying mostly ±2.0; Fig. 7) than in the SSHA observations (ranging mostly ±1.0; Fig. 7).

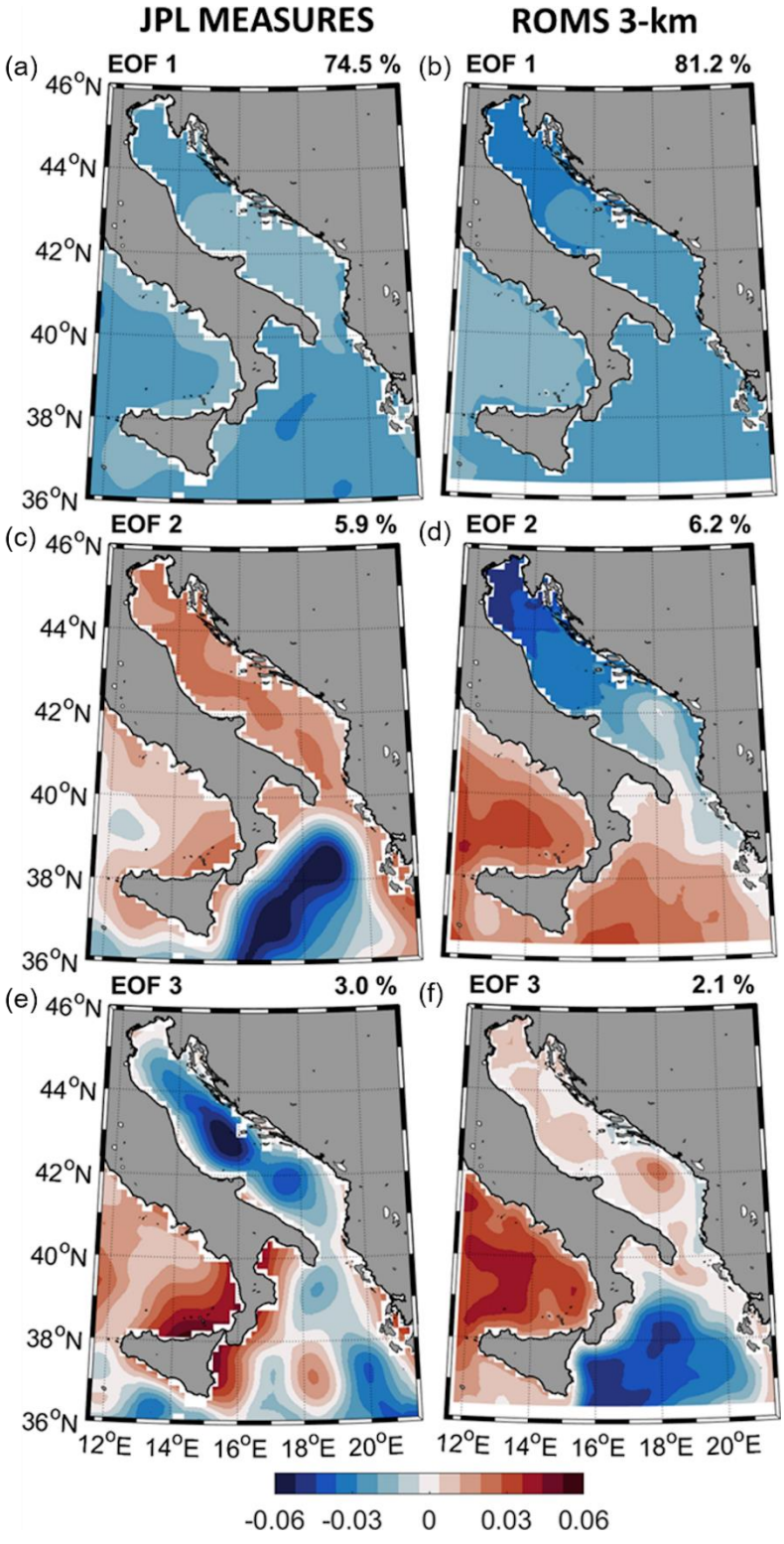

Figure 6. Three main normalized spatial EOF components derived during the 1993–2017 period from the SSHA from the JPL MEASURES gridded product (a, c, e) and the SSH results of the AdriSC ROMS 3 km model (b, d, f).

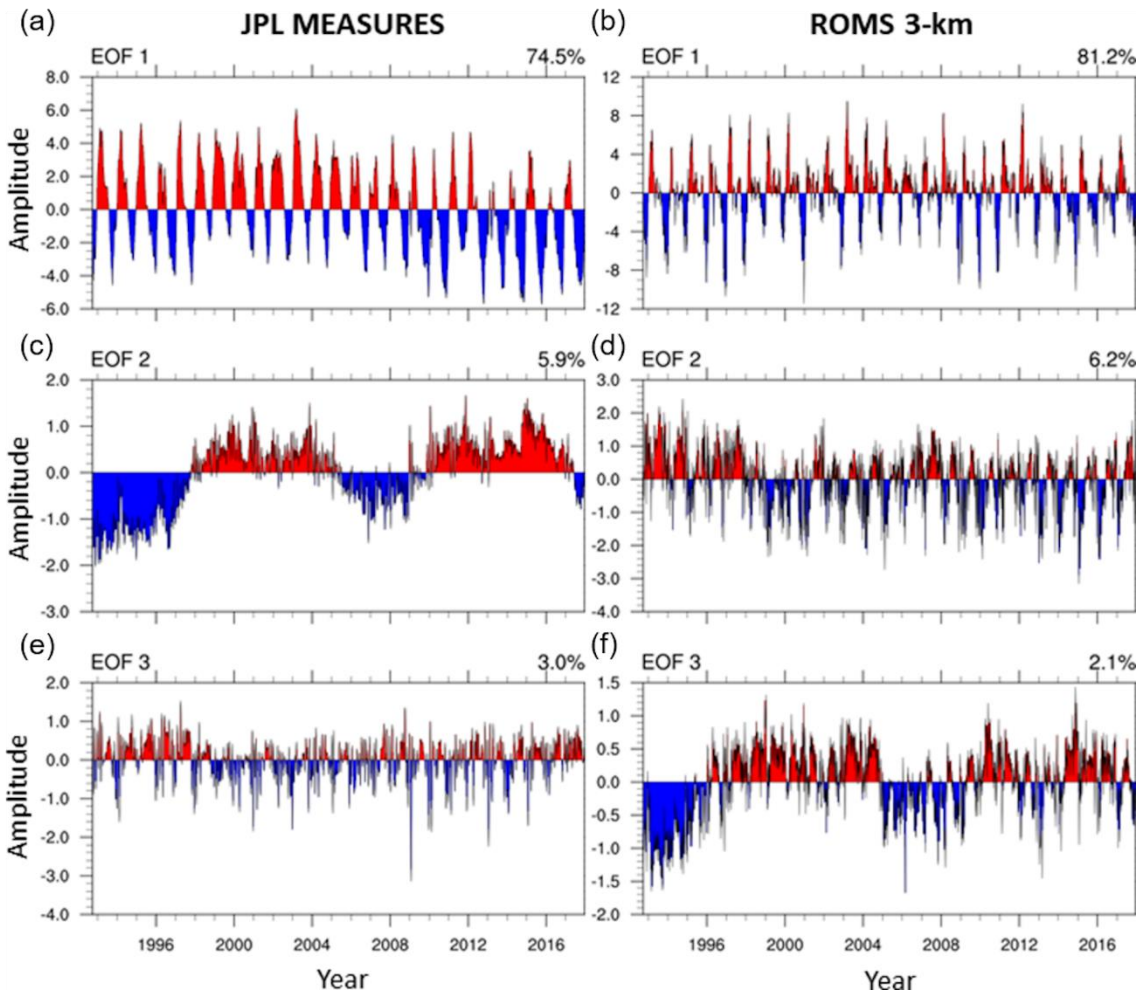

Figure 7. Time series of the amplitudes associated with the three main normalized spatial EOF components derived during the 1993–2017 period from the SSHA from the JPL MEASURES gridded product (a, c, e) and the SSH results of the AdriSC-ROMS 3 km model (b, d, f).

Consequently, as both seasonal and interannual signals are stronger in the AdriSC-ROMS 3 km results compared to the JPL_MEASURES observations, the decadal variability and hence the so-called BiOS signal in the northern Ionian Sea (pattern identified with strongly negative EOF values; Fig. 6), is weaker in the model (2.1 % of the total signal with amplitudes varying ±1.5; Fig. 7) than in the measurements (5.9 % of the total signal with amplitudes ranging ±2.0; Fig. 7). Differences between observations and modelling of the BiOS-driven signal can also be observed during the 2012–2014 period after an intense dense-water formation in 2012 (Mihanović et al., 2013), which had the capacity to reverse the circulation in the northern Ionian Sea (Gačić et al., 2014). The modelled EOF3 reaches a substantially negative value in 2012 and particularly in 2013, while the observations (EOF2) present only a slight decrease in amplitude which mostly remains positive during these years. This may indicate a larger

capacity of the dense waters to change the BiOS-driven patterns during these extremely severe years compared to other BiOS-driven amplitude reversals (e.g. 1997, 2005, and 2009), which are of a similar amplitude ratio in the model and observations. Further, it may be hypothesized that the limited capability of the AdriSC-ROMS 3 km model to reproduce the intensity of the BiOS signal is linked to the insufficient spatial extension of the 3 km domain to the south, where the boundary conditions have too much influence on the results. Despite these limitations, it should also be noted that the time variations of the three main EOFs (Fig. 7) are generally well synchronized between the model and the observations.

The AdriSC-ROMS 3 km sea surface temperature results are further compared to two different remote sensing products, namely AVHRR SST (Fig. 8) and JPL_MUR SST (Fig. 9). Spatial maps are provided for the median of the gridded observations, as well as the median and 1st, 25th, 75th, and 99th percentiles of the biases between model results and observations. The spatial variations of the AVHRR median observations (Fig. 8) show that the lowest temperatures are found in the northern and western parts of the Adriatic Sea, with an average around 17.0 °C. In the middle and southeastern parts of the Adriatic surface temperatures range from 17.5 to 19.0 °C. In the northern Ionian Sea, median temperatures are higher, ranging from 18.0 to 19.8 °C.

Regarding the evaluation, the AdriSC-ROMS 3 km model underestimates the SST in the northern Adriatic, particularly along the plume of the Po river, by as much as -0.8 °C, while in the rest of the Adriatic, biases are lower and range from -0.2 to 0.2 °C. In the Ionian Sea, the model tends to overestimate the SST by up to 0.6 °C along the western coast and by an average of 0.1 °C along the eastern coast. As for the extreme underestimations, the biases reach as low as -2.0 °C in the northern Adriatic, -0.7 °C in the rest of the Adriatic, and -0.5 °C in the Ionian Sea for the 25th percentile, as well as -4.0 °C in the northern Adriatic, -3.0 °C in the rest of the Adriatic and -2.0 °C in the Ionian Sea for the 1st percentile. Small negative biases, down to -0.5 °C, are still present in the northern Adriatic for the 75th percentile, with positive biases up to 0.3 °C for the rest of the Adriatic and up to 1 °C in the Ionian Sea. For the 99th percentile, the entire domain exhibits positive biases around 1.5 °C in the Adriatic and 2 °C in the Ionian Sea.

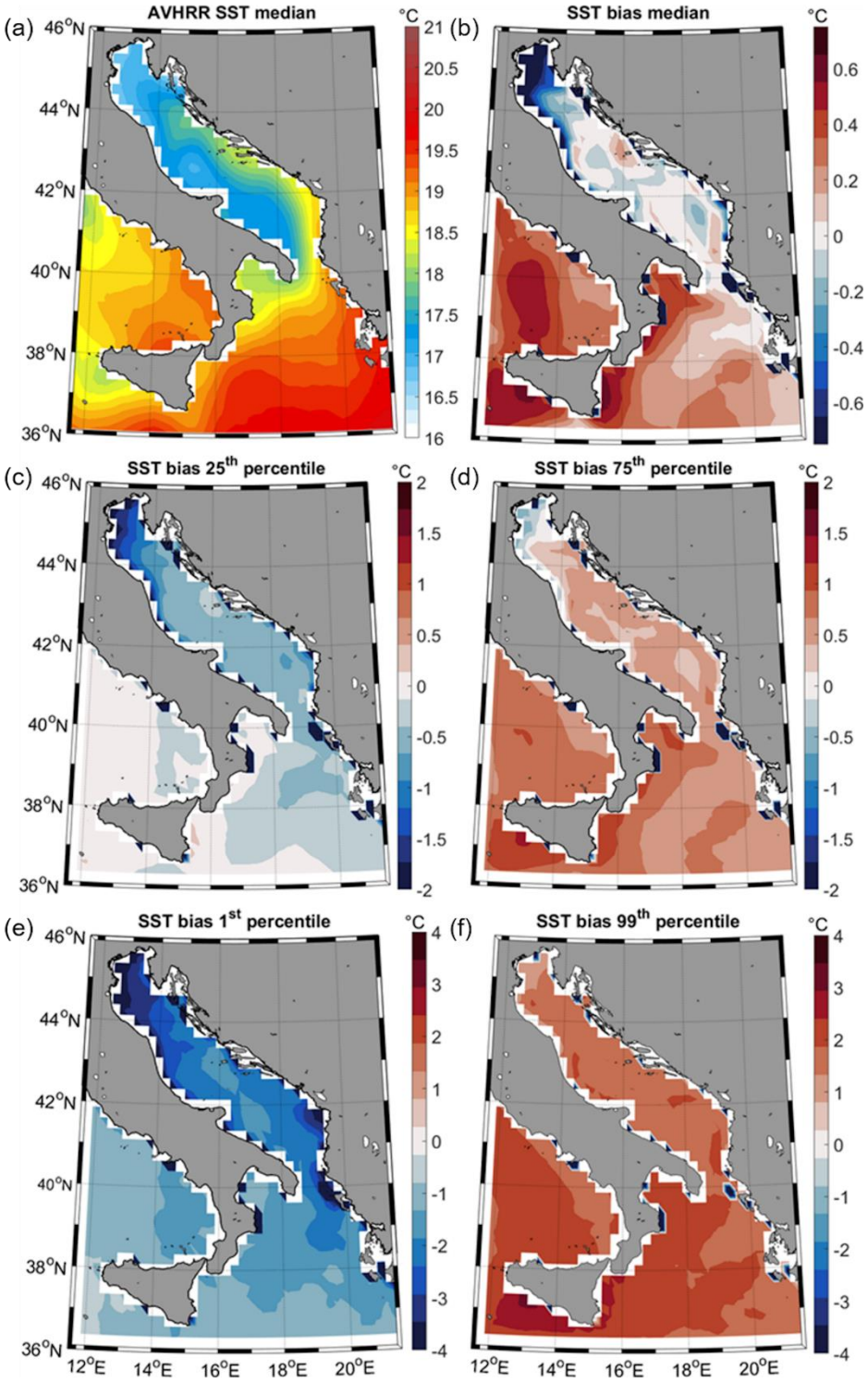

Figure 8. Median of the AVHRR daily sea surface temperature product (a) as well as the median (b) and 25th (c), 75th (d), 1st (e), and 99th (f) percentiles of the daily sea surface temperature biases between AdriSC-ROMS 3 km model results and the AVHRR product during the 1987–2017 period.

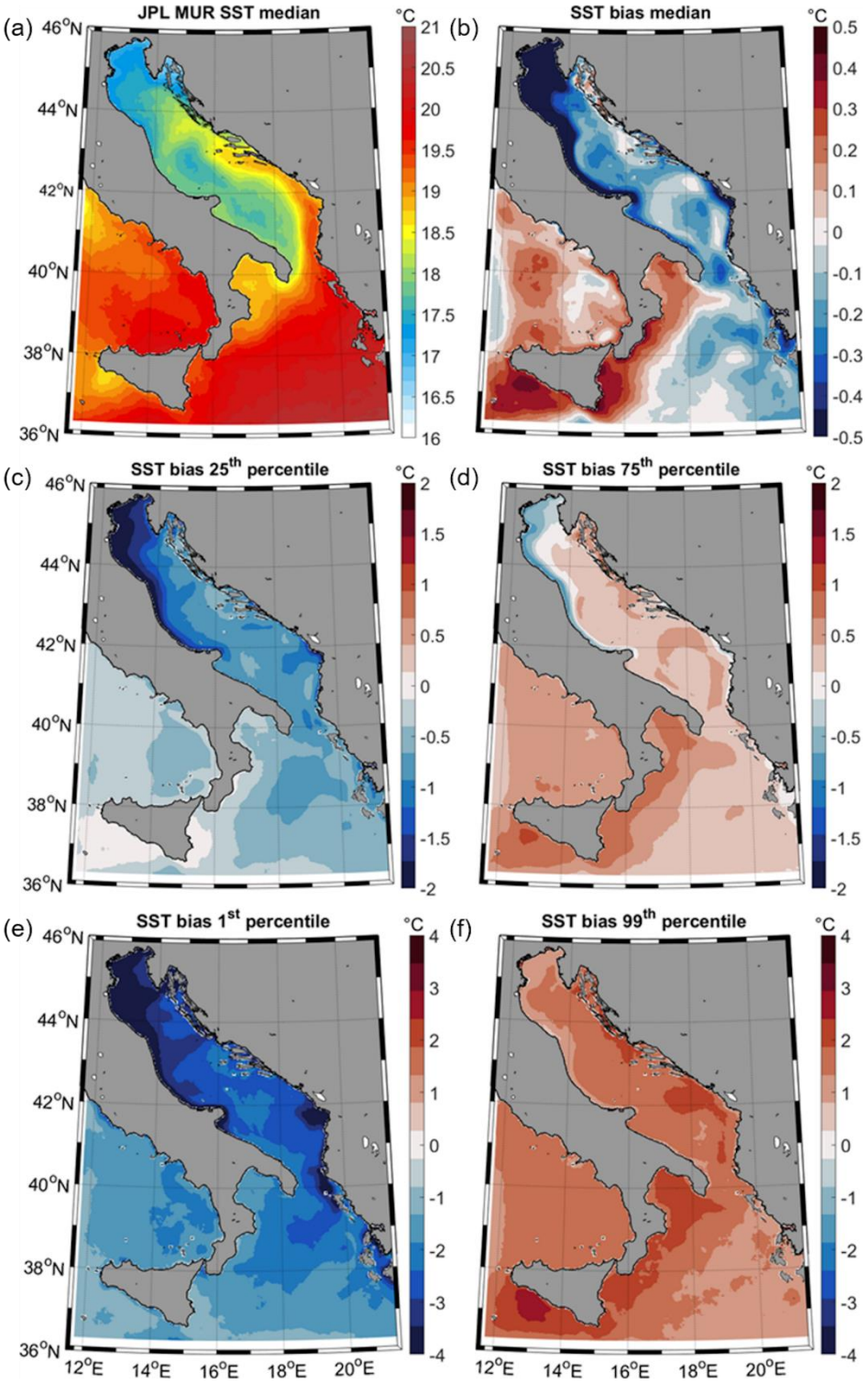

Figure 9. As in Fig. 4 but for the JPL MUR daily sea surface temperature product during the 2002–2017 period.

It should be noted that in some coastal parts of the domain, the observed dark blue patches are artifacts resulting from different representations of the coastline between the AdriSC-ROMS 3 km model and the AVHRR remote sensing product. The other SST dataset analysed in this study (JPL_MUR SST) has a shorter temporal span (i.e. only starts in June 2002) but a higher spatial resolution (i.e. 0.01° instead of 0.25°) and, as a result, provides a more accurate representation of the coastline than AVHRR. The median of the JPL_MUR_SST dataset (Fig.9) shows that the lowest temperatures are present in the northern and northeastern Adriatic, averaging around 17.0 °C. In the middle and western parts of the Adriatic, surface temperatures are around 17.7 °C, while the highest temperatures are in the middle and southeastern Adriatic, ranging from 18.5 to 19.5 °C. In the northern Ionian Sea, median temperatures are mostly around 20.0 °C.

Concerning the evaluation, the AdriSC-ROMS 3 km model generally underestimates the SST, except in the coastal northeastern Adriatic and western part of the Ionian Sea. In the northern Adriatic, the northern part of the western coast along the plume of the Po river, and southernmost part of the eastern coast, negative biases reach below -0.5 °C. In the rest of the Adriatic, as well as the middle and eastern parts of the Ionian Sea, biases reach down to -0.3 °C. A narrow strip of negative median biases may be seen along the eastern coast of the southern Adriatic, matching the plumes of the large Albanian rivers. In terms of the extreme conditions, for the 25th percentile, negative biases reach down to -2.0 °C in the northern Adriatic and northern part of the western coast, -1.0 °C in the rest of the Adriatic, and -0.8 °C in the Ionian Sea. For the 1st percentile, biases reach down to-4.0 °C in the northern Adriatic, northern part of the western coast, and southernmost part of the eastern coast, -3.0 to -2.0 °C in the rest of the Adriatic, and -3.0 °C in the Ionian Sea. For the 75th percentile, small negative biases are present in the northern Adriatic and northern part of the western coast down to -0.5 °C, whereas for the rest of the Adriatic and Ionian Sea, the temperature is overestimated by up to 0.3–0.8 °C. For the 99th percentile, the model overestimates the SST in the whole domain by up to 0.5–2.0 °C.

3.2. Modelled thermohaline properties

The overall skills of the AdriSC-ROMS 3 km and 1 km models to reproduce the observed CTD data are presented in Fig. 10. First, correlations and normalized standard deviations of modelled and observed temperature (Fig. 10a) and salinity (Fig. 10b) for each observational experiment and/or cruise are shown with Taylor diagrams.

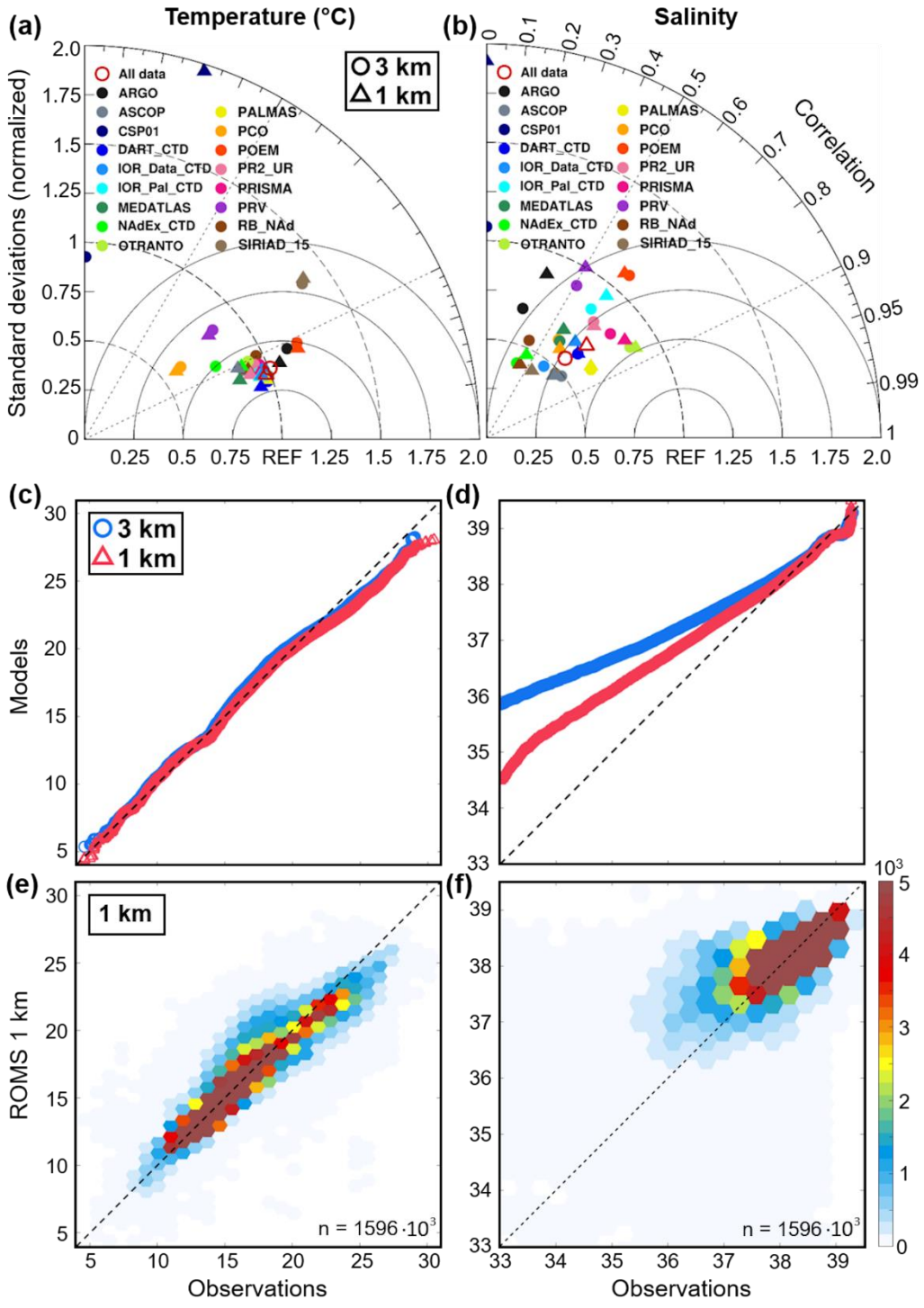

Figure 10. Evaluation of the AdriSC-ROMS 3 km and 1 km temperature (a, c, e) and salinity (b, d, f) results against observations from 17 different datasets with (a, b) Taylor diagrams and (c, d) quantile-quantile plots as well as, only for the 1 km model, (e, f) scatter plots showing the density (number of occurrences) with hexagonal bins and total number of points n.

It should be noted that the CSP01 dataset presents extremely small correlations for the temperature (0.0 and 0.3 for the AdriSC-ROMS 3 km and 1 km models, respectively) and even

anticorrelations for the salinity (-0.2 and -0.4 for the AdriSC-ROMS 3 km and 1 km, respectively), marked as 0.0 on the Taylor diagram for practical reasons. Additionally, for the AdriSC-ROMS 1 km model, the CSP01 dataset also exhibits large standard deviations around 1.9 for both temperature and salinity. Since all the other datasets show relatively similar results, it is suspected that CSP01 may not be a reliable dataset for this evaluation and is treated as an outlier and removed from further analysis. For all the other observational experiments and/or cruises, the overall results (hereafter referred to as all data) reveal that the AdriSC-ROMS 3 km and 1 km models simulated the observed temperatures with good accuracy (i.e. correlations around 0.9 and normalized standard deviations around 1.0) but do not properly capture the observed salinity (i.e. correlations around 0.7 and normalized standard deviations around 0.5). This most probably highlights the fact that even kilometre-scale ocean models struggle to accurately reproduce the freshwater input from the Adriatic rivers, which play a crucial role in terms of the thermohaline circulation along the coasts (Vilibić et al., 2016, 2018).

Second, the Q-Q plots of temperature and salinity (Fig. 10c and d) reveal that both models can generally represent the observed distributions, with only a small underestimation of the observed temperatures above 22 °C but a substantial overestimation of the observed salinity below 37.5. However, it should be noted that the number of records with salinity lower than 37.5 represents less than 1 % of the entire dataset. Additionally, the AdriSC-ROMS 1 km model presents significantly smaller salinity overestimations than the AdriSC-ROMS 3 km model and is therefore solely used for further evaluation of the modelled thermohaline properties. Finally, the scatter plots (Fig. 10e and f) reveal that the hexagons with the largest number of points follow the reference line for both temperature and salinity, indicating that the vast majority of the AdriSC-ROMS 1 km results correspond well to the observations in both intensity and timing. A more detailed evaluation of the AdriSC-ROMS 1 km thermohaline properties, depending on four depth ranges (i.e. 0–50, 50–200, 200–500, and 500–2000 m), is presented as the median (Fig. 11) and MAD (Fig. 12) of the temperature and salinity biases (i.e. model minus observations), depending on the locations of the *in situ* observations.

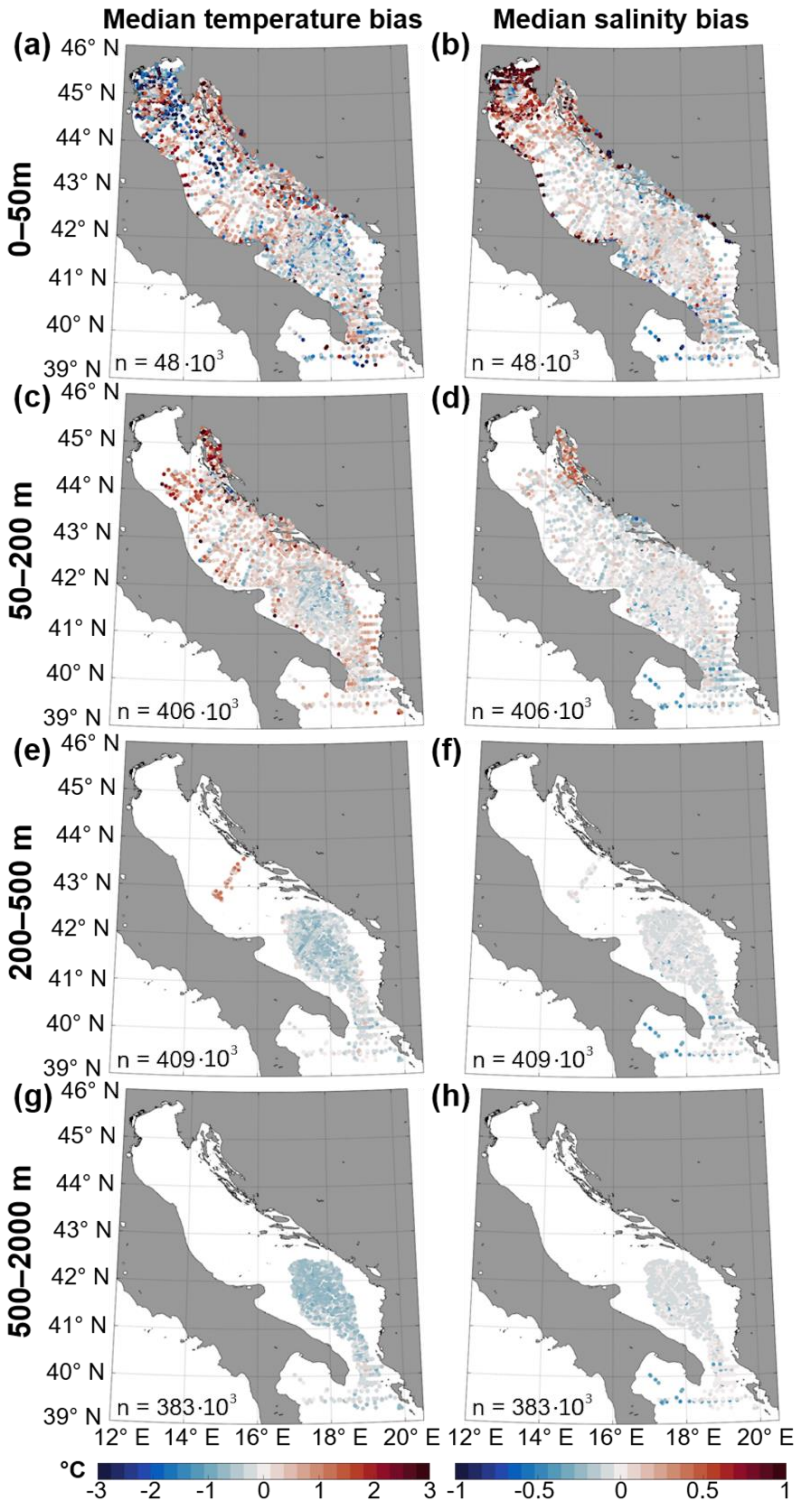

Figure 11. Median of the temperature (left panels) and salinity (right panels) biases between AdriSC-ROMS 1 km model results and CTD observations for depth ranges: (a, b) 0–50 m, (c, d) 50–200 m, (e, f) 200–500 m, and (g, h) 500–2000 m, with the total number of points n (bottom left corner).

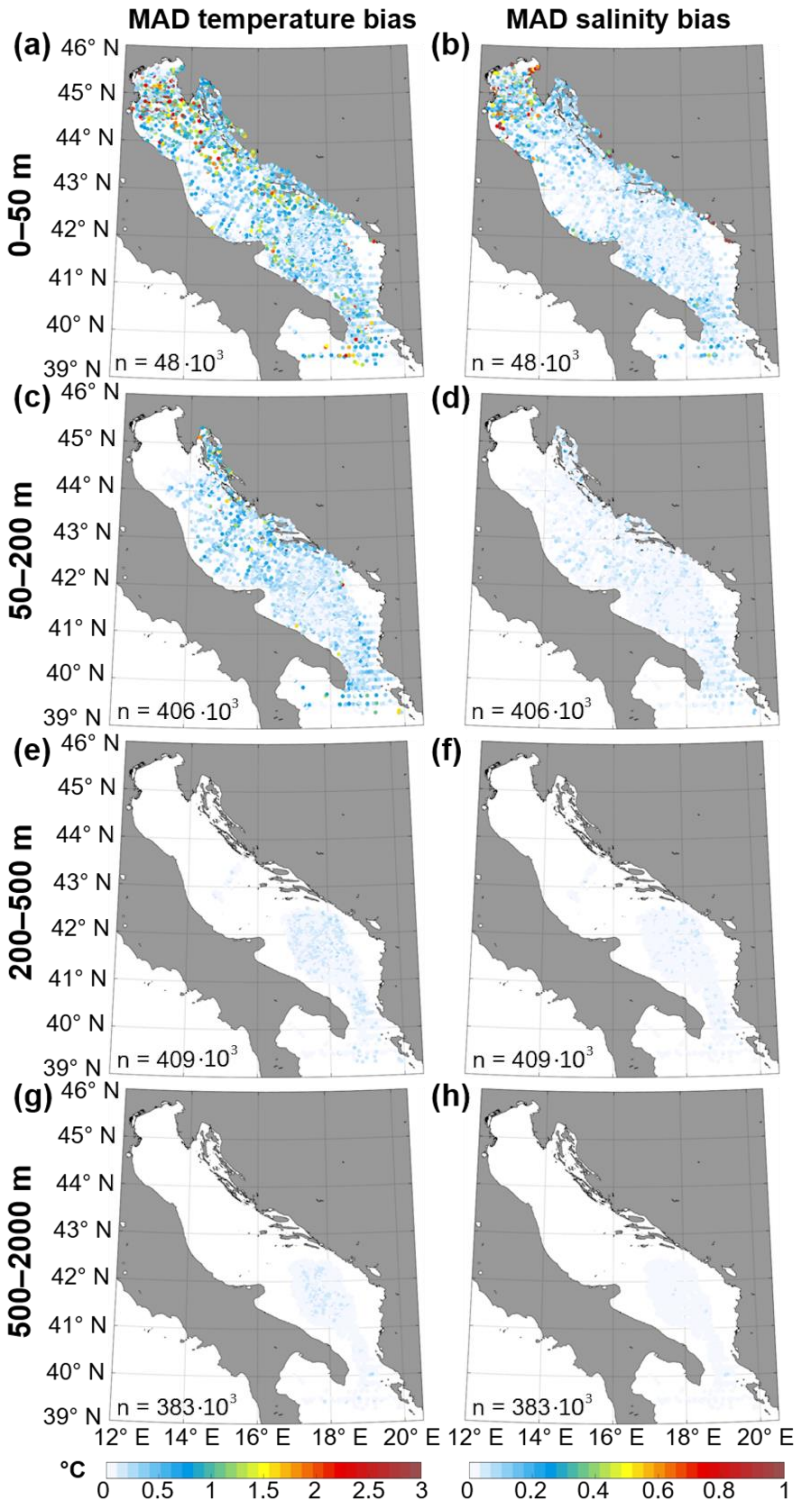

Figure 12. MAD of the temperature (left panels) and salinity (right panels) biases between AdriSC-ROMS 1 km model results and CTD observations for depth ranges: (a, b) 0–50 m, (c, d) 50–200 m, (e, f) 200–500 m, (g, h) 500–2000 m, with the total number of points n (bottom left corner).

For the surface layer (0–50 m), the median temperature and salinity biases (Fig. 11a and b) exhibit large spatial variability. In general, there is a slight prevalence of temperature underestimation and salinity overestimation in the surface layer in the whole Adriatic. Notably, biases are most pronounced in the northern Adriatic, with dominant negative values for temperature and positive values for salinity. In this area, the median temperature bias is ranging from -4 to 2 °C and MAD is ranging from 0.0 to 0.9 °C (the values are calculated as the 5th and 95th percentiles of the spatial distributions, respectively). The median salinity bias ranges from -0.6 to 4.3 with MAD ranging from 0.0 to 1.4. The large overestimation of salinity in the upper layer of the northern Adriatic is most probably influenced by the inaccurate representation of river discharges in the model, especially of the Po river, which has the largest outflow in the Adriatic Sea (average discharge of 1500 $m^3 s^{-1}$; Raicich, 1996; Supić and Orlić, 1999). Strong negative temperature biases are also present in the middle Adriatic ranging from -2.4 to 0.5 °C with MAD from 0.0–0.4 °C.

Furthermore, larger median temperature and salinity biases are present in the northeastern Adriatic coastal areas, particularly in the Kvarner Bay, ranging from -2.0 to 1.3 °C with MAD between 0.0–1.2 °C, and from -0.7 to 2.9 with MAD between 0.0–1.0, respectively. Biases in the western coastal part of the Adriatic range from -1.0 to 1.5 °C with MAD from 0.0–0.3 °C for temperature, and from -0.8 to 1.5 with MAD from 0.0–0.2 for salinity. In the middle eastern (including the Dalmatian Islands) and the southern Adriatic, biases are in the range from -1.8 to 0.8 °C with MAD between 0.0–0.9 °C for temperature, and -0.9 to 1.7 with MAD from 0.0–1.0 for salinity (with only -0.4 to 0.3 in the southern Adriatic).

For the upper intermediate layer (50–200 m), the model reproduces dominantly warmer temperatures, except in the southern Adriatic where the biases range between -0.7 and 0.4 °C with MAD from 0.0–0.2 °C (Fig. 11c and 12c). The largest temperature overestimations are located in the northeastern Adriatic, with biases up to 3.0 ± 0.8 °C, as well as in the middle Adriatic and the middle eastern coastal areas, with biases up to 1.5 ± 0.8 °C. Concerning the salinity, the model generally underestimates the observations (Fig. 11d) except in the northeastern Adriatic where positive salinity biases up to 0.5 (with MAD between 0–0.1) are dominant.

For the lower intermediate layer (200–500 m), positive temperature biases up to 1.5 °C adjacent to negative biases down to -1.0, with MAD from 0.0–0.2 °C, are located in the middle Adriatic and more precisely in the Jabuka Pit, the collector of the northern Adriatic dense

waters (Vilibić and Supić, 2005), while negative biases down to -0.8 are present in the southern Adriatic (Fig. 11e and 12e). Salinity biases are slightly negative with values down to -0.1 ± 0.0 (Fig. 11f and 12f).

For the deeper layers (500–2000 m), temperature is underestimated in the southern Adriatic Pit and in the northern Ionian Sea with biases ranging from -0.8 to -0.1 °C with MAD from 0.0–0.1 °C (Fig. 11g and 12g). Similarly, salinity biases are relatively low and range from -0.1 to 0.0 ± 0.0 (Fig. 11h and 12h). Overall, the spatial analysis of the CTD stations depending on the depth reveals that the capability of the AdriSC-ROMS 1 km model to reproduce temperature and salinity is generally better in deeper parts of the Adriatic than in the coastal areas and the shallow northern Adriatic shelf.

The last kind of analysis in this section is an in-depth climatological and seasonal evaluation of the AdriSC-ROMS 1 km thermohaline properties performed for seven predefined subdomains (Fig. 3b). For the northern Adriatic subdomain (Fig. 13), the AdriSC-ROMS 1 km model is overall lacking accuracy in reproducing the thermohaline properties. The monthly temperature climatology is reproduced relatively well most of the year (i.e. biases ranging from -0.6 to 0.6 °C) except in August, September, and October when the differences can reach down to -1.6 °C (Fig. 13a). The salinity is not well represented, especially in the second half of the year, with persistently higher values by up to 0.7 (Fig. 13b).

Regarding the seasonal variations, the vertical profiles of the median temperature biases show a strong underestimation reaching down to -1.0 °C in spring and -2.0 °C in summer in the surface layer (Fig. 13d). However, during these two seasons, a large overestimation of the temperature is present below 10 m and up to 3.8 °C at 30 m of depth. In autumn, temperature is mostly negatively biased, and the underestimation reaches down to -0.7 °C. Winter temperature biases are rather small throughout the whole water column. In addition, salinity is strongly overestimated at the surface independently of the season (Fig. 13e), with winter having the smallest biases (below 0.5) and summer having the largest biases (up to 2.1). Below 20 m, the salinity biases are smaller and the seasonal variability is weaker.

The analysis of the T-S diagrams reveals that the model performs well in reproducing dense water masses. Given that the northern Adriatic is a well-known and one of the most researched dense-water formation sites (Zore-Armanda, 1963; Vilibić and Supić, 2005; Mihanović et al., 2013, 2018; Vilibić et al., 2016), these results are promising. The model appears to be less accurate in the density ranges below 25 kg m^{-3}, where there is an overestimation of density

(Fig. 13g, h). In addition, despite the lack of accuracy of the model for salinities under 36 and temperatures over 24 °C, most of the observations are well captured in the T-S diagram with the AdriSC-ROMS 1 km model.

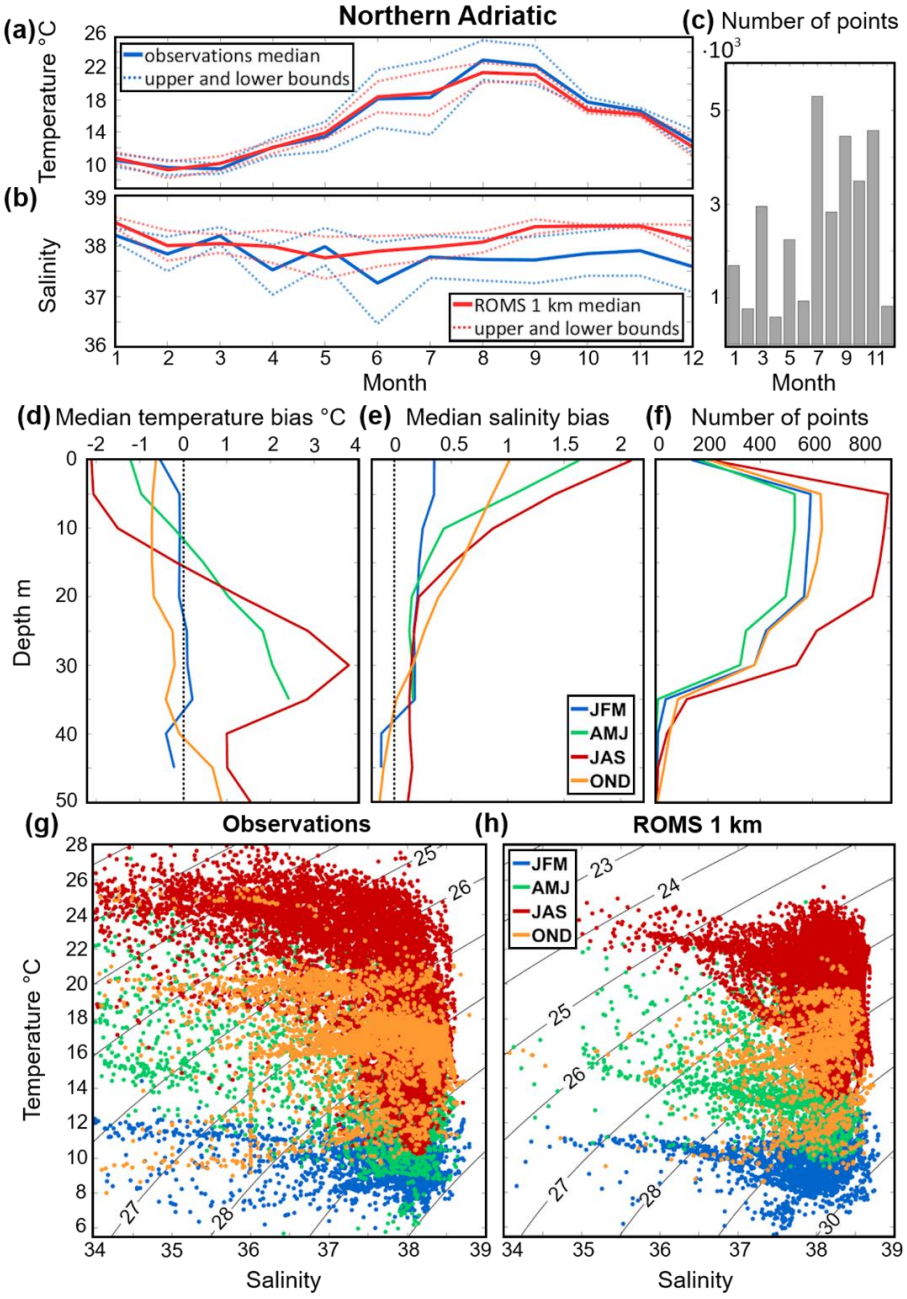

Figure 13. Northern Adriatic subdomain. Monthly climatology of AdriSC-ROMS 1 km and *in situ* (a) median temperature, (b) median salinity, and their variabilities (i.e. upper and lower bounds defined as ±MAD) as well as (c) the number of observations per month. Seasonal variations of the (d) temperature and (e) salinity biases between the model and observations depending on the depth as well as (f) the number of observations per depth. Seasonal T-S

diagrams for (g) the CTD observations and (h) the AdriSC-ROMS 1 km model with PDA isolines.

For the western coast subdomain (Fig. 14), the AdriSC-ROMS 1 km model seems to represent the monthly temperature climatology well (Fig. 14a) despite a tendency towards higher positive biases from May to November (up to 2.0 °C). It should be noted that the highest bias is found in July when the amount of available data is quite small (Fig. 14c). Moreover, the salinity climatology is reproduced with good accuracy throughout the entire year (Fig. 14b).

Seasonally, the strongest temperature biases are observed in summer and autumn: (1) mostly negative in the first 20 m reaching down to -1.0 °C and (2) becoming positive below 20 m (up to 1.0 °C) until 200 m, where they decrease (Fig. 14d). Winter temperature biases are generally small and decrease with depth, reaching nearly 0 °C below 100 m. In spring, the temperature biases are negative in the surface but become positive below 20 m down to 100 m, similarly to the other seasons. Salinity biases seem to be the strongest in the surface, with an underestimation of -1.0 in spring and an overestimation up to 1.5 in winter (Fig. 14e). However, a very small number of observations were recorded at this depth (Fig. 14f). Also, salinity biases are small throughout the water column independently of the season.

The seasonal analysis of the T-S diagrams shows that the AdriSC-ROMS 1 km model can reproduce the seasonal properties of the western coast subdomain water masses (Fig. 14g, h), where the outflow of freshened waters from the northern Adriatic occurs (Artegiani et al., 1997; Lipizer et al., 2014; Burrage et al., 2009).

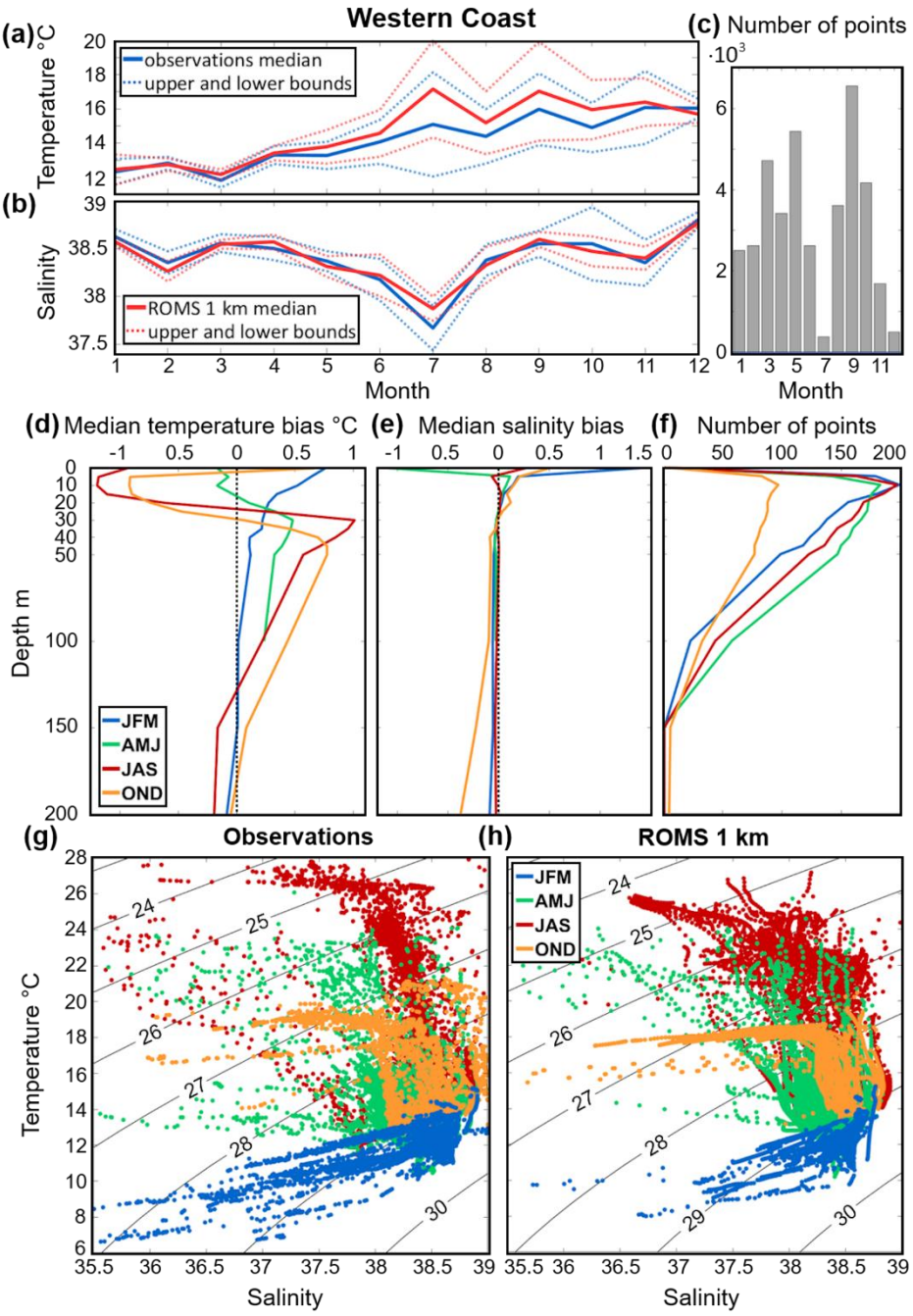

Figure 14. Western coast subdomain. Monthly climatology of AdriSC-ROMS 1 km and *in situ* (a) median temperature, (b) median salinity, and their variabilities (i.e. upper and lower bounds defined as ±MAD) as well as (c) the number of observations per month. Seasonal variations of the (d) temperature and (e) salinity biases between themodel and observations depending on the depth as well as (f) the number of observations per depth. Seasonal T-S diagrams for (g) the CTD observations and (h) the AdriSC-ROMS 1 km model with PDA isolines.

For the deep Adriatic subdomain (Fig. 15), the modelled monthly temperature and salinity medians are consistently lower than the observations throughout the year. The highest biases occur in winter and spring, reaching almost -0.7 °C for the temperature (Fig. 15a), while the differences in salinity are smaller than -0.1 (Fig. 15b).

Further, seasonal analysis shows that the temperature biases are mostly negative, reaching down to -2.0 °C in the surface in summer, and associated with a small number of observations (Fig. 15d), while below 50 m they are mostly smaller than -0.5 °C (Fig. 15f). More precisely, the underestimation of observations is minimized between 50 and 300 m for all seasons, except in winter when biases reach down to -0.5 °C. However, stronger temperature underestimations are present in the deeper layers between 300 and 900 m of depth but rapidly decrease below 900 m. Salinity is overestimated in summer and winter in the surface layer and mostly underestimated for all the other depths and seasons, with biases smaller than -0.1 (Fig. 15e).

Seasonal analysis of the T-S diagrams shows that the model performs well regardless of the season, with slightly narrower temperature and salinity ranges and an overestimation of densities under 26.5 kg m^{-3}, particularly in summer (Fig. 15g, h). The densest waters are captured relatively well by the model, which is important as the deep Adriatic subdomain is a well-known dense-water formation and accumulation site (Vilibić and Orlić, 2001, 2002; Manca et al., 2002; Mantziafou and Lascaratos, 2004, 2008).

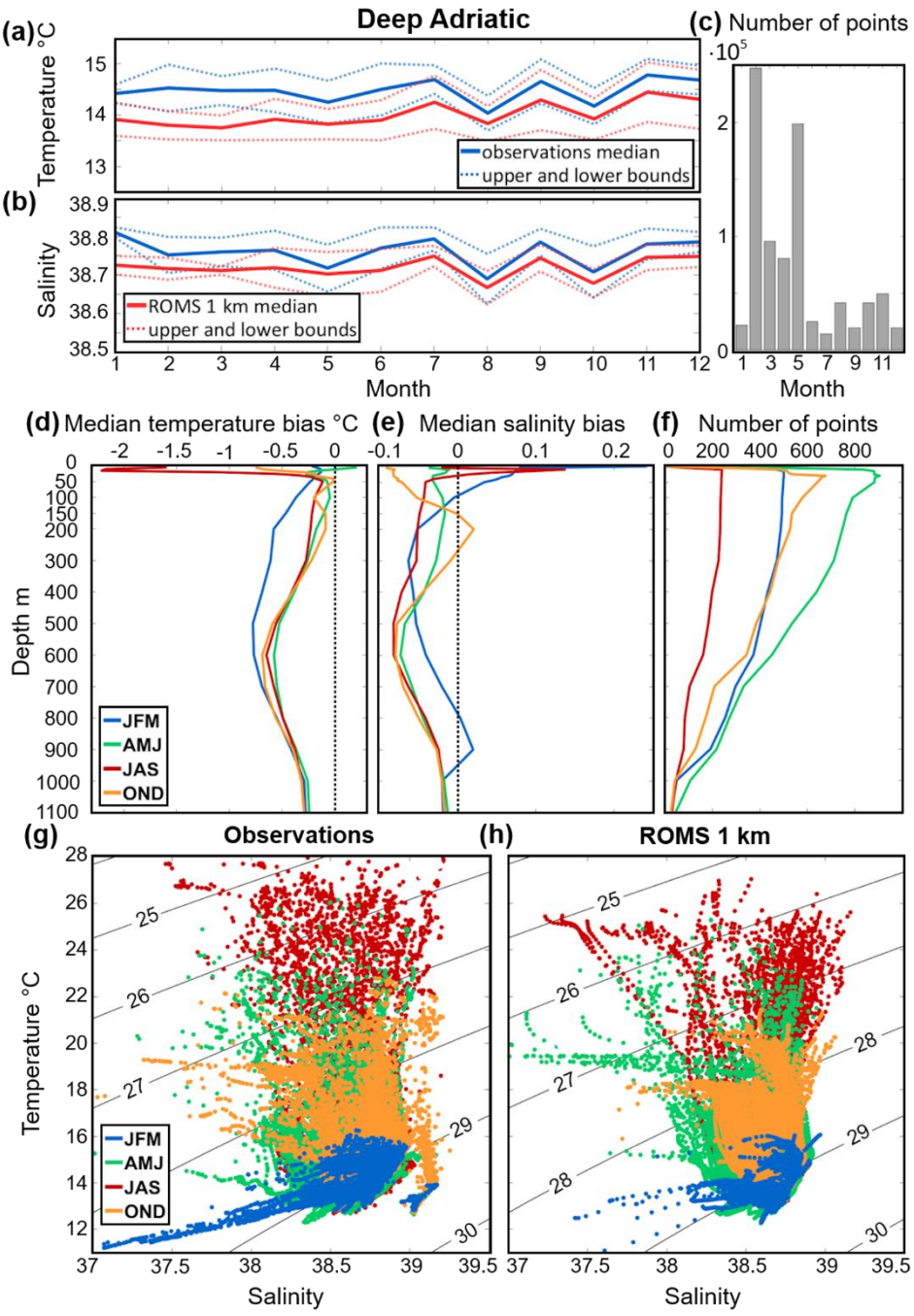

Figure 15. Deep Adriatic subdomain. Monthly climatology of AdriSC-ROMS 1 km and *in situ* (a) median temperature, (b) median salinity, and their variabilities (i.e. upper and lower bounds defined as ±MAD) as well as (c) the number of observations per month. Seasonal variations of the (d) temperature and (e) salinity biases between the model and observations depending on the depth as well as (f) the number of observations per depth. Seasonal T-S diagrams for (g) the CTD observations and (h) the AdriSC-ROMS 1 km model with PDA isolines.

For the middle Adriatic subdomain (Fig. 16), the AdriSC-ROMS 1 km demonstrates great capability in reproducing the monthly temperature climatology, except in December when the difference reaches 0.5 °C (Fig. 16a). Salinity is also well captured with slightly lower modelled values up to 0.1 in January, July and October (Fig. 16b).

Seasonally, negative temperature biases are present near the surface for all seasons except winter when the bias is slightly positive (Fig. 16d). In summer, temperature biases reach down to -1.0 °C near the surface but become positive below 20 m. In autumn, temperature is mostly underestimated by the model throughout the water column, while in spring negative biases change the sign under 100 m. Temperature in winter is slightly overestimated at all depths. Concerning the salinity, biases are mostly underestimated at the surface, except in summer at 5 m and below, where there is an overestimation up to almost 0.2 (Fig. 16e). Under 40 m, salinity biases are negative with the largest underestimations in autumn (below -0.1).

The analysis of the T-S diagrams shows that the model performs well for all seasons, except in summer when the underestimation of temperature and overestimation of salinity in the surface layer can be clearly seen as the overestimation of PDA (hereafter referred as density) below 26 kg m^{-3} (Fig. 16g, h).

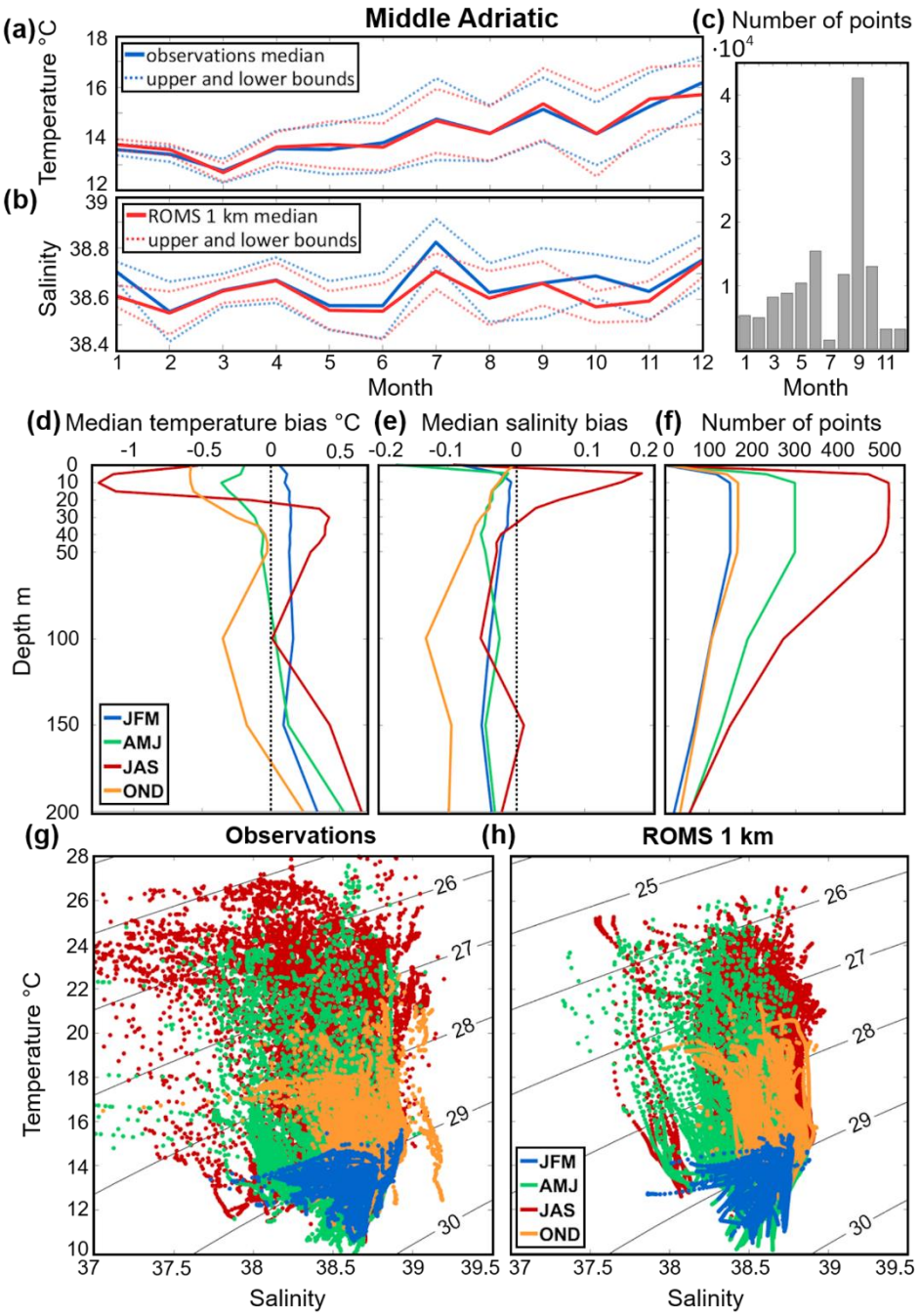

Figure 16. Middle Adriatic subdomain. Monthly climatology of AdriSC-ROMS 1 km and *in situ* (a) median temperature, (b) median salinity and their variabilities (i.e. upper and lower bounds defined as ±MAD) as well as (c) number of observations per month. Seasonal variations of the (d) temperature and (e) salinity biases between the model and observations depending on the depth as well as (f) number of observations per depth. Seasonal T-S diagrams for (g) the CTD observations and (h) the AdriSC-ROMS 1 km model with PDA isolines.

For the Kvarner Bay subdomain (Fig. 17), concerning the monthly climatology (Fig. 17a), the AdriSC-ROMS 1 km model reproduces temperatures better during winter, spring and autumn (biases around 0.1–0.5 °C) than during summer (biases reaching up to 2.0 °C), similarly to the northern Adriatic subdomain. Salinity is captured relatively well with larger biases (around 0.1–0.5) in March, May, June and December (Fig. 17b).

The seasonal analysis shows small positive temperature biases occurring in winter in the first 25 m of depth, but they become quasi-null below 25 m (Fig. 17d). Vertical profiles of temperatures are best reproduced in autumn when the biases are quite small. In spring, temperature is mostly overestimated under 10 m with biases growing with depth and surpassing 0.5 °C. In summer, negative temperature biases are found in the surface and large overestimations occur below 20 m of depth, reaching around 1.5 °C. Salinity is overestimated for all seasons in the whole water column, with biases being higher in surface. Unlike for temperature, the best results for salinity are obtained in summer and spring with small biases under 20 m of depth (Fig. 17e). In autumn and winter at 5 m depth, when the largest number of observations were recorded (Fig. 17f), the biases reach around 0.3 and 0.4, respectively.

Moreover, the seasonal analysis of the T–S diagrams shows that the model performs well independently of the season but with a slightly narrower salinity range, especially for salinity lower than 37.0 (Fig. 17g, h). The densest waters are well captured, which is important as the Kvarner Bay subdomain is a known dense-water formation site (Mihanović et al., 2013; Janeković et al., 2014; Benetazzo et al., 2014, Vilibić et al., 2016; Denamiel et al., 2021).

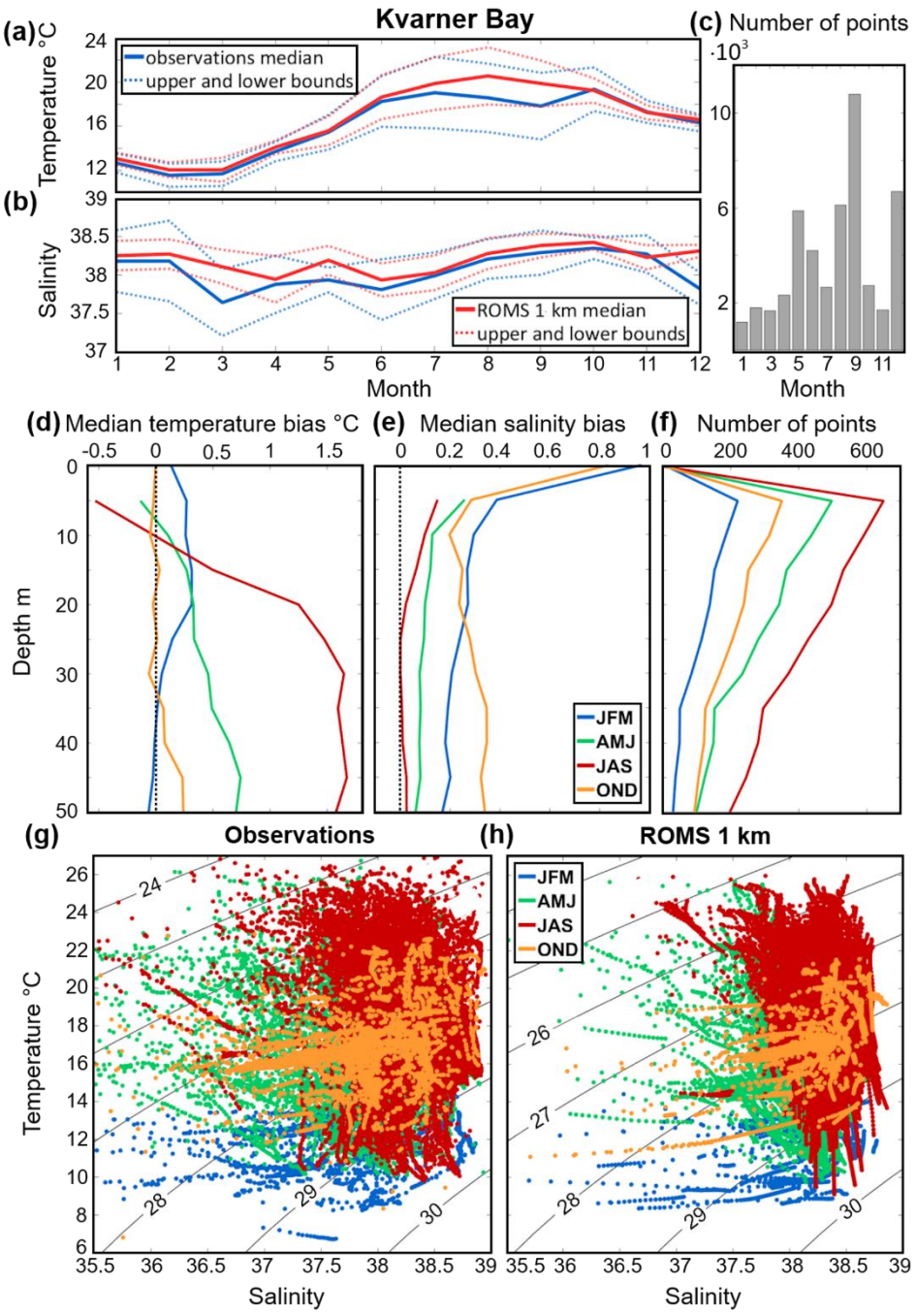

Figure 17. Kvarner Bay subdomain. Monthly climatology of AdriSC-ROMS 1 km and *in situ* (a) median temperature, (b) median salinity and their variabilities (i.e. upper and lower bounds defined as ±MAD) as well as (c) number of observations per month. Seasonal variations of the (d) temperature and (e) salinity biases between the model and observations depending on the depth as well as (f) number of observations per depth. Seasonal T-S diagrams for (g) the CTD observations and (h) the AdriSC-ROMS 1 km model with PDA isolines.

For the Dalmatian Islands subdomain (Fig. 18), similarly to the Kvarner Bay subdomain, the AdriSC-ROMS 1 km model seems capable of reproducing the temperature monthly climatology (Fig. 18a) for all the months, except from July to September when modelled values are significantly higher (reaching from 0.7–2.0 °C). Modelled salinities have slightly lower values throughout the year, especially in summer and autumn with biases down to -0.2 (Fig. 18b).

Seasonal analysis of the temperature reveals that the largest biases occur in summer, being negative in the first 10 m of depth but positive in the deeper layers, where they reach up to 1.0 °C at 30 m of depth (Fig. 18d). In autumn, the biases are negative in the first 40 m of depth and positive below. Spring and winter both have small biases throughout the water column. Salinity biases are largest in winter and spring in the surface. Below 10 m of depth, the highest underestimations occur in summer and autumn (Fig. 18e). The analysis of the T-S diagrams shows that the model performs well for all seasons. However, as for the other subdomains, the model overestimates the densities under 25 kg m^{-3} (Fig. 18g, h).

For the Otranto–Ionian subdomain (Fig. 19), the analysis of the monthly climatology reveals that the temperature and salinity values are well captured by the AdriSC-ROMS 1 km model, showing slightly negative differences for the most of the year for both variables (reaching down to -0.4 °C and -0.1, respectively; Fig. 19a, b).

Seasonally, the largest temperature variations occur in the first 200 m of depth, with the highest biases in summer (Fig. 19d). Below 200 m, the biases are similar for all seasons, with values around -0.2 °C extending down to 1000 m of depth. Salinity biases are largest between 100 and 200 m of depth, reaching under -0.1 for all seasons except summer (Fig. 19e). Below this depth, the biases reduce and approach 0.0 at 600 m of depth, beyond which they become positive. The analysis of the T-S diagrams shows that the model captures well the seasonal distributions of the water masses (Fig. 19g, h). However, for salinity smaller than 37.5 and density smaller than 25 kg m^{-3}, the modelled values slightly overestimate the observations.

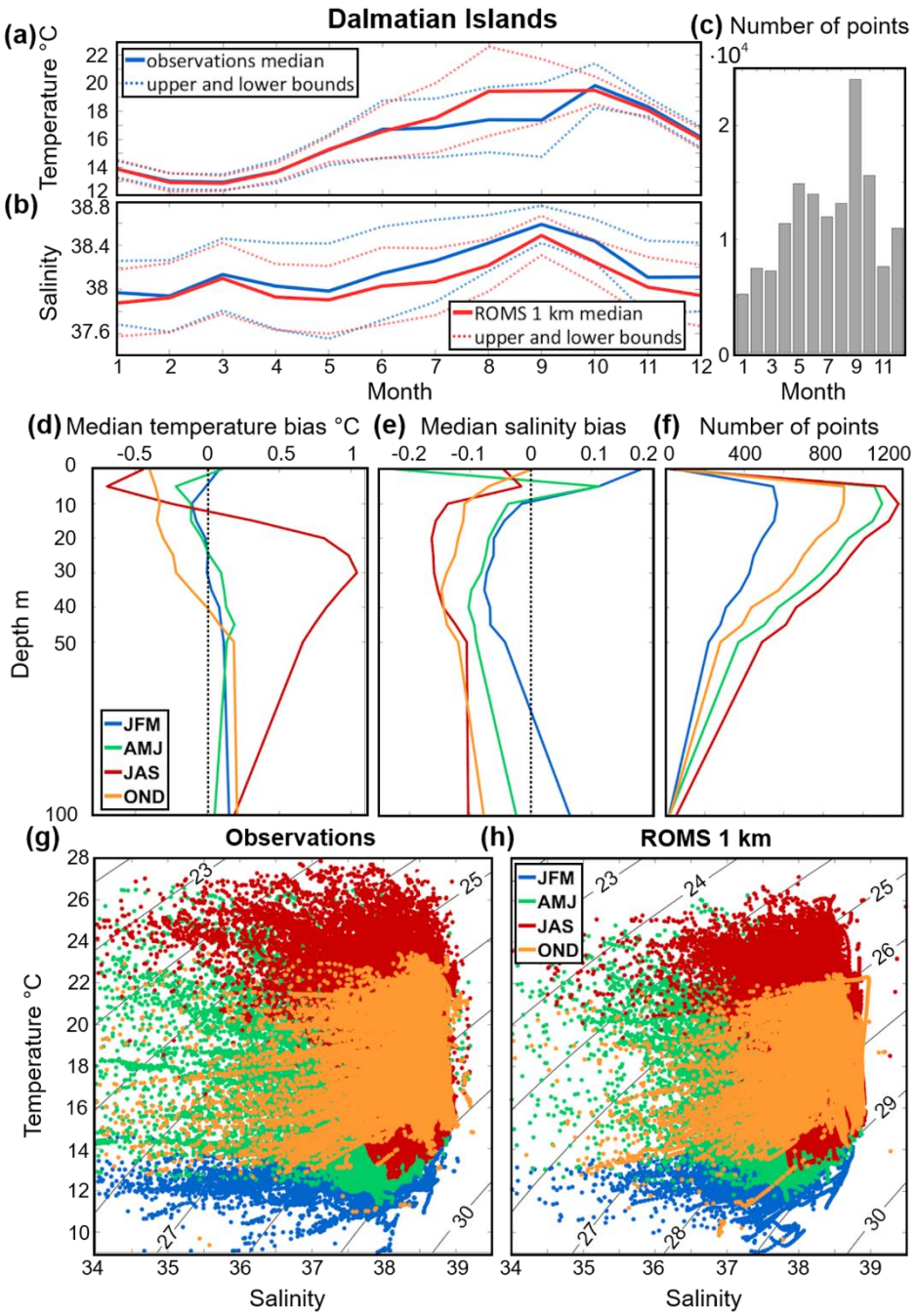

Figure 18. Dalmatian Islands subdomain. Monthly climatology of AdriSC-ROMS 1 km and *in situ* (a) median temperature, (b) median salinity and their variabilities (i.e. upper and lower bounds defined as ±MAD) as well as (c) number of observations per month. Seasonal variations of the (d) temperature and (e) salinity biases between the model and observations depending on the depth as well as (f) number of observations per depth. Seasonal T-S diagrams for (g) the CTD observations and (h) the AdriSC-ROMS 1 km model with PDA isolines.

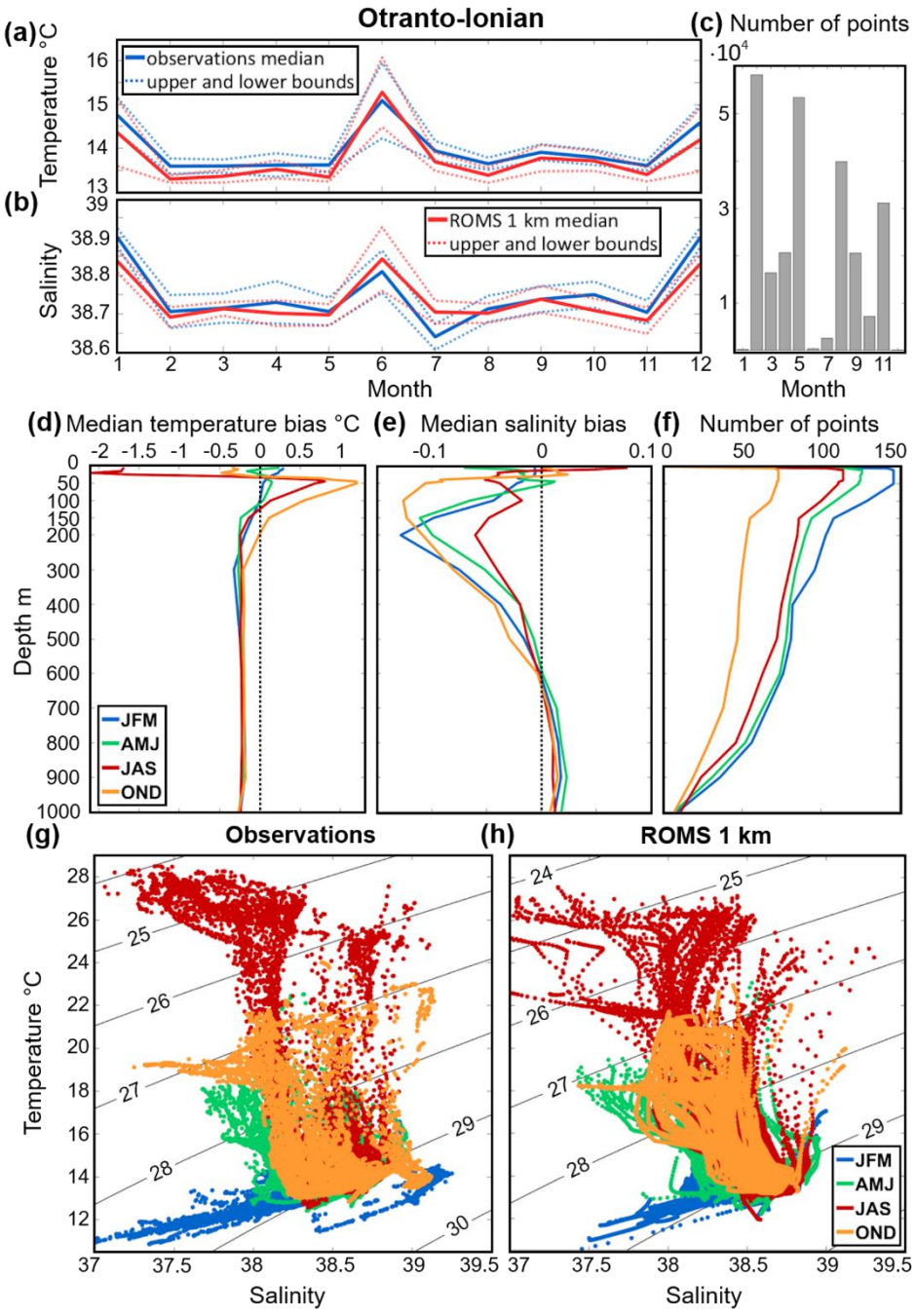

Figure 19. Otranto–Ionian subdomain. Monthly climatology of AdriSC-ROMS 1km and *in situ* (a) median temperature, (b) median salinity and their variabilities (i.e. upper and lower bounds defined as ±MAD) as well as (c) number of observations per month. Seasonal variations of the (d) temperature and (e) salinity biases between the model and observation depending on the depth as well as (f) number of observations per depth. Seasonal T-S diagrams for (g) the CTD observations and (h) the AdriSC-ROMS 1 km model with PDA isolines.

3.3. Modelled dynamical properties

A basic skill assessment of the AdriSC-ROMS 3 km and 1 km models to reproduce the observed ADCP and RCM hourly measurements is presented in Fig. 20. First, correlations and normalized standardized deviations of the modelled and observed ocean current speeds (Fig. 20a) and directions (Fig. 20b) for each dataset are depicted with Taylor diagrams. Following these analyses, the AdriSC-ROMS 3 km and 1 km models appear to reproduce the observed current speeds with correlations between 0.2 and 0.5 and normalized standardized deviations ranging from 0.7–1.2 as well as the current directions with correlations around 0.2 and normalized standardized deviations between 0.8 and 1.0. However, the Q-Q plot analyses of current speeds and directions (Fig. 20c and d) reveal that both models are, in fact, perfectly capable of representing the observed distributions, except for a small overestimation of the current speeds above 0.5 m s^{-1}. Consequently, the low correlations obtained for the Taylor diagrams must have been uniquely linked to a lack of synchronization between hourly observations and model results. It should also be noted that the number of records with speeds higher than 0.5 m s^{-1} represents less than 1 % of the entire dataset. Additionally, the current speed overestimations are smaller for the AdriSC-ROMS 1 km results than for those of the AdriSC-ROMS 3 km model. Therefore, the 1 km model is solely used for further evaluation of the modelled dynamical parameters.

Moreover, the scatter plot analyses (Fig. 20e and f) indicate that the hexagons with the highest density of records generally follow the reference line for both current speeds and directions. However, due to the previously mentioned lack of synchronization, modelled current speeds, and especially modelled current directions, can be extremely spread out compared to the observations. Despite the inherent challenges of reproducing the ocean dynamics at the hourly scale, the scattering of the AdriSC-ROMS 1 km results may also be influenced by uncertainties linked to the time references of the observational dataset. Indeed, due to the lack of metadata availability for certain datasets, some observations, possibly provided in local time, have been compared with model results in Universal Time Coordinated (UTC). Further, it should be noted that the two vertical lines visible on the current direction scatter plot represent inconsistencies identified in the JP2 dataset for two stations and have been excluded from further analyses.

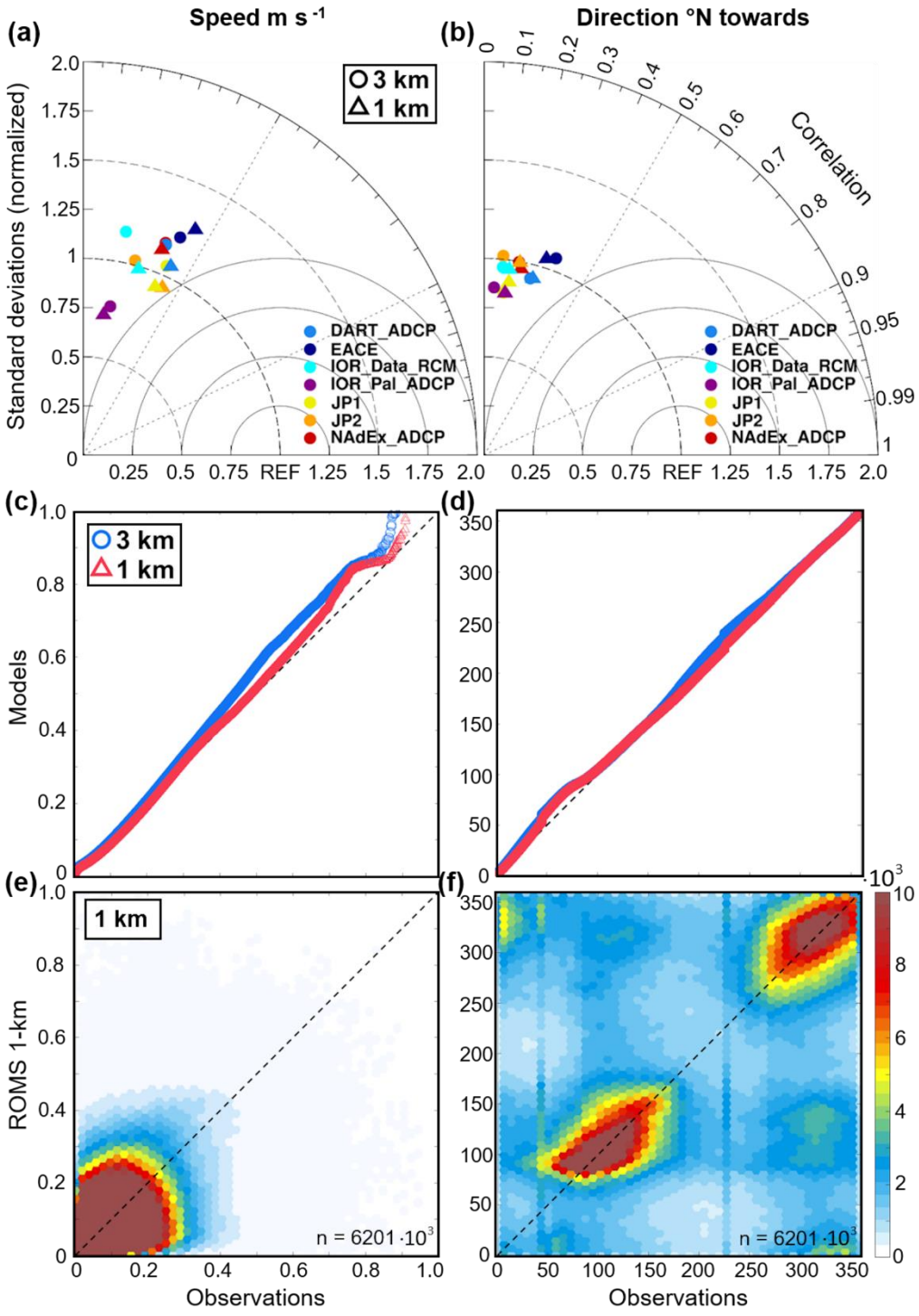

Figure 20. Evaluation of the AdriSC-ROMS 3 km and 1 km current speeds (a, c, e) and directions (b, d, f) against observations from seven different datasets with (a, b) Taylor diagrams and (c, d) quantile–quantile plots as well as, only for the 1 km model, (e, f) scatter plots showing the density (number of occurrences) with hexagonal bins and total number of points n.

Further, an in-depth climatological and seasonal evaluation of the AdriSC-ROMS 1 km dynamical properties is performed for seven different datasets (Fig. 3c). In the case of the DART_ADCP dataset (Fig. 21), the monthly climatology differences of the modelled and the observed current speeds can reach up to 0.02 m s^{-1} in October and down to -0.05 m s^{-1} in March (Fig. 21a), while the direction differences reach down to -39 ° in September. Concerning seasonal variations, the vertical profiles of the modelled and observed current speeds (Fig. 21d) indicate an underestimation reaching -0.03 m s^{-1} in winter and -0.02 m s^{-1} in spring. The largest differences occur in autumn, reaching down to -0.05 m s^{-1}, while in summer, very small biases are present throughout the water column, except at 5 m depth. The rose plots (Fig. 21e) depicting modelled and observed current direction reveal that the observed distributions are similarly reproduced by the model independently of the season. It can be seen that the occurrences of the eastward current direction are overestimated, while the northeastward direction is underestimated.

For the JP2 dataset (Fig. 22), the AdriSC-ROMS 1 km reproduced the monthly climatology of current speed with good accuracy (Fig. 22a), which is supported by a large number of observations throughout the year (Fig. 22c). The largest difference of 0.02 m s^{-1} is reached in November. However, the current direction climatology is mostly overestimated, reaching up to 87.43 ° in June (Fig. 22b). Seasonal vertical profiles of the modelled and observed current speed (Fig. 22d) show an overestimation under 10 m in winter and autumn, reaching up to 0.03 m s^{-1}. Extremely small biases are present in spring and summer down to 40 m depth, where they reach 0.02 m s^{-1}. According to the rose plots (Fig. 22e), the main current directions within this dataset are well reproduced for all seasons, with a slight overestimation of occurrences of all directions, except the eastward direction, which is strongly underestimated independently of the season. This systematic underestimation may be ascribed to the inaccurate representation of the coastline in the model at the locations of the extracted points.

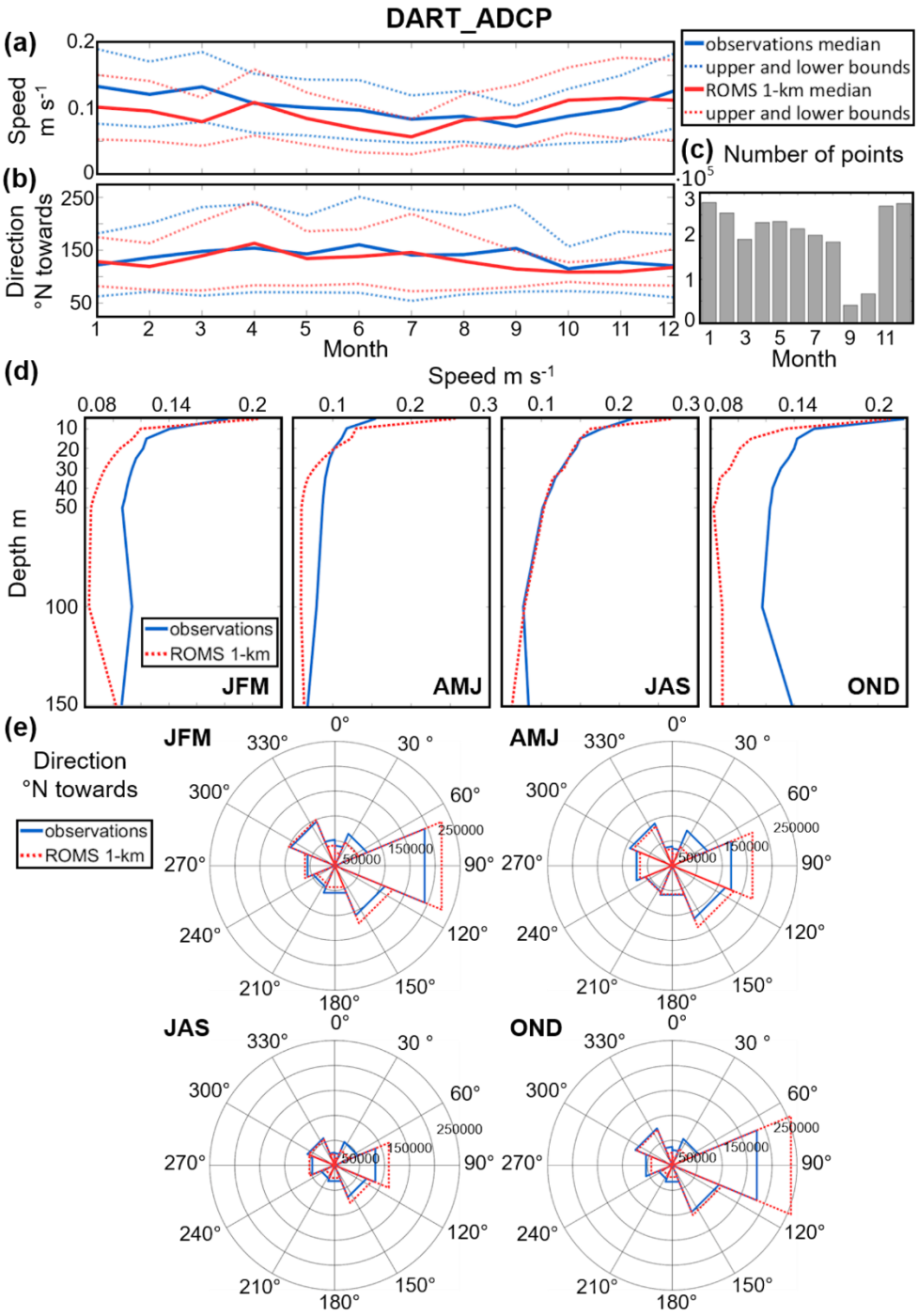

Figure 21. DART_ADCP dataset. Monthly climatology of AdriSC-ROMS 1 km and *in situ* (a) median speed, (b) median direction, and their variabilities (i.e. upper and lower bounds defined as ±MAD), as well as (c) the number of observations per month. Seasonal variations of the (d) speed from the model and observations depending on the depth. Seasonal rose plots of the (e) direction for ADCP observations and the AdriSC-ROMS 1 km model.

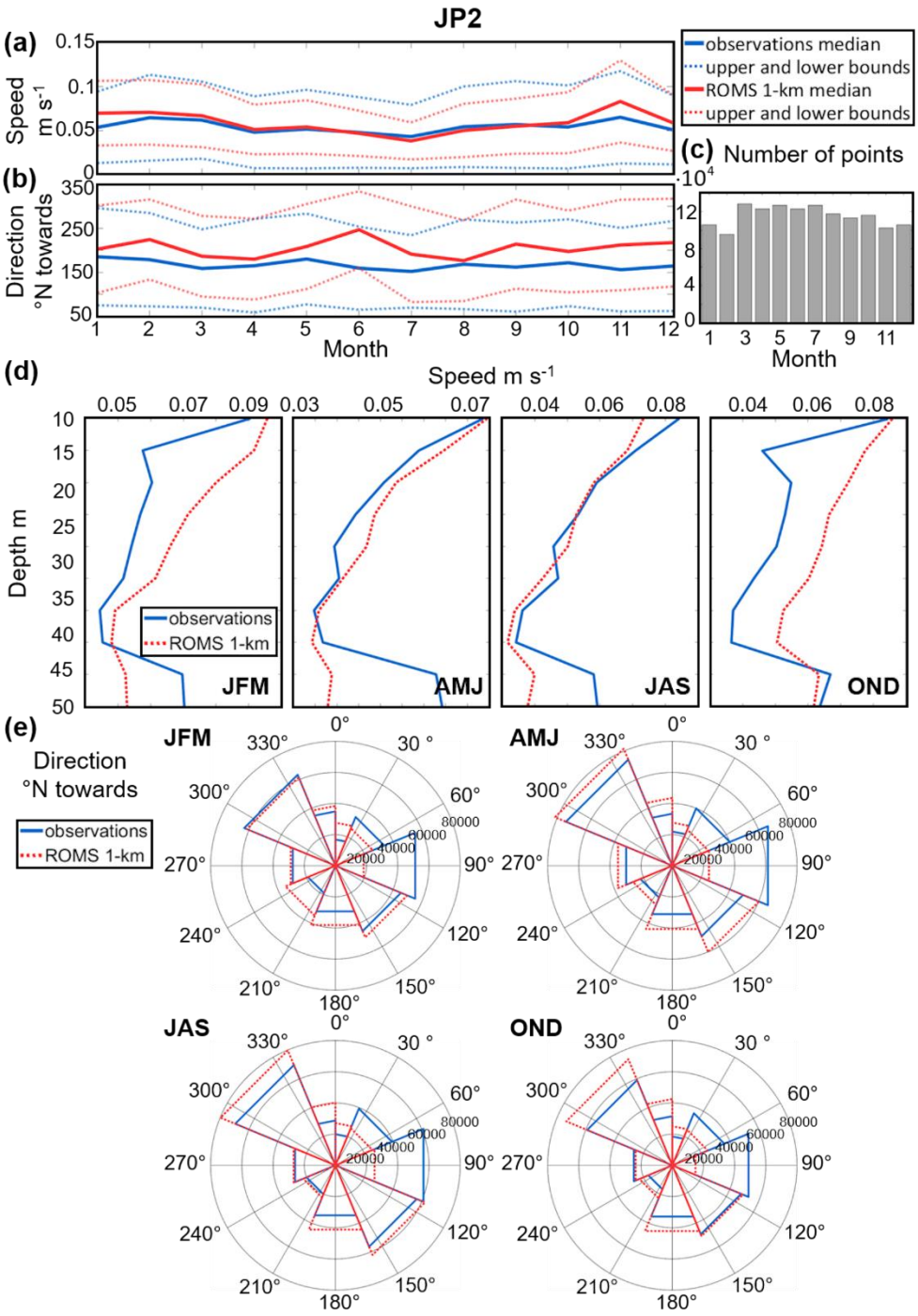

Figure 22. JP2 dataset. Monthly climatology of AdriSC-ROMS 1 km and *in situ* (a) median speed, (b) median direction, and their variabilities (i.e. upper and lower bounds defined as ±MAD), as well as (c) the number of observations per month. Seasonal variations of the (d) speed from the model and observations depending on the depth. Seasonal rose plots of the (e) direction for ADCP observations and the AdriSC-ROMS 1 km model.

For the IOR_Data_RCM dataset (Fig. 23), the monthly climatology of current speed is well represented by AdriSC-ROMS 1 km in summer and autumn, while differences are more pronounced in winter and spring, varying between -0.03 and 0.03 m s^{-1} (Fig. 23a). The current direction climatology is reproduced with good accuracy by the model, except in winter when biases reach up to 50 ± 29 ° in January (Fig. 23b). Regarding the seasonal variations, the vertical profiles of the modelled speed are generally in good agreement with the observed speed in the first 40 m (Fig. 23d). Within this layer, very small differences are present in winter and autumn, while in summer and spring, the model tends to underestimate the observed speed down to -0.02 m s^{-1}. Below this depth, the observations are underestimated for all seasons. To be noted is that the number of observations is largest in the first 50 m, whereas 99.5 % of all the data is concentrated within the first 100 m. The rest of the data (i.e. 0.5 %) are spread between 100 and 900 m of depth, and thus only the first 100 m are presented on the vertical plots. The rose plots of the modelled and observed current direction (Fig. 23e) reveal that the observed distributions are similarly reproduced by the model independently of the season. The direction differences are slightly larger in autumn for the eastern currents.

For the JP1 dataset (Fig. 24), AdriSC-ROMS 1 km seems to mostly underestimate the observed current speed climatology by an average of -0.02 ± 0.01 m s^{-1} (Fig. 24a). The current direction differences vary largely from February to July, while from August to January, when the number of observations is significantly larger (Fig. 24c), the differences are small, reaching up to 17 ± 17 ° (Fig. 24b). Concerning the seasonal variations, the vertical profiles reveal that the model systematically underestimates the observed speed throughout the water column (Fig. 24d). The smallest biases are present in winter and spring, reaching around 0.01 m s^{-1} and 0.02 m s^{-1} on average, respectively. In summer and autumn, the biases reach around 0.03 m s^{-1} and 0.04 m s^{-1} on average, respectively. The rose plots of the modelled and observed current direction show that the observed distributions are similarly reproduced by the model for all seasons. In summer and autumn, the southeastward and northwestward current directions are overestimated, while the westward direction is slightly underestimated.

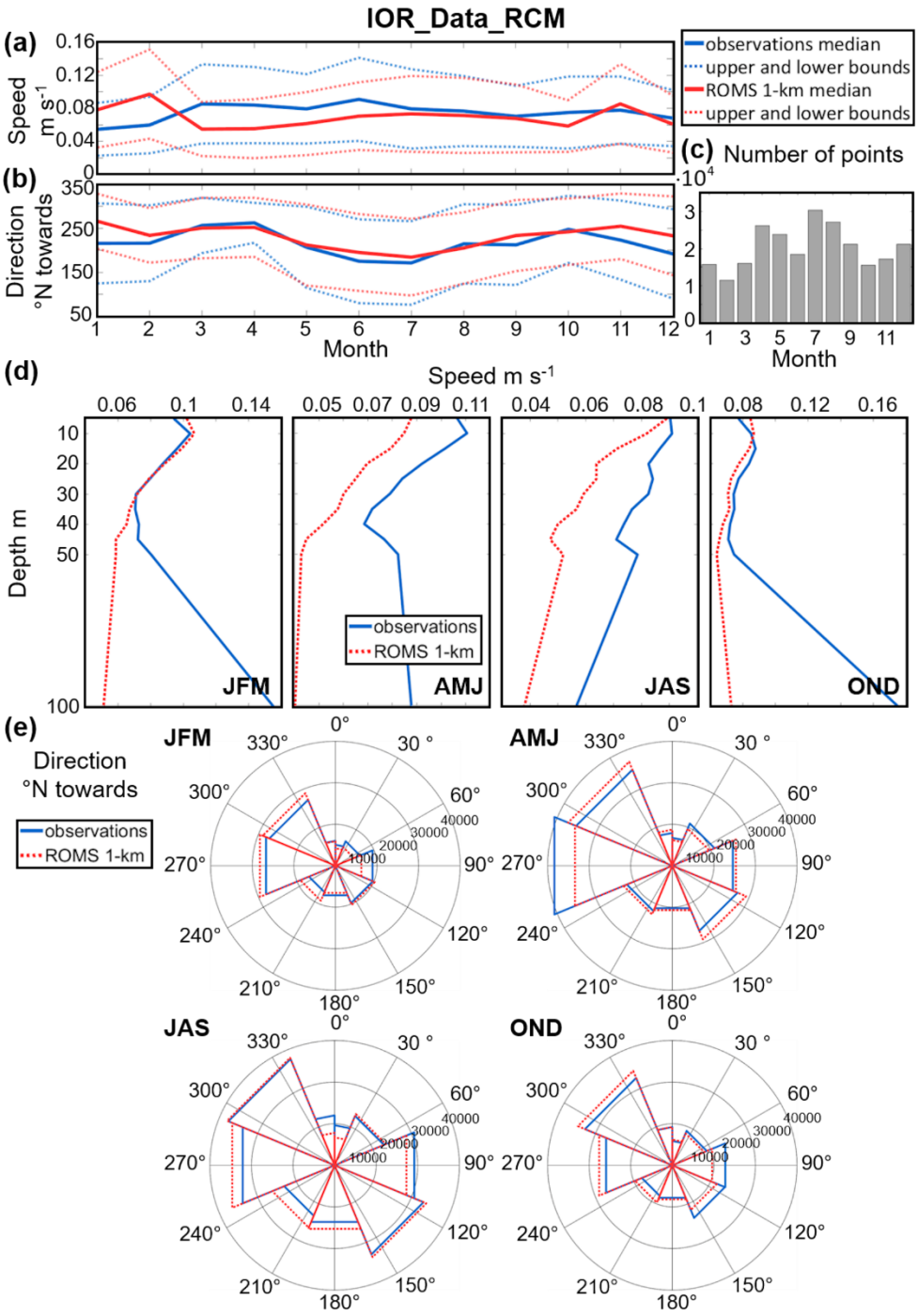

Figure 23. IOR_Data_RCM dataset. Monthly climatology of AdriSC-ROMS 1 km and *in situ* (a) median speed, (b) median direction, and their variabilities (i.e. upper and lower bounds defined as ±MAD), as well as (c) the number of observations per month. Seasonal variations of the (d) speed from the model and observations depending on the depth. Seasonal rose plots of the (e) direction for RCM observations and the AdriSC-ROMS 1 km model.

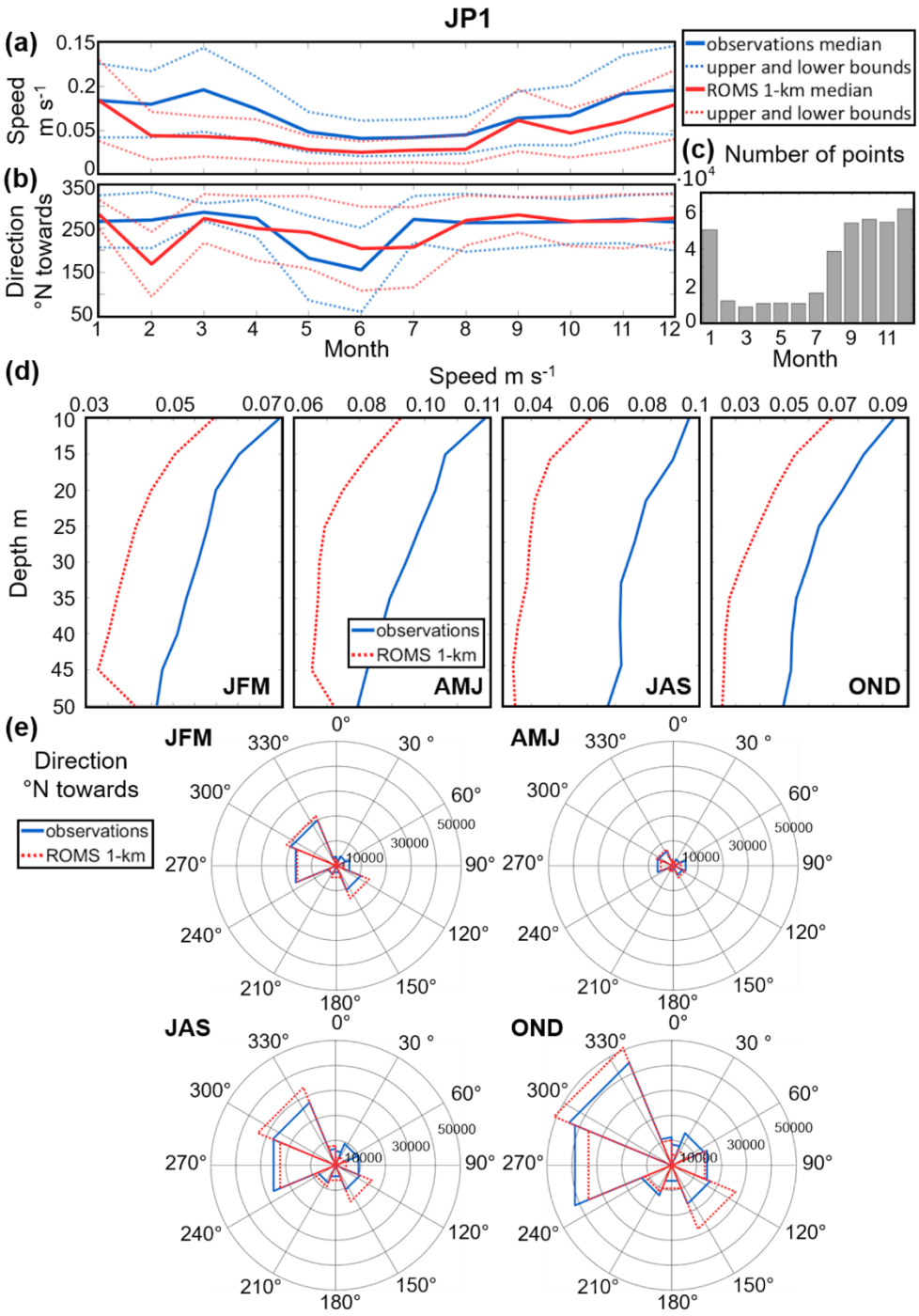

Figure 24. JP1 dataset. Monthly climatology of AdriSC-ROMS 1 km and *in situ* (a) median speed, (b) median direction and their variabilities (i.e. upper and lower bounds defined as ±MAD) as well as (c) number of observations per month. Seasonal variations of the (d) speed from the model and observations depending on the depth. Seasonal rose plots of the (e) direction for ADCP observations and the AdriSC-ROMS 1 km model.

First, it should be noted that the IOR_Pal_ADCP dataset (Fig. 25) has a gap in observations in January and February (Fig. 25c). For the rest of the year, the AdriSC-ROMS 1 km model mostly underestimates the observed current speed by an average of -0.03 ± 0.01 m s^{-1} (Fig. 25a). The current direction (Fig. 20b) is also generally underestimated by -42 ± 29 ° to -8 ± 22 °. Seasonal vertical profiles of the modelled and observed current speed (Fig. 25d) show an underestimation of observations for all seasons. The lowest biases are present in winter and summer, reaching 0.03 m s^{-1} and 0.02 m s^{-1} on average, respectively. The largest current speed biases are in spring and autumn, averaging around 0.05 m s^{-1} and 0.04 m s^{-1}, respectively. The current direction rose plots (Fig. 25e) reveal that the model overestimates the occurrences of the main eastward and south-eastward current directions, while other directions are mostly underestimated, regardless of the season.

For the NAdEx_ADCP dataset (Fig. 26), the AdriSC-ROMS 1 km model properly reproduces the observed current speed with very small differences throughout the year, except in January and November when they reach up to 0.02 ± 0.00 m s^{-1} (Fig. 26a). Additionally, in this dataset, no observations were recorded in September and October (Fig. 26c). The monthly climatology of current direction (Fig. 26b) reveals relatively small differences, except in August and December when they reach down to -62 ± 17 °. Regarding the seasonal variations, the vertical profiles of the modelled speeds slightly underestimate the observed speeds by 0.01 m s^{-1} on average, except in autumn when the biases reach around 0.02 m s^{-1}. The rose plots (Fig. 26e) show that the observed current direction distributions are well reproduced by the model with small differences independently of the season.

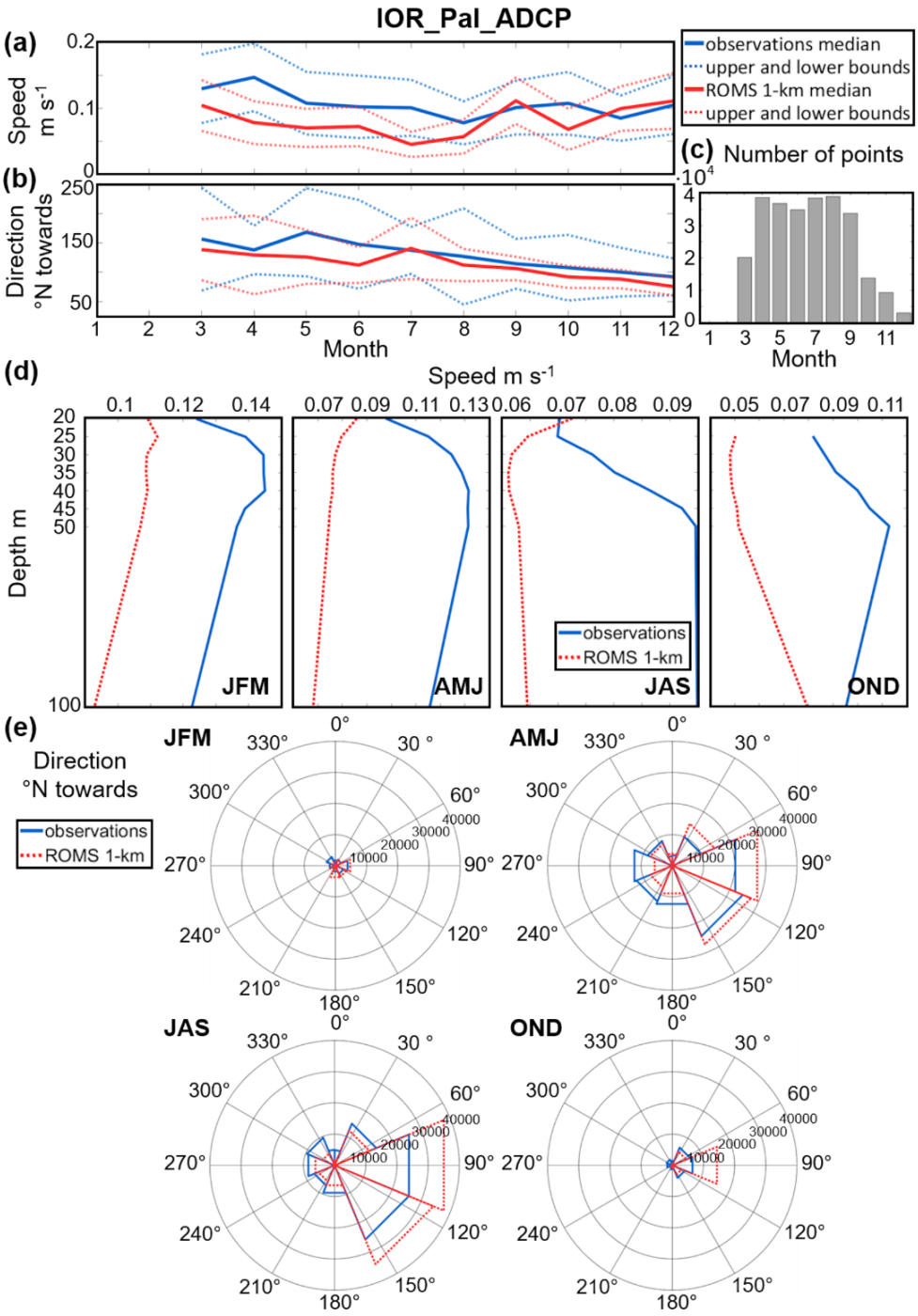

Figure 25. IOR_Pal_ADCP dataset. Monthly climatology of AdriSC-ROMS 1 km and *in situ* (a) median speed, (b) median direction and their variabilities (i.e. upper and lower bounds defined as ±MAD) as well as (c) number of observations per month. Seasonal variations of the (d) speed from the model and observations depending on the depth. Seasonal rose plots of the (e) direction for ADCP observations and the AdriSC-ROMS 1 km model.

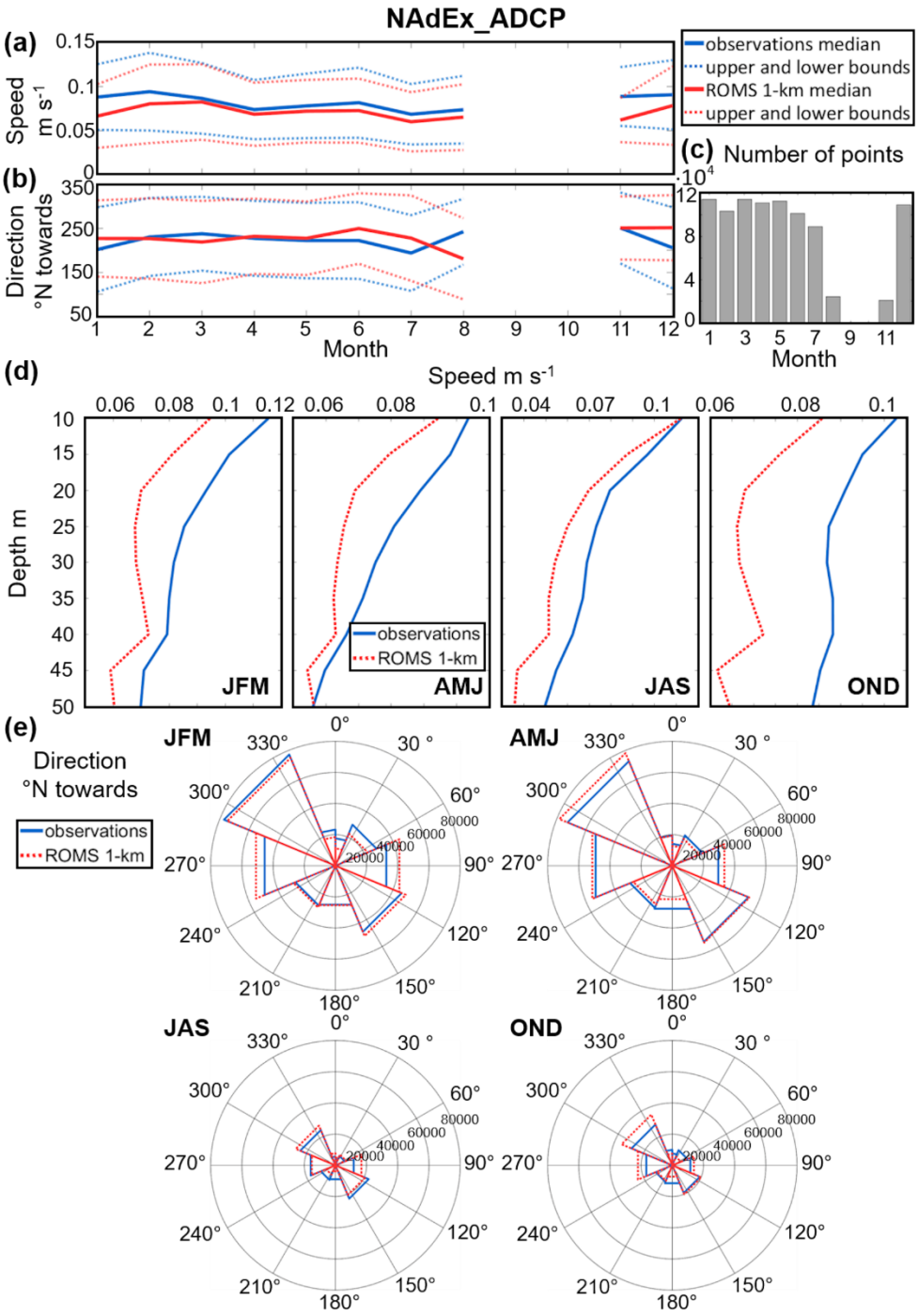

Figure 26. NAdEx_ADCP dataset. Monthly climatology of AdriSC 1–km and *in situ* (a) median speed, (b) median direction and their variabilities (i.e. upper and lower bounds defined as ±MAD) as well as (c) number of observations per month. Seasonal variations of the (d) speed from the model and observations depending on the depth. Seasonal rose plots of the (e) direction for ADCP observations and the AdriSC-ROMS 1 km model.

Lastly, the EACE dataset (Fig. 27) has a large gap in the observations from July to October (Fig. 27c). For the rest of the year, the AdriSC-ROMS 1 km model overestimates the observed current speed by up to 0.04 ± 0.02 m/s in winter, only 0.02 ± 0.00 m s^{-1} in December and underestimates down to -0.01 ± 0.00 m s^{-1} in spring (Fig. 27a). The current directions (Fig. 27b) are largely underestimated in January and February by -112 ± 79 ° and -119 ± 10 °, respectively. On the other hand, the direction differences are significantly smaller and positive in spring whereas negative in autumn. Seasonal vertical profiles of the modelled and observed current speeds (Fig. 27d) confirm the overestimation of observations in winter reaching 0.03 m s^{-1}, on average as well as a slight underestimation in spring up to 0.01 m s^{-1}. Finally, the current direction rose plots (Fig. 27e) reveal that the model underestimates in winter and overestimates in spring, the occurrences of the main northwestward current direction.

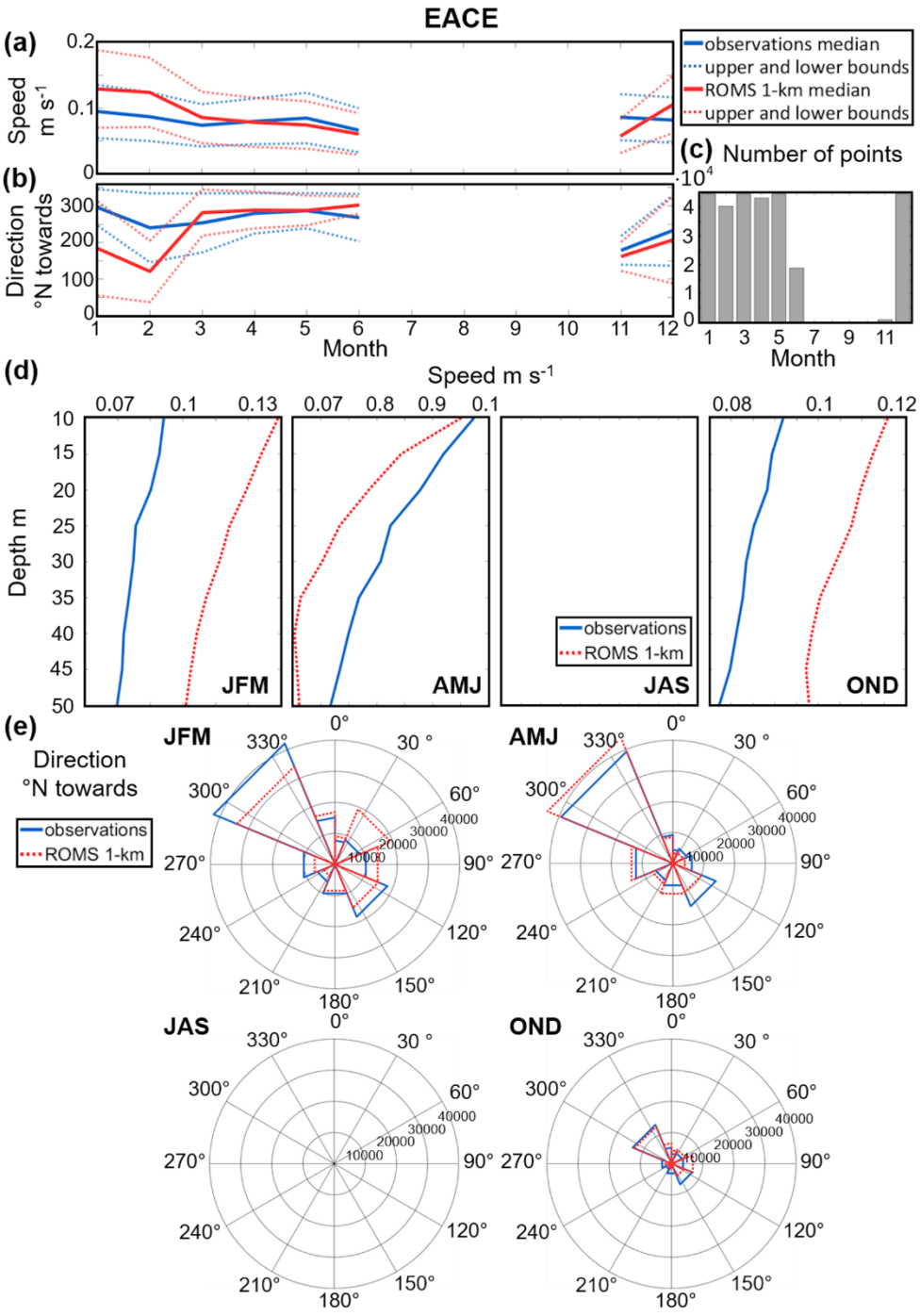

Figure 27. EACE dataset. Monthly climatology of AdriSC-ROMS 1 km and *in situ* (a) median speed, (b) median direction and their variabilities (i.e. upper and lower bounds defined as ±MAD) as well as (c) number of observations per month. Seasonal variations of the (d) speed from the model and observations depending on the depth. Seasonal rose plots of the (e) direction for ADCP observations and the AdriSC-ROMS 1 km model.

3.4. Discussion

The evaluation of the AdriSC-ROMS 3 km sea surface properties reveals that the model is capable of reproducing the BiOS, even though with a weaker intensity due to the overestimation of both seasonal and interannual signals. The SST is also quite well reproduced, despite presenting a persistent cold bias within the Adriatic Sea. In the Mediterranean climate community, the overall cold SST bias, which is present particularly during summer, is a well-known feature of ocean models. First, Akhtar et al. (2018), in their assessment of the impact of model resolution and coupling in the Mediterranean Sea, indicated that coupled atmosphere-ocean models are more likely to generate negative SST biases. Second, a comparison of SST results from six different models with remote sensing products (Darmaraki et al., 2019) revealed cold biases ranging from about -0.3 to -1.0 °C on average over the entire Mediterranean Sea. The cold summer SST biases are also known to be higher in the northern Adriatic Sea, reaching below -3 °C on average (e.g. L'Hévéder et al., 2013; Di Luca et al., 2014; Sevault et al., 2014; Parras-Berrocal et al., 2020). Consequently, it can be concluded that the results obtained with the AdriSC-ROMS 3 km model fall within the known ranges of cold SST biases of the Mediterranean models.

However, following these first results, the high-resolution AdriSC models also seem to improve the representation of summer SST, as the 25th percentile – which is most likely indicative of summer month biases – reaches a maximum value of -2 °C near the Po river and averages -0.75 °C over the entire Adriatic Sea. As explained in Parras-Berrocal et al. (2020), the cold summer SST biases of the AdriSC-ROMS 3 km model can result from (1) a deficit of solar radiation in the AdriSC atmospheric model, which exhibits systematic temperature underestimation (up to 5 °C) in summer (Denamiel et al., 2021b), (2) some intrinsic shortcomings of the AdriSC ocean model such as vertical mixing and turbidity, and (3) the method of imposing river temperatures by using the ERA-Interim skin temperatures near river estuaries, which is a crude approximation, particularly for larger Adriatic rivers such as the Po or the Albanian rivers. Also, it is known that the optical properties of water play a crucial role in modelling the turbidity, which is responsible for most of the downward shortwave radiation absorption in the upper layer and thus potentially the presence of cold SST biases. Hence, the evaluation of AdriSC-ROMS 3 km SST results highlights potential limitations in the implemented dQ/dSST procedure, aimed at mitigating issues linked to the optical properties of Adriatic waters.

Further, the evaluation of the AdriSC-ROMS 1 km thermohaline properties reveals that the model is generally capable of reproducing, with mostly good accuracy, the temperature and salinity in all analysed subdomains. In the middle Adriatic, the western coast, and the middle eastern coastal parts of the Adriatic (e.g. Dalmatian Islands subdomain), monthly climatologies are well represented. However, the largest biases are found in the surface layer (up to 50 m of depth) during summer with a maximum of ±1.0 °C for temperature and ±0.2 for salinity. These biases are most probably associated with the previously mentioned issues related to the optical properties of Adriatic waters and/or river discharges. Additionally, in the deepest parts of the southern Adriatic, as well as the Strait of Otranto and the northernmost part of the Ionian Sea, persistent negative temperature biases of about -0.25 °C on average are obtained, while the salinity biases remain lower than ± 0.1. However, in certain areas, at specific depths and times of the year, the AdriSC-ROMS 1 km model lacks accuracy. In general, the largest differences are found in the northern Adriatic, with negative temperature biases in summer (reaching down to -2.0 °C) and large positive salinity biases (up to 2.0) in the surface layer. As seen previously in the SST evaluation, the cold bias is likely linked to the improper estimation of the Po river temperature, while the overestimation of salinity for the lowest values may result from the improper estimation of Po freshwater fluxes. As similar results (i.e. overestimation of surface salinity and overestimation of the summer temperature in surface) are also found in the northeastern coastal part of the Adriatic and a large scatter of the lowest salinity values is present in Fig. 10, the AdriSC-ROMS models seem to struggle to reproduce the proper river plume dynamics in the northern Adriatic.

Nevertheless, these results represent an improvement compared to previous Mediterranean RCMs evaluated in the Adriatic Sea, which exhibited salinity biases above 3.0 and temperature biases below -3.0 °C in the northern Adriatic (e.g. L'Hévéder et al., 2013; Di Luca et al., 2014; Sevault et al., 2014; Parras-Berrocal et al., 2020). In the Jabuka Pit, where strong positive temperature biases are adjacent to negative ones, the representation of bathymetry by the model (e.g. 1 km resolution, flattening due to the smoothing procedure) may have influenced the location and amount of dense water collected. However, it should be noted that within the middle Adriatic subdomain, including the Jabuka Pit, the coldest more saline waters are well represented by the AdriSC-ROMS 1 km model, as evident in the T-S diagram. In addition, independently of the subdomains, the analysis of vertical profiles shows that temperature and salinity biases often present a peak near the thermocline or halocline depth, which could be attributed to an inaccurate representation of vertical diffusivity and vertical mixing in the

AdriSC-ROMS models. However, a more thorough investigation is required to discern whether the vertical biases stem from the AdriSC-ROMS model setup itself or from the MEDSEA fields used as initial and boundary conditions.

Furthemore, the evaluation of the AdriSC-ROMS 1 km dynamical properties reveals that the model is generally in good agreement with observed hourly ocean current speed and direction. However, there is a certain mismatch in time between the model results and observations, which may be ascribed to a lack of synchronization between hourly observations and model results, along with uncertainties linked to the observational dataset time references. This demonstrates the difficulties inherent in reproducing ocean dynamics and evaluating model results at the hourly scale. Concerning the datasets, the RCM measurements (i.e. IOR_Data_RCM dataset), mainly located along the eastern coast (including islands) and some offshore locations, are well reproduced by the model, with relatively small biases (up to ± 0.03 m s^{-1} for speed and a maximum of 50 ° for direction). The ADCP measurements of current speed in the middle eastern coastal area (i.e. JP1 and JP2 datasets) are relatively well captured (biases up to 0.04 m s^{-1}), while more significant differences arise for current direction (biases up to 87 °). In addition, a systematic underestimation of the occurrences of the main current directions may be linked to a misrepresentation of the coastline in the model at certain locations. Also, ocean current measurements along the transect across the Palagruža Sill (i.e. DART_ADCP and IOR_Pal_ADCP datasets) are modelled with a general underestimation of current speed (down to -0.05 m s^{-1}) and an overestimation of the occurrences of the main current direction, which can be linked to the bathymetry representation in the model (e.g. 1 km resolution, smoothing procedure).

Lastly, the ADCP measurements in the northeastern Adriatic (i.e. NAdEx_ADCP dataset) are reproduced mostly with good accuracy, with a slight underestimation of current speed (down to -0.02 m s^{-1}). However, this presents a significant improvement compared to the results of the ALADIN/HR-ROMS modelling system, which was evaluated on the same set of measurements from the NAdEx experiment (Vilibić et al., 2018). Indeed, the authors demonstrated that the model strongly underestimates the observed current speeds by 50 %–80 % on average, while the AdriSC-ROMS 1 km underestimates current speed by only 18 % on average. This highlights the fact that, in the northeastern Adriatic, higher horizontal and vertical ocean and atmospheric model resolutions, better resolving the complex bathymetry and orography, are required to reproduce the mesoscale variability of winds, particularly the hurricane-strength bora winds, as demonstrated by Denamiel et al. (2021).

4. MULTI–MODEL ANALYSIS OF THE ADRIATIC DENSE-WATER DYNAMICS

This chapter analyses different state-of-the-art modelling approaches to dense-water dynamics during the 2014–2015 period. The results of the following four different simulations are analysed and compared: the latest reanalysis product for the Mediterranean Sea, a recently evaluated fine-resolution atmosphere-ocean Adriatic Sea climate model, and a long-running Adriatic Sea atmosphere-ocean forecast model used in both hindcast and data assimilation modes.

4.1. Comparative evaluation during the 2014–2015 period

A brief comparative evaluation of the four simulations is performed in order to quantify the skills of the ocean models against 18987 CTD measurements (Fig. 28c). The number of observations, depending on the depth, is (1) 7698 for the 0–50 m range, (2) 7582 for the 50–200 m range, (3) 2130 for the 200–500 m range, and (4) 1577 for the 500–1200 m range. The observations partially cover the northern Adriatic, the Kvarner Bay, the Palagruža Sill, and the SAP.

A Taylor diagram (Fig. 28a) illustrates the correlations and normalized standard deviations of the modelled and observed temperature and salinity for each simulation. For MEDSEA, the correlations for temperature and salinity are 0.77 and 0.01, respectively, representing the lowest values among all simulations, while the standard deviations are 1.20 and 0.48, respectively. ROMS-hind and ROMS-full show almost the same correlations (approximately 0.94) for temperature, with standard deviations of 0.93 and 1.01, respectively. For salinity, the correlations are 0.90 and 0.93, and the standard deviations are 0.84 and 0.89, respectively. The AdriSC-ROMS correlation is 0.92 for temperature and 0.89 for salinity, with standard deviations of 0.99 and 0.64, respectively. Based on the Taylor diagram, MEDSEA demonstrates overall poorer performance compared to ROMS-hind/full and AdriSC-ROMS, which show similar results.

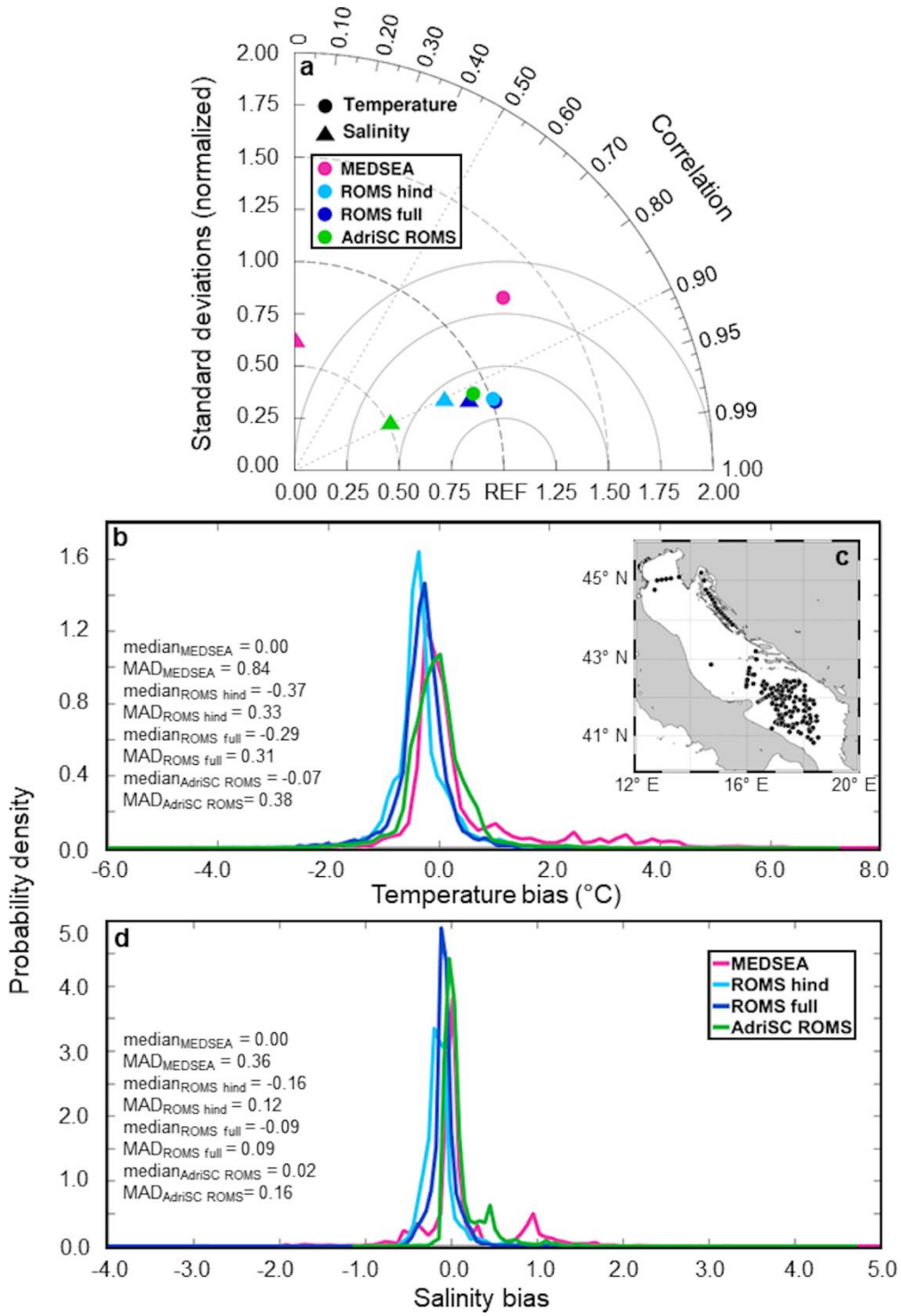

Figure 28. Comparison of the results of the four simulations against CTD observations in the form of (a) a Taylor diagram, (b) probability density functions of the biases between the model results and *in situ* (b) temperature and (d) salinity observations, and (c) a map with the locations of CTD observations (black dots).

For the temperature biases (Fig. 28b), the ROMS-hind distribution has a median of -0.37, associated with a large peak, and a MAD of ± 0.33 °C. The ROMS-full distribution has a smaller peak and a median of -0.29 ± 0.30 °C. The MEDSEA distribution has a median of 0.00 ± 0.84 °C, with a heavier tail of positive biases up to 4.5 °C. The AdriSC-ROMS distribution has the lowest peak and a median of -0.04 ± 0.61 °C. Therefore, the ROMS simulations systematically underestimate the sea temperature, but the assimilation reduces the biases. The median temperature bias is smaller in AdriSC-ROMS and MEDSEA, but they have the largest MADs due to an overestimation of temperatures in MEDSEA (up to 4.5 °C) and both an over- and underestimation of temperatures between -2 and +2 °C in AdriSC-ROMS.

For the salinity biases (Fig. 28d), the ROMS-hind distribution has the lowest peak and a median of -0.16 ± 0.12. The ROMS-full distribution has a larger peak and a median of -0.09 ± 0.09. The MEDSEA distribution has a median of 0.00 ± 0.36, a tail of negative biases down to -2.0, and a heavy tail of positive biases with a secondary peak at approximately 1.0. The AdriSC-ROMS distribution has a slightly larger peak than MEDSEA and a median of 0.02 ± 0.16, with very low probabilities for negative biases below -0.2 but a heavy tail up to around 1.0 and a secondary peak around 0.4. Hence, the ROMS-full and hind simulations both underestimate the observed salinities, but the assimilation reduces the biases. The AdriSC-ROMS model tends to overestimate the salinity, while the MEDSEA results display the largest over- and underestimations of salinities.

In addition, the comparison of the performance of models with different resolutions may be affected by the double-penalty effect (Crocker et al., 2020). This effect implies that, in pointwise comparison with observations, the finer-resolution models tend to be penalized more than the coarser-resolution models, potentially leading to worse verification results. When a model has sufficient resolution to reproduce a small-scale feature but simulates it incorrectly, it is penalized twice: once for not reproducing the feature where it should have been and once for simulating it where it has not been observed. Contrarily, if a model resolution is not sufficient to reproduce a feature, it will be penalized only once for not capturing the feature. This phenomenon might partially explain why the AdriSC-ROMS model (1 km resolution) presents larger bias variability in both temperature and salinity compared to the ROMS-hind and ROMS-full models (2 km resolution).

4.2. Analysis of the extremes

To analyse how the different models capture the extremes during the 2014–2015 period, the spatial distributions of daily maximum wind stresses, daily maximum upward turbulent heat fluxes, and their associated timing are presented in Fig. 29 and 30, while the spatial distributions of daily maximum bottom PDAs, minimum temperatures and maximum salinities, along with their associated timing, are presented in Fig. 31, 32 and 33, respectively.

4.2.1. Wind stresses and upward turbulent fluxes

It should be noted that ERA5, which forces the MEDSEA reanalysis, produces very small wind stresses over the whole basin (Fig. 29a), barely reaching 0.4 N m^{-2} in the northern Adriatic, while ALADIN-HR-hind and ALADIN-HR-full wind stress results (Fig. 29c, e) are extremely similar despite the variational scheme of the assimilation changing the wind stresses (i.e. the differences between the ALADIN-HR-hind and full wind stresses are at least an order of magnitude smaller than their differences in relation to the other atmospheric models). Further, AdriSC-WRF, the only kilometre-scale atmospheric model used in this comparison, generates the largest extremes overall for both wind stresses (> 1.5 N m^{-2} ; Fig. 29g) and upward turbulent heat fluxes (> 1100 W m^{-2} ; Fig. 30g). However, for the upward turbulent fluxes, ERA5 produces maximum heat losses comparable to AdriSC-WRF (Fig. 30a, g), while ALADIN-HR-full maximum heat losses are at least two times smaller than in ALADIN-HR-hind (Fig. 30c, e). In fact, ALADIN-HR-full has the smallest maximum heat losses of all simulations and shows a patchy spatial distribution, with the smallest values over the middle of the northern Adriatic, barely reaching 750 W m^{-2} in February–March. Therefore, both MEDSEA and ALADIN-HR-full are strongly influenced by the assimilation (e.g. sea surface temperature coming from remote sensing products or variational changes of the heat flux forcing, respectively).

Another important point is that the turbulent heat fluxes are strongly influenced by the sea surface temperature and relative humidity, which are, in turn, influenced by solar radiation. The maximum heat losses are thus more likely to be found in December 2014–January 2015 – due to a difference in air-sea temperatures of about 3–4 °C having a larger contribution to the upward turbulent heat flux calculation than the intensity of the wind stresses (Fairall et al., 1996) – than in early February–March 2015, when the temperature differences are smaller. In the northern Adriatic, the Trieste jet is seen by both ALADIN-HR models and the AdriSC-WRF, with wind stress maxima reaching 0.8 and 1.3 N m^{-2}, respectively.

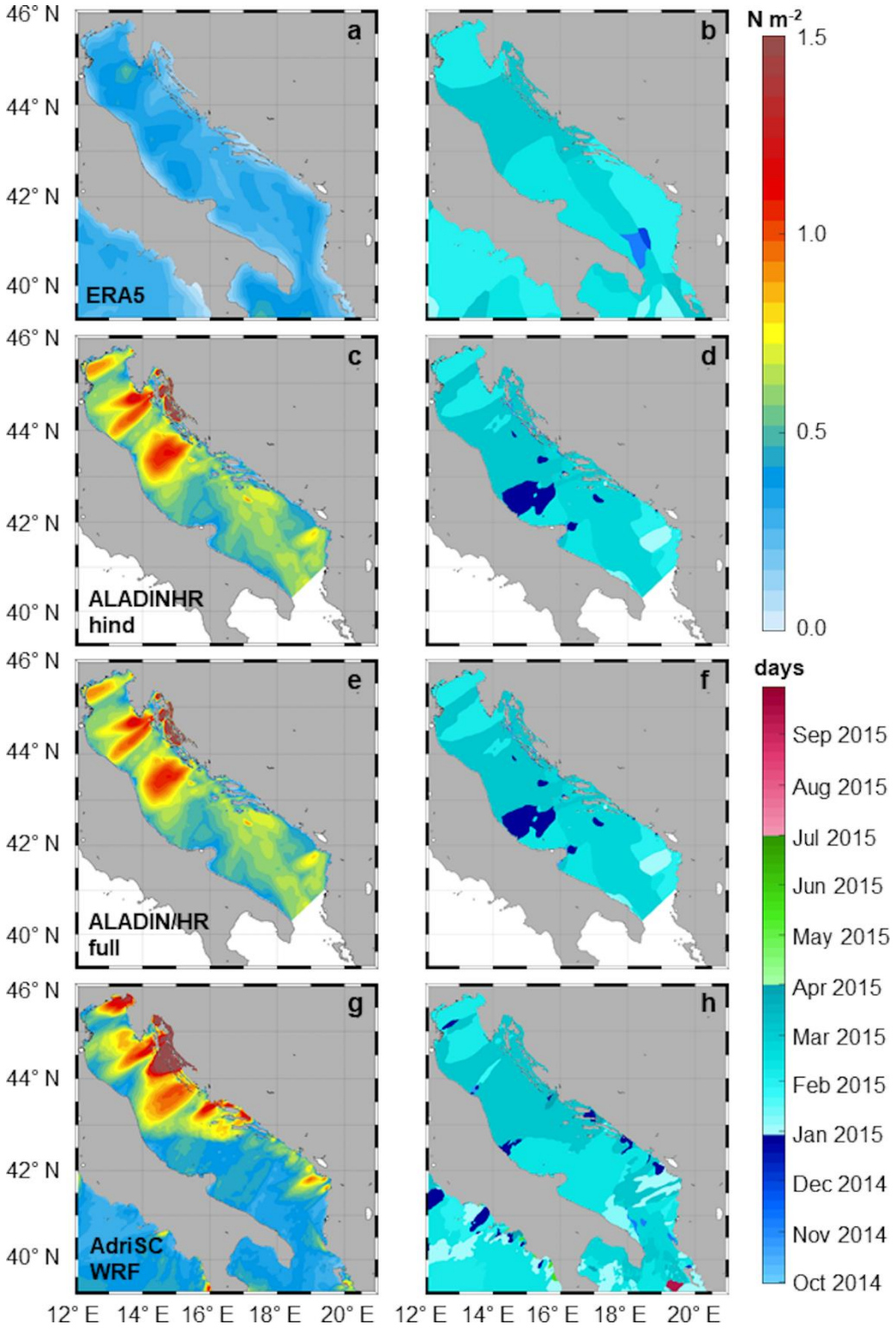

Figure 29. Spatial distribution of maximum surface wind stresses and their corresponding timing for (a, b) ERA5, (c, d) ALADIN-HR-hind, (e, f) ALADIN-HR-full, and (g, h) AdriSC-WRF.

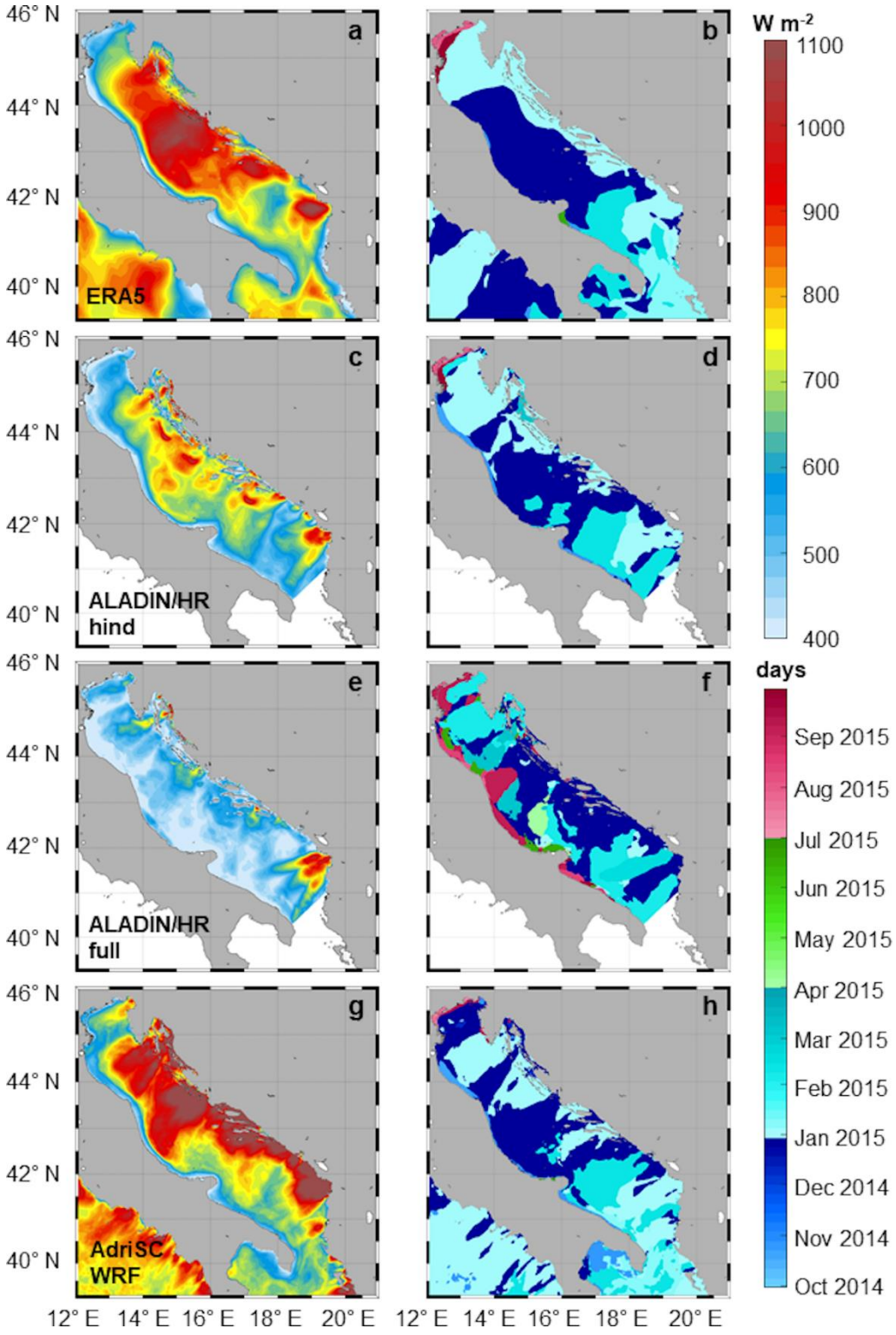

Figure 30. Spatial distribution of maximum upward turbulent heat fluxes and their corresponding timing for (a, b) ERA5, (c, d) ALADIN-HR-hind, (e, f) ALADIN-HR-full, and (g, h) AdriSC-WRF.

It is also important to highlight that the Trieste jet produced by both ALADIN-HR models is extended further offshore than in the AdriSC-WRF simulation. For the upward turbulent fluxes, ERA5 and both ALADIN-HR simulations produce a small intensity along the Trieste jet (less than 600 W m^{-2}) between January and March 2015, while AdriSC-WRF reaches 850 W m^{-2} in December 2014. The largest values of maximum wind stresses are found in the Kvarner Bay and along the Senj jet for all simulations, including ERA5. They reach up to 1.3 N m^{-2} for both ALADIN-HR models and more than 1.5 N m^{-2} for AdriSC-WRF over a far wider area than the other models. In this region, for the upward turbulent heat fluxes, the maximum values are reached by ERA5 (i.e. 900 W m^{-2} despite not reproducing the bora jets) and AdriSC-WRF (larger than 1100 W m^{-2}), while ALADIN-HR-hind and ALADIN-HR-full reach 850 W m^{-2} and barely 750 W m^{-2}, respectively.

In the middle Adriatic, strong wind stresses up to 1.2 N m^{-2} for both the ALADIN-HR models and the AdriSC-WRF model are produced along the Karlobag and Sukošan jets. However, AdriSC-WRF extends the Karlobag jet to the middle of the Adriatic, with values (up to 1.5 N m^{-2}) several times larger than those achieved with the ALADIN-HR simulations. It also produces some strong wind stresses up to 1.3 N m^{-2} along the Dalmatian coast, where other bora jets are known to be located. In terms of upward turbulent fluxes, the maximum values are, on average, 900 W m^{-2} for ERA5, 800 W m^{-2} for ALADIN-HR–hind, larger than 400 W m^{-2} for ALADIN-HR-full, and larger than 1100 W m^{-2} along the eastern Adriatic coast for AdriSC-WRF. In the southern Adriatic, maximum wind stresses in ALADIN-HR-hind and ALADIN-HR-full reach up to 0.7 N m^{-2} but are smaller along the coastline. In the AdriSC-WRF simulation, the wind stresses remain relatively small in the southern Adriatic (less than 0.5 N m^{-2}) aside from a small patch of larger values off the southern Montenegrin coast. For the upward turbulent fluxes, the results obtained with ERA5 and AdriSC-WRF are quite similar, with strong intensities along the eastern coast (on average, 900 and 1000 W m^{-2}, respectively) and values less than 700 W m^{-2} offshore.

Overall, for all models, maxima of wind stresses are associated with bora events, while upward turbulent heat fluxes seem to be influenced by the seasonal variations of the sea surface temperature (SST) more than by the wind stresses. In other words, the largest input to the upward turbulent heat fluxes comes from the bora wind, yet a small fraction – found to influence maxima of the heat fluxes – comes from SST. This is the reason why maxima of heat fluxes occur mostly during bora episodes in late December to early February (Fig. 30), whereas the maxima of wind stresses occur mostly during bora episodes in early February to early

March (Fig. 29). Additionally, the AdriSC-WRF model generates the strongest dynamics with, on average, the strongest maximum wind stresses and the maximum heat losses, while ERA5 has the weakest wind stresses, and ALADIN/HR–full has the smallest heat losses.

4.2.2. Potential density anomalies

In the northern Adriatic, all simulations produce the highest maximum PDA values during late winter (February–March 2015; Fig. 31b, d, f, h). They reach up to 29.4 kg m^{-3} on the shelf for MEDSEA; up to 29.6 kg m^{-3} along the coast but below 29.3 kg m^{-3} on the shelf for ROMS-hind; up to 29.8 kg m^{-3} along the coast and, on average, 29.5 kg m^{-3} on the shelf for ROMS-full; and finally, above 29.8 kg m^{-3} along the coast and, on average, 29.7 kg m^{-3} for AdriSC-ROMS (Fig. 31a, c, e, g).

In the Kvarner Bay, both MEDSEA and ROMS-hind have extremely small maximum PDAs (below 29.0 kg m^{-3}), indicating no dense-water formation in this area. In contrast, both ROMS-full and AdriSC-ROMS produce large maximum PDAs (up to 29.6 and 29.7 kg m^{-3}, respectively). However, ROMS-full presents patch-like PDA distributions, with maxima occurring partly during winter and partly during spring, while AdriSC-ROMS has more homogeneous values over the whole Kvarner Bay, with maxima occurring mostly in winter but also in September in a few very small areas.

Further, off the Kvarner Bay, ROMS-full produces a large patch of extremely dense waters (> 29.8 kg m^{-3}), which does not seem to be smooth and continuous with the previous data assimilation cycle spatial PDA distributions over the rest of the Adriatic domain. In this case, data assimilation corrects the initial state of the ocean model at the start of the assimilation cycle as the most cost-effective mechanism for correcting suboptimal atmospheric (hydrostatic and coarser) forcing and ocean model vertical and horizontal resolution constraints. Also, this patch occurred in February and is located just southwest from the glider data assimilated in the model, which is the strongest contributor to the data assimilation cost function at this point (Janeković et al., 2020).

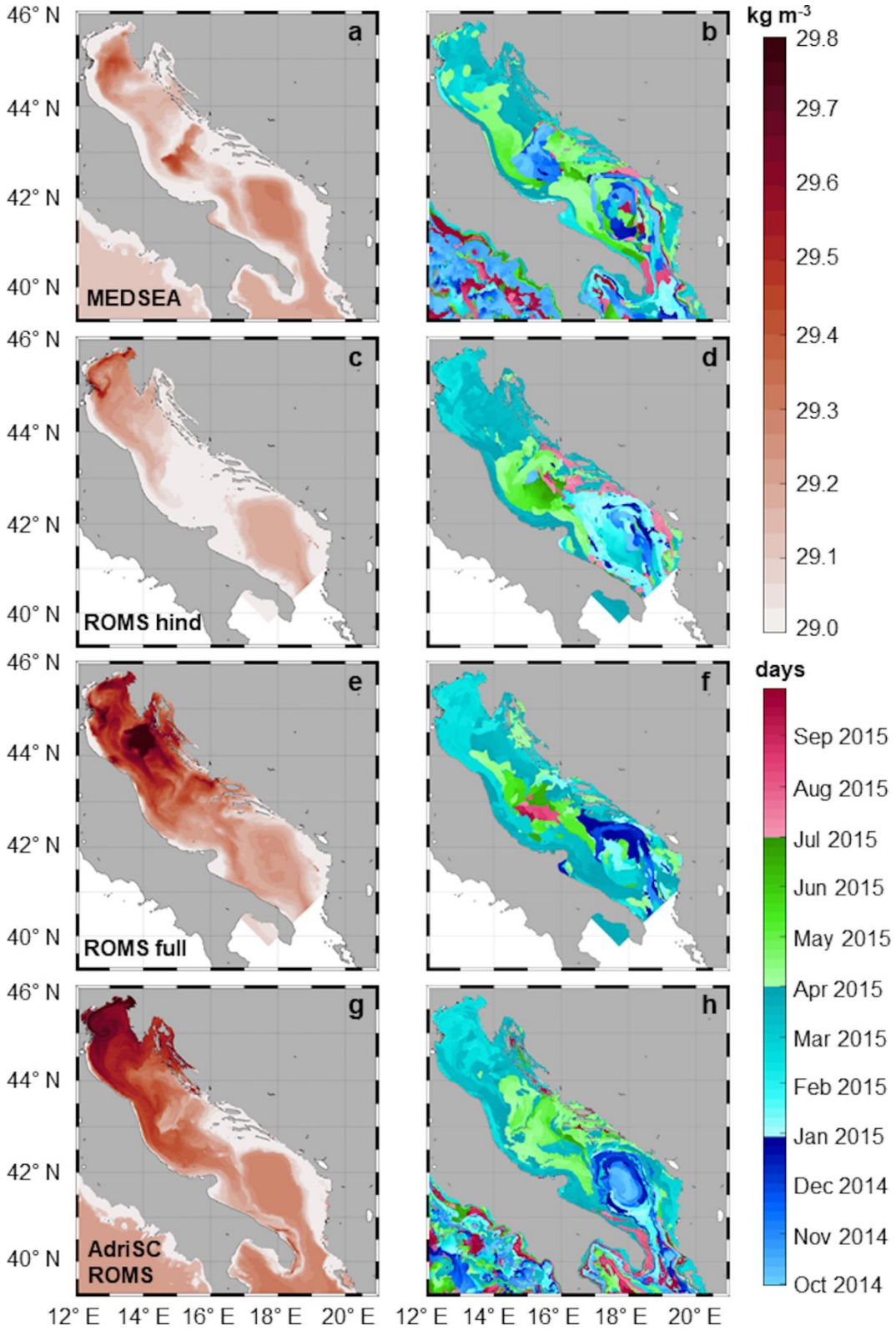

Figure 31. Spatial distribution of maximum bottom PDAs and their corresponding timing for (a, b) MEDSEA, (c, d) ROMS-hind, (e, f) ROMS-full, and (g, h) AdriSC-ROMS.

In the middle Adriatic, ROMS-hind shows relatively low maximum PDAs (below 29.1 kg m^{-3}), but the other models present interesting spatial variations. In the Jabuka Pit, which is a known dense-water reservoir, maximum PDAs reach up to 29.5 kg m^{-3} in MEDSEA during autumn 2014 (i.e. the highest PDA values over the entire basin), up to 29.6 kg m^{-3} in ROMS-full during spring and summer, and only up to 29.4 kg m^{-3} in AdriSC-ROMS during spring.

Further, in ROMS-full and AdriSC-ROMS simulations, the PDA maxima are highest in the western part of the middle Adriatic in late winter and spring, resembling the dense-water outflow that normally peaks up to two months after its generation in the northern Adriatic. However, in ROMS-full, some high values of maximum PDAs (about 29.4 kg m^{-3}) are also present along the Dalmatian islands, which is not an area known for the formation or accumulation of dense waters due to the extensive freshwater discharge of the Neretva River. In the southern Adriatic, within the SAP and mostly during winter, maximum PDAs reach up to 29.4 kg m^{-3} in MEDSEA, only 29.2 kg m^{-3} in ROMS-hind, up to 29.3 kg m^{-3} in ROMS-full, and up to 29.4 kg m^{-3} in AdriSC-ROMS. Along the western side of the SAP, where dense waters are known to cascade through canyon systems (Rubino et al., 2012), ROMS-full and AdriSC-ROMS produce some transport of dense waters (> 29.3 kg m^{-3}), mostly in late spring for AdriSC-ROMS and in March for ROMS-full. Also, MEDSEA, ROMS-hind, and AdriSC-ROMS present relatively low maximum PDAs (< 29.0 kg m^{-3}) in the coastal area east of the SAP, a shelf strongly influenced by the Albanian rivers (Artegiani et al., 1997), while ROMS-full has slightly higher values reaching up to 29.2 kg m^{-3}.

Overall, in the northern Adriatic and the Kvarner Bay, where the dense waters are generated during strong bora events, MEDSEA and ROMS-hind have smaller maximum PDAs (29.4 and 29.6 kg m^{-3}, respectively) than ROMS-full and AdriSC-ROMS (29.7 and 29.8 kg m^{-3}, respectively). However, in AdriSC-ROMS, extreme dense waters are generated homogeneously over the entire northern Adriatic, while they appear as patches in ROMS-full, with a maximum found off the southern tip of Istria, along the Senj jet. This can be attributed to the 4D-Var data assimilation four-day cycling which updates the initial state of the ROMS model. Surprisingly, in the Jabuka Pit – a known collector of the dense waters – the PDAs of ROMS-full are higher than in the AdriSC-ROMS simulation, indicating that either AdriSC-ROMS is overly dissipative or that the impact of assimilation is significant in ROMS-full. In the SAP, maximum bottom PDAs are produced in all simulations, generally during late autumn and early winter (December 2014–January 2015), indicating that northern Adriatic dense waters did not reach the bottom of the SAP by the end of any simulation.

Additionally, the spatial distributions of minimum bottom temperature and the corresponding timing of the minimums for the four simulations are shown in Fig. 32. In general, the lowest temperatures are produced in the northern Adriatic, reaching down to 5 °C, along the western coast and in Kvarner Bay, while highest minimums are found in the shallower parts of southern Adriatic, reaching up to 15 °C. For MEDSEA, minimum temperatures mostly occurred in winter, particularly in the western part of the middle Adriatic during spring, whereas in the Jabuka Pit minimum temperatures were produced in autumn 2014 (Fig. 32a and b). For ROMS-hind, the main difference is in the Jabuka Pit, where the minimums occurred in summer (Fig. 32c and d). ROMS-full minimums mostly happened in winter but also in spring in a part of Kvarner Bay and in the middle Adriatic (Fig. 32e and f). It can be seen that ROMS-full produced the smallest temperatures in a patch in the northern Adriatic. For AdriSC-ROMS, temperature minimums are also present mostly in winter, while in parts of the middle Adriatic, including the Jabuka Pit, they occurred in spring (Fig. 32g and h). In the SAP, minimums are mostly produced in autumn, and partly in winter and spring by all models.

The spatial distributions of maximum bottom salinity, along with the corresponding timing of the maximums, are displayed on Fig. 33 for all simulations. The smallest maximum salinities are obtained in the northern Adriatic, Kvarner Bay and along the western coast, with values reaching down to 38.2, while the largest salinities are produced in the southern Adriatic up to 39.2. MEDSEA results are characterized by the biggest contrast between these areas. Maximums occurred in summer, mainly in the coastal areas, whereas in the middle Adriatic they predominantly happened in autumn (Fig. 33a and b). ROMS-hind results resemble MEDSEA results but with slightly smaller maximums in the middle and southern Adriatic. The timing of the maximum salinities is mostly in late autumn and winter, as well as in summer in parts of northern Adriatic and some coastal areas (Fig. 33c and d). To summarize, ROMS-full produced slightly larger maximums than ROMS-hind, with the largest differences offshore of Kvarner Bay. Also, maximums are mostly produced in winter in the northern Adriatic and Kvarner Bay, in summer along the western coast and in spring in the middle Adriatic (Fig. 33e and f). AdriSC-ROMS results revealed large maximum salinities (above 38.5) over the whole Adriatic except in very narrow coastal parts. The timing of the maximums is mostly in summer for the northern and northeastern Adriatic, as well as along the eastern coast, whereas the rest of the Adriatic reached maximum salinity in autumn (Fig. 33g and h).

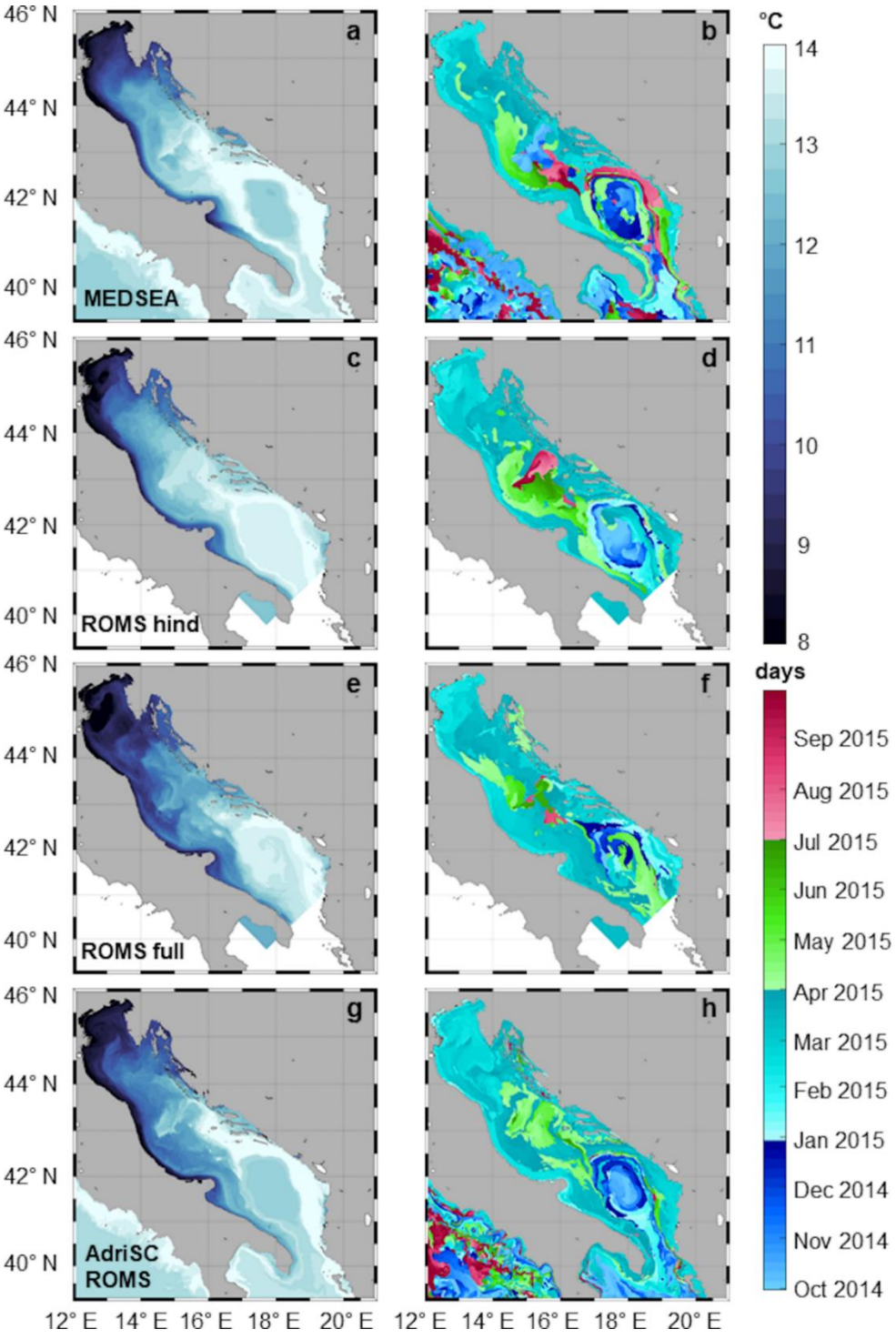

Figure 32. Spatial distribution of minimum bottom temperature and corresponding time of the minimums for (a, b) MEDSEA, (c, d) ROMS-hind, (e, f) ROMS-full and (g, h) AdriSC-ROMS.

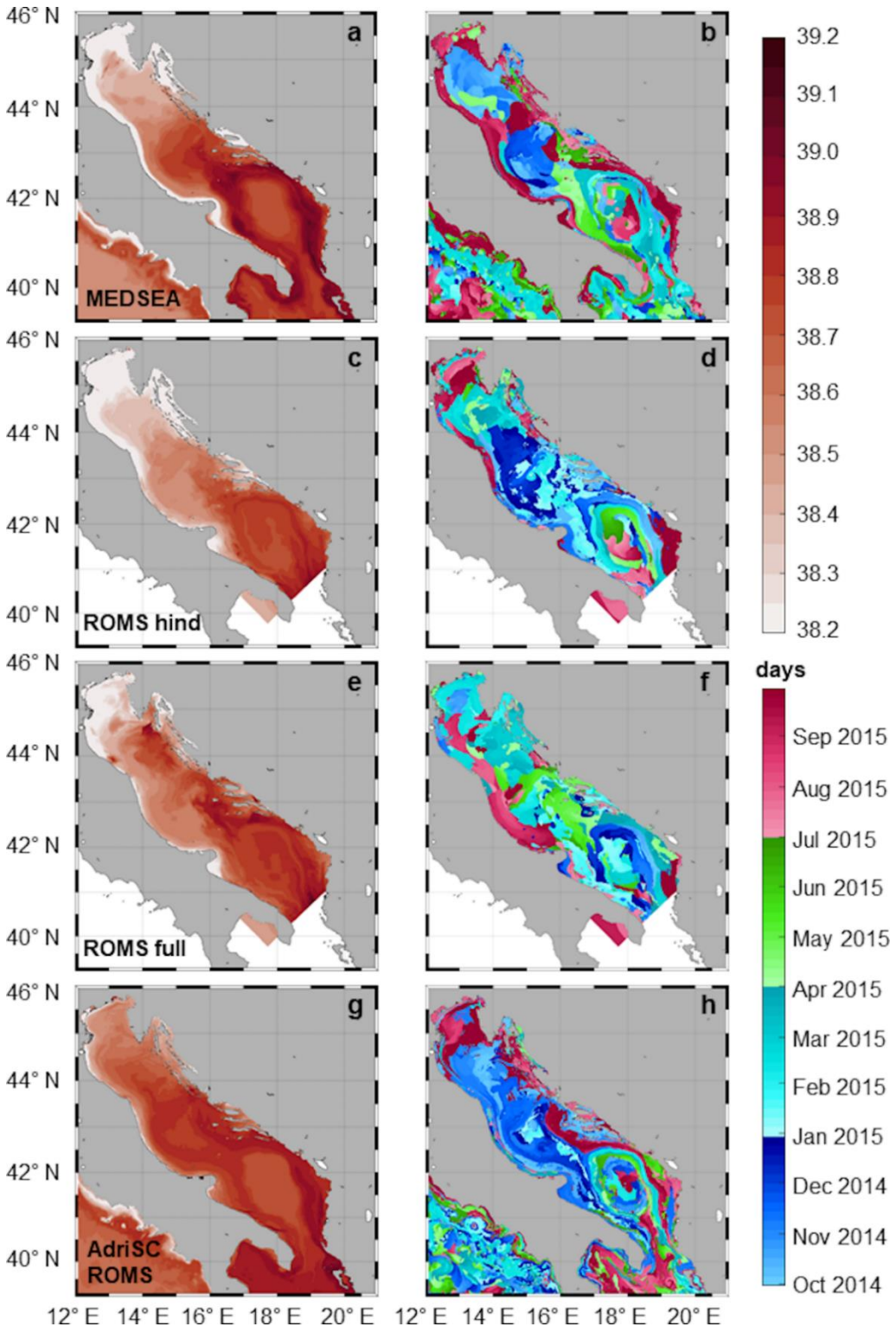

Figure 33. Spatial distribution of maximum bottom salinity and corresponding time of the maximums for (a, b) MEDSEA, (c, d) ROMS-hind, (e, f) ROMS-full and (g, h) AdriSC-ROMS.

4.3. Dense-water dynamics

4.3.1. Subdomain-averaged time series

To better understand how the different models capture the dense-water dynamics within the Adriatic basin, the daily results are presented as time series spatially averaged over the known sites of generation and collection of dense waters (Fig. 34–38). In the northern Adriatic, all models present three prominent peaks of wind stresses (Fig. 34a), capturing the three severe bora events that occur during the NAdEx campaign over the following dates: 28 December 2014–1 January 2015, 3–7 February, and 3–6 March 2015. These dominant wind stress events are also associated with peaks of upward turbulent heat fluxes in all models (Fig. 34c). However, the intensities of the ERA5 wind stress peaks (0.15, 0.3, and 0.2 N m^{-2}) are half those in ALADIN-HR-full, ALADIN-HR-hind, and AdriSC-WRF, which are all similar (peaks at 0.3, 0.6, and 0.5 N m^{-2}). Further, the intensity of the upward turbulent heat flux peaks is often smaller and more spread or shifted over time in ALADIN-HR-full (peaks at 300, 450, and 300 W m^{-2}) than in the other models due to the variational scheme used in the assimilation. It should be noted that the strongest peaks in upward turbulent heat fluxes are always reached by ERA5 and/or AdriSC-WRF (peaks at 600, 400, and 350 W m^{-2}), while ALADIN-HR-hind produced slightly smaller intensities in general (peaks at 500, 350, and 300 W m^{-2}).

Concerning the associated bottom PDA time variations (Fig. 35a), it should be first noted that the AdriSC-ROMS PDAs are systematically higher than in the other models by 0.2–0.8 kg m^{-3} due to higher salinity (differences of about 0.3–0.6; Fig. 38a). Second, for all simulations, the maximum values are obtained between February and March 2015, when the dense-water generation occurs (Vilibić et al., 2018). Further, in February 2015, a large increase of bottom PDAs – probably driven by the assimilation of the Arvor-C, towed CTD, and glider data, which influenced two four-day cycles – is seen in ROMS-full, which reaches values nearly as high as those in AdriSC-ROMS.

The PDAs without seasonality show that all models reproduce the peaks in density due to the bora-driven dense-water formation (Fig. 36a). ROMS-full consistently shows the highest increases in density during these peaks (0.4, 0.35, and 0.3 kg m^{-3}), while MEDSEA reaches the lowest values (below 0.1 kg m^{-3} for the three peaks). However, the MEDSEA and AdriSC-ROMS densities already increased before the first bora event by 0.2 kg m^{-3}, which means that, in fact, the highest peak is reached by AdriSC-ROMS after the first bora event and that MEDSEA density anomalies are close to AdriSC-ROMS values. The PDAs without

seasonality also clearly show a density decrease during spring and summer in all models, when the denser waters are transported from the northern Adriatic towards the south.

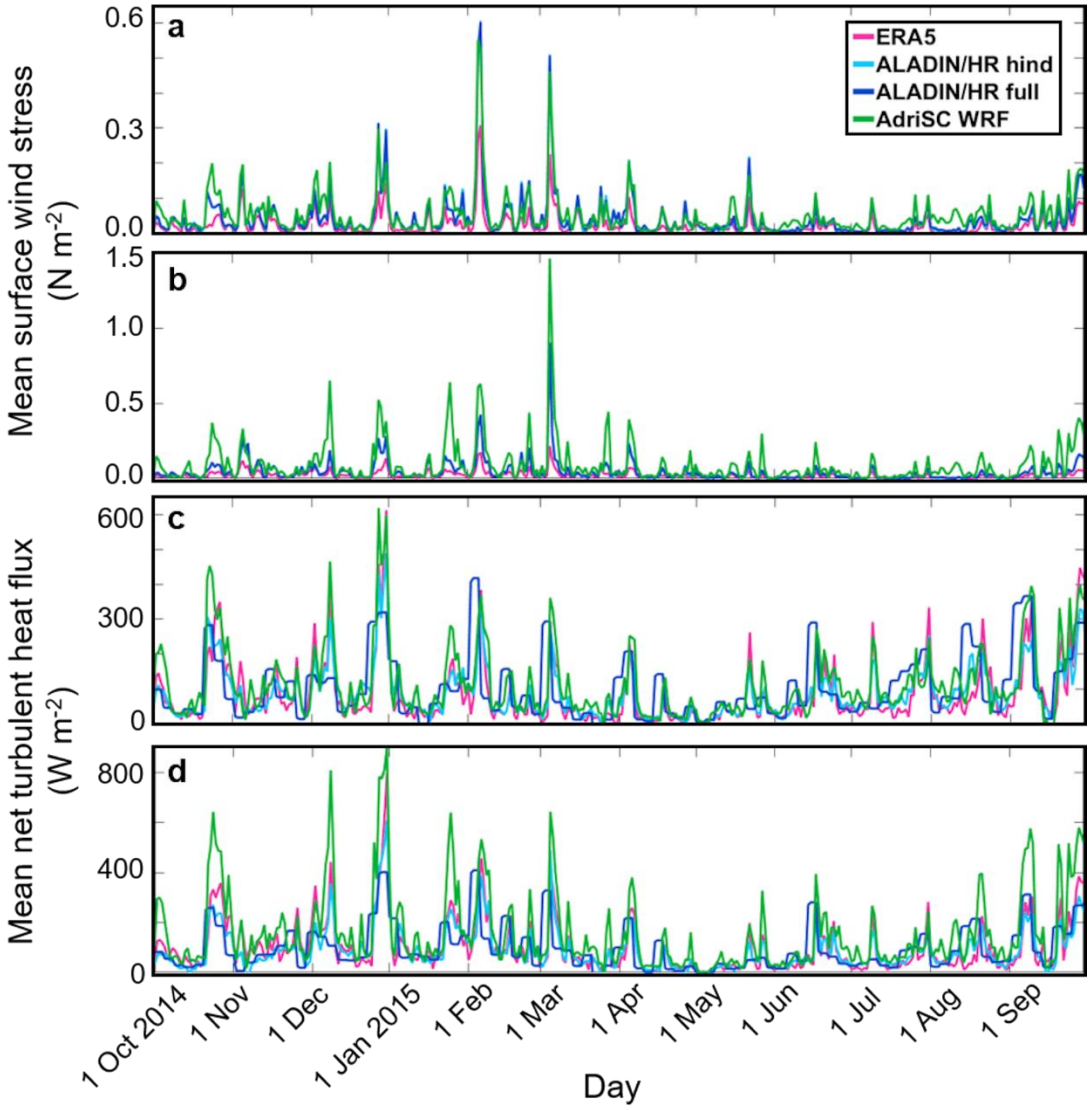

Figure 34. Time series of daily wind stresses and upward turbulent heat fluxes averaged over two subdomains, namely (a, c) the northern Adriatic and (b, d) Kvarner Bay, for the 2014–2015 period and for the four simulations.

In the Kvarner Bay, the three bora peaks of wind stresses (Fig. 34c) and the associated upward turbulent heat fluxes (Fig. 34d) are also seen by all models. However, ERA5-computed wind stresses are always extremely low (below 0.2 N m^{-2}), while AdriSC-WRF produces stronger wind stresses (peaks at 0.5, 0.6, and 1.5 N m^{-2}) compared to ALADIN-HR-full and ALADIN-HR-hind (peaks at 0.25, 0.4, and 0.9 N m^{-2}). The intensity of the upward turbulent heat flux peaks is again consistently lower and more spread or shifted over time in ALADIN-HR-full (peaks at 400, 400, and 300 W m^{-2}) than in the other models (peaks as large as 800,

500, and 600 N m^{-2}). Also, AdriSC-WRF model produces eight wind stress peaks above 0.25 N m^{-2} between December 2014 and April 2015, while ALADIN-HR-hind and ALADIN-HR-full only surpass this threshold for the three main bora events. That is, the non-hydrostatic kilometre-scale AdriSC-WRF model (at 3 km resolution) demontrates the capability to reproduce much higher wind stresses than the hydrostatic ALADIN-HR model (at 8 km resolution, dynamically downscaled to 2 km for the winds only). This is attributed to the impact of the highly non-linear orographic processes on the dynamics of the bora-driven flows (e.g. Grubišić, 2004; Kuzmić et al., 2015). Next, the upward turbulent heat fluxes are less intense in ERA5 and ALADIN-HR-hind than in AdriSC-WRF, indicating smaller cooling rates, which thus should lead to less generation of dense waters.

In terms of bottom PDA analysis (Fig. 35b), similar to the northern Adriatic subdomain, the AdriSC-ROMS model produces the largest values, while MEDSEA and ROMS-hind generally have the smallest values, with differences up to 0.6 kg m^{-3} in February–March 2015. This difference is again mostly driven by salinity, which is the lowest in MEDSEA and again the highest in AdriSC-ROMS (Fig. 38). However, salinity is significantly higher in ROMS-full than in ROMS-hind starting in December 2014, when near-bottom salinity measurements were available continuously in the Kvarner Bay through the NAdEx campaign. Convincingly, these measurements influenced the ROMS-full run, shifting it from ROMS-hind towards the higher measured salinities and closer to the AdriSC-ROMS results.

As for the northern Adriatic subdomain, the PDAs without seasonality show three main peaks linked to bora-driven dense-water formation in all models (Fig. 36b). However, the timing and intensity of the ROMS-full peaks generally differes from the other models (which all behave quite similarly), particularly after the second and third bora events. This shows the impact of assimilating observations from the NAdEx campaign in the ROMS-full model.

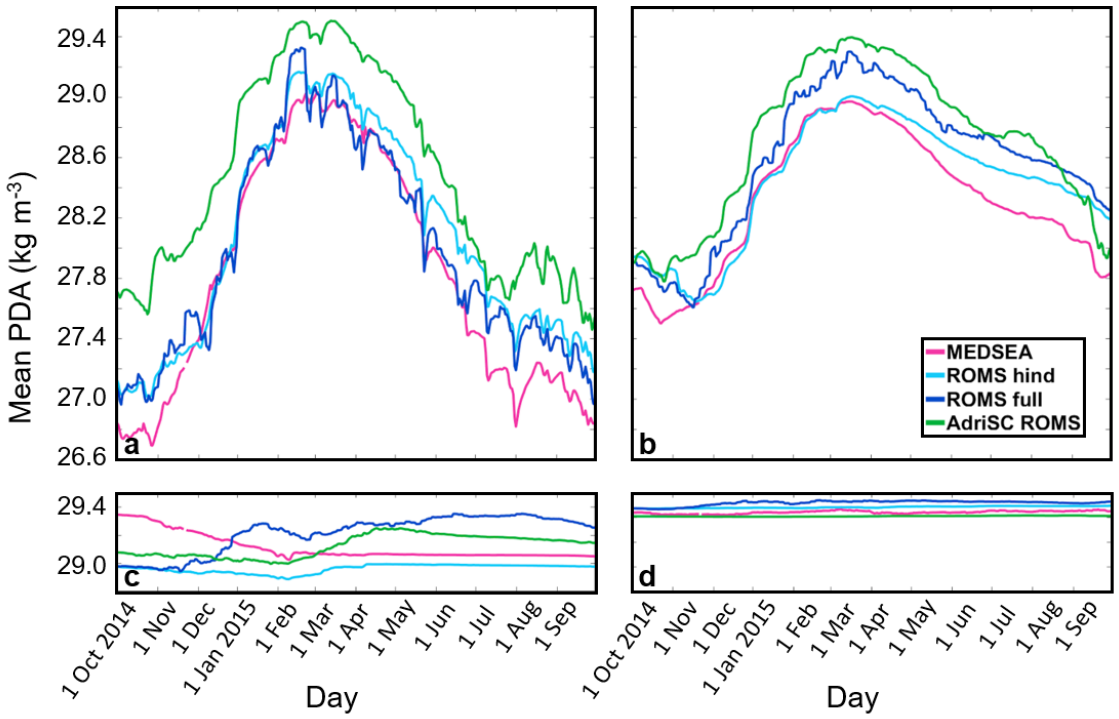

Figure 35. Time series of daily bottom PDAs averaged over four subdomains, namely (a) the northern Adriatic, (b) Kvarner Bay, (c) the Jabuka Pit, and (d) the deep Adriatic, for the 2014–2015 period and for the four simulations.

In the Jabuka Pit (Fig. 35c and 36c), bottom PDAs (with and without seasonality) from the two free model runs (AdriSC-ROMS and ROMS-hind) start increasing from February 2015, coinciding with the arrival of newly generated denser waters from the northern Adriatic, and peak in late April 2015. However, AdriSC-ROMS PDAs are larger than those of ROMS-hind in terms of both mean values (more than 29.1 kg m^{-3} vs. less than 29.0 kg m^{-3}) and, in particular, increase rates (0.2 kg m^{-3} in two months vs. less than 0.1 kg m^{-3} in two months) during the known arrival time of dense waters in the Jabuka Pit (i.e. between March and June 2015). It should be noted that ROMS-full shows an earlier increase in PDAs during December 2014 and January 2015, reaching up to 29.3 kg m^{-3}, similar to the values obtained in AdriSC-ROMS in late April. This increase is probably driven by the availability of measurements during that period. Later, after a small decrease between February and March 2015, ROMS-full PDAs slowly increase until summer. Unlike other simulations, MEDSEA starts with large PDA values in autumn (higher by about 0.2–0.3 kg m^{-3} than other simulations), which then decrease by March down to values slightly higher than those of ROMS-hind and stabilize until September 2015. This indicates that MEDSEA does not capture dense-water arrival in the Jabuka Pit during spring 2015.

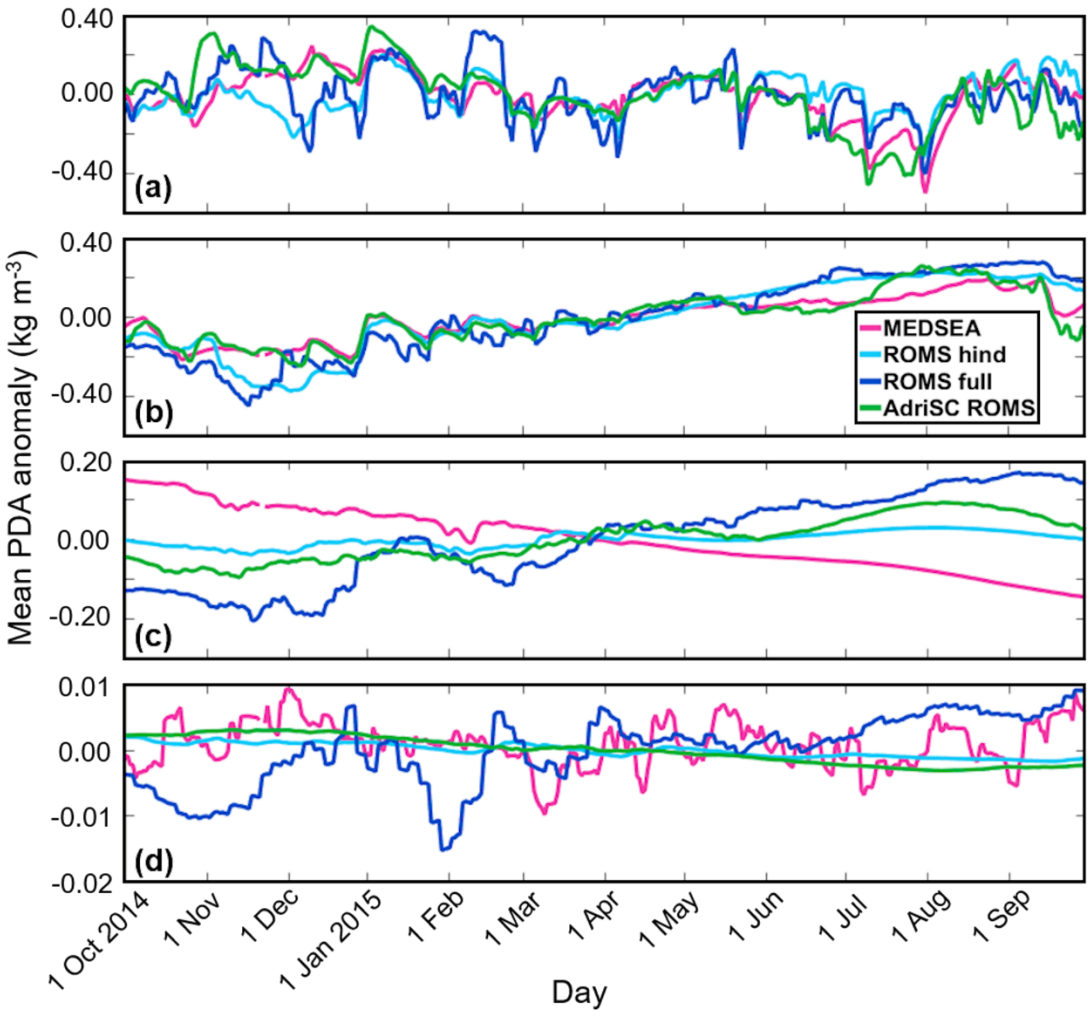

Figure 36. Time series of daily bottom PDAs without seasonality averaged over four subdomains, namely (a) the northern Adriatic, (b) Kvarner Bay, (c) the Jabuka Pit, and (d) the deep Adriatic, for the 2014–2015 period and for the four simulations.

In the deep Adriatic (Fig. 35d), bottom PDA values are comparable in all models, with slightly larger values in ROMS-hind and ROMS-full and smaller values in MEDSEA and AdriSC-ROMS. Further, temporal changes in PDAs are larger in ROMS-full and MEDSEA, as they assimilate deep observations (e.g. by Argo profilers up to 700–800 m), which were available throughout the 2014–2015 period (Kokkini et al., 2020), as can be clearly seen in the PDAs without seasonality (Fig. 36d).

Overall, the analysis of the time series spatially averaged over the subdomains where dense waters are either generated (i.e. the northern Adriatic and Kvarner Bay) or collected (the Jabuka Pit and deep Adriatic) confirms the results obtained for the extreme values. First, the AdriSC climate simulation generates the strongest dynamics among all the models during the bora

events, with the highest intensities in wind stress, upward turbulent heat flux, and bottom PDA (except in the Jabuka Pit and the deep Adriatic). Second, the MEDSEA model, closely followed by the ROMS-hind model, generates the lowest levels of dense waters during the December 2014–March 2015 period. The assimilation in ROMS-full, despite reducing the intensity of the upward turbulent fluxes, tends to increase the bottom PDA values in all the subdomains but particularly in the Kvarner Bay and the Jabuka Pit.

In addition, time series of daily bottom temperature and salinity in four subdomains for all simulations are shown on Fig. 37 and 38, respectively. First, in the northern Adriatic subdomain (Fig. 37a), the largest differences in modelled temperature occurred in autumn 2014 and summer 2015 when MEDSEA gives the highest mean temperatures reaching 20.8 °C in October and 20.3 °C in September, while the other modelled temperatures are around 1–1.5 °C lower. In contrast, winter and spring temperatures have better matching between simulations with smaller differences. The mean temperature minimum in the northern Adriatic occurs at the end of February and beginning of March for all simulations. However, ROMS-full stands out with an uneven temperature curve near the minimum and the lowest values. The mean salinity results (Fig. 38a) reveal a large positive bias in AdriSC-ROMS results ranging from 0.3–1.1 with respect to other simulations.

All models produce maximum mean salinity in summer and minimum values in December 2014, when ROMS-full shows a sharp minimum up to 37, while the other models have higher values. ROMS-hind and ROMS-full mostly differ from March to August with a positive bias around 0.2 for ROMS-hind, whereas ROMS-full shows a sharp minimum in December up to 37. MEDSEA salinity is generally lower than all the other models with a few exceptions.

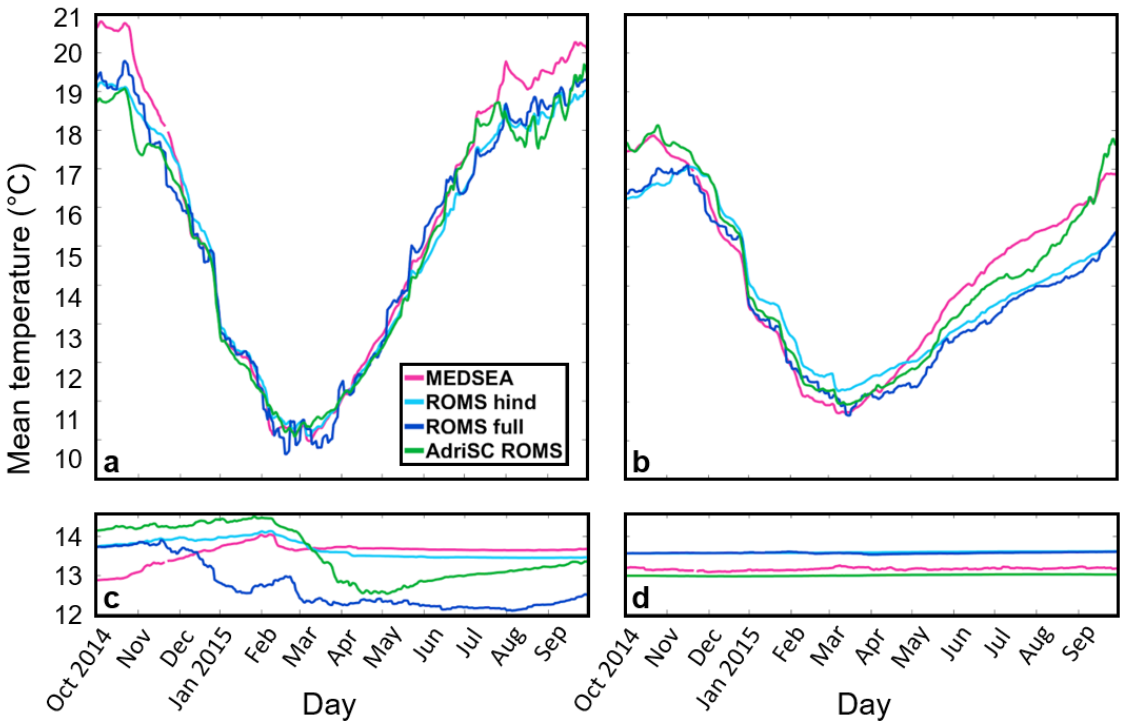

Figure 37. Time series of daily bottom temperature averaged over four subdomains: (a) northern Adriatic, (b) Kvarner Bay, (c) Jabuka Pit and (d) deep Adriatic for the 2014–2015 period and four simulations.

Second, in the Kvarner Bay subdomain (Fig. 37b), the autumn temperatures are more than 1 °C higher for AdriSC-ROMS and MEDSEA than for ROMS-hind and ROMS-full. ROMS-hind temperatures are generally little higher than ROMS-full over the entire 2015. During winter, all simulations give relatively similar results, while the differences become larger in spring and summer. AdriSC-ROMS and MEDSEA showed similar temperatures to ROMS-full until April when the biases increased by up to 1–2 °C. Regarding the mean salinity (Fig. 38b), as in the previous subdomain, AdriSC-ROMS showed a large positive bias up to 0.6, as well as a similar timing of the minimums and maximums for all simulations. In the entire 2015, ROMS-full salinities are higher than ROMS-hind, particularly during February and March whereas the MEDSEA salinities are mostly very low compared to other models. The obtained salinities in Kvarner Bay are generally higher than in the northern Adriatic, particularly in late autumn and winter.

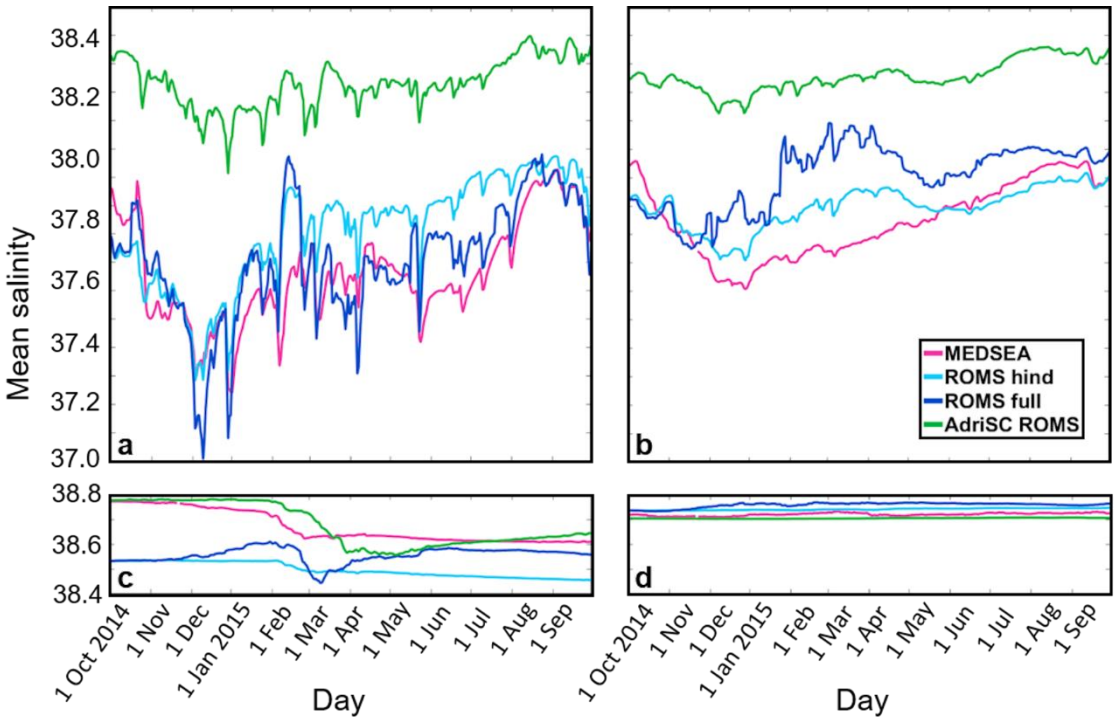

Figure 38. Time series of daily bottom salinity averaged over four subdomains: (a) northern Adriatic, (b) Kvarner Bay, (c) Jabuka Pit and (d) deep Adriatic for the 2014–2015 period and four simulations.

Third, in the Jabuka Pit subdomain (Fig. 37c), the models show the mean temperature quite differently. AdriSC-ROMS gave higher temperatures until March (up to 14.5 °C), followed by a decrease to around 12.5 °C in April and then a gradual increase. Both ROMS-full and ROMS-hind exhibited similar temperatures (around 13.8 °C) by December, when ROMS-full started decreasing, reaching a minor peak in February and continued to decrease until it reached almost 12 °C. In contrast, ROMS-hind increased up to 14 °C until mid-February, then decreased and remained around 13.5 °C throughout the year. MEDSEA results resemble ROMS-hind but with lower values in autumn. Regarding the mean bottom salinity, AdriSC-ROMS gives similar results to MEDSEA but with a minimum ocurring a month later. The ROMS-full and ROMS-hind salinities are lower than in other models by around 2.5 in autumn (Fig. 38c). ROMS-full produced an increase in winter, a minimum in March and another increase during spring, while ROMS-hind slightly decreased throughout 2015.

Lastly, in the deep Adriatic subdomain (Fig. 37d), the mean bottom temperature remains nearly monotonic for all simulations. ROMS-full and ROMS-hind demonstarted the highest values, while AdriSC-ROMS showed the lowest temperatures, differing by 0.5 °. MEDSEA results are slightly higher than those of AdriSC-ROMS. Mean salinity is similarly produced in

the deep Adriatic for all models (Fig. 38d). Larger values are obtained with ROMS-full and smallest values with the AdriSC-ROMS simulation.

4.3.2. Time evolution of the bottom PDA spatial distributions

To better visualize the evolution in time and space of dense waters, the spatial distributions of the daily bottom PDAs are analysed on specific dates:. 1 March (Fig. 39), 1 April (Fig. 40), 1 May (Fig. 41), and 1 June 2015 (Fig. 42), as well as throughout the 2014–2015 period. Before the first bora event on 28 December 2014, dense waters are mostly present in the deep Adriatic, with bottom PDA values ranging from 29.2 kg m^{-3} for ROMS-hind and ROMS-full to over 29.3 kg m^{-3} for MEDSEA and AdriSC-ROMS. However, in the Jabuka Pit, MEDSEA shows PDA values up to 29.5 kg m^{-3} in November 2014, which slowly decrease to 29.2 kg m^{-3} before the first bora event, whereas ROMS-full produces values below 29.25 kg m^{-3} around 20 December 2014. During the first bora event, in AdriSC-ROMS (and not in other models), dense waters (above 29.4 kg m^{-3}) are immediately generated along the northern Adriatic coast (i.e. along the Trieste jet). These dense waters are then transported toward the Po River delta and the northern Adriatic shelf. Denser waters (exceeding 29.45 kg m^{-3}) are generated and transported in AdriSC-ROMS from the Gulf of Trieste at the end of January and also in the Kvarner Bay in both AdriSC-ROMS (with values up to 29.3 kg m^{-3}) and ROMS-full (with values up to 29.45 kg m^{-3}).

Further, in ROMS-full, just before the second bora event, patches of extremely dense waters (above 29.4 kg m^{-3} and up to more than 29.5 kg m^{-3}) emerge on the northern Adriatic shelf and offshore from the Kvarner Bay. At the same time, in AdriSC-ROMS, the dense waters start to be transported from the northern Adriatic shelf towards the western Adriatic coast, along the Po River plume. Between the second bora event and 3 March 2015 (i.e. the third bora event), a larger amount of dense water is generated in the northern Adriatic (along the Trieste jet and in the shelf) by all models, with PDA surpassing 29.5 kg m^{-3} in AdriSC-ROMS and in ROMS-hind and ROMS-full, and up to 29.4 kg m^{-3} in MEDSEA. However, it should be noted that MEDSEA only registers dense waters on the northern shelf, not along the Trieste jet. Furthermore, a larger amount of dense waters (above 29.5 kg m^{-3}) are generated within and off the Kvarner Bay and transported along the Po River plume towards the Jabuka Pit and the southern Adriatic in ROMS-full and AdriSC-ROMS. However, due to the availability of assimilated measurements, ROMS-full first generates dense waters off the Kvarner Bay and

then within bay. In contrast, AdriSC-ROMS clearly transports the dense waters generated within the Kvarner Bay westward along the bora jets.

On 1 March 2015 (Fig. 39), dense waters start to be collected within the Jabuka Pit in both ROMS-full and AdriSC-ROMS, while no dense water is transported that far south in MEDSEA and ROMS-hind. Between the third bora event and 1 April 2015, for ROMS-full and AdriSC-ROMS, after an initial increase along the bora jets, dense waters (above 29.5 kg m^{-3}) are transported along the western coast from the northern Adriatic and the Kvarner Bay towards the south and partially collected in the Jabuka Pit. ROMS-hind also shows some dense-water transport (with PDAs barely reaching 29.2 kg m^{-3}) from the northern Adriatic towards the Jabuka Pit. However, in MEDSEA, the dense waters generated in the northern shelf (up to 29.45 kg m^{-3}) seem to slowly dissipate without being transported.

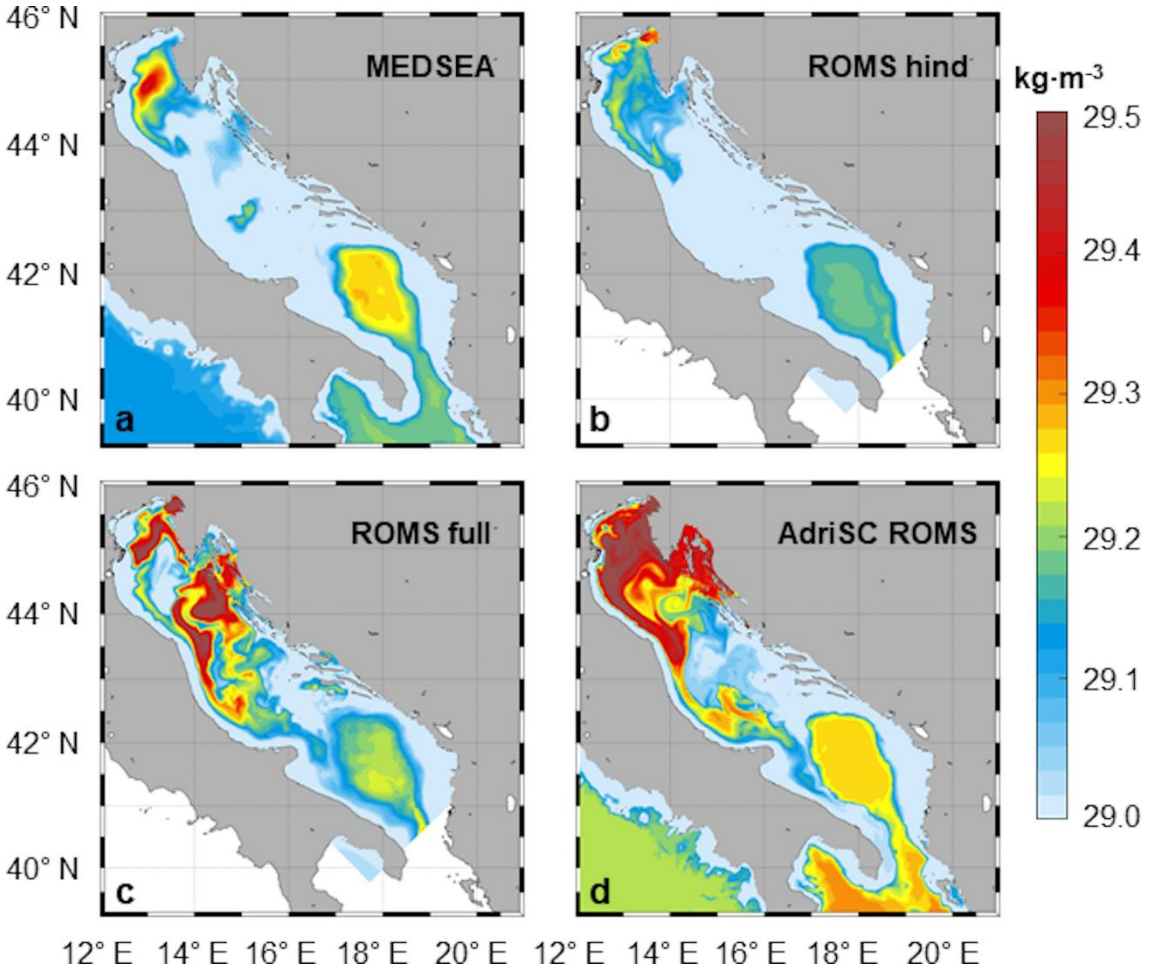

Figure 39. Spatial distribution of bottom PDAs on 1 March 2015 for (a) MEDSEA, (b) ROMS-hind, (c) ROMS-full, and (d) AdriSC-ROMS simulations.

On 1 April (Fig. 40), the northern Adriatic dense waters decreased to PDA values below 29.3 kg m^{-3} in MEDSEA, barely reaching 29.2 kg m^{-3} in ROMS-hind, mostly below 29.35 kg m^{-3} in AdriSC-ROMS, and they even totally disappeared in ROMS-full. For ROMS-full and AdriSC-ROMS, dense waters (up to 29.35 and above 29.5 kg m^{-3} , respectively) still remain within the Kvarner Bay. Between 1 April and 1 May 2015, in ROMS-full and AdriSC-ROMS, continuous transport towards the south results in a larger amount of dense waters being collected in the Jabuka Pit, from where they start to cascade towards the SAP via the deepest parts of the Palagruža Sill (Rubino et al., 2012). Notably, the cascading occurs along a narrower and more western path in AdriSC-ROMS compared to ROMS-full.

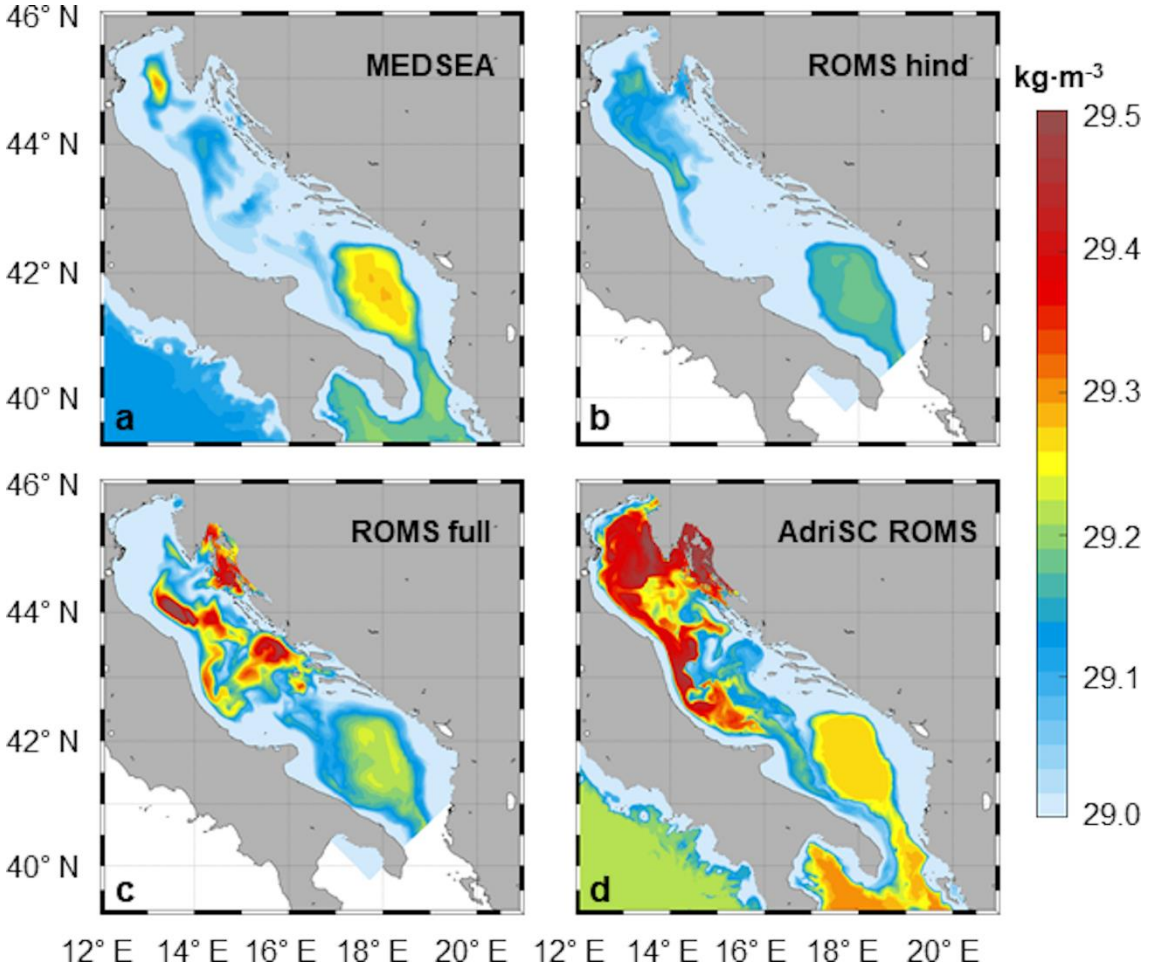

Figure 40. Same as in Fig. 12 but for 1 April 2015.

On 1 May 2015 (Fig. 41), no dense water is present in the MEDSEA and ROMS-hind models, except within the SAP. Dense waters (PDA above 29.3 kg m^{-3}) remain within the Kvarner Bay, the Jabuka Pit, and along the western coast in ROMS-full and AdriSC-ROMS. Between 1 May and 1 June 2015, the remaining dense waters are either transported towards the south or, for the most part, collected within the Kvarner Bay and the Jabuka Pit in both ROMS-full and AdriSC-ROMS. The collection of dense waters within the Kvarner Bay (particularly in AdriSC-ROMS, where PDAs are above 29.45 kg m^{-3} over most of the bay) can be explained by the fact that this area is much deeper than the open northern Adriatic. On 1 June 2015 (Fig. 42), however, the dense waters collected within the Jabuka Pit have much higher PDAs in ROMS-full (above 29.4 kg m^{-3}) than in AdriSC-ROMS (below 29.3 kg m^{-3}) despite AdriSC-ROMS clearly producing a greater amount of dense waters during the three bora events. This can be explained either by AdriSC-ROMS being too dissipative or by the strong impact of the assimilation in ROMS-full.

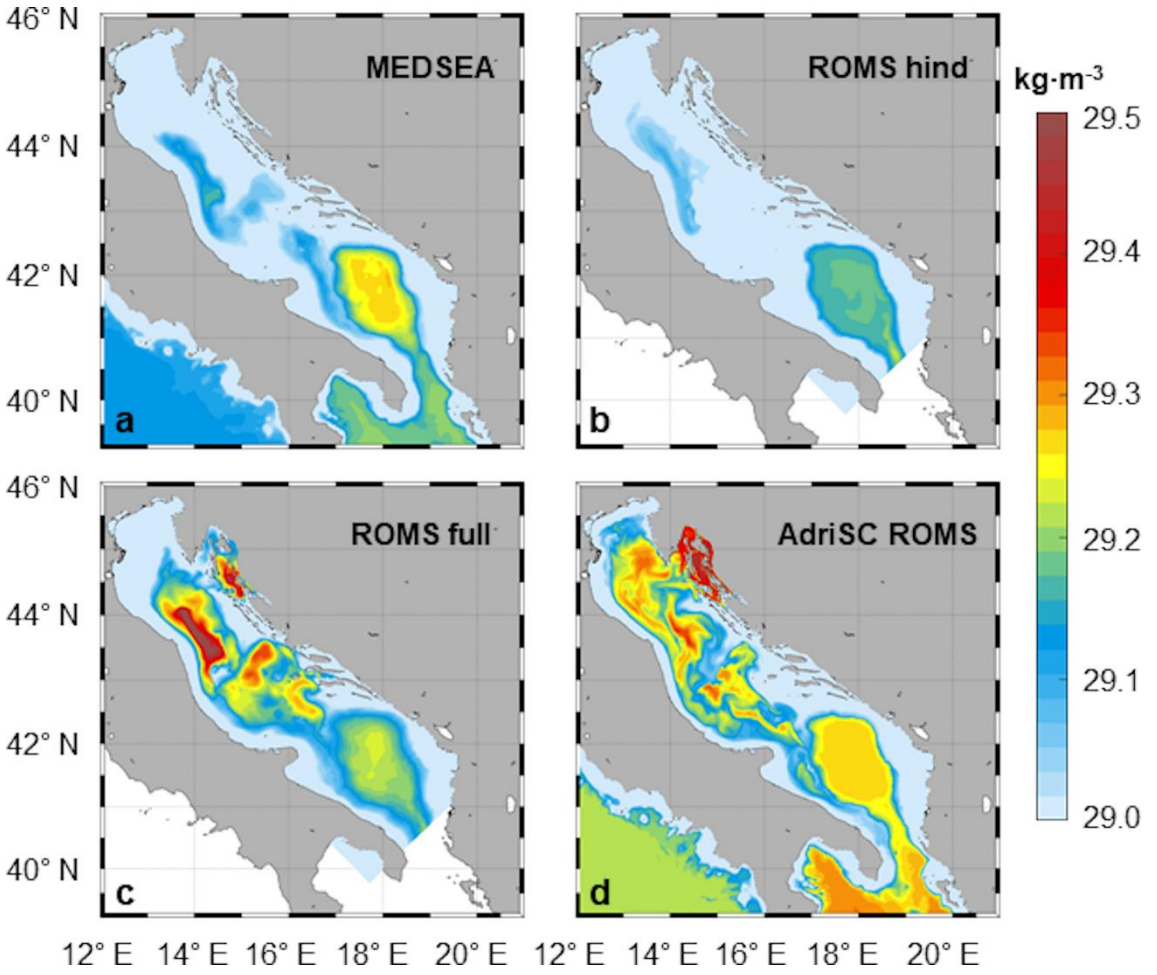

Figure 41. Same as in Fig. 12 but for 1 May 2015.

After 1 June 2015 (Fig. 42), dense waters remain within the Kvarner Bay until the end of June in ROMS-full and until the end of September in AdriSC-ROMS. Within the Jabuka Pit, they remain until the end of September, with PDA values above 29.25 kg m^{-3} in ROMS-full but barely reaching 29.2 kg m^{-3} in AdriSC-ROMS. Overall, AdriSC-ROMS generates a larger amount of dense waters compared to other models due to its stronger atmospheric forcing, while MEDSEA and ROMS-hind do not properly reproduce the dense-water dynamics in the Adriatic basin. However, ROMS-full collects a larger amount of dense waters in the Jabuka Pit than all the other models. These findings suggest that AdriSC-ROMS is probably too dissipative during the transport of dense waters from the northern Adriatic and Kvarner Bay towards the south.

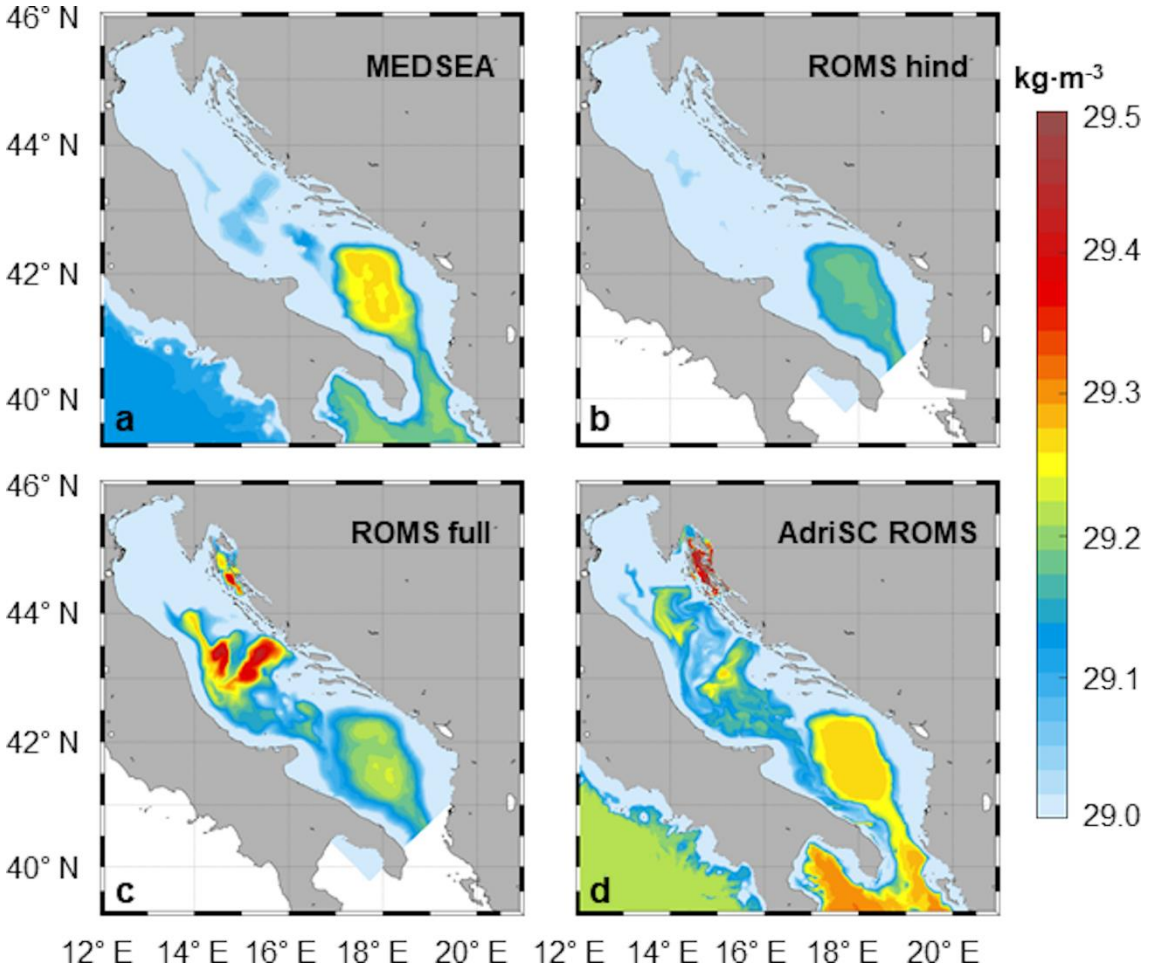

Figure 42. Same as in Fig. 12 but for 1 June 2015.

Further, the patchy distribution of very dense waters obtained in ROMS-full during winter and spring can be attributed to the assimilation of data in four-day cycles, for which CTD measurements – collected at some given sites and for some specific days – played a significant role in adjusting the Adriatic dynamical solutions (Janeković et al., 2020). This demonstrates

the importance of the coverage and the long-term availability of assimilated data. A better representation of the dense-water dynamics within the Adriatic basin in ROMS-hind can thus be envisioned (and is possible, as demonstrated by the results of the AdriSC model) before performing the data assimilation which currently cannot fully compensate for the accumulated shortcomings of the ALADIN-HR and ROMS-hind models.

4.3.3. Daily volume transports along selected transects

To quantify the dense-water outflow across different sections of the northern and middle Adriatic, the volume transports of dense water, defined by the PDA threshold of 29.2 kg m^{-3}, through four transects (T1–T4) are presented in Fig. 43. The direction of transport is defined as positive towards the northwest (transects T1, T3, and T4) or the northeast (transect T2).

In general, MEDSEA and ROMS-hind transports are the lowest across all transects, which is expected, as their overall PDA values are found to be the lowest of all simulations. With the same argument, the AdriSC-ROMS transport is the highest for all transects, except for T4, where the ROMS-full transport prevails (Fig. 43d). The transports produced by MEDSEA at T1 are mostly very low, peaking at -0.03 Sv in February (Fig. 43a). ROMS-hind transport varies there between -0.07 and -0.01 Sv in February, while the largest absolute values are produced during March, reaching -0.30 Sv. ROMS-full transports at T1 are similar in magnitude to those of ROMS-hind, but the timing is different. In February, the transport reaches -0.20 Sv, whereas in March, the values are smaller, reaching only -0.04 Sv. AdriSC-ROMS transports at T1 are extremely high from February to April compared to the other simulations. The largest southeastward transports are produced in February, almost reaching -1.00 Sv, while in March and April, they reach -0.80 Sv.

At T2, both MEDSEA and ROMS-hind transports are null or almost null on all days since they do not produce dense waters with PDA values above 29.2 kg m^{-3} within the Kvarner Bay (Fig. 43b). ROMS-full transports are largest in February and in the first half of March (peak at -0.20 Sv), when intense measurements were carried out in the Kvarner Bay. AdriSC-ROMS transports are also the highest in February and March, peaking at -0.60 Sv, while the values in April reach -0.20 Sv. AdriSC-ROMS transports indicate that the ratio between dense water originating from the northern Adriatic and the Kvarner Bay is roughly 60 : 40, which is similar to the transport ratio derived for the massive dense-water generation in winter 2012 (Janeković et al., 2014). As for T3 and T4, both MEDSEA and ROMS-hind transports are null throughout the whole period. ROMS-full transports at T3 vary around -0.05 Sv from the middle of

February to the end of May (Fig. 43c), being the highest in the second half of March, reaching -0.20 Sv.

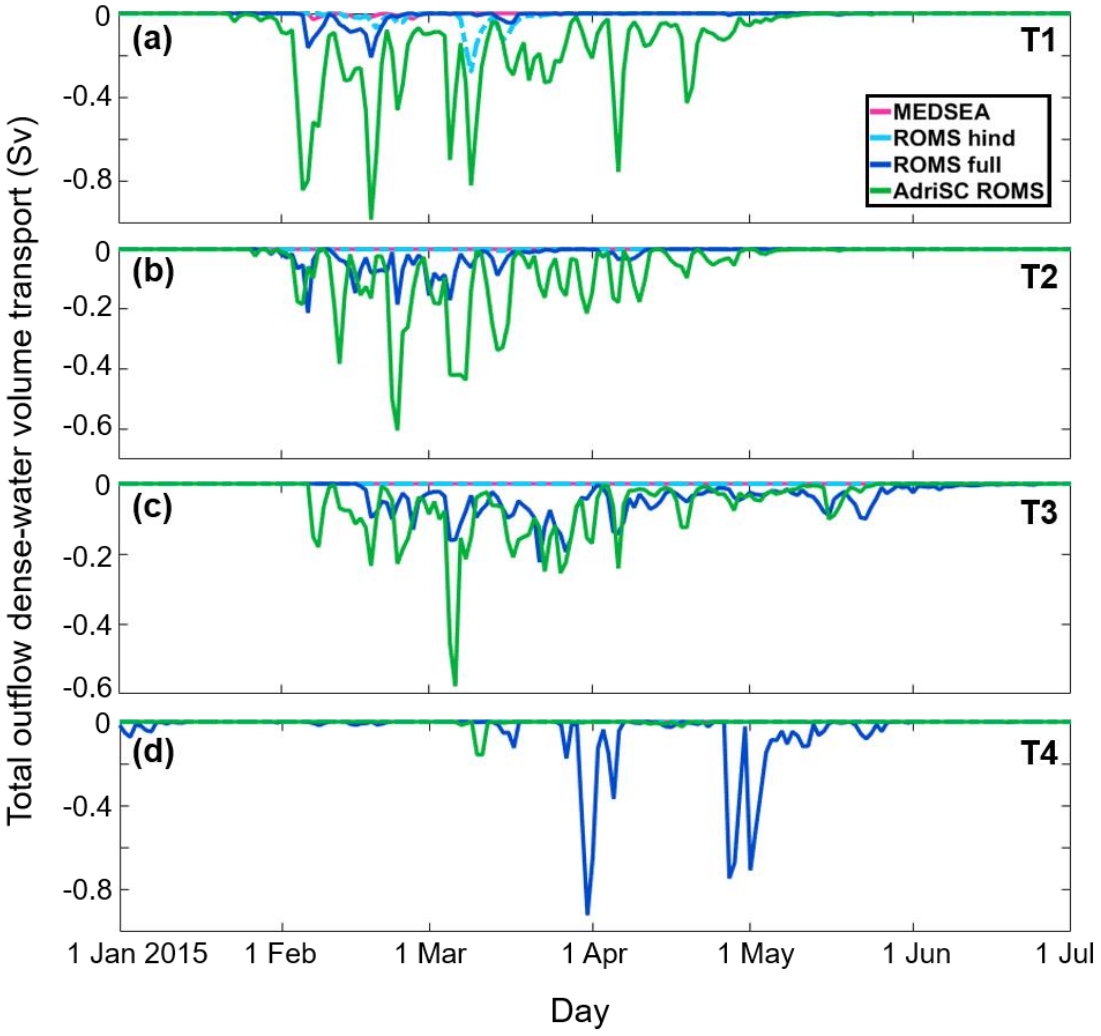

Figure 43. Daily volume transport rates of dense-water outflow with PDA values higher than 29.2 kg m^{-3} integrated over the transects (a) T1, (b) T2, (c) T3, and (d) T4.

Further, the results reveal certain similarities in the behaviour of ROMS-full and AdriSC-ROMS transports. The dense-water transports at T3 are lagged for about 2 to 3 weeks (depending on the simulation) after the transports at T1 and T2, from which an estimate of bottom density current may be computed (approximately 0.10–0.17 m s^{-1}). Lastly, ROMS-full transports are extremely large at T4, much larger than in AdriSC-ROMS, peaking during March-April with values reaching -0.90 and -0.70 Sv, respectively. For the rest of the time, the transports are relatively small, bringing into question whether these outbursts of dense water are driven by the assimilated data or by an outflow of dense waters with high densities that are produced by ROMS-full northwest of transect T4 in the Jabuka Pit.

4.4. Discussion

This multi-model analysis has demonstrated the complexity of reproducing the dense-water dynamics within the Adriatic basin, as the presented models produced different or even divergent results despite all thorough evaluation in previous studies (Escudier et al., 2021; Janeković et al., 2104; Vilibić et al., 2018; Pranić et al., 2021; Denamiel et al., 2021b, 2022). However, it is important to consider that the presented results belong to different model categories. MEDSEA is a reanalysis product covering the entire Mediterranean Sea for the 1987–2019 period. ALADIN-HR-ROMS does not cover the entire Adriatic Sea and is used, in this study, either in hindcast mode (hind) or in fully assimilated mode with four-day cycles (full) for the 2014–2015 period. Finally, AdriSC represents the evaluation run of a climate model covering the full Adriatic for the 1987–2017 period. This implies that numerical schemes (e.g. discretization, parametrization) and the setup (e.g. physics, resolution, forcing) used in these models, as well as the type of simulation performed (free run vs. assimilated run), strongly influence the quality of the presented results. As this study only compares state-of-the-art models (ERA5, WRF, and ALADIN in the atmosphere and NEMO and ROMS in the ocean), the differences in numerical schemes will not be discussed hereafter because it is difficult to quantify how they impact the dense-water dynamics, as they vary from model to model. However, the different model setups will be analysed with the aim to better understand their impact on the bora-driven dense-water dynamics in the Adriatic basin.

4.4.1. Impact of the resolution and the physics on the bora dynamics

First, the ERA5 reanalysis at 25 km resolution has been demonstrated to be incapable of capturing the bora dynamics (Denamiel et al., 2021a). Consequently, in this study, ERA5 wind stresses are 2 to 3 times smaller than the AdriSC-WRF and ALADIN-HR results. However, in both the northern Adriatic and the Kvarner Bay, heat losses calculated from the ERA5-MEDSEA model – via bulk formulae using sea-surface-temperature-assimilating remote sensing products – are comparable to the ALADIN-HR-ROMS-hind model (Fig. 34). These heat losses are still underestimated compared to the AdriSC model, particularly within the Kvarner Bay and the Gulf of Trieste, as well as along all bora jets (Fig. 29).

Second, the hydrostatic ALADIN-HR model at 8 km resolution and dynamically downscaled wind fields to 2 km, has already been demonstrated to reproduce the basic bora dynamics (Horvath et al., 2009). However, our results reveal that within the Kvarner Bay region, ALADIN-HR wind stresses are not as intense and do not cover as wide an area as the

non-hydrostatic AdriSC-WRF model. Indeed, the bora cross-flow variability in the Kvarner Bay might occur at a kilometre scale, particularly during deep bora events (Kuzmić et al., 2015), while bora pulsations have a strong sub-kilometre spatial component, posing a challenge for proper quantification in any kilometre-scale atmospheric model. Nevertheless, Denamiel et al. (2021a) demonstrated that, during 22 bora events, including 2 in 2015, the AdriSC-WRF 3 km model skillfully reproduced wind speed observations at Pula, Rijeka, Ogulin, Zavižan, Gospić, and Knin stations (all located in the Kvarner Bay region) above 20 m s^{-1} despite overestimating them by up to 5 m s^{-1} below this threshold.

Further, the ALADIN-HR-ROMS-hind heat losses are always smaller than those computed by the AdriSC model. It is documented that hydrostatic atmospheric models are not capable of capturing all the details of the bora jets (Klemp and Durran, 1987; Blockley and Lyons, 1994; Grisogono and Belušić, 2009). Consequently, the hydrostatic approximation used in ALADIN-HR constrains its ability to reproduce the finer-scale details of the bora flow (Horvath et al., 2009). Further, quite surprisingly, the 4D-Var data assimilation scheme used in the ROMS-full assimilation reduces the intensity of the turbulent heat fluxes, creating a dynamical imbalance between the wind stresses (which are similar in comparison to the differences between the different atmospheric models) and the heat losses forcing the ocean model.

Also, the evaluations of the AdriSC-WRF model performed both for the climate run over a 31-year period (Denamiel et al., 2021b) and during extreme bora events (Denamiel et al., 2020a, b, 2021a), have demonstrated that a 3 km resolution effectively represents the atmospheric dynamics within the Adriatic basin. Further, the results of the AdriSC-WRF model at 3 km resolution (particularly the intensity of the winds), have been shown to converge towards the results obtained with the higher-resolution AdriSC-WRF-1.5 km model during bora events (Denamiel et al., 2021a). However, only sub-kilometre-scale atmospheric models can properly capture the highly nonlinear dynamics of bora flows (Kuzmić et al., 2015). Thus, using a 3 km nonhydrostatic model remains a compromise between accuracy and efficiency. This compromise is particularly important when running multi-year climate simulations, having a tremendous computational cost. This is also highlighted by Vodopivec et al. (2022), who conducted a sensitivity study over a 16-year period using different runoff configurations and different sources of atmospheric forcing, and concluded that the atmospheric forcing has a substantial impact on the hydrology and circulation of the Adriatic Sea.

4.4.2. Impact of the resolution and the bathymetry on the dense-water dynamics

In ocean models, resolution significantly impacts the representation of the numerous islands located along the eastern Adriatic coast. More importantly, it impacts the representation of the reservoirs that collect dense waters within the Adriatic basin (i.e. Kvarner Bay, Jabuka Pit, and SAP). To better understand the required horizontal resolution for reproducing the Adriatic Sea dynamics, the spatial distributions of the median and MAD of the Rossby radii, calculated from the AdriSC-ROMS results, are presented for the entire model domain in Fig. 41a and b, respectively. In general, the median Rossby radius decreases from open seas toward shallower coastal areas. The largest values are found to be around 10.0 ± 2.0 km in the open northern Ionian Sea. Median Rossby radii are slightly smaller in the SAP, with values around 7.5 ± 1.3 km, while they decrease sharply on the edges of the pit to around 5.0 ± 1.2 km. In the Jabuka Pit, the radii reach around 4.0 ± 1.2 km, whereas in the rest of the middle Adriatic, they reach around 2.5 ± 1.2 km. The deeper part of the Kvarner Bay presents high variability, with Rossby radii around 2 ± 1.5 km. The northern Adriatic exhibits the smallest median Rossby radii and MAD, approximately 1.0 ± 0.4 km.

Further, the time series of the Rossby radius are presented for the northern Adriatic and Kvarner Bay (Fig. 44c), as well as for the Jabuka Pit and deep Adriatic (Fig. 44d) subdomains. In the northern Adriatic, the radius is in the range of 0.5–1.0 km until April 2015. Then it increases to around 1.5 km until September, followed by a decrease below 1 km. For the Kvarner Bay, values obtained from November 2014 to April 2015 are very small (less than 500 m). These values gradually increase, peaking at 3.5 km during summer before decreasing again in September. In the Jabuka Pit, there is a decrease from approximately 4 km to extremely small values around 300 m in February 2015, followed by a subsequent increase. Similarly, the deep Adriatic subdomain shows the same behaviour as the Jabuka Pit, but with values that are almost 4 km larger throughout the whole year. The median Rossby radii values obtained in the SAP align with the findings from a prior study by Kurkin et al. (2020) dedicated to analysing the first Rossby radii in European semi-enclosed basins.

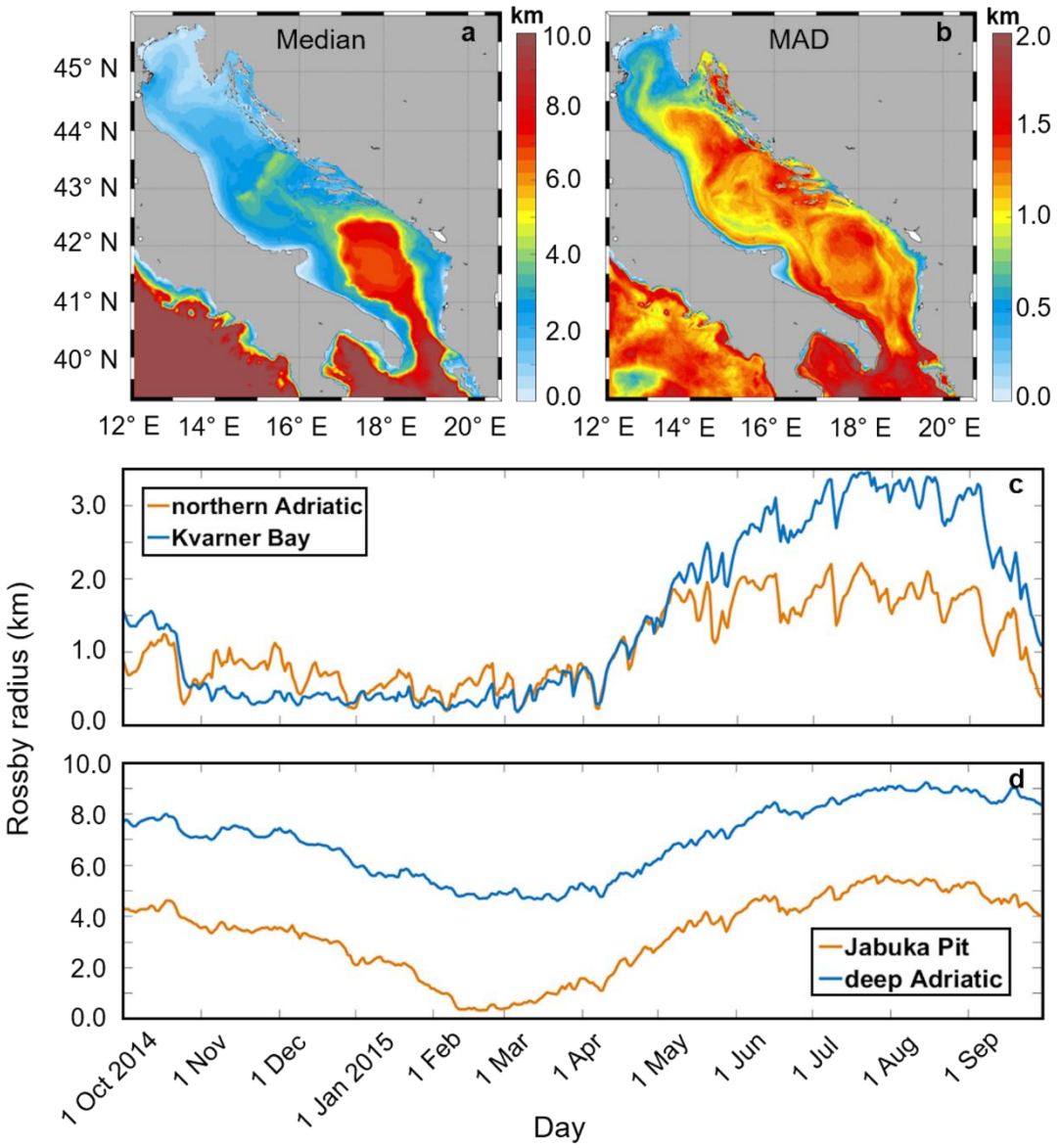

Figure 44. Median and MAD of the first baroclinic Rossby radius of deformation for the AdriSC-ROMS domain (a, b) and time series of the Rossby radius for the northern Adriatic and Kvarner Bay (c), as well as for the Jabuka Pit and deep Adriatic subdomain (d).

Overall, the baroclinic Rossby radii present large variability in the Adriatic Sea, suggesting that even sub-kilometre-scale ocean models are needed to simulate the full range of processes within the region, particularly the dense-water dynamics. However, for climate simulations, a horizontal resolution finer than 1 km is currently not feasible. Further, different digital terrain models (DTMs) have been used to generate the bathymetries of the presented models. To evaluate the joint impact of resolution and bathymetry, MEDSEA and ROMS (hind and full) bathymetries are compared to the AdriSC-ROMS model at 1 km resolution (Fig. 28b, c). It is evident that the MEDSEA model is shallower than AdriSC-ROMS within the Kvarner Bay and

the Jabuka Pit (by 60–80 m), but also in the middle of the SAP (by more than 100 m). Consequently, the capacity of the MEDSEA model to naturally collect the dense waters within the known Adriatic reservoirs is decreased compared to the AdriSC-ROMS model, thus relying more heavily on the assimilation of the available data.

In the ROMS-hind and ROMS-full models, the bathymetry also appears generally shallower than in AdriSC-ROMS within the Kvarner Bay and along the canyon system between the Jabuka Pit and the SAP (by 20–40 m). This is particularly important, as it might explain the differences in terms of the paths seen between ROMS-full and AdriSC-ROMS when the dense waters are transported from the Jabuka Pit towards the SAP. However, concerning the Jabuka Pit and the SAP, the alternating positive and negative differences in bathymetry between ROMS (full and hind) and AdriSC-ROMS indicate certain shifts in locations. Whether and how these shifts in location impact the dense-water dynamics remains unclear based on the results presented in this study. Finally, it is important to highlight that the AdriSC-ROMS model uses 35 vertical sigma layers, while the ROMS (full and hind) model incorporates only 20. Given that bora-driven dense-water dynamics require proper resolution in both surface (for the sea temperature cooling) and bottom (for the dense-water transport) layers, the finer vertical resolution used in AdriSC-ROMS may play a major a role in the overall performance of the model.

4.4.3. Impact of the salinity forcing on the dense-water generation

Dense-water generation is highly sensitive to the background salinity content provided through either open boundaries or direct river outflows imposed on ocean models. First, in ROMS-hind, Janeković et al. (2014) quantified an underestimation of salinity by 0.2–0.5 in a simulation of the massive dense-water formation in 2012. After updating the outdated river climatologies that largely overestimated the discharges, Vilibić et al. (2016) confirmed that even the simulations using the most realistic river representation underestimate the background salinity content within the Adriatic basin. As the AREG model (forcing ROMS-full) is set up with the old river climatologies and has a low salinity content over the entire Adriatic basin, far too much fresh water is inputted through the ROMS-hind open lateral boundary located in the southern Adriatic. Consequently, the ROMS-hind results presented in this study for the 2014–2015 period have low basin-wide salinities and therefore generate dense waters with lower bottom PDA values.

Next, the AdriSC-ROMS model has been thoroughly evaluated over a 31-year period in Pranić et al. (2021). In the northern Adriatic, despite inaccuracies in salinity below 36 due to the Po River misrepresentation, the AdriSC-ROMS model reproduced well the dense-water masses. Second, in the Kvarner Bay, AdriSC-ROMS salinities were demonstrated to be excessively high, which could lead to a general overestimation of the dense-water bottom PDAs in this region. In the SAP, the evaluation revealed that the salinities and the densest waters are relatively well-captured by the AdriSC-ROMS model. Additionally, salinities in MEDSEA are closer to the AdriSC-ROMS results in the southern Adriatic (i.e. Jabuka Pit and deep Adriatic subdomains) and to the ROMS-hind results in the northern Adriatic (i.e. northern Adriatic and Kvarner Bay subdomains) during the entire 2014–2015 period (Fig. 38). It can thus be safely assumed that the old river climatologies used in MEDSEA result in low salinities over the northern part of the Adriatic basin and hence lower bottom PDAs during the bora-driven dense-water generation events. Finally, besides the river discharges, the surface freshwater E - P fluxes (i.e. evaporation - precipitation fluxes) also determine the surface salinity of the northern Adriatic Sea. The E - P fluxes are taken into account in all ocean models presented in this study but are derived from diverse atmospheric models. Consequently, the differences in E - P fluxes might contribute to variations in dense-water results.

4.4.4. Impact of the assimilation on the ocean dynamics

First, in ROMS-full, the 4D-Var data assimilation is applied in four-day cycles, implying that the ocean dynamical properties are not continuously smooth in time between the cycles, as the ROMS-full model adjusts the initial state at the beginning of each cycle. Consequently, despite the large improvement in terms of the ocean fields used to minimize the cost function of the assimilation, the continuous process of dense-water generation and transport over time is not properly reproduced in ROMS-full. For example, since salinity is generally underestimated in ROMS-hind, the data assimilation performed in ROMS-full constantly attempts to adjust salinities (and therefore bottom PDAs) to higher values. However, data availability fluctuates considerably during the investigated period and, for example, is more concentrated in the Kvarner Bay during the February–March 2015 period or along a northern Adriatic transect (Po–Rovinj) surveyed with a monthly or bimonthly frequency. As a consequence, this leads to extremely high bottom PDAs being present off the Kvarner Bay before the actual generation of dense waters within the Kvarner Bay or along the Trieste jet in the ROMS-full model.

Second, MEDSEA, unlike ROMS-full, uses a 3D-Var assimilation approach which is known to lose the temporal information contained in the observations through averaging (Janeković et al., 2020). Generally, during the 2014–2015 period, MEDSEA assimilates fewer data than ROMS-full, which benefited from the observations collected during the NAdEx campaign. Consequently, MEDSEA is incapable of adjusting its solution in order to capture the proper dense-water dynamics. For example, in the Jabuka Pit, MEDSEA provides a constant decrease in bottom PDAs from autumn 2014 to winter 2015, which is opposite to all the other models and is probably driven by the availability of the assimilated observations (e.g. Argo data). However, ROMS-full is likely to have assimilated the same observations within the Jabuka Pit but also assimilated Arvor-C and drifter data obtained off the Kvarner Bay during the NAdEx campaign. Further, during the winter, when bora episodes occur, only a small number of SST cloud-free scenes are available for assimilation in ERA5. As a result, MEDSEA, contrary to ROMS-full, is mostly incapable of generating the bora-driven dense waters and hence of transporting and collecting them within the Jabuka Pit.

5. ADRIATIC SEA DENSE-WATER CLIMATOLOGY (1987–2017)

In this chapter, the climatology of the Adriatic dense waters during a three-decade period (1987–2017) is estimated with the results derived from the AdriSC kilometre-scale ocean climate simulation. The thermohaline properties modelled by AdriSC-ROMS 1 km are analysed and discussed. The analyses are divided based on the three main phases of dense-water (DW) dynamics – generation, spreading and accumulation. The focus is directed towards locations where the generation and accumulation of dense waters take place, as well as the dense-water spreading pathways.

5.1. Dense-water generation

This section describes the DW generation during the 1987–2017 period in two subdomains: the northern Adriatic (NA) and the Kvarner Bay (KB; Fig. 4).

First, the daily time series of averaged bottom PDA, temperature and salinity are analysed for the NA and KB domains (Fig. 45). In the NA, the seasonal variability of PDA, temperature and salinity is larger compared to the KB. In general, bottom PDAs in the NA vary between 27.0 and 30.0 kg m^{-3}, while in the KB they range from 27.7 to 29.9 kg m^{-3} (Fig. 45a). A sharp increase of PDA during winter reaching a peak in February is followed by a sharp decrease until the end of summer when the minimums of PDA are produced. DW with PDA equal or larger than 29.2 kg m^{-3} are generated throughout most of the years, except for 2014 in the NA and 1990, 1994–1997, 2007 and 2014 in the KB. The years with the strongest DW generation (indicated by a PDA maximum larger than 29.5 kg m^{-3}) are 1989, 1991, 1999, 2000, 2002–2006, 2008, 2012, 2013 and 2017 in the NA, and 1987, 1989, 1993, 1999, 2000, 2002, 2004–2006, 2008, 2012, 2013 and 2017 in the KB. Also, PDA maximums are often smaller in the KB than in the NA (by 0.1–0.4 kg m^{-3}). In the KB, a smaller secondary peak in PDA is also noticable during summer, associated with DW accumulation in the deepest KB sections. In autumn, the larger PDA simulated in the KB compared to the NA indicates delayed mixing of the entire water column due to the greater depths within the KB.

Further, in the NA, bottom temperatures vary between 6.5 and 21.0 °C, while in the KB, they vary between 8.0 and 17.0 °C (Fig. 45b). Temperatures in the KB are generally higher during winter, whereas in the NA, they peak in summer due to its shallower depth, reacting faster to surface heat flux changes. The lowest temperatures were produced during the extreme winter of 2012 in both subdomains. Regarding salinity, the values are overall larger in the KB than in the NA. In the 1987–1999 period, salinity varies between 37.6 and 38.4 in the NA and

between 38.0 and 38.4 in the KB (Fig. 45c). Larger salinities are produced in the 2000–2008 period in both subdomains, followed by a decrease until 2011, which is marked by a steep increase in both subdomains leading to large salinities in the 2012–2013 period. Notably, in 2012, salinity in the KB reached a peak larger than in the NA (by more than 0.1), while the temperature was lower in the NA (by ~2.5 °C), which led to very similar extreme PDAs in both subdomains. Similarly, in 1987, substantially larger salinity in the KB resulted in larger PDAs than in the NA. However, 1987 is the first year of the simulation and even though this year has been documented to have strong DW formation events (Vilibić et al., 2001), it should be considered with caution due to possible influence of the initial conditions despite the spin-up period. Further, a slight salinity decrease is produced from 2014, followed by an average increase, peaking at 38.7 in 2017. In addition, a general positive trend can be noticed for salinity during the 31-year period. Interestingly, this long-term salinity variability is following salinity changes in other Adriatic sections and the phases of the BiOS regimes (Gačić et al., 2010; Mihanović et al., 2015, 2021).

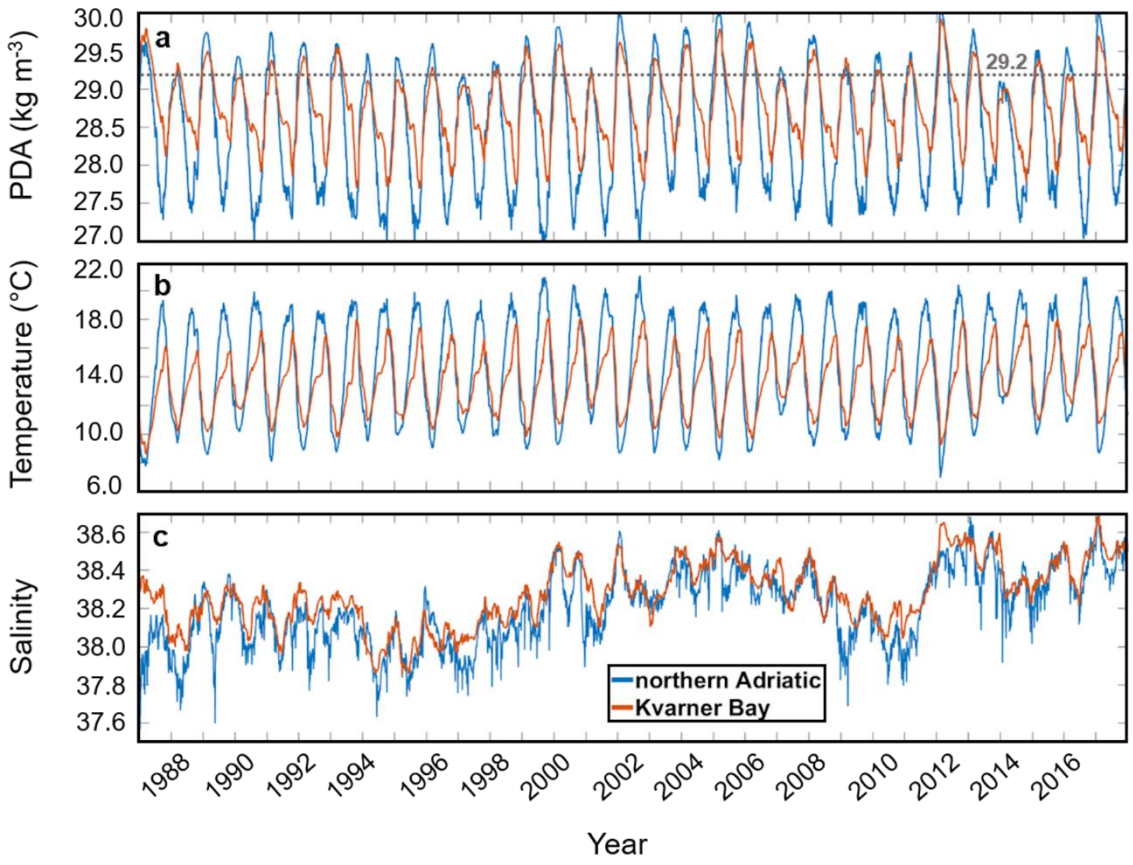

Figure 45. Daily time series of bottom (a) PDA, (b) temperature and (c) salinity for the northern Adriatic and Kvarner Bay subdomains during the 1987–2017 period.

Second, the PDFs of maximum bottom PDA, as well as bottom temperature and salinity for the DOY with maximum PDA during the winter (JFM) seasons of the 1987–2017 period are presented in Fig. 46 for both subdomains. In general, maximum PDAs are larger in the NA where the highest probabilities are produced for the PDAs around 29.7 kg m^{-3} (Fig. 46a). In contrast, in the KB, the most probable PDAs range between 29.3 and 29.6 kg m^{-3}.

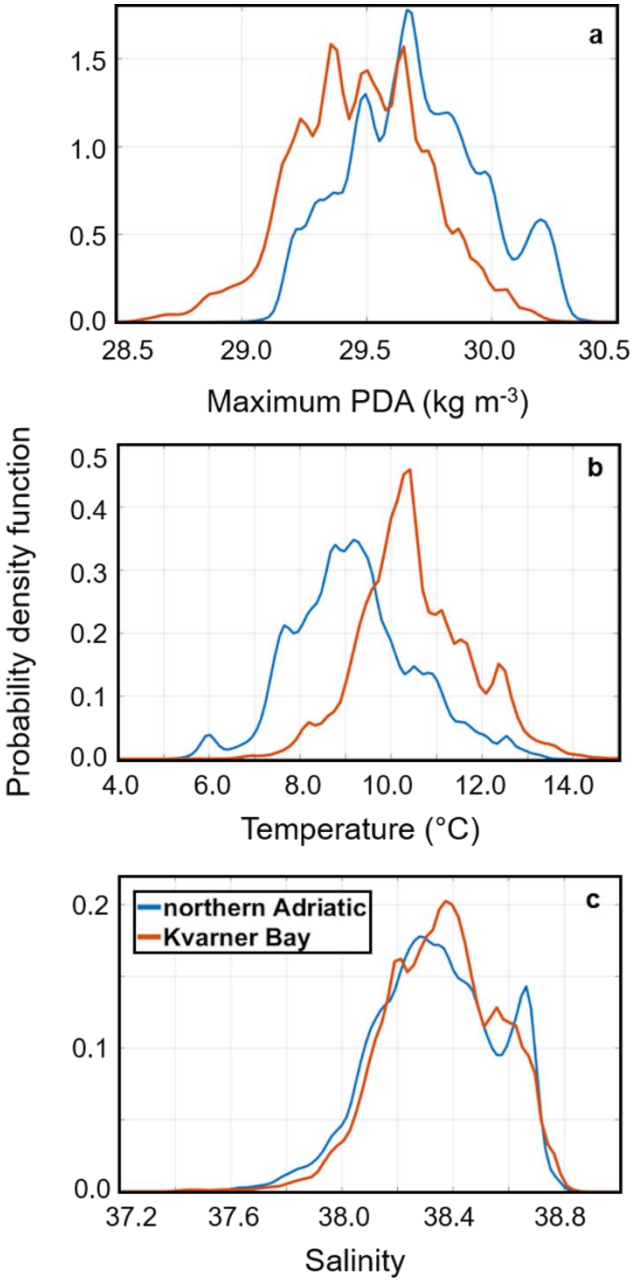

Figure 46. Probability density functions of (a) maximum bottom PDA as well as bottom (b) temperature and (c) salinity for the DOY with maximum PDA in the northern Adriatic and Kvarner Bay subdomains during the JFM seasons of the 1987–2017 period.

Furthermore, the temperatures are generally higher in the KB, with the highest probabilities for values around 10–11 °C, while in the NA, the most probable temperatures are around 9 °C (Fig. 46b). Conversely, the salinity PDFs are very similar in both subdomains, with salinities mostly distributed between 37.8 and 38.8 (Fig. 46c). However, slightly higher probabilities are found for salinities around 38.4 in the KB and below 38.3 in the NA. Convincingly, DW generated in the NA is denser mainly due to its lower temperatures, while the salinity difference between two DW formation sites remains small. It should be noticed that even though the maximum heat losses occur over the KB during DW formation (e.g., Dorman et al., 2007; Janeković et al., 2014), the coldest bottom temperatures are found in the NA due to the depth of the KB (up to 3 times deeper than the NA).

Third, the maximum bottom PDA, DOY of maximum PDA, as well as the bottom temperature and salinity at the DOY of maximum PDA during the JFM seasons in the 1987–2017 period are presented as box plots for both subdomains (Fig. 47 and 48). In the NA, the years with the smallest maximum PDAs (median < 29.5 kg m^{-3}) and therefore the weakest DW generation are: 1988, 1997, 1998, 2001, 2007, 2009 and 2014 (Fig. 47a). The years with the strongest DW generation (median of maximum PDAs > 30.0 kg m^{-3}) are: 2002, 2005, 2012 and 2017. For instance, in 2012, maximum PDA in the NA reached 30.5 kg m^{-3}, which is in accordance with the measurements in the Gulf of Trieste, where a maximum PDA of around 30.5 kg m^{-3} was recorded (Mihanović et al., 2013). The remaining majority of the years belongs to the category with maximum PDAs between 29.5 and 30.0 kg m^{-3}.

In the KB, distributions of maximum PDAs are generally smaller than those in the NA (Fig. 47b). Median maximum PDAs larger than 30.0 kg m^{-3} are produced only in February–March 2012, which is confirmed by sparse observations in that area indicating a maximum PDA of around 30.0 kg m^{-3} (Mihanović et al., 2013). In one half of the remaining years, PDAs range between 29.5 and 30.0 kg m^{-3}, while in the other half, they are smaller than 29.5 kg m^{-3}. The box plots of the DOY of maximum PDA are similar to those for the NA but with a slight prevalence of the later part of the JFM period. The median of the DOY of the maximum PDA in the NA varies between 25 and 70, revealing the differences in the timing of the DW generation between years. For example, in 2002, the major DW generation event occurred in January without further increases in PDA afterward. Conversely, in 2011, the highest PDA is produced in March, indicating substantial late-winter cooling. Further, some years have a wide range in the distributions of the DOY of the maximum PDA, suggesting either several presumably weak DW events occurring at different parts of the NA or a slow transport of DW

in the bottom layers of the NA shelf, potentially due to some external forcing (Vilibić et al., 2008). In the KB, some years with wider range in distributions of the DOY of the maximum PDA are also present. This indicates the existence of several cooling events spanning over different sections of the KB. Although bora winds can vary spatially over the KB depending on the events (Grisogono and Belušić, 2009), major events encompassing the whole region during which the PDAs are highest were not reproduced.

Finally, in 2012, the year of the most extreme DW generation, the temperature at the DOY of maximum PDA reached the lowest values around 4.0 °C, in both DW generation sites (Fig. 48), with median values around 6.0 and 8.0 °C in the NA and KB, respectively. Also, the salinity reached the largest values in 2012 in the KB (~ 38.5), indicating the intrusion of high-salinity waters into the KB due to a low freshwater load observed during the most of the preceding year (Mihanović et al., 2013). In the NA, the salinities were slightly larger in some other years with smaller maximum PDA than in 2012 (Fig. 48c, d). As the salinities are constantly increasing in the whole Adriatic, maintaining such a trend in the future (Soto-Navarro et al., 2020), along with similar intensities of surface cooling observed in the severe winter of 1929 (Vatova, 1934) and projected during bora events (Denamiel et al., 2020), may imply the generation of even denser DW in the future climate.

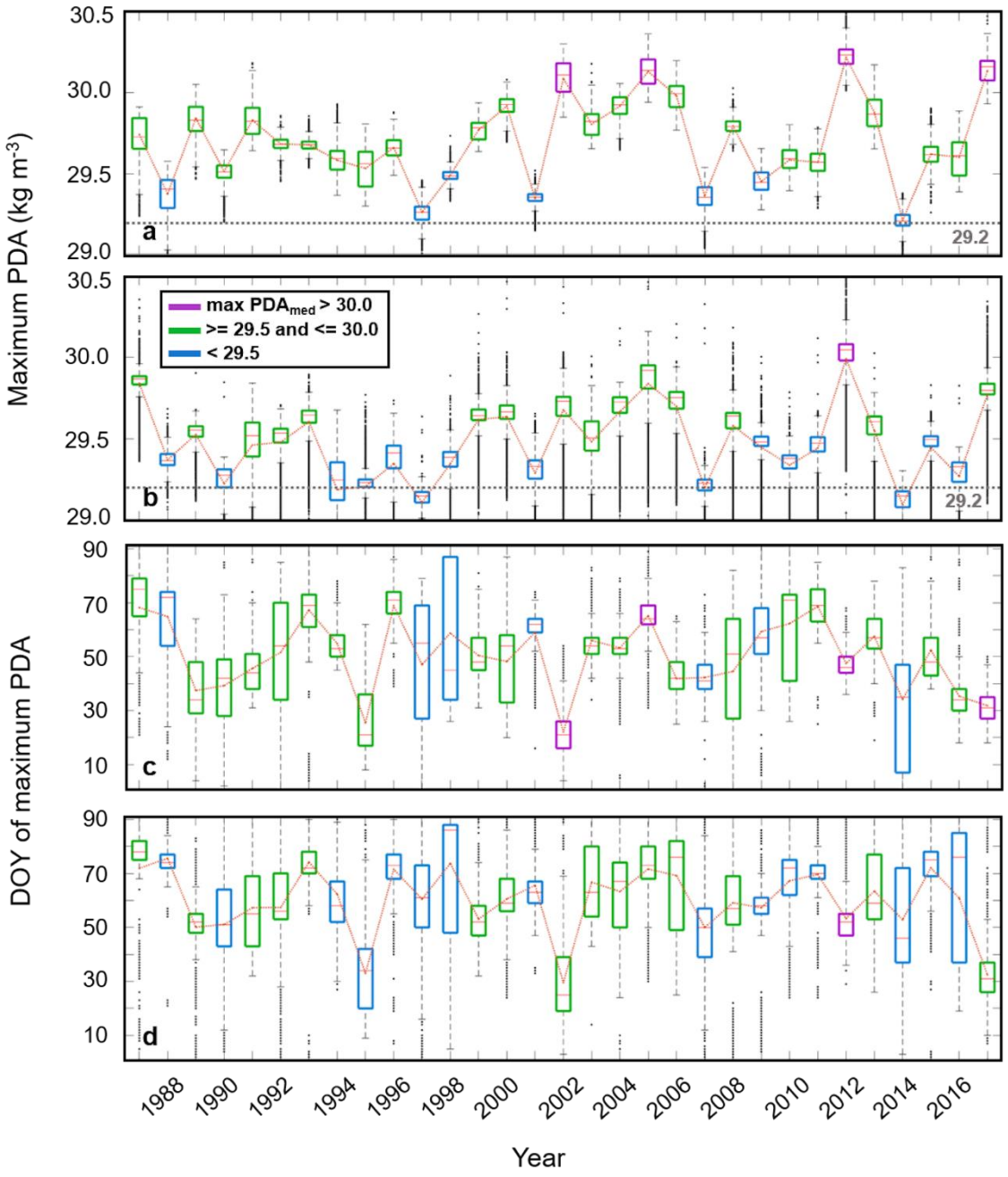

Figure 47. Box plots of maximum bottom PDA and DOY of maximum PDA for the (a, c) northern Adriatic and (b, d) Kvarner Bay subdomains in the 1987–2017 period. The red line inside each box plot denotes the median of the distribution. The orange dotted line connects the mean values of the distributions.

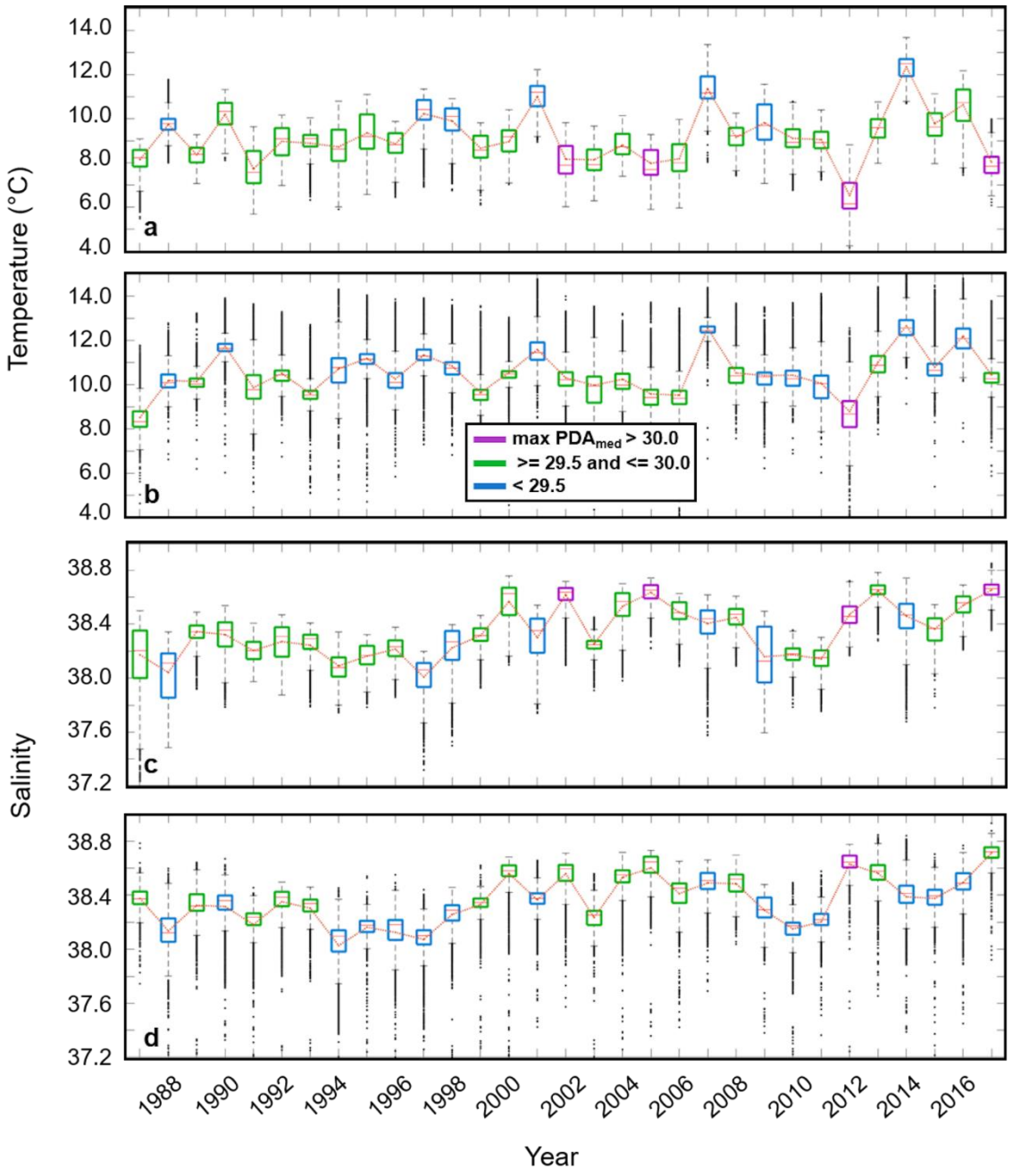

Figure 48. Box plots of bottom temperature and salinity at the DOY of maximum PDA for the (a, c) northern Adriatic and (b, d) Kvarner Bay subdomains in the 1987–2017 period. The red line inside each box plot denotes the median of the distribution. The orange dotted line connects the mean values of the distributions.

5.2. Dense-water spreading

This section analyses the spreading of the bottom dense waters (PDA > 29.2 kg m^{-3}) accross nine transects in the Adriatic Sea (Fig. 4).

First, the time series of monthly bottom dense-water mass transported outward through the nine transects are presented in Fig. 49. At T1, located on the southern edge of the northern Adriatic, indicating the DW outflow solely from the NA, the transported DW mass mostly varies around $-10.0 \cdot 10^{11}$ kg, slightly surpassing this value in 2003 and 2017. The largest amount of DW is transported through T1 in February 2012, sharply peaking at $-20.0 \cdot 10^{11}$ kg. The amounts of transported DW through T2, marking the boundary between the open sea and the northern half of the Kvarner Bay and indicating DW mass outflow from the KB only, mostly vary down to around $-5.0 \cdot 10^{11}$ kg and exceptionally to $-6.8 \cdot 10^{11}$ kg in February 2012. A comparison between T2 and T1 bottom DW mass outflow, suggests that the outflow from the KB is 2–3 times lower than the outflow from the NA, attributing 25–35% of the total dense waters to the KB. Although differing in methodology (mass vs. volume transports), our estimates are somehow smaller than those by Janeković et al. (2014), who quantified the contribution of KB DW waters to be around 40% during the winter of 2012. Further southeast, at T3 in the middle Adriatic, the bottom DW mass varies down to around $-1.0 \cdot 10^{11}$ kg, while larger values around $-2.0 \cdot 10^{11}$ kg are obtained in 2003, 2006 and 2012. The decrease possibly reflects enhanced mixing between DW and ambient waters known to occur in this region (Vilibić and Mihanović, 2013) and strongly modifying DW outflow. The T4 transect, located north of the Jabuka Pit in the middle Adriatic, shows mostly smaller amounts of transported DW mass except in 1988, 2000 and 2012 (near $-2.0 \cdot 10^{11}$ kg or larger).

Significant differences are evident between the two transects located in the Palagruža Sill and divided by the island of Palagruža, T5a and T5b, of which T5a is closer to the western coast. Until the mid-1990s, the monthly transported DW mass is much larger at T5b (reaching down to $-6.0 \cdot 10^{11}$ kg) than at T5a (down to $-2.0 \cdot 10^{11}$ kg), after which there is a period of reduced DW transport until 1999. From 2000 to 2017, a reversal occurs with the transported DW mass being larger at T5a (down to $-3.0 \cdot 10^{11}$ kg) compared to T5b (mostly less than $1.0 \cdot 10^{11}$ kg). This may indicate a major change in DW dynamics over the northern Adriatic shelf – e.g., due to circulation changes or differences between DW and the ambient water densities – as DW arriving through T5b cascades initially to the Jabuka Pit before being transported along deepest sections of the Palagruža Sill (Vilibić et al., 2004). In contrast, DW arriving through

T5a are directly coming from the northern Adriatic shelf, detouring the Jabuka Pit along the western shelf. Further, at T6 in the northwestern part of the southern Adriatic, very large amounts of DW mass are transported in specific years (1989, 2000, 2002–2006, 2008, 2012, 2013 and 2017), with the largest mass transported in April 2005 reaching $-70.0 \cdot 10^{11}$ kg. This DW time series resemble the DW time series at T5a, indicating that the most of these DW are transported downslope along the western sections of the Southen Adriatic Pit towards its deeper layers (e.g., Gondola Slide, Bari Canyon, Foglini et al., 2016; Langone et al., 2016).

Interestingly, strong quasi-decadal variations in the bottom DW mass outflow may be seen at all transects, except the one in the Strait of Otranto. For example, a reduced outflow may be seen in the 1994–1998 period, when the salinities of the Adriatic were substantially lowered due to EMT/BiOS-driven enhanced advection of low-salinity Western Mediterranean waters into the Adriatic (Vilibić et al., 2012). Consequently, the PDA was generally lower in the Adriatic, reflecting also to the PDA of the DW in both NA and KB. In contrast, larger bottom DW mass outflow was reproduced during 2003–2006, coinciding with the maximum of inflow of saline waters occurring due to strong cyclonic phase of the BiOS (Mihanovć et al., 2015).

The remaining transects, T7 and T8, are located in the Strait of Otranto, where T7 is a full-length transect and T8 is a shorter transect closer the western coast. The time series reveal completely different dynamics at T7 and T8 compared to the other transects: DW transport at T7 is predominantly driven by open-ocean convection in the SAP (e.g., Bensi et al., 2013; Querin et al., 2013), while DW transport at T8 is also strongly influenced by the properties of the DW coming over the Palagruža Sill, determining its fraction that sinks to the SAP versus the fraction remaining along the shelf. There is always at least around $-5.0 \cdot 10^{11}$ kg transported each month through T7, with variations down to around $-30.0 \cdot 10^{11}$ kg and a few exceptional peaks down to $-47.0 \cdot 10^{11}$ kg. At T8, the monthly bottom DW mass ranges mostly down to $-0.5 \cdot 10^{11}$ kg. In some years, this value is surpassed and in another few years such as 2012, the values exceed $-1.0 \cdot 10^{11}$ kg at the beginning of the year. Notably, the substantial bottom DW mass outflow in 2012 at T6 and T7 indicates massive DW production in the northern Adriatic during the winter, being capable to sustain both the strong downslope currents along the western SAP of its denser fraction and strong bottom current along the shelf of its lighter fraction, extending up to the Strait of Otranto. The same refers to 1987, which is also recognized as a year when massive DW production was observed (Vilibić and Orlić, 2001).

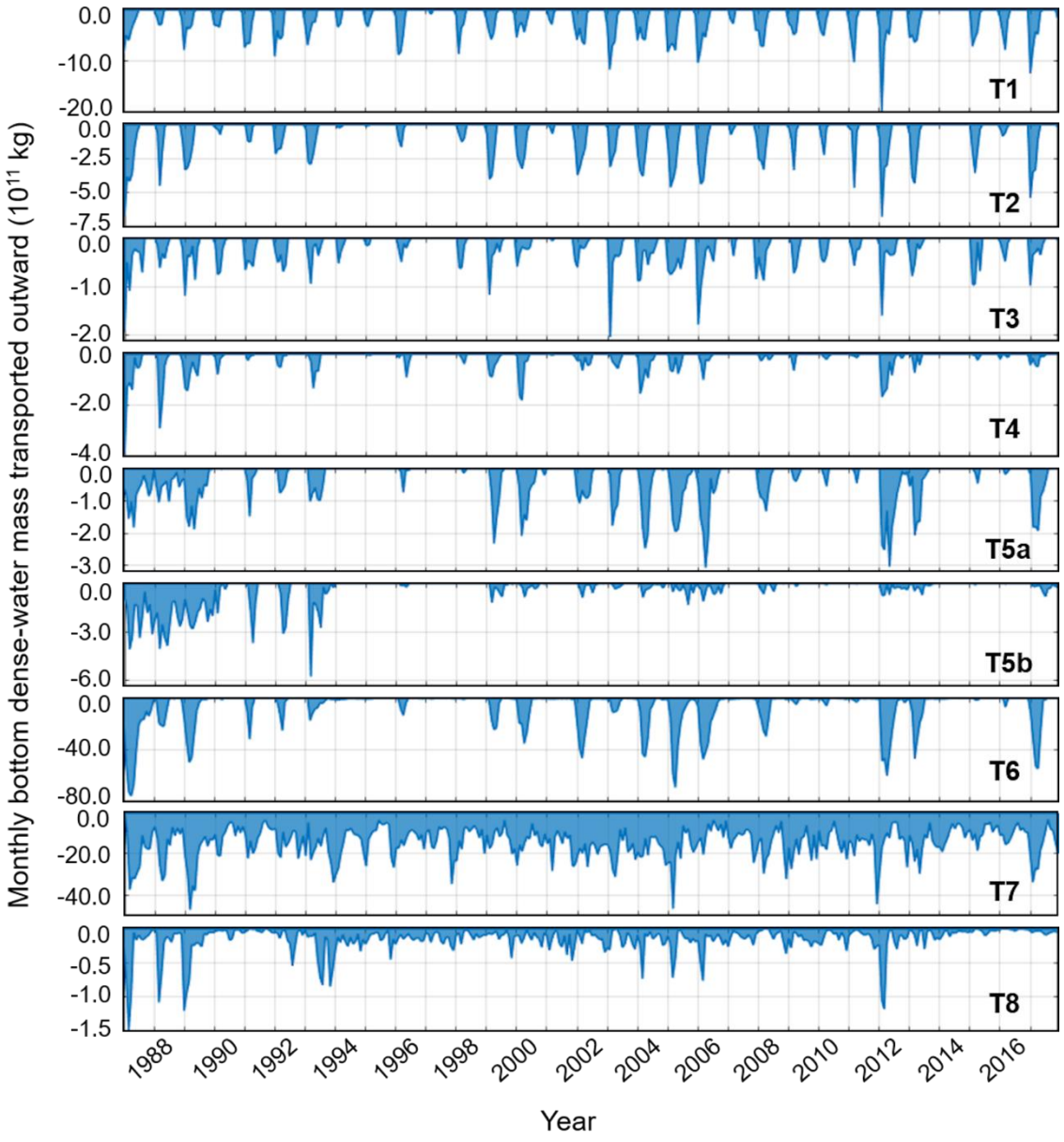

Figure 49. Time series of monthly bottom dense-water mass transported outward at transects: T1, T2, T3, T4, T5a, T5b, T6, T7 and T8 for the 1987–2017 period.

Second, the time series of daily median and maximum bottom dense-water outflow rate in a month across nine transects are presented in Fig. 50 and 51, respectively. The median outflow rates at T1 (down to $-4.0 \cdot 10^5$ kg s^{-1}) are, on average twice the rates at T2 (down to $-2.0 \cdot 10^5$ kg s^{-1}). The maximum outflow rates at T1 reached $-18.5 \cdot 10^5$ kg s^{-1} in February 2012, while the largest maximum rate at T2 is obtained in February 2004 ($-9.0 \cdot 10^5$ kg s^{-1}). The median outflow rates at T3 and T4 are mostly smaller than $-0.5 \cdot 10^5$ kg s^{-1}. The maximum DW rates at T3 reach around $-2.0 \cdot 10^5$ kg s^{-1}, while at T4 they are mostly smaller than $-2.7 \cdot 10^5$ kg s^{-1} reaching down to $-5.0 \cdot 10^5$ kg s^{-1} in 2004. Similarly to the transported DW mass analysis, median DW outflow

rates at T5b exceed those at T5a until the mid-1990s, whereas in the 2000–2017 period, the rates are very small at T5b, surpassing $-1.0 \cdot 10^5$ kg s^{-1} in some years. Maximum rates are also larger at T5b in the first period, but later they generally become similar in magnitude.

At T6, median outflow rates are larger until 1994, during 1999–2007, in 2012, 2013 and 2017, reaching approximately $-25 \cdot 10^5$ kg s^{-1}. During the same periods, maximum DW rates reach down to $-45.0 \cdot 10^5$ kg s^{-1}. Again, T7 exhibits distinct behaviour of DW outflow rates compared to other transects, the median rates mostly vary between -1.0 and $-10 \cdot 10^5$ kg s^{-1}, surpassing this value in several years. The maximum DW outflow rates at T7 are mostly smaller than $-25.0 \cdot 10^5$ kg s^{-1}. At T8, the median DW outflow rates are mostly very low ($< 0.1 \cdot 10^5$ kg s^{-1}) except in 1988–1989, 1993, 2004–2006 and 2012 when they can reach values larger than $-0.4 \cdot 10^5$ kg s^{-1}. However, the maximum DW rates are reached at the end of 1993, 2000, 2001 and the beginning of 2012.

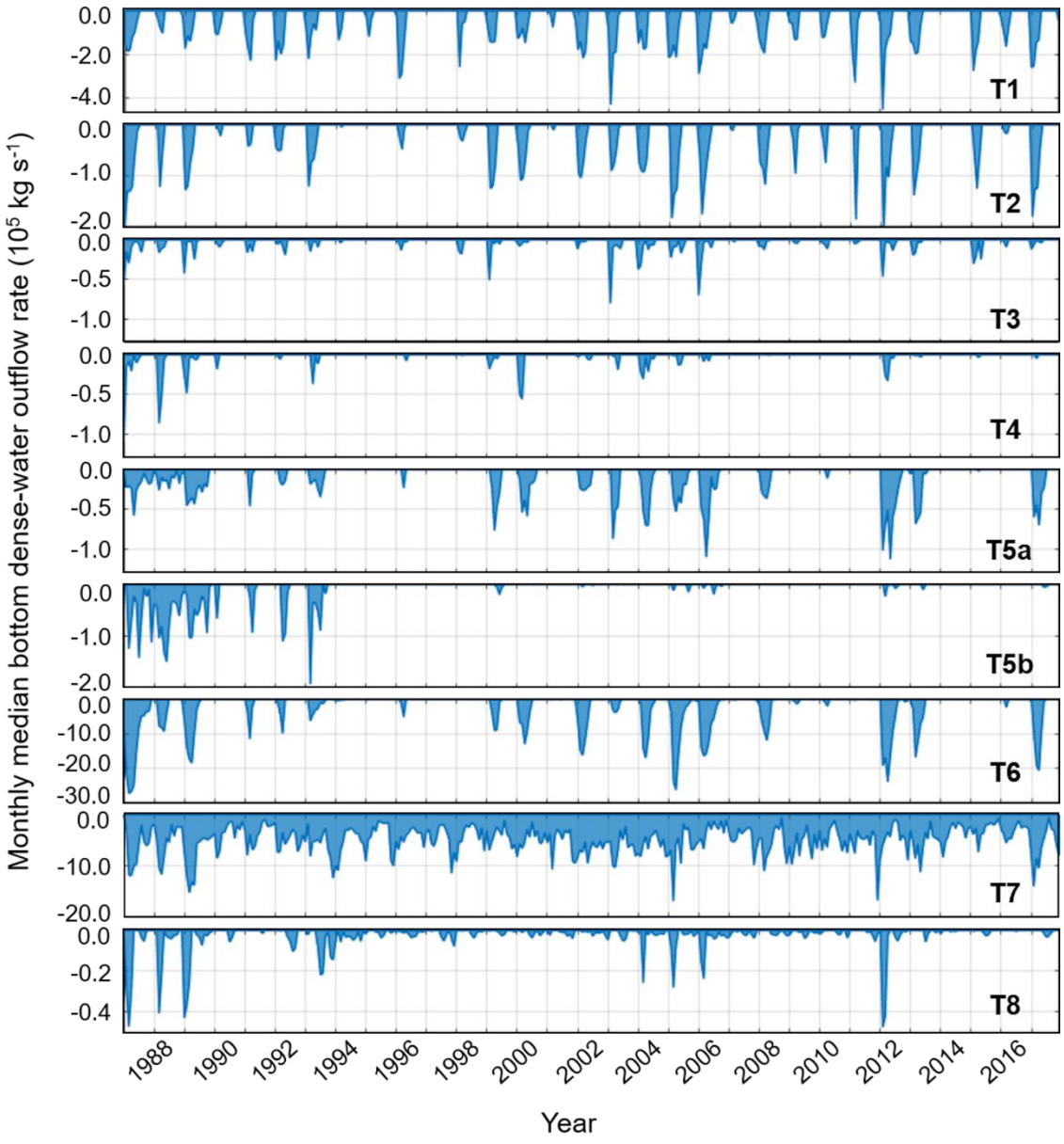

Figure 50. Time series of daily median bottom dense-water outflow rate in a month at transects: T1, T2, T3, T4, T5a, T5b, T6, T7 and T8 for the 1987–2017 period.

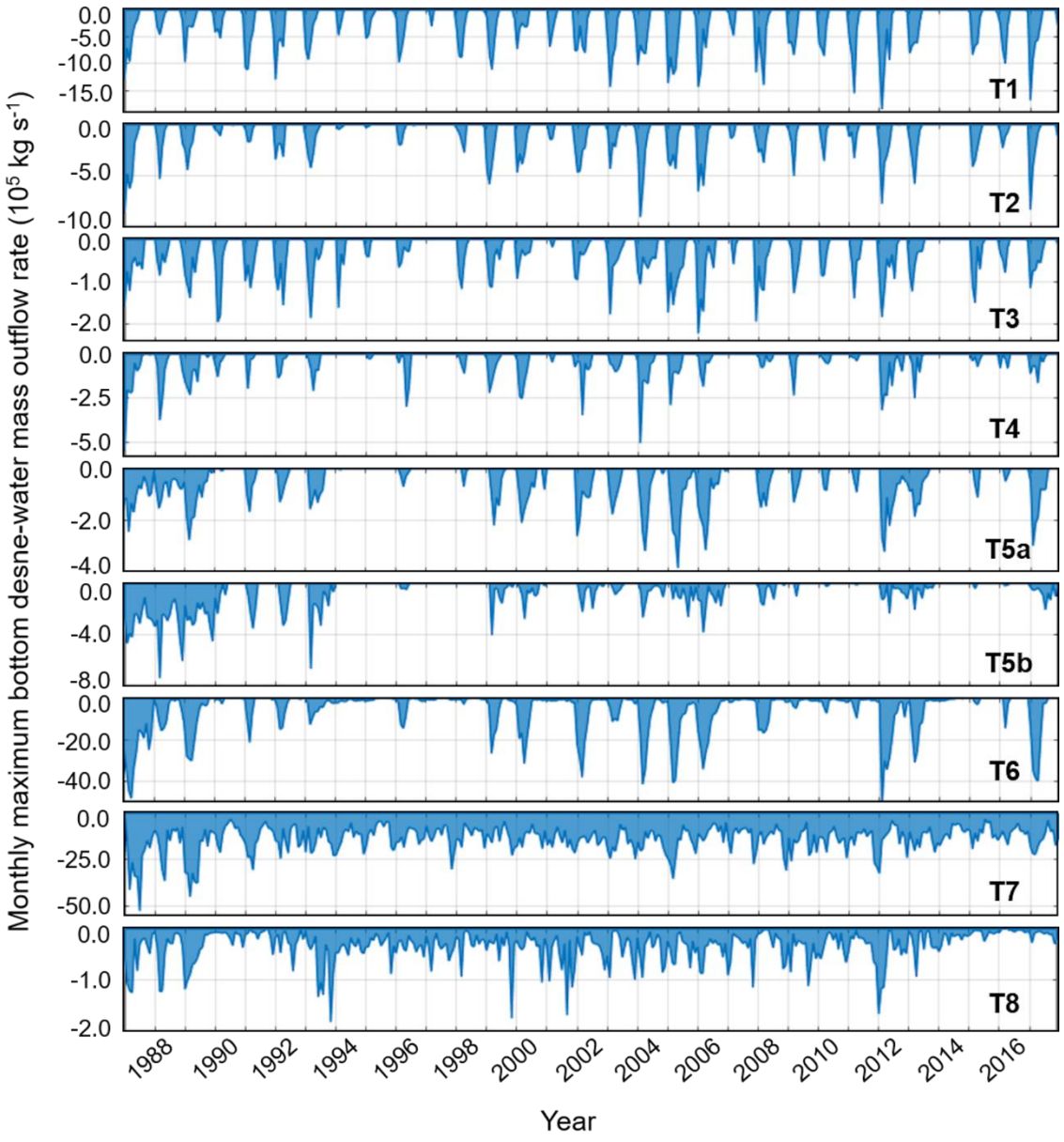

Figure 51. Time series of daily maximum bottom dense-water outflow rate in a month at transects: T1, T2, T3, T4, T5a, T5b, T6, T7 and T8 for the 1987–2017 period.

Next analysis is the 1987–2017 climatology of monthly bottom dense-water mass transported outward at nine transects (Fig. 52). At T1, the largest amounts of DW mass are transported from January to April in the range from $-2.9 \cdot 10^{11}$ kg (January) to $-5.1 \cdot 10^{11}$ kg (March). Similar distribution is obtained at T2 but with smaller values ranging from $-1.8 \cdot 10^{11}$ to $-2.6 \cdot 10^{11}$ kg. At T3, the transported DW mass is largest from February to May, ranging from $-0.2 \cdot 10^{11}$ kg to almost $-0.5 \cdot 10^{11}$ kg, while T4 shows smaller amounts, reaching almost $-0.3 \cdot 10^{11}$ kg. At T5a, the largest values are obtained in March (approximately $-0.8 \cdot 10^{11}$ kg) and they further decrease until June. The neighbouring transect T5b, shows its largest transported DW mass in March and May (down to $-0.2 \cdot 10^{11}$ kg), generally having smaller values than T5a. This

double maximum may be related to (1) direct outflow over the deepest parts of the Palagruža Sill occurring simultaneously in March, with the outflow along southern sections of the sill (T5a), and (2) a delayed outflow of DW originating either from old waters residing in the Jabuka Pit or from a spillover of new DW that first cascade into the pit and then overflow the deepest parts of the Palagruža Sill. Further southeast, at T6, the distribution peaks in March and April, reaching around -12.0 $\cdot 10^{11}$ kg, while in May, it reaches -4.0$\cdot 10^{11}$ kg, resembling the seasonality reproduced at T5a. Indeed, a delay between bottom DW mass outflow at T1 and other transects reveals the average time needed for the DW to travel until it cascades into the SAP. On average, it rapidly reaches the northwestern perimeter of the Jabuka Pit in less than a month, but the Jabuka Pit serves as an obstacle and collector of the densest water, after which the DW requires an additional month to be transported downslope to the deep SAP (if having sufficiently high PDA).

Further, at T7, the transported DW mass remains large throughout the year, increasing from January to March, when it reaches -20.0$\cdot 10^{11}$ kg, and then decreasing slowly until August down to -8.2$\cdot 10^{11}$ kg, after which it increases to -17.8$\cdot 10^{11}$ kg in December. These two maxima may resemble the outflow of DW from the SAP after its generation (the March maximum), while the December maximum could result from enhanced circulation and exchange of water masses in the Strait of Otranto, known to occur in late autumn/early winter (e.g., Mihanović et al., 2021). Undoubtedly, the general circulation and water mass exchange between the SAP and the northern Ionian Sea is a driver of the DW outflow throughout the year, considering the average capacity of the SAP to accumulate DW is about two years (Vilibić and Orlić, 2002). At T8, the bottom DW mass outflow values remain around -0.10$\cdot 10^{11}$ kg from January to March, decreasing until May. Larger values are obtained in July and August, reaching down to -0.14$\cdot 10^{11}$ kg, while the largest transported DW mass is produced in November (-0.16$\cdot 10^{11}$ kg) and December (-0.13$\cdot 10^{11}$ kg). At this shallow transect (up to 200 m), pulsations of the SAP and water exchange in the Strait of Otranto may cause the transport of DW along the shelf, sustaining a minimal DW outflow along a shelf throughout the year.

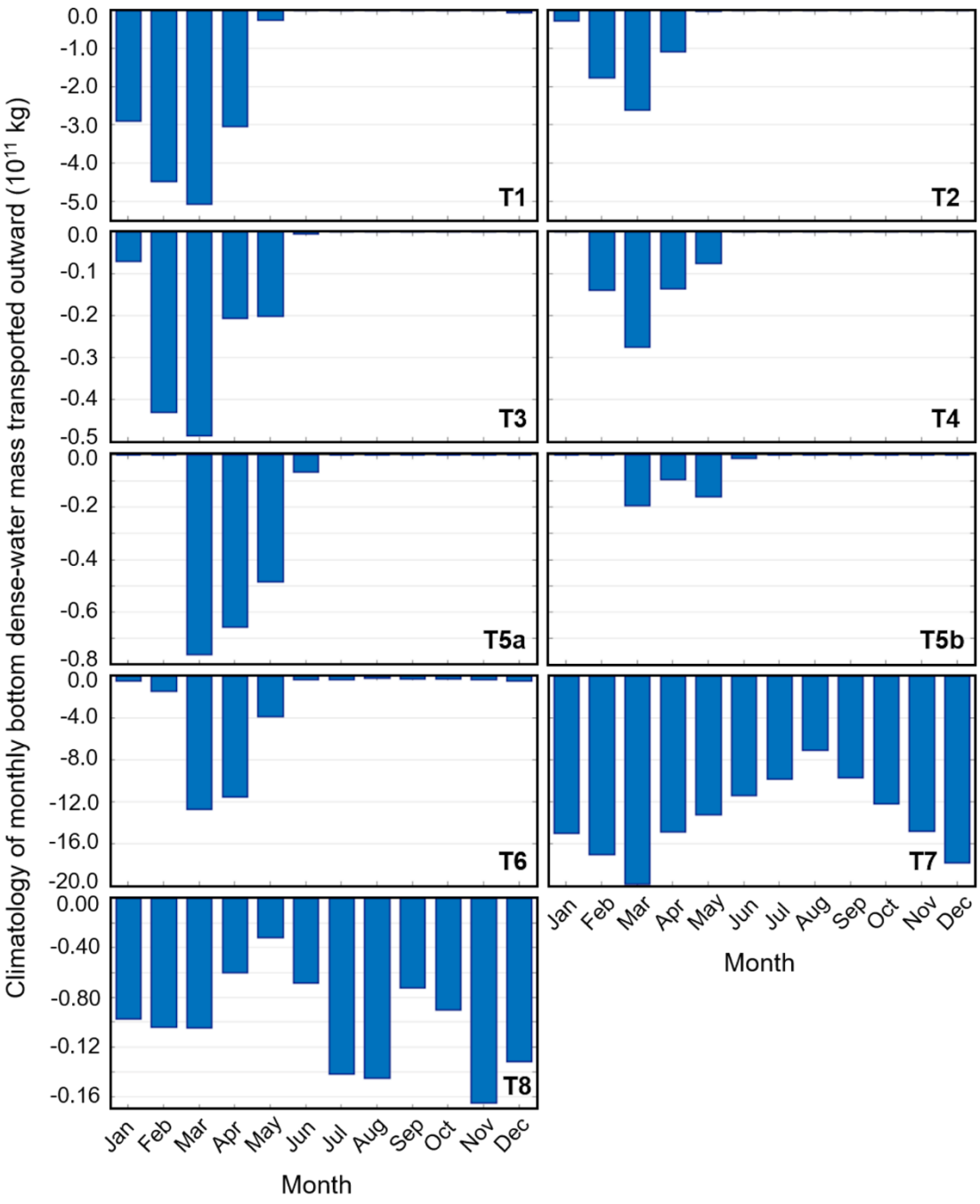

Figure 52. Climatology of monthly bottom dense-water mass transported outward at transects: T1, T2, T3, T4, T5a, T5b, T6, T7 and T8 for the 1987–2017 period.

Moreover, the 1987–2017 climatologies of median and maximum daily bottom dense-water outflow rate in a month at nine transects are presented in Fig. 53 and 54, respectively. The median outflow rate at T1 ranges between $-6.4 \cdot 10^4$ and $-14.6 \cdot 10^4$ kg s^{-1} from January to April, peaking in March. The maximum DW outflow rates are large in February ($-7.1 \cdot 10^5$ kg s^{-1}) as well as in January and March reaching down to $-6.3 \cdot 10^5$ kg s^{-1}. At T2, the largest median and maximum rates occur in February ($-5.1 \cdot 10^4$ kg s^{-1} and $-2.3 \cdot 10^5$ kg s^{-1}, respectively) and March

(-7.5·10^4 kg s^{-1} and -2.5·10^5 kg s^{-1}, respectively). Generally, the maximum daily bottom DW mass outflow from the DW formation sites is 2 to 3 times higher than its median in a month. At T3, the median outflow rates reach around -0.5·10^4 kg s^{-1} in February and March, whereas at T4 they are extremely small (the peak in March is smaller than -0.1·10^4 kg s^{-1}). However, the maximum rates at both transects are quite similar in magnitude, indicating potential strong pulsations of DW occurring along the shelf. At T3, the rates are pronounced from January to May, peaking in March (-0.8·10^5 kg s^{-1}), while at T4, the rates are larger from March to June, also peaking in March (-0.7·10^5 kg s^{-1}).

At T5a, the median DW rates are largest in March, reaching almost -0.2·10^4 kg s^{-1} and then decreasing until May, while at T5b median rates are null for all months. The latter suggests that DW transport over the deepest Palagruža Sill is not persistent, but having pulsations restricted to less than half of the respective months (March to May, when DW cumulative mass outflow is reproduced; Fig. 52). Maximum DW rates are similarly distributed, reaching around -1.0·10^5 kg s^{-}1 in March and April at T5a, and smaller values at T5b, around -0.8·10^5 kg s^{-1} in March and -0.4 ·10^5 kg s^{-1} in May. The similarity between T5a and T5b implies that although the flow is not persistent at the deepest Palagruža Sill section, it might be quite strong on certain days, comparable to the flow along the southern section of the Palagruža Sill. At T6, the median outflow rates are largest in March and April reaching -44.1·10^4 kg s^{-1}, while the maximum rates sharply peak in March (-12.9·10^5 kg s^{-1}) and slowly decrease toward May (-6.8·10^5 kg s^{-1}).

For T7, the median rates increase until March (53.1·10^4 kg s^{-1}), after which they decrease until August (33.2·10^4 kg s^{-1}) and then increase again towards December (50.5·10^4 kg s^{-1}). The maximum DW rates are similarly distributed as the median rates, reaching -18.5·10^5 kg s^{-1} in December, approximately three times larger than the median rates. Lastly, at T8, the median outflow rates peak in July (-0.32·10^4 kg s^{-1}) and August (-0.25·10^4 kg s^{-1}), while for half of year, they remain zero or close to zero. In contrast, the distribution of the maximums is completely different, resembling the cummulative monthly values (Fig. 8), again indicating strong pulsations of the DW, restricted to less than half a month, particulary between December and May. The maximum DW outflow rates have three peaks: in March (-0.36·10^5 kg s^{-1}), July and August (-0.29·10^5 kg s^{-1}), as well as in November (-0.43·10^5 kg s^{-1}). From the analyses of the DW climatologies, it is evident that the peaks of distributions shift from early winter months towards spring as the transect location moves from the northern to the southern Adriatic.

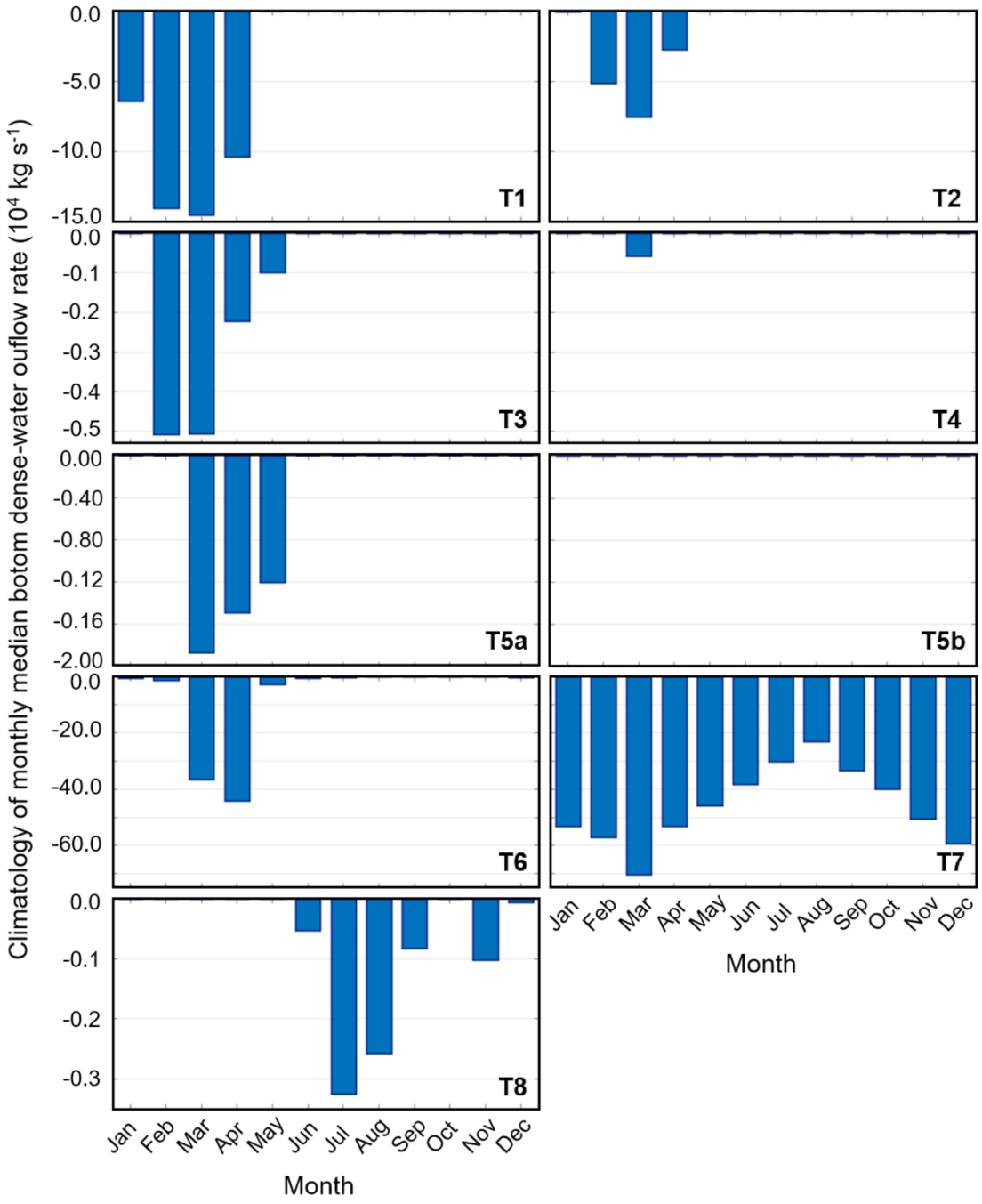

Figure 53. Climatology of daily median bottom dense-water outflow rate in a month at transects: T1, T2, T3, T4, T5a, T5b, T6, T7 and T8 for the 1987–2017 period.

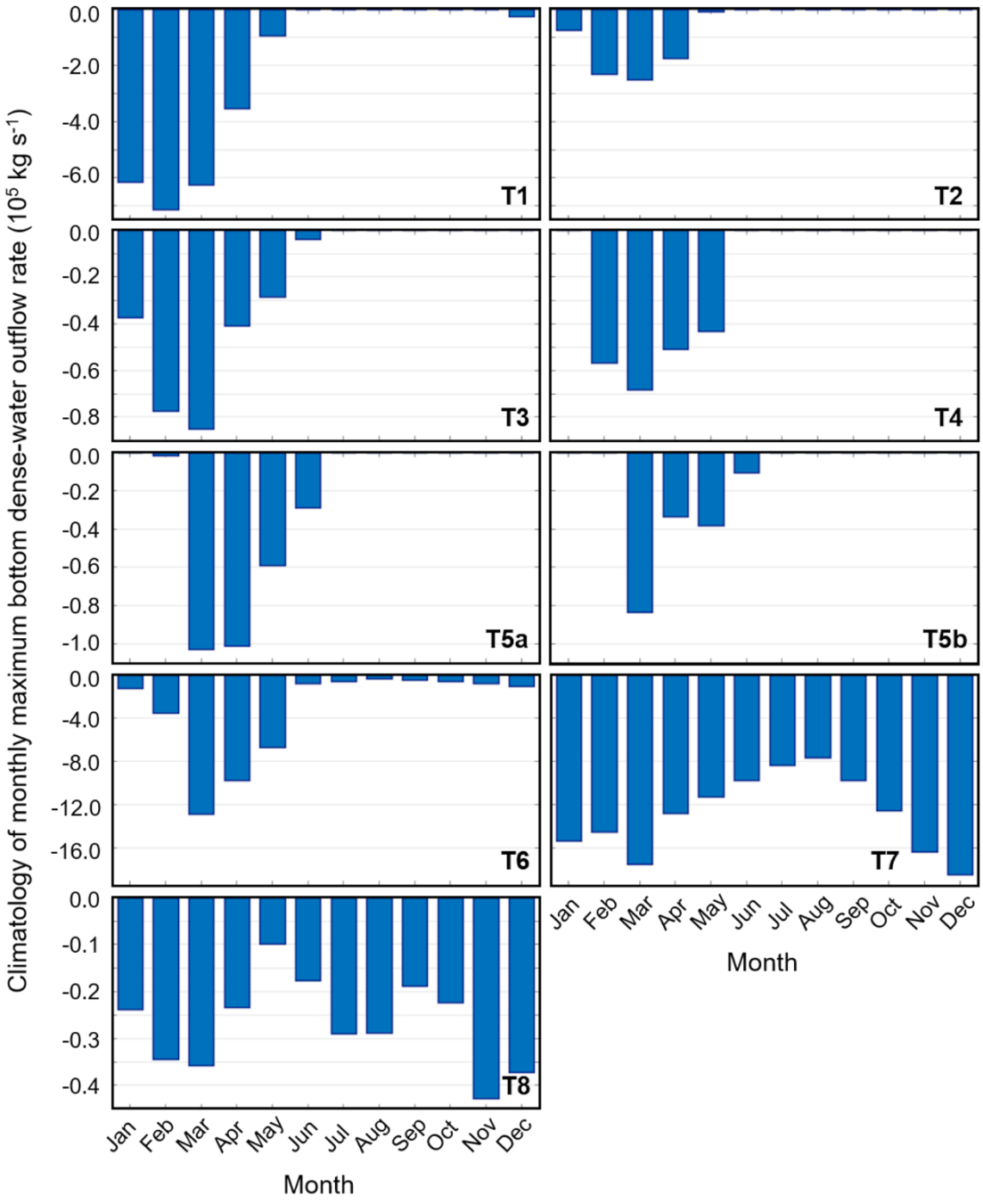

Figure 54. Climatology of daily maximum bottom dense-water outflow rate in a month at transects: T1, T2, T3, T4, T5a, T5b, T6, T7 and T8 for the 1987–2017 period.

5.3. Dense-water accumulation

This section analyses the accumulation of DW during the 1987–2017 period in three accumulation sites defined as three subdomains: the deep Kvarner Bay (DKB), Jabuka Pit (JP) and deep Adriatic (SAP). The JP and the SAP are well-known and well-researched DW accumulation sites (e.g., Zore-Armanda, 1963; Vilibić, 2003; Krasakopoulou et al., 2005; Marini et al., 2006; Querin et al., 2016), while the DKB, being much deeper than the adjacent open northern Adriatic shelf, is the place where the dense waters generated in the KB are gravitationally attracted and reside for much of a year (Janeković et al., 2014; Pranić et al., 2023).

First, the daily time series of bottom PDA in the three subdomains and the PDA rate of change only for the JP and SAP are presented in Fig. 55. The general pattern in the DKB is that the PDA sharply increases at the beginning of the year, when the DW generation is occurring, and then sharply decreases at the end of the year, when vertical mixing of the whole water column is occurring (Vilibić et al., 2018). The years with the largest PDAs (> 29.6 kg m^{-3}) are: 1993, 2000, 2002, 2004–2006, 2012 (up to 30.0 kg m^{-3}) and 2017. Interestingly, two PDA peaks are frequently occurring during a year, the first in February–March when the DW formation is occurring, and the second a few months later, during the summer months. The second maximum probably resembles the post-generation spreading of DW inside the KB and the associated thermohaline circulation, where DW sinks from the shallow parts of the KB as a slow bottom density current and reaches its deepest sections (KBD) in a few months.

In the JP, in some years, there is a sharp increase of PDA at the beginning of the year, but in some of them, there is only approximately linear decrease from the previous year. This means that in the latter years, the generated DW was not dense enough to alter the bottom PDA, i.e, to cascade to the JP. As a consequence, PDA time series exhibits a „saw-tooth“ pattern with large changes every 1–3 years, previously detected in shorter ocean simulations (Mihanović et al., 2018). The years with largest PDA peaks are: 2002, 2005, 2012 (up to 29.75 kg m^{-3}) and 2017, which also have the largest PDA rates of change between 7.0–12.0 10^{-8} kg $m^{-3}s^{-1}$. Indeed, the DW formation in 2017 occurred in January during extremely cold weather conditions over the northern Adriatic (Croatian Meteorological and Hydrological Service; DHMZ, 2018), leading to the generation of DW with a larger PDA difference compared to the deep residing waters, which therefore experienced faster cascading in the JP due to buoyancy effects. Interestingly, the PDA rate of change was somewhat lower in 2012, when the DW

generation occurred in early February (Mihanović et al., 2013). For another year with an extreme PDA rate of change, 2002, the major DW generation event occurred also in January (Fig. 47), supporting the hypothesis that if an exceptional DW event occurs earlier in the northern Adriatic, it generates stronger bottom density currents and exhibits more intense cascading into the JP. Further, as a general rule, the years with smaller PDA peaks also have smaller PDA rates of change.

In the SAP, during the 1989–2000 period PDA generally decreased to 29.23 kg m^{-3} with smaller annual variations. After 2000, the PDA slowly increased each year until 2005, when there was a very sharp rise to 29.30 kg m^{-3} with a PDA rate of change of 6.3 10^{-8} kg $m^{-3}s^{-1}$. This large PDA rate of change is, alongside severe winter and generation of DW in the northern Adriatic, driven by low resident PDA values that were preceeding early 2000s due to the overall EMT/BiOS-driven decrease in salinity and therefore density of the Adriatic dense waters (Vilibić et al., 2012). The next sharp increase in the SAP bottom PDA values occurred during the 2012, reaching slightly less than 29.30 kg m^{-3}, with a rate of change smaller than in 2005, as the preceeding PDA values were much higher than in 2005. Another smaller peak of bottom PDA can be noticed in 2017, restricting the DW cascading during this event just in the JP, with much lower intensity in the SAP. Convincingly, it can be seen that the PDA time series in the SAP also exhibits the saw-tooth pattern already measured by near-bottom sensors at the E2-M3A buoy (Querin et al., 2016), while the AdriSC climate model results indicate large PDA changes occurring there every 5–10 years.

Further, the time series of bottom temperature and salinity in the three subdomains during the 1987–2017 period are presented in Fig. 56. In the DKB, the bottom temperature exhibits strong seasonal oscillations ranging from 8.5–17.5 °C, where a sharp inrease in temperature is the result of vertical mixing reaching the bottom in late autumn (November–December), subsequently decreasing to initial values by February due to consistent wintertime heat losses and cooling events (e.g., Artegiani et al., 1997a). Years with the lowest winter temperatures (< 10 °C) are: 1993, 1999, 2000, 2005, 2006 and 2012. Additionally, a general positive temperature trend can be noticed during the 31–year period. In contrast, bottom salinity demonstrates completely different behaviour from temperature, with strong interannual oscillations and multi-year periods of smaller and larger values. Smaller salinites within the 37.9–38.4 range are produced during the 1987–1999 period, followed by a period of larger salinites in the 38.2–38.7 range from 2000–2008, resembling the BiOS cycles, as noticed for the DW generation. After 2008, a short period of smaller salinities occured from 2009–2011.

In 2012, very large salinities surpassing 38.7 coincided with very low temperatures (down to 9 °C), indicating the accumulation of extremely dense waters. Similar situation was produced previously in 2005 and later in 2017. Furthermore, it is interesting to notice that a sharp temperature increase in late autumn typically coincides with an increase in salinity, revealing the advection of higher salinity open Adriatic waters in autumn, which are decreasing buoyancy and allowing for vertical mixing to reach the bottom. Salinity is again dropping during the DW generation, indicating that the generated and advected waters to the DKB have lower salinity, as coming from shallower regions with more prononunced cooling effects.

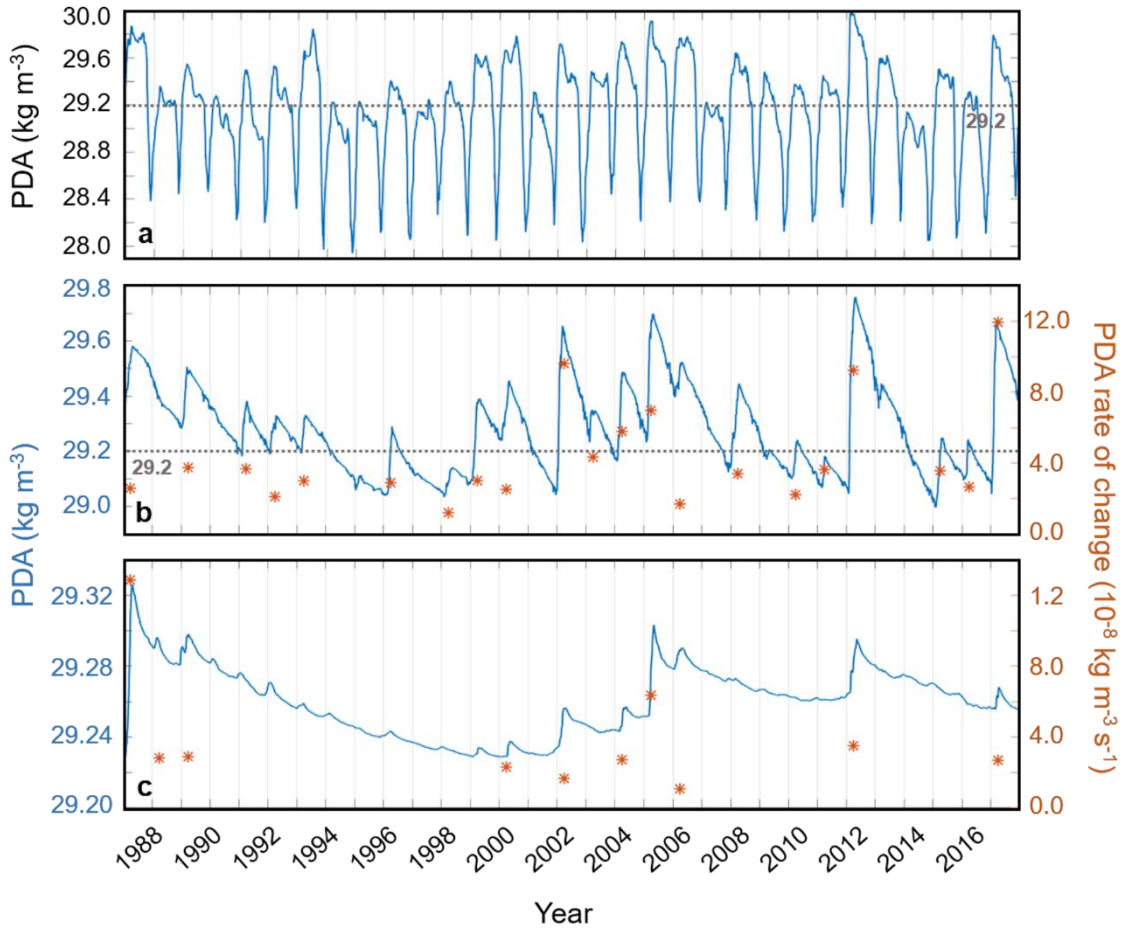

Figure 55. Daily time series of bottom PDA in the (a) deep Kvarner Bay, (b) Jabuka Pit and (c) deep Adriatic as well as the bottom PDA rate of change for Jabuka Pit and deep Adriatic subdomains in the 1987–2017 period.

In the other two subdomains bottom temperature and salinity exhibit different behaviours than in the DKB, as expected due to their greater pit depths and the fact that vertical mixing is not usually reaching the bottom. In the JP, some years have a large late-winter temperature decrease that is a result of colder DW cascading into the pit. Conversely, in years lacking this

cascading phenomenon, the temperature tends to continue rising. The temperature mostly varies within the 10.5–13.5 °C range, with larger drops in 2002 and 2012, while the highest peak is produced at the beginning of 2015. Salinity is generally smaller until 2000 (around 38.4–38.5), when it increases up to 38.7. After a brief period of smaller values (2009–2011), a drastic increase in salinity is obtained from 2012–2015 followed by relatively large values. Aside from the long-term trends, BiOS-driven quasi-decadal oscillations in salinity can be seen, consistent with other investigated series. In all years except 2012, a drop in temperature is conjoined with a drop in salinity, indicating that the DW generated in the northern Adriatic has lower salinity than the residing waters in the JP. Notably, in 2012, a sharp salinity increase is associated with a sharp decrease in temperature, indicating the arrival of highly saline waters in the northern Adriatic during autumn 2011, reaching DW sites in winter 2012.

In the SAP, bottom temperature and salinity exhibit similar behaviour, showing a positive trend towards the end of the 31-year period. The temperature generally ranges between 12.3 and 13.2 °C, with the largest drops occurring in 2002, 2005 and 2012 when it decreased by slightly more than 0.2 °C during winter. Salinity ranges between 38.60 and 38.73, with several larger jumps such as from 2001–2002, in 2005 and from 2011–2012. It is noteworthy that during the 1988–2001 period the salinity-to-temperature ratio decreased, which is probably linked to the Eastern Mediterranean Transient (EMT; Klein et al., 1999). The ratio was later restored until the mid-2000s over a period of four to five years. In addition, a saw-tooth pattern is observed in both temperature and salinity time series in the JP and SAP. Differently than in the JP, the decrease in temperature in 2012 at the bottom of the SAP is conjoined with the decrease in salinity, so that the precondition of highly saline waters prevented much stronger cascading of DW there.

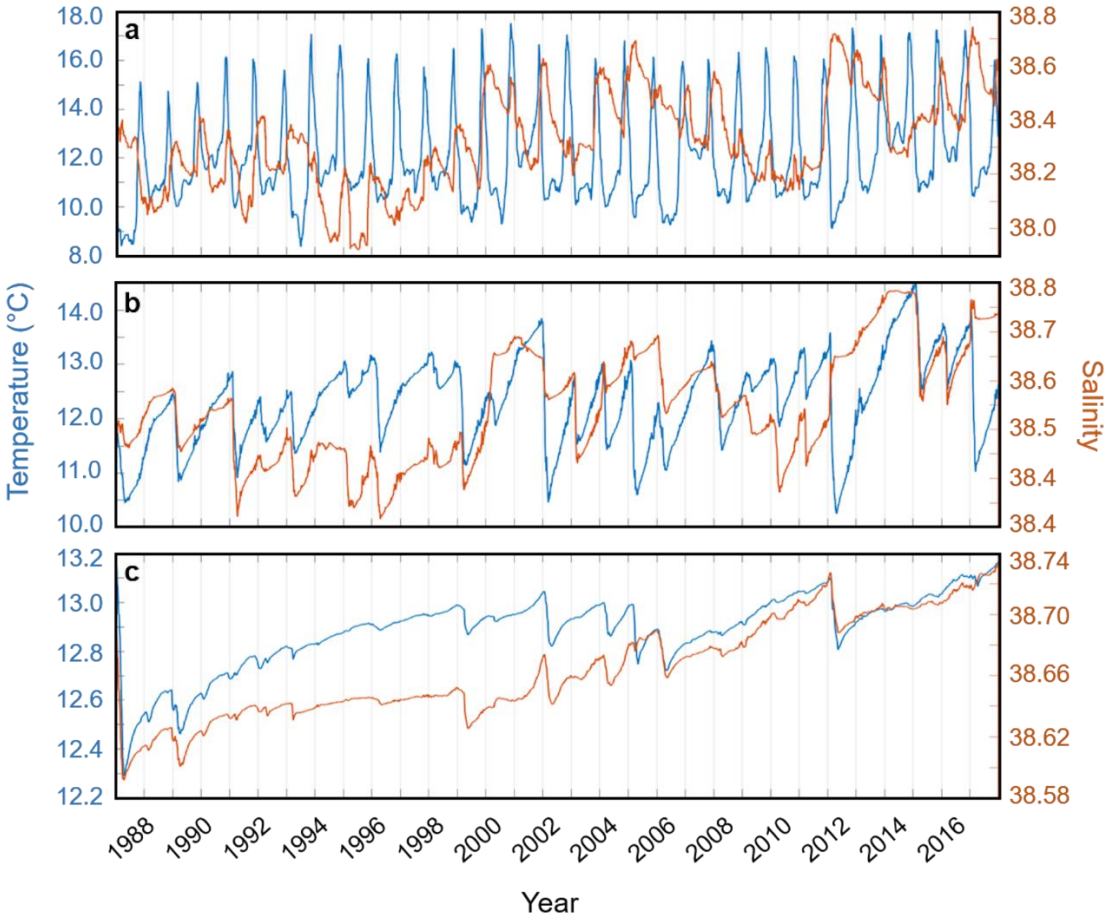

Figure 56. Daily time series of bottom temperature and salinity in the (a) deep Kvarner Bay, (b) Jabuka Pit and (c) deep Adriatic subdomains in the 1987–2017 period.

The next analysis is presented in the form of box plots of the maximum bottom PDA, DOY of maximum PDA as well as the bottom temperature and salinity at the DOY of maximum PDA for the DKB, JP and SAP (Fig. 57, 58 and 59, respectively).

In the DKB, the waters with the largest maximum PDAs (> 30.0 kg m^{-3}) were accumulated in 2012 during late February and early March, coinciding with low temperatures around 8.5 °C and very large salinities up to 38.7 (Fig. 57). In contrast, 2014 was the year with smallest maximum PDAs (< 29.2 kg m^{-3}), along with high temperatures (around 12.0 °C) and moderate salinities (~38.3–38.4). As the bottom DKB waters are renewed every year, such higher temperatures were a consequence of unusually small heat losses and the complete absence of DW during the winter of 2014 (Mihanović et al., 2018), following a very wet year and autumn of 2013 (DHMZ, 2014). In 2001 and 2007, the largest maximum PDAs (< 29.5) are obtained at the end of the year, while for other years, the mean DOY of maximum PDA mostly varies in the first half of the year. Positive trends in temperature and salinity can be noticed during

the 31-year period, which accounts for the fact that the average density of the accumulated waters did not change significantly throughout the simulation.

In the JP (Fig. 58), the 1990–2001 period is characterized by smaller maximum PDAs (< 29.5 kg m^{-3}), while the 2002–2017 period has stronger interannual variations with several years of larger maximum PDAs (> 29.5 kg m^{-3}). If PDA in a year is preceded by the lower PDA (i.e. if cascading of DW occurred in a year), the median of the distributions of DOY of maximum PDA spans between DOY 70 (early March) and DOY 120 (late April). This indicates that the time difference between reaching maximum PDA in the JP and generation in the NA and KB is about 2–3 months, although cascading to JP begins month or less after DW generation. Convincingly, the DW cascading to the JP lasts for 1–2 months. Mean temperatures mostly vary between 9.5–12.5 °C, while mean salinities range between 38.25–38.75. The difference between DW formation years is apparent, e.g., between 2006 and 2012: while the bottom JP temperatures reached around 9 °C after DW cascading in both years (to note, 10.0 °C was the minimal temperature observed in JP during 2012; Mihanović et al., 2013), salinity difference between these two years reached 0.2. As for the other series, a general positive trend can be noticed for the temperature and salinity distributions.

In the SAP, a continuous decrease in the maximum PDA is reproduced from around 29.32 kg m^{-3} in 1989 to 29.23 kg m^{-3} in 1998, while temperature and salinity both increased from 12.5 to 12.8 °C and from 38.60 to 38.63, respectively (Fig. 59). After that, maximum PDAs increased in several years until 2005, reaching up to 29.33 kg m^{-3}. A subsequent period of decrease is interrupted by a jump in 2012 and again in 2017. If PDA in a year is preceded by the lower PDA (i.e. if cascading of DW occurred in a year), median of the distributions of the DOY of maximum PDA are spanning between 90 (late March, in 2002) and 140 (mid May, in 2005). Temperature and salinity both show a positive trend with small variations when the DW cascading occurs.

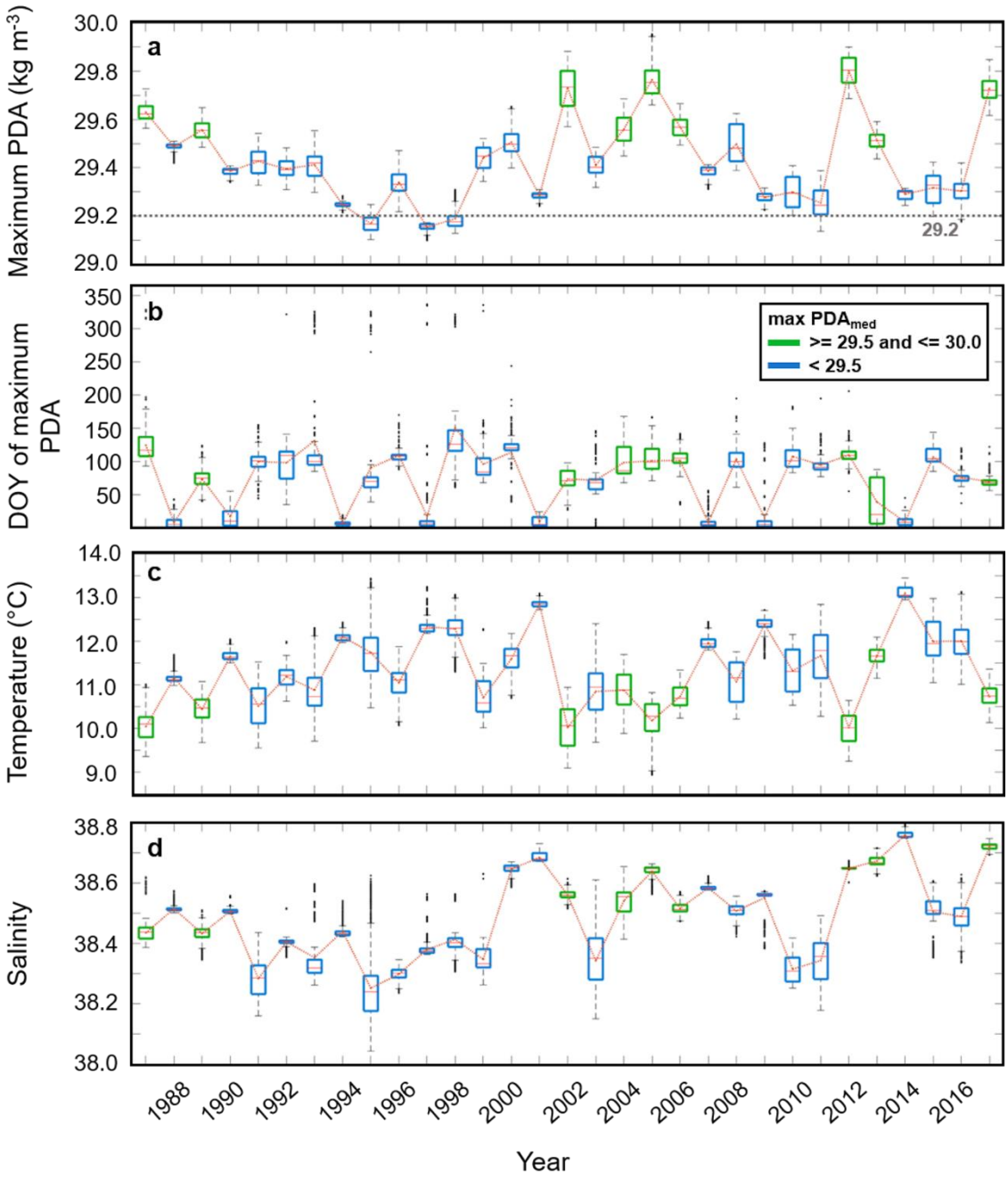

Figure 57. Box plots of (a) maximum bottom PDA, (b) DOY of maximum PDA, (c) bottom temperature and (d) salinity at the DOY of maximum PDA for the deep Kvarner Bay subdomain in the 1987–2017 period. The red line inside each box plot denotes the median of the distribution. The orange dotted line connects the mean values of the distributions.

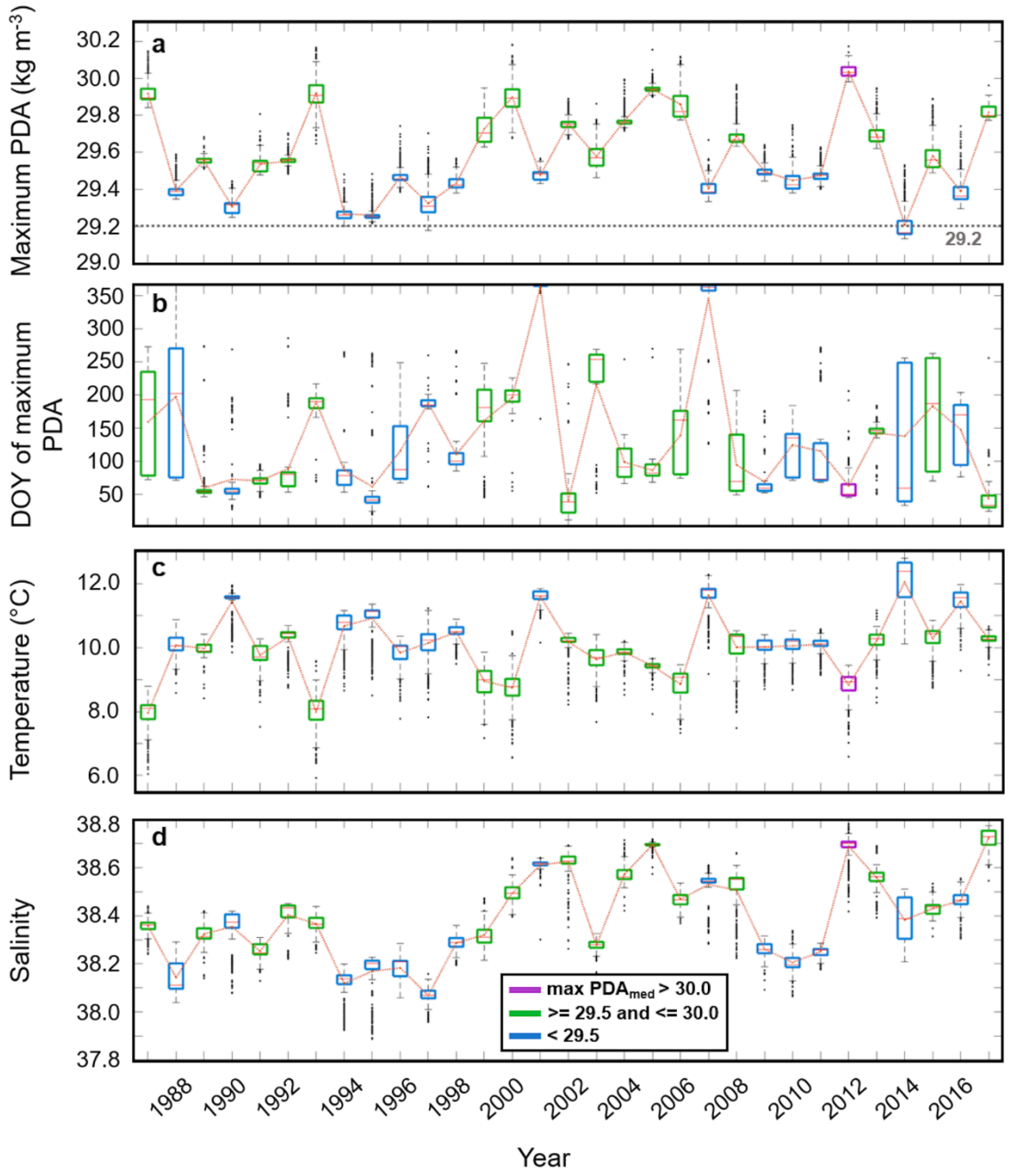

Figure 58. Box plots of (a) maximum bottom PDA, (b) DOY of maximum PDA, (c) bottom temperature and (d) salinity at the DOY of maximum PDA for the Jabuka Pit subdomain in the 1987–2017 period. The red line inside each box plot denotes the median of the distribution. The orange dotted line connects the mean values of the distributions.

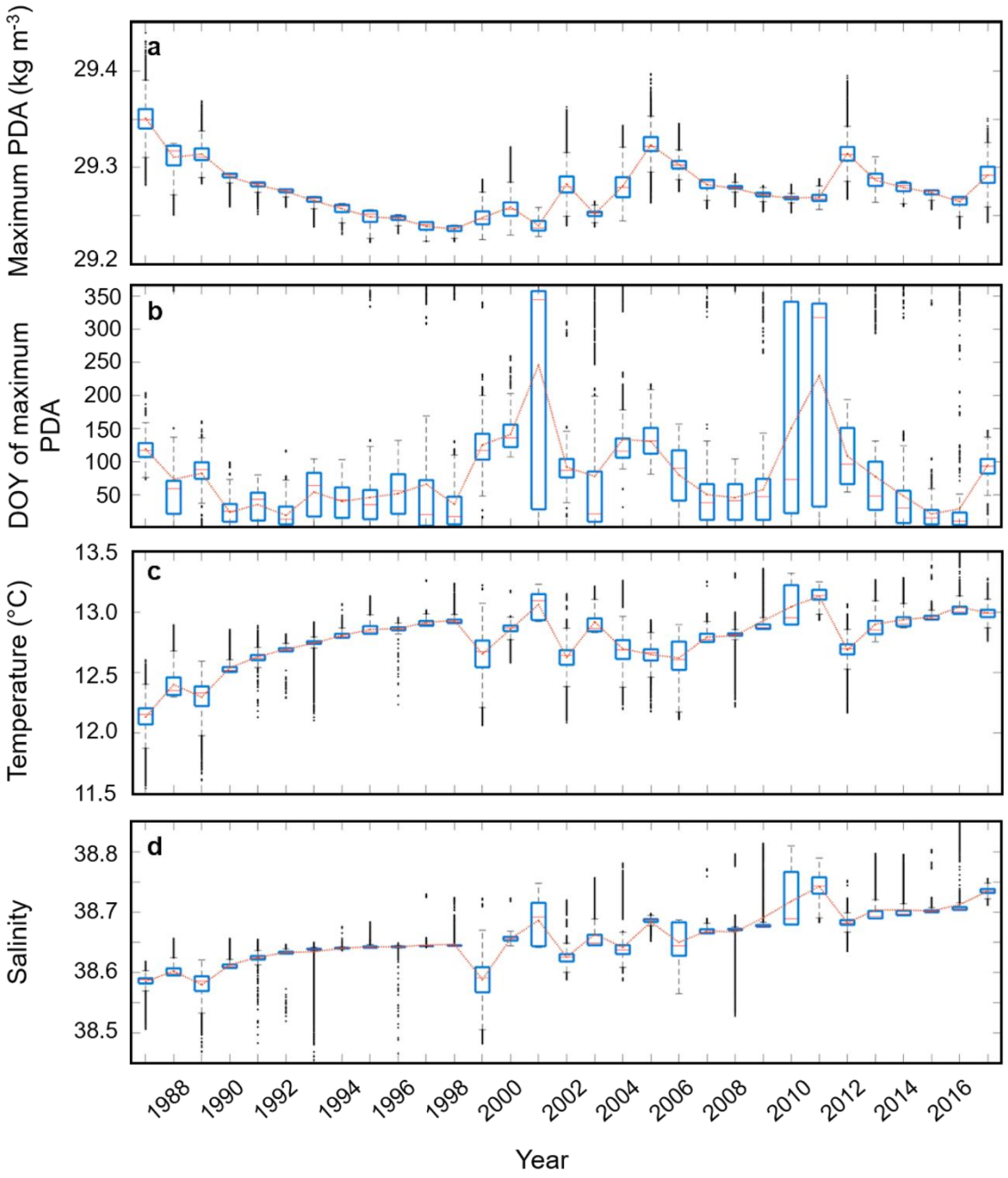

Figure 59. Box plots of (a) maximum bottom PDA, (b) DOY of maximum PDA, (c) bottom temperature and (d) salinity at the DOY of maximum PDA for the deep Adriatic (SAP) subdomain in the 1987–2017 period. The red line inside each box plot denotes the median of the distribution. The orange dotted line connects the mean values of the distributions.

Further, the monthly box plots of bottom PDA, temperature and salinity for the DKB, JP and SAP subdomains are presented on Fig. 60, 61 and 62. In the DKB, PDAs are largest from February to May, peaking in March at around 29.22 kg m^{-3}. Then they decrease until June, keeping these values for almost three months, which are driven by the slow DW spreading from shallower parts of the KB, where DW generation occurs, to the deepest KB sections (KBD). After September, there is a steep decrease in PDA, with a minimum in November around 28.24 kg m^{-3}, when the whole water column is mixed. The temperature follows the PDA distributions but in an inverse manner, with a minimum in March down to 10.5 °C and a maximum in November up to 15.7 °C. Salinity shows its largest values in January and February (around 38.39), after which it decreases, reaching a minimum in October of approximately 38.26, followed by a sharp increase until December and largest variability in November.

In the JP, the smallest PDAs are produced in January around 29.3 kg m^{-3}, after which there is an increase until April, when they reach around 29.35 kg m^{-3}. Therefore, the DW cascading into the JP lasts from February to April on average. Subsequently, from May to December, PDAs slowly decrease to around 29.23 kg m^{-3}, due to the slow mixing with the warmer and more saline intermediate waters. Temperature distributions are very similar to PDA distributions but inversed. Minimum temperatures are reached in April down to 11.7–12.0 °C, after which they increase. Salinities are larger in January and February (around 38.56–38.57) followed by a sharp decrease until May down to 38.52, after which they increase until December, indicating a lag of a month after the temperature changes.

Lastly, monthly box plots in the SAP reveal relatively small variations. PDAs slowly increase from February to peak around 29.26 kg m^{-3} in April and May, after which they slightly decrease until the end of the year. Indeed, these distributions indicate the possibility of DW cascading reaching the bottom of the SAP between late February and May. Temperature and salinity have similar behaviour, decreasing until April and May and then slowly increasing until December. The monthly variations in median temperature and salinity are approximately 0.5 °C and slightly larger than 0.01, respectively.

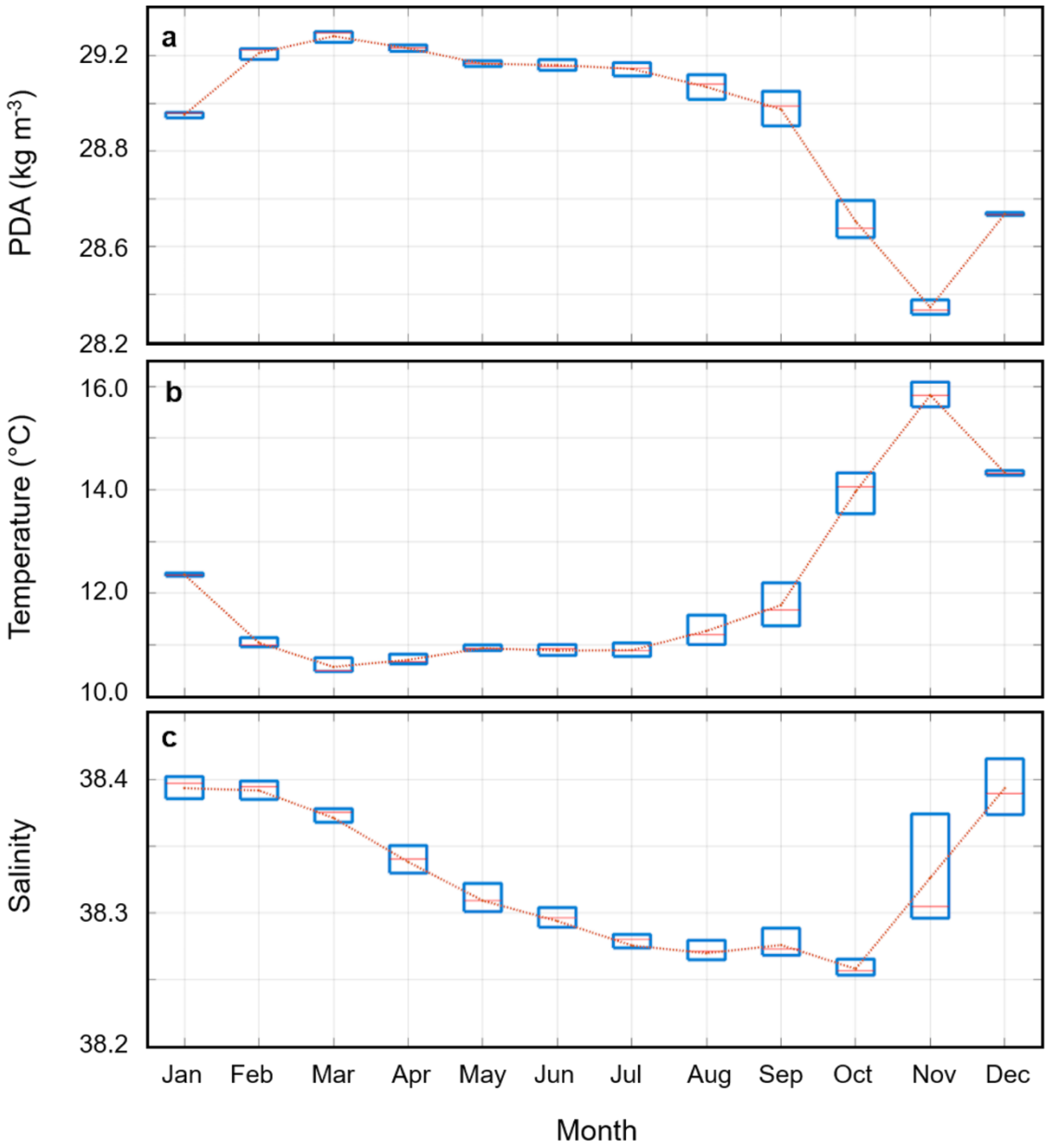

Figure 60. Annual courses of monthly box plots of (a) bottom PDA, (b) temperature and (c) salinity for the deep Kvarner Bay subdomain in the 1987–2017 period. The red line inside each box plot denotes the median of the distribution. The orange dotted line connects the mean values of the distributions.

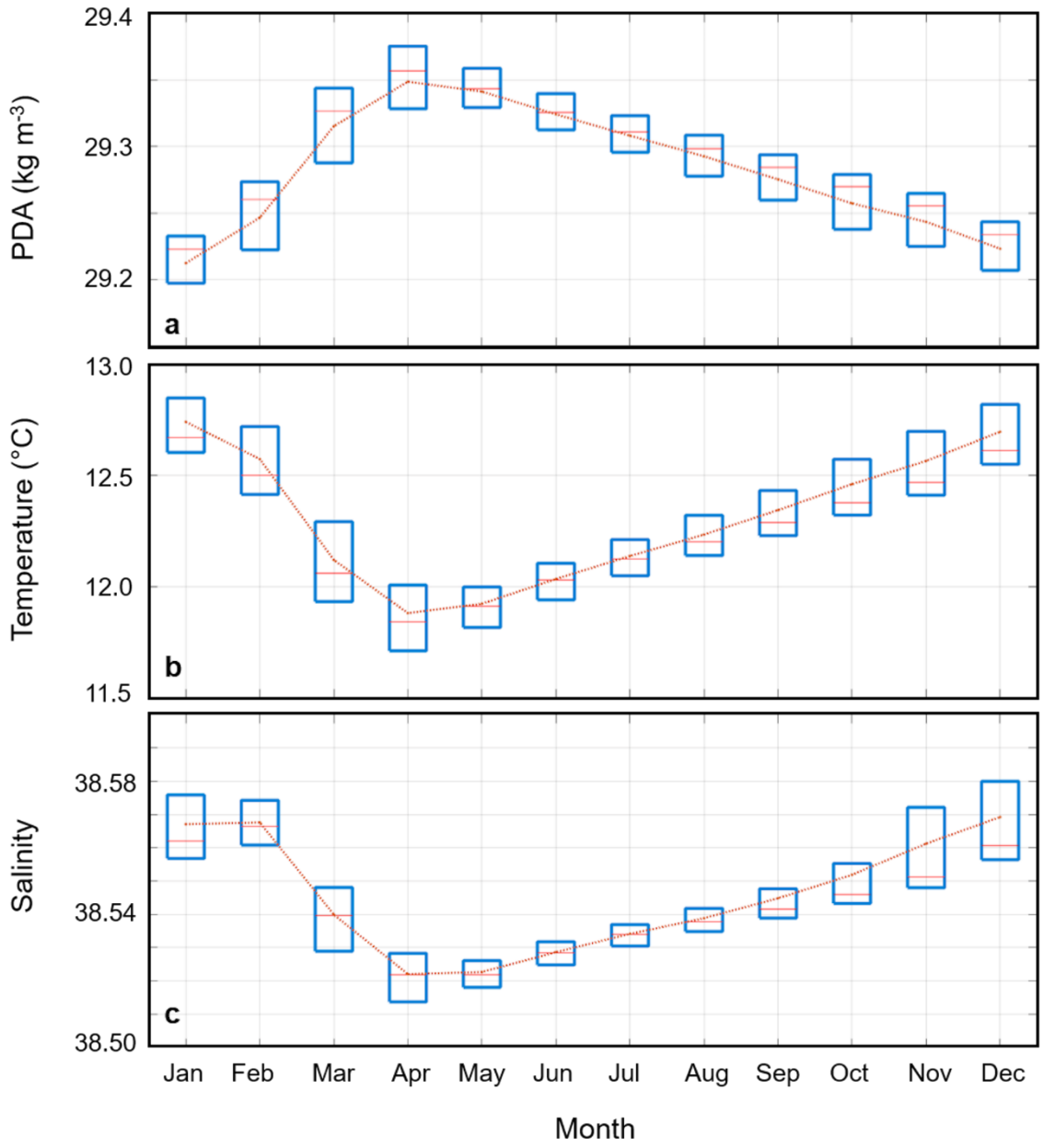

Figure 61. Annual courses of monthly box plots of (a) bottom PDA, (b) temperature and (c) salinity for the Jabuka Pit subdomain in the 1987–2017 period. The red line inside each box plot denotes the median of the distribution. The orange dotted line connects the mean values of the distributions.

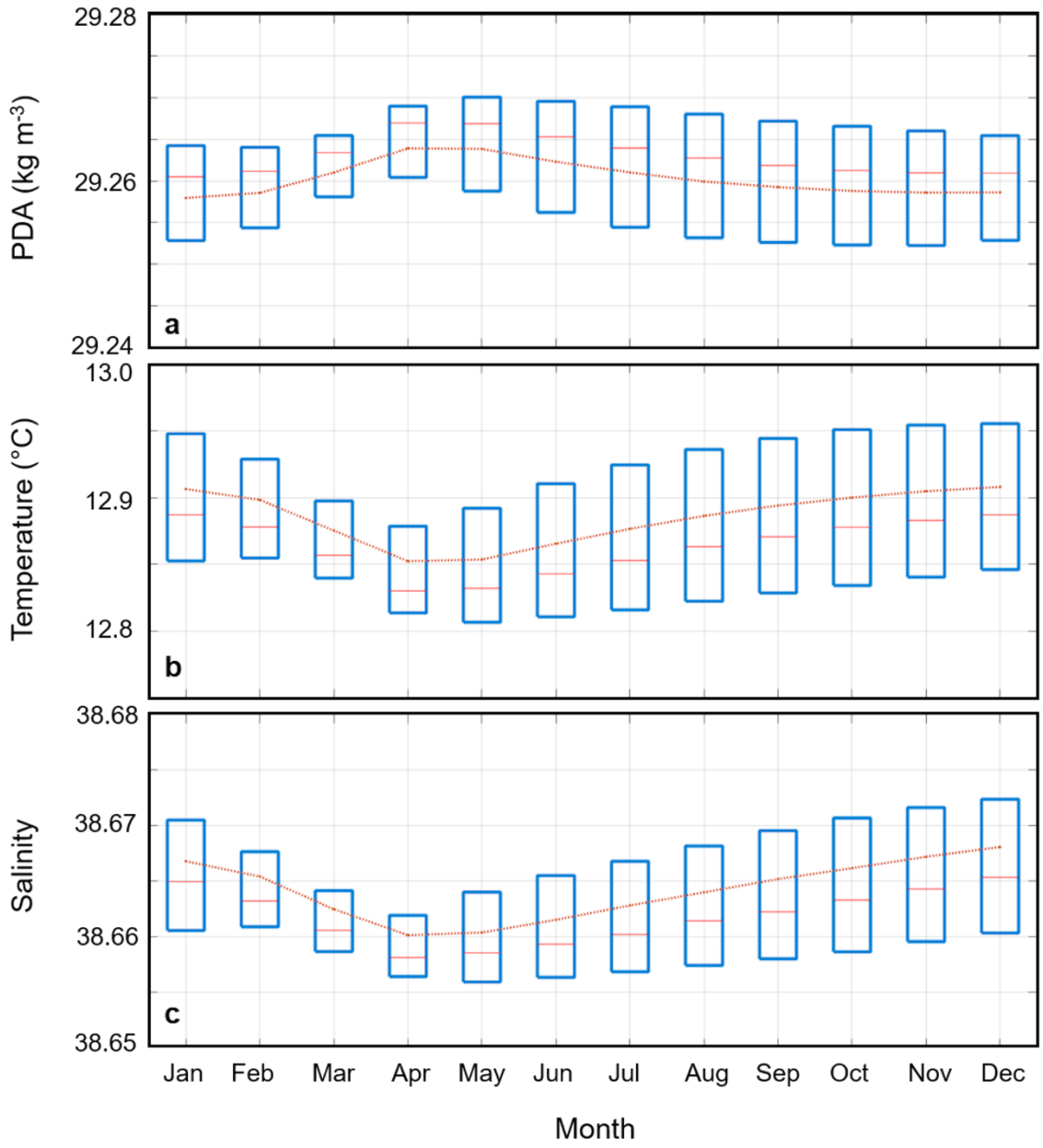

Figure 62. Annual courses of monthly box plots of (a) bottom PDA, (b) temperature and (c) salinity for the deep Adriatic (SAP) subdomain in the 1987–2017 period. The red line inside each box plot denotes the median of the distribution. The orange dotted line connects the mean values of the distributions.

5.4. Discussion

The presented analyses provide a long-term overview of the modelled DW generation, spreading and accumulation processes in the Adriatic Sea using kilometre-scale climate model results. Concerning DW generation in the NA and KB, the results show that bottom winter temperatures are lower in the NA compared to the KB and bottom temperature distributions during maximum bottom PDAs demonstrate lower values in the NA. Therefore, the cooling rates during severe bora outbreaks – that are larger over the KB than over the NA (e.g., Janeković et al., 2014) – are less important for the temperature decrease (and therefore PDA increase) than the ocean volume to be cooled, which is proportionate to its depth. The bottom salinites are generally larger in the KB, as the NA salinities are influenced by the large river loads spreading over the entire NA during the stratification period (April–October). Still, the salinity distributions during maximum PDAs when the freshwater load is constrained to coastlines (e.g., Artegiani et al., 1997a), are very similar between the two generation sites. The PDFs of thermohaline properties reveal that in the AdriSC simulation, the differences in maximum PDA in winter months between the NA and KB are mostly influenced by the differences in temperature. Although DW generation is less intense and less common in the KB than in the NA, the PDA in the KB surpassed 29.2 kg m^{-3} in most years, reaching extreme values in winter of 2012, closely resembling those in the NA.

Further, the analyses of DW spreading show that the transects at the Otranto Strait exhibit completely different dynamics compared to other transects in the Adriatic, as being driven also by open-ocean convection in the middle of the SAP, while the variability in the SAP gyre modulates the coastal DW flow south of the Bari Canyon. Also, the maximums of the monthly bottom DW outflow rate distributions shift from winter towards spring months as the transect locations are moving from northwest to southeast. The contribution of the KB site to the overall DW mass outflow is estimated between 25–35%, which is slightly lower compared to the estimates from Janeković et al. (2014) during the winter of 2012.

Regarding the DW accumulation, the PDA in the DKB undergoes annual changes due to mixing of the whole water column in autumn (November–December) and it is mostly larger than 29.2 kg m^{-3} during winter. In contrast, the thermohaline properties in the JP and SAP differ from the DKB and exhibit a distinct saw-tooth-like pattern. The hypothesis about the saw-tooth modulation was first presented by Querin et al. (2016) for the SAP and later supported by Mihanović et al. (2018) for the JP. According to the AdriSC simulation, the

bottom layer of the SAP is renewed every 5–10 years, aligning with previous research findings. The deep waters in the JP are renewed more frequently, every 1–3 years, given its substantially shallower depth compared to the SAP, thus requiring less buoyancy to reach the bottom.

Furthermore, the PDA rate of change is larger in the JP than in the SAP, which is expected as JP is closer to the DW generation area, and it reaches maximum in different years in the JP and the SAP. Interannual variability in salinity is similar between the DKB and JP, connected mostly by basin-wide variability driven by exchanges of BiOS regimes and the EMT. In contrast, it is different in the SAP, mostly influenced by DW cascading and vertical salinity exchanges driven by double diffusions and deep circulation (Querin et al., 2016). Both temperature and salinity trends are positive in all accumulation sites (DKB, JP and SAP), continuing the trends that are found in centennial Adriatic climatologies (Lipizer et al., 2014). Finally, monthly climatologies revealed an inverse relationship between distributions of temperature and PDA in all accumulation sites, while the behaviour of salinity is similar to temperature only in the JP and SAP.

6. CONCLUSIONS

In this thesis, the performance of the AdriSC ocean climate simulation has been evaluated for the 1987–2017 period. The main novelty of this research lies, firstly, in the implementation – for the very first time, to the best of the author's knowledge – of a kilometre-scale one-way coupled atmosphere-ocean model for long-term climate studies, which still presents many challenges (Schär et al., 2020), and, secondly, the amount of *in situ* data used to perform the evaluation of both daily thermohaline and hourly dynamical properties of the AdriSC ocean models. The findings of the evaluation can be summarized as follows:

- The AdriSC-ROMS 3 km model has been found to show skill in reproducing (1) the observed decadal signal of SSHA, interpreted as the BiOS cycles, despite presenting a weaker intensity compared to the seasonal and interannual variabilities, and (2) the observed SST, despite exhibiting a persistent negative bias within the Adriatic, which is probably linked to the summer cold bias found in the AdriSC-WRF 3 km model (Denamiel et al., 2021b).

- The AdriSC-ROMS 1 km model has been found to be more suitable at reproducing the observed daily temperatures and salinities, as well as hourly ocean currents than the AdriSC-ROMS 3 km model, thus highlighting the need for higher-resolution ocean climate simulations in the Adriatic Sea.

- The detailed analysis of the AdriSC-ROMS 1 km simulation revealed that (1) for the daily temperature and salinity, better results are found in the deepest parts than in the shallow shelf and coastal parts, particularly for the surface layer of the Adriatic Sea, while, (2) for the hourly ocean currents, better results are found for the RCMs and ADCPs located along the eastern coast and the northeastern shelf than for the ADCPs located in the middle eastern coastal area and the deeper part of the Adriatic Sea.

- The AdriSC-ROMS 1 km model was found (1) to perform well in reproducing the seasonal thermohaline properties of the water masses over the entire Adriatic Sea, despite a common overestimation of PDAs lower than 26 kg m^{-3}, and (2) consequently, to be a suitable modelling framework for studying the long-term thermohaline circulation triggered by the DW formation.

Further, with the aim to enhance our understanding of the bora-driven dense-water dynamics in the Adriatic Sea, the results of the AdriSC simulation have been analysed and

compared with three different state-of-the-art modelling approaches, including a reanalysis, a hindcast and a data assimilated simulation for the 2014–2015 period. The main findings of the model intercomparison are summarized as follows:

- In the NA and the KB, DW generation is better captured in ROMS-full and AdriSC-ROMS than in MEDSEA and ROMS-hind, which generate smaller volumes of DW. During bora events, AdriSC model generates the strongest dynamics with the largest intensities in wind stresses, upward turbulent heat fluxes and bottom PDAs. Moreover, extreme DW are generated continuously in time and over the entire northern Adriatic in AdriSC-ROMS, while they appear as isolated patches in ROMS-full. Also, in the AdriSC simulation, due to its higher spatial resolution, the densest waters are collected within the KB, where they remain for the longest amount of time.

- The transport of DW along the western coast is not quantitatively captured by both MEDSEA and ROMS-hind. Conversely, in the JP, ROMS-full collects the largest amount of DW, indicating that AdriSC-ROMS is might be excessively dissipative. In the SAP, the results show that the northern Adriatic DW did not reach the bottom of the pit by the end of any simulation, classifying the winter of 2015 as moderate in terms of DW formation over the northern Adriatic shelf.

- The impact of the resolution of the atmospheric models is most evident in the ERA5 results, which strongly underestimate the wind stresses. However, the heat losses are comparable between the models but are mostly underestimated compared to AdriSC-WRF. Concerning the hydrostatic approximation, the non-hydrostatic model AdriSC-WRF reproduces more intense wind stresses with larger spatial coverage and stronger heat losses than the hydrostatic ALADIN-HR model.

- The ocean models are highly sensitive to the salinity input, a factor crucial in DW generation. In particular, the usage of outdated river climatologies causes lower salinities in ROMS-hind and MEDSEA, consequently leading to reduced bottom PDAs, while AdriSC-ROMS reproduces higher salinities and PDAs.

- When compared to ROMS-hind, data assimilation in ROMS-full tends to increase the bottom PDA values in all subdomains, particularly in the KB and the JP. Although assimilation made a large improvement in terms of the ocean fields, the fields reflect initial state adjustments at the beginning of each assimilation cycle and hence do not

produce long and smooth temporal transitions. In addition, the lack of vertical resolution in the ROMS-full model probably contributes to the improper representation of DW dynamics.

This research revealed that models running over long temporal scales can outperform coarse-resolution reanalysis products and assimilated simulations in reproducing Adriatic dense-water dynamics if the following requirements are met: (1) kilometre- or finer-resolution atmosphere-ocean models and non-hydrostatic atmospheric models, (2) fine vertical resolutions in both atmosphere and ocean, (3) proper forcing of the open boundaries of the models, and (4) appropriate representation of the air-sea interactions (e.g. formulation of the surface wind drag). Nevertheless, in addition to these prerequisites, 4D-Var data assimilation could be used to solve other model problems – such as sea surface temperature drifts, high mixing of the dense waters, etc. – often found in long-term hindcasts and short-term forecasts. However, such an approach would be extremely expensive in terms of the required numerical and observational resources.

Lastly, the results of the AdriSC-ROMS 1 km model have been used to estimate the 31-year-long DW climatology in the Adriatic Sea, and the main findings are summarized below:

- Concerning DW generation, the differences in maximum PDA during winter months between the NA and KB are primarily influenced by the differences in temperature. Furthermore, the cooling rates during severe bora outbreaks are found to be less important for the temperature decrease (and thus, for the PDA increase) than the volume of the ocean to be cooled. Notably, in the KB, a smaller secondary peak in PDA was found during summer, which is linked to DW accumulation in the deepest KB sections.

- Regarding the spreading, the KB generation site contributes an estimated 25–35% to the overall DW mass outflow. The maximums of the monthly bottom DW outflow rate distributions shift from winter towards spring months as the transect locations move from northwest to southeast. However, the transects at the Strait of Otranto exhibit distinct dynamics compared to other transects in the Adriatic Sea because of the large influence of the open-ocean convection in the middle of the SAP.

- In terms of accumulation, the PDA in the DKB is changing annually, while the thermohaline properties in the JP and SAP differ from those in DKB and exhibit saw-tooth-like behaviour. The bottom layer of the SAP is renewed every 5–10 years, while

the deep waters in the JP are renewed more frequently, every 1–3 years, as being substantially shallower than the SAP. The interannual variability of salinity in the DKB and JP differs from the SAP due to different driving mechanisms. Moreover, in all accumulation sites, temperature distributions show inverse behaviour compared to the PDA, while the behaviour of salinity is similar to temperature only in the JP and SAP. In addition, positive long-term trends in both temperature and salinity are found in all accumulation sites.

In conclusion, the added value of high-resolution coastal models in climate research of complex coastal regions such as the Adriatic Sea has been demonstrated in this thesis. In future research, the AdriSC climate simulations are expected to expand our understanding of the dynamics of the Adriatic–Ionian region. Nonetheless, finding the right balance between numerical model accuracy (i.e. resolution) and efficiency (i.e. computational resources and runtime) – depending on the temporal and spatial scales of the studied processes – remains one of the main issues of the climate modelling community. However, with continuous technological and scientific advancements, this challenge could be addressed in the near future.

7. PROŠIRENI SAŽETAK

Zbog nepotpune prostorno-vremenske pokrivenosti oceanografskih mjerenja, istraživanje dinamike i varijabilnosti procesa u moru velikim se dijelom oslanja na razvoj i unaprijeđenja numeričkih modela. U posljednjih nekoliko desetljeća, napravljen je značajan napredak u modeliranju Jadranskoga mora s ciljem savladavanja izazova koji proizlaze iz geomorfologije ovog područja, a koju čini kompleksna obala s preko 1200 otoka, batimetrija koja seže od plitkog šelfa na sjeveru (30 m u prosjeku) do duboke kotline na jugu (oko 1230 m) i planinski lanci koji okružuju poluzatvoreni jadranski bazen. Nadalje, atmosferski i oceanski procesi u Jadranu se odvijaju u širokom rasponu prostornih i vremenskih skala, od dugotrajnih procesa na većim prostornim skalama (npr. termohalina cirkulacija) do kratkotrajnih događaja koji variraju na manjim prostornim skalama (npr. olujna bura). Zbog navedenih obilježja, Jadran predstavlja vrlo zahtjevno područje za numeričko modeliranje atmosfere i mora.

Jedan od glavnih čimbenika koji utječe na dinamiku Jadranskoga mora je termohalina cirkulacija Jadrana na koju veliki utjecaj ima stvaranje guste vode. Gusta voda nastaje hlađenjem mora uslijed puhanja bure na sjevernojadranskom šelfu i u kvarnerskom zaljevu gdje se stvara NAddW (engl., North Adriatic dense Water), te procesom duboke konvekcije u južnojadranskoj kotlini gdje nastaje AdDW (engl., Adriatic Deep Water). Istraživanje guste vode u Jadranu je od velike važnosti zbog njenog utjecaja na dinamiku Jadranskog i Sredozemnog mora te biogeokemijska svojstva mora i živi svijet Jadrana.

Općenito, numerički modeli imaju široku primjenu u oceanografiji, a razlikuju se po sposobnosti reprodukcije različitih oceanografskih svojstava i procesa. Jedna od bitnih značajki numeričkih modela je njihova prostorna i vremenska razlučivost o kojoj ovisi kvaliteta rezultata modela. U posljednjih nekoliko desetljeća, numeričke studije visoke razlučivosti u Jadranu bile su uglavnom usmjerene na kraća vremenska razdoblja do nekoliko godina, dok su simulacije klimatskih modela na kilometarskoj skali tek nedavno provedene u području Jadrana. Istraživanja Jadrana oceanskim modelima razlučivosti do 3 km u počecima su se najviše bavila stvaranjem sjevernojadranske guste vode na sjevernojadranskom šelfu i stvaranjem jadranske duboke vode u južnojadranskoj kotlini te njenom međugodišnjom varijabilnosti. U tom razdoblju, atmosferska polja koja su se koristila za forsiranje oceanskih modela uglavnom su bila izvedena iz klimatoloških podataka ili iz ECMWF (engl. European Centre for Medium-Range Weather Forecasts) globalnih reanaliza. Međutim, mnoge studije su pokazale da ECMWF reanalize, zbog svoje prostorne homogenosti i grube rezolucije, ne mogu

ispravno reproducirati ekstremne događaje, kao što je puhanje bure koje pokreće stvaranje guste vode u sjevernom Jadranu. U posljednjem desetljeću, brojne studije su koristile modele kilometarske rezolucije na ograničenom području za simuliranje procesa pokretanih ekstremnim uvjetima u Jadranskome more. Tu spadaju primjerice ekstremni valovi, olujni uspori, hlađenje površine mora, vertikalno mješanje i stvaranje guste vode koji se događaju tijekom oluja bure ili juga.

Osim atmosferskog forsiranja, velik utjecaj na numeričko modeliranje Jadrana ima i način uvođenja riječnih dotoka te odabir rubnih uvjeta na otvorenim granicama. Naime, korištenje starih klimatologija rijeka i nedostatak novijih mjerenja, posebice uz istočnu obalu Jadrana, rezultiralo je precjenjivanjem riječnih priljeva i sprječavanjem stvaranja guste vode u obalnom području istočnog Jadrana. Drugi izvori pogrešaka su primjerice neadekvatni uvjeti na otvorenim granicama modela te nepravilne parametrizacije određenih procesa.

Što se tiče klimatskog modeliranja koje podrazumijeva simulacije od nekoliko desetljeća, Jadran se pretežito proučavao regionalnim klimatskim modelima razvijenima za Sredozemno more. Međutim, zbog relativno grube horizontalne rezolucije (reda veličine 10 km), regionalni klimatski modeli ne mogu razlučiti kompleksnu obalnu morfologiju Jadrana te nisu sposobni reproducirati procese na manjim prostornim i kraćim vremenskim skalama. Kako bi se kvantificirao utjecaj klimatskih promjena u Jadranu, važna je adekvatna reprezentacija interakcija atmosfera-more tijekom ekstremnih događaja na klimatskim skalama. Atmosferski regionalni klimatski modeli općenito ne uspijevaju reproducirati te procese, posebice u sjevernom Jadranu gdje se ne mogu koristiti za proučavanje dinamike bure.

Na temelju prethodnih istraživanja, javila se potreba za atmosferskim modelima veće razlučivosti koji su sposobni reproducirati dinamiku vjetra i interakciju mora i atmosfere u sjevernom Jadranu, te za dugotrajnijim klimatskim simulacijama. U ovom radu će se predstaviti atmosfersko-oceanski klimatski model visoke rezolucije Adriatic Sea and Coast (AdriSC) koji je razvijen s ciljem poboljšanja reproduciranja dinamike Jadranskoga mora. Atmosferska komponenta modela AdriSC je model WRF (engl. Weather Research and Forecasting; Skamarock i sur., 2005) razlučivosti do 3 km, dok oceansku komponentu čini model ROMS razlučivosti do 1 km. Modelom AdriSC je izvršena 31-godišnja klimatska simulacija u razdoblju od 1987. do 2017. godine.

U prvom dijelu disertacije napravljena je temeljita evaluacija oceanske komponente klimatske simulacije AdriSC usporedbom s opsežnim skupom oceanografskih mjerenja.

Analizirani su parametri površine mora, termohalini i dinamički parametri. Općenito, evaluacija klimatskog modela visoke rezolucije ima brojne izazove koji obuhvaćaju dostupnost, nepotpunost i nedostatak izmjerenih podataka kao i nesavršenosti mjernih sustava, što utječe na interpretaciju rezultata evaluacije. Također, međusobna usporedba klimatskih modela otežana je navedenim ograničenjima.

Nakon evaluacije, rezultati simulacije su primjenjeni u istraživanju dinamike guste vode u Jadranskome moru. Napravljena je međusobna usporedba četiri različite simulacije guste vode u Jadranu u razdoblju od 2014. do 2015. godine, kada su obavljani ciljani oceanografski eksperimenti i mjerenja. Osim AdriSC simulacije, korišten je modelarski sustav koji uključuje asimilaciju podataka, te najnovija oceanska fizikalna reanaliza za Sredozemno more. Utvrđene su glavne prednosti i nedostaci različitih pristupa te je zaključeno da klimatski modeli koji ispunjavaju određene preduvjete, mogu nadmašiti modele s asimilacijom podataka u reprodukciji dinamike guste vode u Jadranu.

U posljednjem dijelu ovog doktorskog istraživanja analizom termohalinih parametara simuliranih oceanskim modelom AdriSC razlučivosti 1 km, načinjena je 31-godišnja klimatologija procesa stvaranja, širenja i akumulacije guste vode u Jadranskome moru od 1987. do 2017. godine čime je dan dugoročan pregled navedenog procesa u povijesnom razdoblju.

Naposljetku, klimatske simulacije modela visoke razlučivosti AdriSC pokazale su se korisnima za proučavanje dinamike jadransko–jonskog područja. No, jedan od najvažnijih izazova klimatskog modeliranja u područjima kao što je Jadransko more jest pronalazak ravnoteže između numeričke točnosti rezultata modela i učinkovitosti izvršavanja simulacije, koji bi se u budućnosti uz daljnji razvoj znanosti i tehnologije mogao prevladati.

8. LITERATURE

Akhtar, N., Brauch, J., and Ahrens, B.: Climate modeling over the Mediterranean Sea: impact of resolution and ocean coupling, Clim. Dyn., 51, 933–948, https://doi.org/10.1007/s00382-017-3570-8, 2018.

Alpers, W., Ivanov, A., and Horstman, J.: Observations of Bora Events over the Adriatic Sea and Black Sea by Spaceborne Synthetic Aperture Radar, Mon. Weather Rev., 137, 1150–1161, https://doi.org/10.1175/2008MWR2563.1, 2009.

Amante, C. and Eakins, B. W.: ETOPO1 1 arc–minute global relief model: procedures, data sources and analysis, NOAA Technical Memorandum NESDIS NGDC-24, 2009.

Artegiani, A. and Salusti, E.: Field observation of the flow of dense water on the bottom of the Adriatic Sea during the winter of 1981, Oceanol. Acta, 10, 387–391, 1987.

Artegiani, A., Bregant, D., Paschini, E., Pinardi, N., Raicich, F., and Russo, A.: The Adriatic Sea general circulation, part I: air-sea interactions and water mass structure, J. Phys. Oceanogr., 27, 1492–1514, https://doi.org/10.1175/1520-0485(1997)027<1492:TASGCP>2.0.CO;2, 1997.

Atlas, R., Hoffman, R. N., Ardizzone, J., Leidner, S. M., Jusem, J. C., Smith, D. K., and Gombos, D.: A cross-calibrated, multiplatform ocean surface wind velocity product for meteorological and oceanographic applications, Bull. Am. Meteorol. Soc., 92, 157–174, https://doi.org/10.1175/2010BAMS2946.1, 2011.

Balsamo, G., Albergel, C., Beljaars, A., Boussetta, S., Brun, E., Cloke, H., Dee, D., Dutra, E., Muñoz-Sabater, J., Pappenberger, F., de Rosnay, P., Stockdale, T., and Vitart, F.: ERA–Interim/Land: a global land surface reanalysis data set, Hydrol. Earth Syst. Sci., 19, 389–407, https://doi.org/10.5194/hess-19-389-2015, 2015.

Batistić, M., Garić, R., Molinero, J.C.: Interannual variations in Adriatic Sea zooplankton mirror shifts in circulation regimes in the Ionian Sea. Clim. Res., 61, 231–240. https://doi.org/10.3354/cr01248, 2014.

Beg Paklar, G., Isakov, V., Koračin, D., Kourafalou, V., Orlić, M.: A case study of bora-driven flow and density changes on the Adriatic shelf (January 1987), Cont. Shelf Res., 21, 1751–1783, https://doi.org/10.1016/S0278-4343(01)00029-2, 2001.

Belušić, D., Klaić, Z. B.: Estimation of bora wind gusts using a limited area model, Tellus A, 56, 296–307, https://doi.org/10.1111/j.1600-0870.2004.00068.x, 2004.

Belušić, D., Žagar, M. Grisogono, B.: Numerical simulation of pulsations in the bora wind, Q. J. Roy. Meteorol. Soc., 133, 1371–1388, https://doi.org/10.1002/qj.12, 2007.

Belušić, D., Hrastinski, M., Večenaj, Ž., Grisogono, B.: Wind regimes associated with a mountain gap at the northeastern Adriatic coast, J. Appl. Meteorol. Clim., 52, 9, 2089–2105, https://doi.org/10.1175/JAMC-D-12-0306.1, 2013.

Belušić, A., Prtenjak, M. T., Güttler, I., Ban, N., Leutwyler, D., Schär, C.: Near-surface wind variability over the broader Adriatic region: Insights from an ensemble of regional climate models, Clim. Dyn., 50, 4455–4480, https://doi.org/10.1007/s00382-017-3885-5, 2017.

Benetazzo, A., Bergamasco, A., Bonaldo, D., Falcieri, F.M., Sclavo, M., Langone, L., and Carniel, S.: Response of the Adriatic Sea to an intense cold air out– break: Dense water dynamics and wave-induced transport. Prog. Oceanogr. 128, 115–138, https://doi.org/10.1016/j.pocean.2014.08.015, 2014.

Bensi, M., Cardin, V., Rubino, A., Notarstefano, G., and Poulain, P.– M.: Effects of winter convection on the deep layer of the Southern Adriatic Sea in 2012, J. Geophys. Res. Oceans, 118, 6064– 6075, https://doi.org/10.1002/2013JC009432, 2013.

Blockley, J. A. and Lyons, T. J.: Airflow over a two-dimensional escarpment, III: Nonhydrostatic flow, Q. J. Roy. Meteorol. Soc., 120, 79–109, https://doi.org/10.1002/qj.49712051507, 1994.

Boldrin, A., Carniel, S., Giani, M., Marini, M., Bernardi Aubry, F., Campanelli, A., Grilli, F., Russo, A.: Effects of bora wind on physical and biogeochemical properties of stratified waters in the northern Adriatic, J. Geophys. Res. Oceans, 114, C08S92, https://doi.org/10.1029/2008JC004837, 2009.

Borenas, K. M., Wahlin, A. K., Ambar, I., Serra, N.: The Mediterranean outflow splitting – a comparison between theoretical models and CANIGO data. Deep-Sea Res. II, 49, 4195–4205, https://doi.org/10.1016/S0967-0645(02)00150-9, 2002.

Bowman, A. W., Azzalini, A.: Applied Smoothing Techniques for Data Analysis. New York: Oxford University Press Inc., ISBN 0191545694, 1997.

Buljan M., Zore-Armanda, M. (1971), Osnovi oceanografije i pomorske meteorologije, II dopunjeno izdanje, Institut za oceanografiju i ribarstvo, Split.

Burrage, D. M., Book, J. W., and Martin, P. J.: Eddies and filaments of the Western Adriatic Current near Cape Gargano: Analysis and prediction, J. Mar. Syst., 78, S205–S226, https://doi.org/10.1016/j.jmarsys.2009.01.024, 2009.

Carniel, S., Benetazzo, A., Bonaldo, D., Falcieri, F. M., Miglietta, M. M., Ricchi, A., Sclavo, M.: Scratching beneath the surface while coupling atmosphere, ocean and waves: Analysis of a dense water formation event, Ocean Model., 101, 101–112, https://doi.org/10.1016/j.ocemod.2016.03.007, 2016.

Cavaleri, L. and Bertotti, L.: In search of the correct wind and wave fields in a minor basin, Monthly Weather Review, 125, 1964–1975, https://doi.org/10.1175/1520-0493(1997)125<1964:ISOTCW>2.0.CO;2, 1997.

Cavaleri, L., Bertotti, L., Buizza, R., Buzzi, A., Masato, V., Umgiesser, G., and Zampieri, M.: Predictability of extreme meteo-oceanographic events in the Adriatic Sea, Q. J. R. Meteorol. Soc., 136, 400–413, https://doi.org/10.1002/qj.567, 2010.

Cavaleri, L., Abdalla, S., Benetazzo, A., Bertotti, L., Bidlot, J.-R., Breivik, Ø., Carniel, S., Jensen, R. E., Portilla–Yandun, Rogers, W. E., Roland, A., Sanchez-Arcilla, A., Smith, J. M., Staneva, J., Toledo, Y., van Vledder, G. P., and van der Westhuysen, A. J.: Wave modelling in coastal and inner seas, Prog. Oceanogr., 167, 164–233, https://doi.org/10.1016/j.pocean.2018.03.010, 2018.

Chapman, D. C.: Numerical treatment of cross–shelf open boundaries in a barotropic coastal ocean model, J. Phys. Oceanogr., 15, 1060–1075, https://doi.org/10.1175/1520-0485(1985)0152.0.CO;2, 1985.

Chelton, D. B., deSzoeke, R. A., Schlax, M. G., El Naggar, K., Siwertz, N.: Geographical Variability of the First Baroclinic Rossby Radius of Deformation, J. Phys. Oceanogr., 28(3), 433–460, https://doi.org/10.1175/1520-0485(1998)028<0433:GVOTFB>2.0.CO;2, 1998.

Chiggiato, J., and Oddo, P.: Operational ocean models in the Adriatic Sea: a skill assessment. Ocean Sci. 4, 61–71, https://doi.org/10.5194/os-4-61-2008, 2008.

Cornes, R. C., van der Schrier, G., van den Besselaar, E. J. M., and Jones, P. D.: An ensemble version of the E-OBS temperature and precipitation data sets, J. Geophys. Res. Atmos., 123, 9391– 9409, https://doi.org/10.1029/2017JD028200, 2018.

Courtier, P., Thépaut, J. N., Hollingsworth, A.: A strategy for operational implementation of 4D-Var, using an incremental approach, Q. J. Roy. Meteorol. Soc. 120, 1367–1387, https://doi.org/10.1002/qj.49712051912, 1994.

Crocker, R., Maksymczuk, J., Mittermaier, M., Tonani, M., and Pequignet, C.: An approach to the verification of high-resolution ocean models using spatial methods, Ocean Sci., 16, 831–845, https://doi.org/10.5194/os-16-831-2020, 2020.

Cushman–Roisin, B.,Gačić, M.,Poulain**,** P.-M.,Artegiani, A.: Physical Oceanography of the Adriatic Sea, Past, Present and Future, Springer Netherlands, https://doi.org/10.1007/978-94-015-9819-4, 2001.

Cushman-Roisin, B., Naimie, C. E.: A 3d finite–element model of the Adriatic tides, J. Mar. Syst., 37, 279–297, https://doi.org/10.1016/S0924-7963(02)00204-X, 2002.

Darmaraki, S., Somot, S., Sevault, F., Nabat, P., Cabos Narvaez, W. D., Cavicchia, L., Djurdjevic, V., Li, L., Sannino, G., and Sein, D. V.: Future evolution of Marine Heatwaves in the Mediterranean Sea, Clim. Dyn., 53, 1371–1392, https://doi.org/10.1007/s00382-019-04661-z, 2019.

Denamiel, C., Šepić, J., Ivanković, D., Vilibić, I.: The Adriatic Sea and Coast modelling suite: Evaluation of the meteotsunami forecast component, Ocean Model., 135, 71–93, https://doi.org/10.1016/j.ocemod.2019.02.003, 2019.

Denamiel, C., Pranić, P., Quentin, F., Mihanović, H., Vilibić, I.: Pseudo-global warming projections of extreme wave storms in complex coastal regions: The case of the Adriatic Sea, Clim. Dyn., 55, 2483–2509, https://doi.org/10.1007/s00382-020-05397-x, 2020a.

Denamiel, C., Tojčić, I., Vilibić, I.: Far future climate (2060–2100) of the northern Adriatic air-sea heat transfers associated with extreme bora events, Clim. Dyn., 55, 3043–3066, https://doi.org/10.1007/s00382-020-05435-8, 2020b.

Denamiel, C., Tojčić, I., Vilibić, I.: Balancing accuracy and efficiency of atmospheric models in the northern Adriatic during severe bora events, J. Geophys. Res. Atmos., 126, https://doi.org/10.1029/2020JD033516, 2021a.

Denamiel, C., Pranić, P., Ivanković, D., Tojčić, I., Vilibić, I.: Performance of the Adriatic Sea and Coast (AdriSC) climate component—a COAWST V3.3-based coupled atmosphere-ocean modelling suite: atmospheric dataset, Geosci. Model Dev., 14, 3995–4017, https://doi.org/10.5194/gmd-14-3995-202127, 2021b.

Di Luca, A., Flaounas, E., Drobinski, P., and Lebeaupin–Brossier, C.: The atmospheric component of the Mediterranean Sea water budget in a WRF multi-physics ensemble and observations, Clim. Dyn., 43, 2349–2375, https://doi.org/10.1007/s00382-014-2058-z, 2014.

Dobricic, S., Pinardi, N.: An oceanographic three-dimensional variational data assimilation scheme, Ocean Model., 22, 89–105, https://doi.org/10.1016/j.ocemod.2008.01.004, 2008.

Dorman, C. E., Carniel, S., Cavaleri, L., Sclavo, M., Chiggiato, J., Doyle, J., Haack, T., Pullen, J., Grbec, B., Vilibić, I., Janeković, I., Lee, C., Malačić, V., Orlić, M., Paschini, E., Russo, A., Signell, R. P.: Winter 2003 marine atmospheric conditions and the bora over the northern Adriatic, J. Geophys. Res. Oceans, 112, C03S03, https://doi.org/10.1029/2005JC003134, 2007.

Drobinski, P., Silva, N.D., Panthou, G. et al. Scaling precipitation extremes with temperature in the Mediterranean: past climate assessment and projection in anthropogenic scenarios. Clim. Dyn., 51, 1237–1257, https://doi.org/10.1007/s00382-016-3083-x, 2018.

Dudhia, J.: Numerical study of convection observed during the winter monsoon experiment using a mesoscale two-dimensional model, J. Atmos. Sci., 46, 3077–3107, https://doi.org/10.1175/1520-0469(1989)046<3077:NSOCOD>2.0.CO;2, 1989.

Dudhia, J.: A Multi-Layer Soil Temperature Model for MM5, Sixth PSU/NCAR Mesoscale Model Users' Workshop, Boulder, 22–24 July 1996, 49–50, 1996.

Dukowicz, J. K.: Reduction of pressure and pressure gradient errors in ocean simulations, J. Phys. Oceanogr., 31, 1915–1921, https://doi.org/10.1175/1520-0485(2001)031<1915:RODAPG>2.0.CO;2, 2001.

Dunić, N., Vilibić, I., Šepić, J., Mihanović, H., Sevault, F., Somot, S., Waldman, R., Nabat, P., Arsouze, T., Pennel, R., Jordà, G., and Precali, R.: Performance of multi-decadal ocean simulations in the Adriatic Sea, Ocean Model., 134, 84–109, https://doi.org/10.1016/j.ocemod.2019.01.006, 2019.

Dutour Sikirić, M., Janeković, I., Kuzmić, M.: A new approach to bathymetry smoothing in sigma-coordinate ocean models. Ocean Model. 29, 128–136. https://doi.org/10.1016/j.ocemod.2009.03.009, 2009.

Egbert, G. D., Bennett, A. F., and Foreman, M. G. G.: Topex/Poseidon tides estimated using a global inverse model, J. Geophys. Res., 99, 24821–24852, https://doi.org/10.1029/94JC01894, 1994.

Egbert, G. D. and Erofeeva, S. Y.: Efficient inverse modeling of barotropic ocean tides, J. Atmos. Ocean. Technol., 19, 183–204, https://doi.org/10.1175/1520-0426(2002)0192.0.CO;2, 2002.

Escudier R., Clementi E., Cipollone A., Pistoia J., Drudi M., Grandi A., Lyubartsev V., Lecci R., Aydogdu A., Delrosso D., Omar M., Masina S., Coppini G., Pinardi N.: A high resolution reanalysis for the Mediterranean Sea, Front. Earth Sci., 9, 2296–6463, https://doi.org/10.3389/feart.2021.702285, 2021.

Escudier, R., Clementi, E., Omar, M., Cipollone, A., Pistoia, J., Aydogdu, A., et al.: Mediterranean Sea Physical Reanalysis (CMEMS MED–Currents) (Version 1) [data set]. Copernicus Monitoring Environment Marine Service (CMEMS). https://doi.org/10.25423/CMCC/MEDSEA_MULTIYEAR_PHY_006_004_E3R1, 2020.

Fairall, C.W., Bradley, E.F., Rogers, D.P., Edson, J.B., Young, G.S.: Bulk parameterization of air-sea fluxes for tropical ocean-global atmosphere coupled-ocean atmosphere response experiment, J. Geophys. Res., 101 (C2), 3747–3764, https://doi.org/10.1029/95JC03205, 1996.

Flather, R. A.: A tidal model of the north-west European continental shelf, Mem. Soc. R. Sci Liege, 6, 141–164, 1976.

Foglini, F., Campiani, E., Trincardi, F.: The reshaping of the South West Adriatic Margin by cascading of dense shelf waters. Mar. Geol., 375, 64–81. https://doi.org/10.1016/j.margeo.2015.08.011, 2016.

Gačić, M., Civitarese, G., Miserocchi, S., Cardin, V., Crise, A., and Mauri, E.: The open–ocean convection in the Southern Adriatic: A controlling mechanism of the spring phytoplankton bloom. Cont. Shelf Res., 22, 1897–1908, https://doi.org/10.1016/ S0278-4343(02)00050-X, 2002.

Gačić, M., Borzelli, G. E., Civitarese, G., Cardin, V., and Yari, S.: Can internal processes sustain reversals of the ocean upper circulation? The Ionian Sea example, Geophys. Res. Lett., 37(9), https://doi.org/10.1029/2010GL043216, 2010.

Gačić, M., Civitarese, G., Kovačević, V., Ursella, L., Bensi, M., Menna, M., Cardin, V., Poulain, P.-M., Cosoli, S, Notarstefano, G., and Pizzi, C.: Extreme winter 2012 in the Adriatic: an example of climatic effect on the BiOS rhythm, Ocean Sci., 10, 513–522, https://doi.org/10.5194/os-10-513-2014, 2014.

Garcia–Quintana, Y., Grivault, N., Hu, X., Myers, P. G.: Dense water formation on the Icelandic shelf and its contribution to the North Icelandic Jet, J. Geophys. Res. Oceans, 126, e2020JC016951, https://doi.org/10.1029/2020JC016951, 2021.

Gohm, A., Mayr, G.J., Fix, A. Giez, A.: On the onset of bora and the formation of rotors and jumps near a mountain gap, Q. J. Roy. Meteorol. Soc., 134, 21–46. https://doi.org/10.1002/qj.206, 2008.

Grisogono, B., Belušić, D.: A review of recent advances in understanding the meso- and microscale properties of the severe Bora wind, Tellus A, 61, 1–16. https://doi.org/10.1111/j.1600-0870.2008.00369.x, 2009.

Grubišić, V.: Bora-driven potential vorticity banners over the Adriatic, Q. J. Roy. Meteorol. Soc., 130, 2571–2603, https://doi.org/10.1256/qj.03.71, 2004.

Heggelund, Y., Vikebø, F., Berntsen, J., Furnes, G.: Hydrostatic and non-hydrostatic studies of gravitational adjustment over a slope, Cont. Shelf Res., 24, 2133–2148, https://doi.org/10.1016/j.csr.2004.07.005, 2004.

Hersbach, H., de Rosnay, P., Bell, B., Schepers, D., Simmons, A., Soci, C., Abdalla, S., Alonso-Balmaseda, M., Balsamo, G., Bechtold, P., Berrisford, P., Bidlot, J.-R., de Boisséson, E., Bonavita, M., Browne, P., Buizza, R., Dahlgren, P., Dee, D., Dragani, R., Diamantakis, M., Flemming, J., Forbes, R., Geer, A.J., Haiden, T., Hólm, E., Haimberger, L., Hogan, R., Horányi, A., Janiskova, M., Laloyaux, P., Lopez, P., Munoz-Sabater, J., Peubey, C., Radu, R., Richardson, D., Thépaut, J.-N., Vitart, F., Yang, X., Zsótér, E., and Zuo, H.: Operational global reanalysis: Progress, future directions and synergies with NWP. ECMWF ERA Report Series 27, 2018.

Hersbach, H., Bell, B., Berrisford, P., Hirahara, S., Horányi, A., Muñoz–Sabater, J., et al.: The ERA5 Global Reanalysis, Q. J. Roy. Meteorol. Soc., 146, 1999–2049. https://doi.org/10.1002/qj.3803, 2020.

Horak, J., Hofer, M., Gutmann, E., Gohm, A., and Rotach, M. W.: A process–based evaluation of the Intermediate Complexity Atmospheric Research Model (ICAR) 1.0.1, Geosci. Model Dev., 14, 1657–1880, https://doi.org/10.5194/gmd-14-1657-2021, 2021.

Horvath, K., Ivatek-Šahdan, S., Ivančan–Picek, B., Grubišić, V.: Evolution and structure of two severe cyclonic bora events: Contrast between the northern and southern Adriatic, Weather Forecast., 24, 946–964, https://doi.org/10.1175/2009WAF2222174.1, 2009.

Iermano, I., Moore, A.M., Zambianchi, E.: Impacts of a 4-dimensional variational data assimilation in a coastal ocean model of southern Tyrrhenian Sea, J. Mar. Syst., 154(B), 157–171, https://doi.org/10.1016/j.jmarsys.2015.09.006, 2015.

Ivanov, V. V., Shapiro, G. I., Huthnance, J. M., Aleynik, D. L., Golovin, P. N.: Cascades of dense water around the world ocean, Prog. Oceanogr., 60, 47–98, https://doi.org/10.1016/j.pocean.2003.12.002, 2004.

Ivatek-Šahdan, S. and Tudor, M.: Use of high-resolution dynamical adaptation in operational suite and research impact studies, Meteorol. Z., 13, 99–108, https://10.1127/0941-2948/2004/0013-0099, 2004.

Janeković, I. and Kuzmić, M.: Numerical simulation of the Adriatic Sea principal tidal constituents, Ann. Geophys., 23, 3207–3218, https://doi.org/10.5194/angeo-23-3207-2005, 2005.

Janeković, I., Powell, B.S., McManus, M.A., Sevadjian, J.: 4D-Var data assimilation in a nested, coastal ocean model: A Hawaiian case study, J. Geophys. Res. Oceans, 118, 5022–5035, https://doi.org/10.1002/jgrc.20389, 2013.

Janeković, I., Mihanović, H., Vilibić, I., Tudor, M.: Extreme cooling and dense water formation estimates in open and coastal regions of the Adriatic Sea during the winter of 2012, J. Geophys. Res. Oceans, 119, 3200–3218, https://doi.org/10.1002/ 2014JC009865, 2014.

Janeković, I., Mihanović, H., Vilibić, I., Grčić, B., Ivatek–Šahdan, S., Tudor, M., Djakovac, T.: Using multi-platform 4D-Var data assimilation to improve modeling of Adriatic Sea

dynamics, Ocean Model., 146, 1463–5003, https://doi.org/10.1016/j.ocemod.2019.101538, 2020.

Janjić, Z.: The Step-Mountain eta Coordinate Model: Further developments of the convection, viscous sublayer, and turbulence closure schemes, Mon. Weather Rev., 122, 927–945, https://doi.org/10.1175/1520-0493(1994)1222.0.CO;2, 1994.

Jasprica, N., Čalić, M., Kovačević, V., Bensi, M., Radić, I.D., Garić, R., Batistić, M.: Phytoplankton distribution related to different winter conditions in 2016 and 2017 in the open southern Adriatic Sea (eastern Mediterranean), J. Mar. Syst., 226, 103665, https://doi.org/10.1016/j.jmarsys.2021.103665, 2022.

Jiang, Q., Doyle, J. D.: Wave breaking induced surface wakes and jets observed during a bora event, Geophys. Res. Lett., 32, L17807, https://doi.org/10.1029/2005GL022398, 2005.

Johnson, N. C., Krishnamurthy, L., Wittenberg, A. T., Xiang, B., Vecchi, G. A., Kapnick, S. B., and Pascale, S.: The impact of sea surface temperature biases on North American precipitation in a high-resolution climate model, J. Clim., 33, 2427–2447, https://doi.org/10.1175/JCLI-D-19-0417.1, 2020.

Kain, J. S.: The Kain-Fritsch convective parameterization: an update, J. Appl. Meteo rol., 43, 170–181, https://doi.org/10.1175/1520-0450(2004)0432.0.CO;2, 2004.

Kehler-Poljak, G., Telišman Prtenjak, M., Kvakić, M., Šariri, K., and Večenaj, Ž.: Interaction of sea breeze and deep convection over the northeastern Adriatic Coast: An analysis of sensitivity experiments using a high-resolution mesoscale model, Pure Appl. Geophys., 174, 4197–4224, https://doi.org/10.1007/s00024-017-1607-x, 2017.

Klein, B., Roether, W., Manca, B. B., Bregant, D., Beitzel, V., Kovačević, V., Luchetta, A.: The large deep-water transient in the Eastern Mediterranean. Deep–Sea Res. I, 46, 371–414. https://doi.org/10.1016/S0967-0637.(98)00075-2, 1999.

Klemp, J. B., Durran, D. R.: Numerical modelling of bora winds, Meteorol. Atmos. Phys., 36, 215–227, https://doi.org/10.1007/BF0104515, 1987.

Kotlarski, S., Keuler, K., Christensen, O. B., Colette, A., Déqué, M., Gobiet, A., Goergen, K., Jacob, D., Lüthi, D., van Meijgaard, E., Nikulin, G., Schär, C., Teichmann, C., Vautard, R., Warrach–Sagi, K., and Wulfmeyer, V.: Regional climate modeling on European scales: a joint

standard evaluation of the EURO–CORDEX RCM ensemble, Geosci. Model Dev., 7, 1297–1333, https://doi.org/10.5194/gmd-7-1297-2014, 2014.

Krasakopoulou, E., Frangoulis, C., Psarra, S., Lagaria, A., Giannoudi, L. and Petihakis, G.: Carbonate system variables at the POSEIDON–E1–M3A site (S. Aegean Sea, Eastern Mediterranean), in: 11th Panhel. Symp. Oceanogr. & Fish., 857–860, 2015.

Kurkin, A., Kurkina, O., Rybin, A., and Talipova, T.: Comparative analysis of the first baroclinic Rossby radius in the Baltic, Black, Okhotsk, and Mediterranean seas, Russ. J. Earth Sci., 20, ES4008, https://doi.org/10.2205/2020ES000737, 2020.

Kuzmić, M., Grisogono, B., Li, X., and Lehner, S.: Examining deep and shallow Adriatic bora events, Q. J. Roy. Meteorol. Soc., 141, 3434–3438, https://doi.org/10.1002/qj.2578, 2015.

L'Hévéder, B., Li, L., Sevault, F., and Somot, S.: Interannual variability of deep convection in the Northwestern Mediterranean simulated with a coupled AORCM, Clim. Dyn., 41, 937–960, https://doi.org/10.1007/s00382-012-1527-5, 2013.

Langone, L., Conese, I., Miserocchi, S., Boldrin, A., Bonaldo, D., Carniel, S., Chiggiato, J., Turchetto, M., Borghini, M., Tesi, T.: Dynamics of particles along the western margin of the Southern Adriatic: Processes involved in transferring particulate matter to the deep basin. Mar. Geol., 375, 28–43, https://doi.org/10.1016/j.margeo.2015.09.004, 2016.

Laprise, R.: The Euler Equations of motion with hydrostatic pressure as independent variable, Mon. Weather Rev., 120, 197–207, https://doi.org/10.1175/1520-0493(1992)1202.0.CO;2, 1992.

Larson, J., Jacob, R., and Ong, E.: The model coupling toolkit: a new fortran90 toolkit for building multiphysics parallel coupled models, Int. J. High Perform. Comput. Appl., 19, 277–292, https://doi.org/10.1177/1094342005056115, 2005.

Leredde, Y., Denamiel, C., Brambilla, E., Lauer-Leredde, C., Bouchette, F., Marsaleix, P.: Hydrodynamics in the Gulf of Aigues-Mortes, NW Mediterranean Sea: *In situ* and modelling data, Cont. Shelf Res., 27(18), 2389–2406, https://doi.org/10.1016/j.csr.2007.06.006, 2007.

Levitus, S., Boyer, T.P.: World Ocean Atlas 1994, Volume 4: Temperature, NOAA Atlas NESDIS 4, US Dept. of Commerce, 1994a.

Levitus, S., Burgett, R., Boyer, T.P.: World Ocean Atlas 1994, Volume 3: Salinity, NOAA Atlas NESDIS 3, US Dept. Commerce, 1994b.

Ličer, M., Smerkol1, P., Fettich, A., Ravdas, M., Papapostolou, A., Mantziafou, A., Strajnar, B., Cedilnik, J., Jeromel, M., Jerman, J., Petan, S., Malačič, V., Sofianos, S.: Modeling the ocean and atmosphere during an extreme bora event in northern Adriatic using one-way and two-way atmosphere-ocean coupling, Ocean Sci., 12, 71–86, https://doi.org/10.5194/os-12-71-2016, 2016.

Lipizer, M., Partescano, E., Rabitti, A., Giorgetti, A., and Crise, A.: Qualified temperature, salinity and dissolved oxygen climatologies in a changing Adriatic Sea, Ocean Sci., 10, 771–797, https://doi.org/10.5194/os-10-771-2014, 2014.

Liu, F., Mikolajewicz, U., Six, K. D.: Drivers of the decadal variability of the North Ionian Gyre upper layer circulation during 1910–2010: a regional modelling study. Clim. Dyn., https//doi.org/10.1007/s00382-021-05714-y, 2021.

Ludwig, W., Dumont, E., Meybeck, M., and Heussner, S.: River discharges of water and nutrients to the Mediterranean Sea: major drivers for ecosystem changes during past and future decades?, Prog. Oceanogr., 80, 199–217, https://doi.org/10.1016/j.pocean.2009.02.001, 2009.

Ljubenkov, I.: Hydrodynamic modeling of stratified estuary: case study of the Jadro River (Croatia), J. Hydrol. Hydromech., 63, 29–37, https://doi.org/10.1515/johh-2015-0001, 2015.

Madec, G., Bourdallé–Badie, R., Bouttier, P.–A., Bricaud, C., Bruciaferri, D., Calvert, D., et al.: NEMO Ocean Engine. Paris, France: Notes du Pôle de modélisation de l\'Institut Pierre–Simon Laplace (IPSL), https://doi.org/10.5281/zenodo.1472492, 2017.

Malačić, V. and Petelin, B.: Climatic circulation in the Gulf of Trieste (northern Adriatic), J. Geophys. Res., 114, C07002, https://doi.org/10.1029/2008JC004904, 2009.

Manca, B. B., Kovačević, V., Gačić, M., and Viezzoli, D.: Dense water formation in the Southern Adriatic Sea and spreading into the Ionian Sea in the period 1997–1999, J. Mar. Syst., 33–34, 133–154, https://doi.org/10.1016/S0924-7963(02)00056-8, 2002.

Mantziafou, A. and Lascaratos, A.: An eddy resolving numerical study of the general circulation and deep-water formation in the Adriatic Sea, Deep-Sea Res. I, 51, 251–292, https://doi.org/10.1016/j.dsr.2004.03.006, 2004.

Mantziafou, A. and Lascaratos, A.: Deep-water formation in the Adriatic Sea: interannual simulations for the years 1979–1999, Deep–Sea Res. I, 55, 1403–1427, https://doi.org/10.1016/j.dsr.2008.06.005, 2008.

Marchesiello, P., McWilliams, J. C., and Shchepetkin, A.: Open boundary conditions for long–term integration of regional oceanic models, Ocean Model., 3, 1–20, https://doi.org/10.1016/S1463-5003(00)00013-5, 2001.

Marini, M., Russo, A., Paschini, E., Grilli, F., Campanelli, A.: Short-term physical and chemical variations in the bottom water of middle Adriatic depressions, Clim. Res., 31(2/3), 227–237, http://www.jstor.org/stable/24869280, 2006.

Martin, P. J., Book, J. W., Burrage, D. M., Rowley, C. D., and Tudor, M.: Comparison of model-simulated and observed currents in the central Adriatic during DART, J. Geophys. Res., 114, C01S05, https://doi.org/10.1029/2008JC004842, 2009.

May, P. W.: Climatological flux estimates in the Mediterranean Sea: Part 1. Winds and wind stresses. NORDA Report 54, NSTL Station, Mississippi 39529, 1982.

McKiver, W. J., Sannino, G., Braga, F., and Bellafiore, D.: Investigation of model capability in capturing vertical hydrodynamic coastal processes: a case study in the north Adriatic Sea, Ocean Sci., 12, 51–69, https://doi.org/10.5194/os-12-51-2016, 2016.

Mears, C. A., Scott, J., Wentz, F. J., Ricciardulli, L., Leidner, S. M., Hoffman, R., and Atlas, R.: A near-real-time version of the Cross-Calibrated Multiplatform (CCMP) ocean surface wind velocity data set, J. Geophys. Res. Oceans, 124, 6997–7010, https://doi.org/10.1029/2019JC015367, 2019.

Mejia, J. F., Koracin, D., and Wilcox, E. M.: Effect of coupled global climate models sea surface temperature biases on simulated climate of the western United States, Int. J. Climatol., 38, 5386–5404, https://doi.org/10.1002/joc.5817, 2018.

Melanotte–Rizzoli, P., Manca. B. B., D'Alcala, M. R., Theocharis, A., Bergamasco, A., Bregant, D., et al.: A synthesis of the Ionian Sea hydrography, circulation and water mass pathways during POEM–Phase I, Prog. Oceanogr., 39, 153–204. - https://doi.org/10.1016/S0079-6611(97)00013-X, 1997.

Mihanović, H., Vilibć, I., Carniel, S., Tudor, M., Russo, A., Bergamasco, A., Bubić, N., Ljubešić, Z., Viličić, D., Boldrin, A., Malačić, V., Celio, M., Comici, C., and Raicich, F.: Exceptional dense water formation on the Adriatic shelf in the winter of 2012, Ocean Sci., 9, 561–572, https://doi.org/10.5194/os-9-561-2013, 2013.

Mihanović, H., Vilibić, I., Dunić, N., Šepić, J.: Mapping of decadal middle Adriatic oceanographic variability and its relation to the BiOS regime. J. Geophys. Res. Oceans, 120, 5615–5630, https://doi.org/10.1002/2015JC010725, 2015.

Mihanović, H., Janeković, I., Vilibić, Bensi, M., and Kovačević, V.: Modelling Interannual Changes in Dense Water Formation on the Northern Adriatic Shelf, Pure Appl. Geophys., 175, 4065–4081, https://doi.org/10.1007/s00024-018-1935-5, 2018.

Mihanović, H., Vilibić, I., Šepić, J., Matić, F., Ljubešić, Z., Mauri, E., Gerin, R., Notarstefano, G., Poulain, P.-M.: Observation, preconditioning and recurrence of exceptionally high salinities in the Adriatic Sea. Front. Mar. Sci., 8, 672210. https://doi.org/10.3389/fmars.2021.672210, 2021.

Mlawer, E. J., Taubman, S. J., Brown, P. D., Iacono, M. J., and Clough, S. A.: Radiative transfer for inhomogeneous atmospheres: RRTM, a validated correlated–k model for the longwave, J. Geophys. Res., 102, 16663, https://doi.org/10.1029/97JD00237, 1997.

Moore, A.M., Arango, H.G., Broquet, G., Edwards, C., Veneziani, M., Powell, B.S., et al.: The Regional Ocean Modeling System (ROMS) 4-dimensional variational data assimilation systems: Part II – performance and application to the California current system. Prog. Oceanogr., 91, 50–73, http://dx.doi.org/10.1016/j.pocean.2011.05.003, 2011.

Oddo, P., Pinardi, N., and Zavatarelli, M.: A numerical study of the interannual variability of the Adriatic Sea (2000–2002). Sci. Total Environ., 353, 39–56, https://doi.org/10.1016/j.scitotenv.2005.09.061, 2005.

Oddo, P., Pinardi, N., Zavatarelli, M., Coluccelli, A.: The Adriatic basin forecasting system. Acta Adriat., 47 (Suppl.), 169–184, 2006.

Oddo, P., and Guarnieri, A.: A study of the hydrographic conditions in the Adriatic Sea from numerical modelling and direct observations (2000–2008), Ocean Sci., 7, 549–567, https://doi.org/10.5194/os-7-549-2011, 2011.

Orlanski, I.: A simple boundary condition for unbounded hyperbolic flows, J. Comput. Phys., 21, 251–269, https://doi.org/10.1016/0021-9991(76)90023-1, 1976.

Orlić, M., Dadić, V., Grbec, B., Leder, N., Marki, A., Matić, F., Mihanović, H., Beg Paklar, G., Pasarić, M., Pasarić, Z., Vilibić, I.: Wintertime buoyancy forcing, changing seawater

properties and two different circulation systems produced in the Adriatic, J. Geophys. Res. Oceans, 112, C03S07, https://doi.org/10.1029/2005JC003271, 2007.

Orlić, M., Dadić, V., Grbec, B., Leder, N., Marki, A., Matić, F., Mihanović, H., Beg Paklar, G., Pasarić, M., Pasarić, Z., and Vilibić, I.: Wintertime buoyancy forcing, changing seawater properties and two different circulation systems produced in the Adriatic, J. Geophys. Res., 112(C3), https://doi.org/10.1029/2005JC003271, 2006.

Pano, N. and Abdyli, B.: Maximum floods and their regionalization on the Albanian hydrographic river network, in: International Conference on Flood Estimation, 6–8 March 2002, CHR. Report II,17, Bern, Switzerland, 379–388, 2002.

Pano, N., Frasheri, A., and Avdyli, B.: The climatic change impact in water potential processe on the Albanian hydrographic river network, in: International Congress on Environmental Modelling and Software, 5–8 July 2010, Ottawa, Ontario, Canada, available at: https://scholarsarchive.byu.edu/iemssconference/2010/all/266, 2010.

Parras-Berrocal, I. M., Vazquez, R., Cabos, W., Sein, D., Mañanes, R., Perez–Sanz, J., and Izquierdo, A.: The climate change signal in the Mediterranean Sea in a regionally coupled atmosphere-ocean model, Ocean Sci., 16, 743–765, https://doi.org/10.5194/os-16-743-2020, 2020.

Pinardi, N., Allen, I., Demirov, E., De Mey, P., Korres, G., Lascaratos, A., Le Traon, P.-Y., Maillard, C., Manzella, G., Tziavos, C.: The Mediterranean ocean Forecasting System: first phase of implementation (1998–2001), Ann. Geophys., 21, 3–20, https://doi.org/10.5194/angeo-21-3-2003, 2003.

Pinardi, N., Coppini, G.: Operational oceanography in the Mediterranean Sea: the second stage of development, Ocean Sci., 6, 263–267. https://doi.org/10.5194/os-6-263-2010, 2010.

Poli, P., Hersbach, H., Dee, D. P., Berrisford, P., Simmons, A. J., Vitart, F., Laloyaux, P., Tan, D. G., Peubey, C., Thépaut, J. N., Trémolet, Y., Hólm, E.V., Bonavita, M., Isaksen, L., and Fisher, M.: ERA-20C: An atmospheric reanalysis of the twentieth century. J. Clim., 29(11), 4083–4097, https://doi.org/10.1175/JCLI-D-15-0556.1, 2016.

Powell, B. S., Arango, H.G., Moore, A.M., Di Lorenzo, E., Milliff, R.F., Foley, D.: 4DVAR data assimilation in the Intra-Americas Sea with the Regional Ocean Modeling System (ROMS), Ocean Model., 25, 173–188, https://doi.org/10.1016/j.ocemod.2008.04.008, 2008.

Prein, A. F., Langhans, W., Fosser, G., Ferrone, A., Ban, N., Goergen, K., Keller, M., Tölle, M., Gutjahr, O., Feser, F., Brisson, E., Kollet, S., Schmidli, J., van Lipzig, N. P. M., and Leung, R.: A review on regional convection-permitting climate modeling: Demonstrations, prospects and challenges, Rev. Geophys., 53, 323–361, https://doi.org/10.1002/2014RG000475, 2015.

Pullen, J., Doyle, J., and Signell, R.: Two-way air-sea coupling: a study of the Adriatic, Mon. Weather Rev., 134, 1465–1483, https://doi.org/10.1175/MWR3137.1, 2006.

Pullen, J., Doyle, J. D., Haack, T., Dorman, C., Signell, R. P., Lee, C. M.: Bora event variability and the role of air–sea feedback, J. Geophys. Res. Oceans, 112, C03S18. https://doi.org/10.1029/2006JC003726, 2007.

Querin, S., Bensi, M., Cardin, V., Solidoro, C., Bacer, S., Mariotti, L., Stel, F., Malačič, V.: Saw–tooth modulation of the deep-water thermohaline properties in the southern Adriatic Sea. Journal of Geophysical Research, 121, 4585–4600, https://doi.org/10.1002/2015JC011522, 2016.

Querin, S., Cossarini, G., Solidoro, C.: Simulating the formation and fate of dense water in a midlatitude marginal sea during normal and warm winter conditions. J. Geophys. Res. Oceans 118, 885–900, https://doi.org/10.1002/jgrc.20092, 2013.

Raicich, F.: Notes on the flow rates of the Adriatic rivers. Technical Report RF 02/94, 8 pp., CNR. Istituto sperimentale talassografico, Trieste, Italy, 1994.

Ricchi, A., Miglietta, M. M., Falco, P. P., Benetazzo, A., Bonaldo, D., Bergamasco, A., Sclavo, M., and Carniel, S.: On the use of a coupled ocean-atmosphere-wave model during an extreme cold air outbreak over the Adriatic Sea, Atmos. Res., 172–173, 48–65, https://doi.org/10.1016/j.atmosres.2015.12.023, 2016.

Schär, C., Frei, C., Luthi, D., and Davies, H. C.: Surrogate climatechange scenarios for regional climate models, Geophys. Res. Lett., 23, 669–672, https://doi.org/10.1029/96GL00265, 1996.

Schär, C., Fuhrer, O., Arteaga, A., Ban, N., Charpilloz, C., Di Girolamo, S., Hentgen, L., Hoefler, T., Lapillonne, X., Leutwyler, D., Osterried, K., Panosetti, D., Rüdisühli, S., Schlemmer, L., Schulthess, T. C., Sprenger, M., Ubbiali, S., and Wernli, H.: Kilometer–Scale Climate Models: Prospects and Challenges, B. Am. Meteorol. Soc., 101, E567–E587, https://doi.org/10.1175/BAMS-D-18-0167.1, 2020.

Sevault, F., Somot, S., Alias, A., Dubois, C., Lebeaupin Brossier, C., Nabat, P., Adloff, F., Déqué, M., and Decharme, B.: A fully coupled Mediterranean regional climate system model: design and evaluation of the ocean component for the 1980–2012 period, Tellus A, 66, 23967, https://doi.org/10.3402/tellusa.v66.23967, 2014

Shapiro, G. I., Hill, A. E.: The alternative density structures of cold/saltwater pools on a sloping bottom: The role of friction, J. Phys. Oceanogr., 27, 2381–2394, https://doi.org/10.1175/1520-0485(2003)033<0390:TADSOC>2.0.CO;2, 2003.

Shchepetkin, A.F., McWilliams, J.C.: The regional oceanic modeling system: a split–explicit, free-surface, topography-following coordinate ocean model, Ocean Model., 9, 347– 780 404. https://doi.org/10.1016/j.ocemod.2004.08.002, 2005.

Shchepetkin, A.F., McWilliams, J.C.: Correction and commentary for "Ocean forecasting in terrain-following coordinates: Formulation and skill assessment of the regional ocean modeling system" by Haidvogel et al., J. Comput. Phys., 227, pp. 3595–3624, J. Comp. Phys. 228, 8985–9000, https://doi.org/10.1016/j.jcp.2009.09.002, 2009.

Signell, R. P., Chiggiato, J., Horstmann, J., Doyle, J. D., Pullen, J., Askari, F.: High-resolution mapping of Bora winds in the northern Adriatic Sea using synthetic aperture radar, J. Geophys. Res., 115, C04020, https://doi.org/10.1029/2009JC005524, 2010.

Simoncelli, S., Masina, S., Axell, L., Liu, Y., Salon, S., Cossarini, G., Bertino, L., Xie, J., Samuelsen, A., Levier, B., et al.: MyOcean regional reanalyses: overview of reanalyses systems and main results, Mercator Ocean J 54: Special issue on main outcomes of the MyOcean2 and MyOcean follow-on projects. https://www.mercator-ocean.fr/wp-content/uploads/2016/03/JournalMO-54.pdf, 2016.

Simoncelli, S., Fratianni, C., Pinardi, N., Grandi, A., Drudi, M., Oddo, P., and Dobricic, S.:_Mediterranean Sea Physical Reanalysis (CMEMS MED-Physics)_ (Version 1) [Data set]. Copernicus Monitoring Environment Marine Service (CMEMS). https://doi.org/10.25423/MEDSEA_REANALYSIS_PHYS_006_004, 2019.

Skamarock, W. C., Klemp, J. B., Dudhia, J., Gill, D. O., Barker, D. M., Wang, W., Powers, J. G.: A description of the Advanced Research WRF Version 2, NCAR Technical Note NCAR/TN468+STR, https://doi.org/10.5065/D6DZ069T, 2005.

Smith, R.B.: Aerial observations of the Yugoslavian Bora. J. Atmos. Sci., 44, 269–297, https://doi.org/10.1175/1520-0469(1987)044<0269:AOOTYB>2.0.CO;2, 1987.

Smolarkiewicz, P. K. and Grabowski, W. W.: The multidimensional positive definite advection transport algorithm: nonoscillatory option, J. Comput. Phys., 86, 355–375, https://doi.org/10.1016/0021-9991(90)90105-A, 1990.

Somot, S., Sevault, F., and Déqué, M.: Transient climate change scenario simulation of the Mediterranean Sea for the twenty-first century using a high-resolution ocean circulation model, Clim. Dyn., 27, 851–879, https://doi.org/10.1007/s00382-006-0167-z, 2006.

Somot, S., Ruti, P., Ahrens, B., Coppola, E., Jordà, G., Sannino, G., and Solmon, F.: Editorial for the Med-CORDEX special issue. Clim. Dyn., 51, 771–777, https://doi.org/10.1007/s00382-018-4325-x, 2018.

Soto–Navarro, J., Jordá, G., Amores, A., Cabos, W., Somot, S., Sevault, F.: 2020. Evolution of Mediterranean Sea water properties under climate change scenarios in the Med-CORDEX ensemble. Clim. Dyn., 54, 2135–2165, https://doi.org/10.1007/s00382-019-05105-4, 2020.

Sperrevik, A. K., Röhrs, J., and Christensen, K. H.: Impact of data assimilation on Eulerian versus Lagrangian estimates of upper ocean transport, J. Geophys. Res. Ocean., 122, 5445–5457, https://doi.org/10.1002/2016JC012640, 2017.

Stiperski, I., Ivančan-Picek, B., Grubišić, V., Bajić, A.: Complex bora flow in the lee of Southern Velebit. Q. J. Roy. Meteorol. Soc., 138: 1490–1506, https://doi.org/10.1002/qj.1901, 2012.

Taylor, K.: Summarizing multiple aspects of model performance in a single diagram, J. Geophys. Res, 106, 7183–7192, https://doi.org/10.1029/2000JD900719, 2001.

Theocharis, A., Krokos, G., Velaoras, D., and Korres, G.: An internal mechanism driving the alternation of the Eastern Mediterranean dense/deep water sources. In: Eusebi Borzelli, G.L., Gačić M., Lionello, P., Malanotte-Rizzoli, P. (Eds.), The Mediterranean Sea: Temporal Variability and Spatial Patterns, Geophysical Monograph Series. AGU, pp. 113–137. https://doi.org/10.1002/9781118847572.ch8, 2014.

Thorne, P. W. and Vose, R. S.: Reanalyses suitable for characterizing long-term trends, Bull. Am. Meteorol. Soc., 91, 353–361, https://doi.org/10.1175/2009bams2858.1, 2010.

Tonani, M., Teruzzi, A., Korres, G., Pinardi, N., Crise, A., Adani, M., et al.: The Mediterranean Monitoring and Forecasting Centre, a component of the MyOcean system. Proceedings of the Sixth International Conference on EuroGOOS 4–6 October 2011, Sopot, Poland. Edited by H. Dahlin, N.C. Fleming and S. E. Petersson. First published 2014, EuroGOOS Publication no. 30. ISBN 978-91-974828-9-9, 2014

Tudor, M., Ivatek-Šahdan, S., Stanešić, A., Horvath, K., and Bajić, A.: Forecasting weather in Croatia using ALADIN numerical weather prediction model, in: Climate Change and Rgional/Local Responses, edited by: Zhang, Y. and Ray, P., InTech, Rijeka, Croatia, 59–88, https://doi.org/10.5772/55698, 2013.

Tudor, M., Stanešić, A., Ivatek-Šahdan, S., Hrastinski, M., Odak Plenković, I., Horvath, K., Bajić, A. and Kovačić, T.: Operational validation and verification of ALADIN forecast in meteorological and hydrological service of Croatia, Croat. Meteorol. J., 50 (50), 47–70, https://hrcak.srce.hr/155403, 2015.

Umlauf, L. and Burchard, H.: A generic length-scale equation for geophysical turbulence models, J. Mar. Res., 61, 235–265, https://doi.org/10.1357/002224003322005087, 2003.

Varga, Á. J. and Breuer, H.: Sensitivity of simulated temperature, precipitation, and global radiation to different WRF configurations over the Carpathian Basin for regional climate applications, Clim. Dynam., 55, 2849–2866, https://doi.org/10.1007/s00382-020-05416-x, 2020.

Vested, H. J., Berg, P. and Uhrenholdt, T.: Dense water formation in the northern Adriatic, J. Mar. Syst., 18, 135–160, https://doi.org/10.1016/S0924-7963(98)00009-8, 1998.

Vilibić, I. and Orlić, M.: Least squares tracer analysis of water masses in the South Adriatic (1967–1990), Deep-Sea Res. I, 48, 2297–2330, https://doi.org/10.1016/S0967-0637(01)00014-0, 2001.

Vilibić, I. and Orlić, M.: Adriatic water masses, their rates of formation and transport through the Otranto Strait, Deep-Sea Res. I, 49, 1321–1340, https://doi.org/10.1016/S0967-0637(02)00028-6, 2002.

Vilibić, I.: An analysis of dense water production on the North Adriatic shelf. Estuar. Coastal Shelf Sci., 56, 861–867, https://doi.org/10.1016/S0272-7714(02)00277-9, 2003.

Vilibić, I., Grbec, B., Supić, N.: Dense water generation in the north Adriatic in 1999 and its recirculation along the Jabuka Pit, Deep–Sea Res. I, 51, 1457–1474. https://doi.org/10.1016/j.dsr.2004.07.012, 2004.

Vilibić, I., and Supić, N.: Dense water generation on a shelf: the case of the Adriatic Sea, Ocean Dyn., 55, 403–415, https://doi.org/10.1007/s10236-005-0030-5, 2005.

Vilibić, I., Beg Paklar, G., Žagar, N., Mihanović, H., Supić, N., Žagar, M., Domijan, N., Pasarić, M.: Summer breakout of trapped bottom dense water from the northern Adriatic. J. Geophys. Res. Oceans, 113, C11S02, https://doi.org/10.1029/2007JC004535, 2008.

Vilibić, I., Matijević, S., Šepić, J., Kušpilić, G.: Changes in the Adriatic oceanographic properties induced by the Eastern Mediterranean Transient, Biogeosciences, 9, 2085–2097, https://doi.org/10.5194/bg-9-2085-2012, 2012.

Vilibić, I., Mihanović, H.: Observing the bottom density current over a shelf using an Argo profiling float, Geophys. Res. Lett., 40, 910–915, https://doi.org/10.1002/grl.50215, 2013.

Vilibić I., Pištalo, D., Šepić J.: Long-term variability and trends of relative geostrophic currents in the middle Adriatic, Cont. Shelf Res., 93, 70–80, https://doi.org/10.1016/j.csr.2014.12.003, 2014.

Vilibić, I., Mihanović, H., Janeković, I., Šepić, J.: Modelling the formation of dense water in the northern Adriatic: sensitivity studies, Ocean Model., 101, 17–29, https://doi.org/10.1016/j.ocemod.2016.03.001, 2016.

Vilibić, I., Mihanović, H., Janeković, I., Denamiel, C., Poulain, P.- M., Orlić, M., Dunić, N., Dadić, V., Pasarić, M., Muslim, S., Gerin, R., Matić, F., Šepić, J., Mauri, E., Kokkini, Z., Tudor, M., Kovač, Ž., Džoić, T.: Wintertime dynamics in the coastal north-eastern Adriatic Sea: the NAdEx 2015 experiment, Ocean Sci., 14, 237–258, https://doi.org/10.5194/os-14-237-2018, 2018.

Vilibić, I., Zemunik, P., Šepić, J., Dunić, N., Marzouk, O., Mihanović, H., Denamiel, C., Precali, R., and Djakovac, T.: Present climate trends and variability in thermohaline properties of the northern Adriatic shelf, Ocean Sci., 15, 1351–1362, https://doi.org/10.5194/os-15-1351-2019, 2019.

Vilibić, I., Pranić, P., Denamiel, C.: North Adriatic Dense Water: lessons learned since the pioneering work of Mira Zore-Armanda 60 years ago, Acta Adriat., https://doi.org/10.32582/aa.64.1.11, 2023.

Vörösmarty, C., Fakers, B., and Tucker, B.: River discharge database, version 1.0 (RivDIS vLO), volumes 0 through 6, in: A contribution to IHP-V Theme 1, Technical Documents Series, Technical report, UNESCO, Paris, France, 1996.

Wahlin, A. K.: Topographic steering of dense currents with application to submarine canyons, Deep–Sea Res. I, 49, 305–320, https://doi.org/10.1016/S0967-0637(01)00058-9, 2002.

Wahlin, A. K.: Downward channeling of dense water in topographic corrugations, Deep–Sea Res. I, 51, 577–590, https://doi.org/10.1016/j.dsr.2003.11.002, 2004.

Warner, J. C., Armstrong, B., He, R., Zambon, J. B.: Development of a Coupled Ocean–Atmosphere–Wave–Sediment Transport (COAWST) Modeling System. Ocean Model. 35, 230–244, https://doi.org/10.1016/j.ocemod.2010.07.010, 2010.

Weatherall, P., Marks, K. M., Jakobsson, M., Schmitt, T., Tani, S., Arndt, J. E., Rovere, M., Chayes, D., Ferrini, V., and Wigley, R.: A new digital bathymetric model of the world's oceans, Earth and Space Science, 2, 331–345, https://doi.org/10.1002/2015EA000107, 2015.

Yang, B., Zhang, Y., Qian, Y., Song, F., Leung, L. R., Wu, P., Guo, Z., Lu, Y., and Huang, A.: Better monsoon precipitation in coupled climate models due to bias compensation, npj Clim. Atmos. Sci., 2, 43, https://doi.org/10.1038/s41612-019-0100-x, 2019

Yaremchuk, M., Martin, P., Koch, A., Beattie, C.: Comparison of the adjoint and adjoint–free 4dVar assimilation of the hydrographic and velocity observations in the Adriatic Sea, Ocean Model., 97, 129–140, https://doi.org/10.1016/j.ocemod.2015.10.010, 2016.

Zavatarelli, M., Pinardi, N., Kourafalou, V.H., and Maggiore, A.: Diagnostic and prognostic model studies of the Adriatic Sea general circulation: Seasonal variability, J. Geophys. Res., 107, 3004, https://doi.org/10.1029/2000JC000210, 2002.

Zavatarelli, M. and Pinardi, N.: The Adriatic Sea modelling system: a nested approach, Ann. Geophys., 21, 345–364, https://doi.org/10.5194/angeo-21-345-2003, 2003.

Zore–Armanda, M.: Les masses d'eau de la mer Adriatique. Acta Adriat., 10, 5–88, 1963.

9. CURRICULUM VITAE

Petra Pranić graduated in Physics at the Faculty of Science of the University of Split in September 2018, majoring in "Computational Physics". During her studies, she received two Dean's awards and a scholarship from the city of Split. In 2019, she started working at the Institute of Oceanography and Fisheries in Split as a research assistant on the project of the Croatian Science Foundation titled "Adriatic Decadal and Interannual Oscillations: Observations, Modeling and Consequences" (ADIOS) under the leadership of Dr. Ivica Vilibić, and enrolled in the Interdisciplinary Doctoral Study in Oceanology at the Faculty of Science of the University of Zagreb.

Her current field of scientific research focuses on analyzing atmosphere-ocean numerical models in the Adriatic Sea. More particuraly, her work consists of model skill assessments and analyses of ocean waves in future climate, evaluation of an atmospheric and oceanic historical climate simulation, and studies of the variability of the Adriatic–Ionian thermohaline circulation and Adriatic dense-water dynamics.

In her scientific career so far, Petra Pranić has authored six scientific papers indexed in CC (Current Contents Connect). She is the first author of two papers, both published in Q1 ranked world journals with high impact factors. She presented her research at three international scientific conferences/workshops as the first author of the abstract and has completed four international scientific schools.

In addition, she participated in the activities of three projects of the Interreg Croatia–Italy programme: „Ecological Observing System in the Adriatic Sea: oceanographic observations for biodiversity“ (ECOSS), „Climate challenges on coastal and transitional changing areas: weaving a cross – Project Adriatic Response“ (CHANGE WE CARE) and „Climate Responses for the Adriatic Region“ (CREATE).

10. PUBLISHED SCIENTIFIC PAPERS

1. Denamiel, C., **Pranić, P.**, Quentin, F., Mihanović, H., Vilibić, I.: Pseudo-global warming projections of extreme wave storms in complex coastal regions: the case of the Adriatic Sea. Clim. Dyn., 55, 2483–2509, https://doi.org/10.1007/s00382-020-05397-x, 2020.
2. Denamiel, C., **Pranić, P.**, Ivanković, D., Tojčić, I., Vilibić, I.: Performance of the Adriatic Sea and Coast (AdriSC) climate component – a COAWST V3.3-based coupled atmosphere-ocean modelling suite: atmospheric dataset. Geosci. Model Dev., 14, 3995–4017, https://doi.org/10.5194/gmd-14-3995-2021, 2021.
3. **Pranić, P.**, Denamiel, C., Vilibić, I.: Performance of the Adriatic Sea and Coast (AdriSC) climate component – a COAWST V3.3-based one-way coupled atmosphere-ocean modelling suite: ocean results. Geosci. Model Dev., 14, 5927–5955, https://doi.org/10.5194/gmd-14-5927-2021, 2021.
4. Denamiel, C., Tojčić, I., **Pranić, P.**, Vilibić, I.: Modes of the BiOS-driven Adriatic Sea thermohaline variability. Clim. Dyn., 59, 1097–1113, https://doi.org/10.1007/s00382-022-06178-4, 2022.
5. **Pranić, P.**, Denamiel, C., Janeković, I., Vilibić, I.: Multi-model analysis of Adriatic dense-water dynamics, Ocean Sci., 19, 649–670, https://doi.org/10.5194/os-19-649-2023, 2023.
6. Vilibić, I., **Pranić, P.**, Denamiel, C.: North Adriatic Dense Water: lessons learned since the pioneering work of Mira Zore-Armanda 60 years ago, Acta Adriat., https://doi.org/10.32582/aa.64.1.11, 2023.